Technical University of Denmark

DTU

Entrained Flow Gasification of Biomass

Qin, Ke; Jensen, Anker Degn; Jensen, Peter Arendt; Lin, Weigang

Link back to DTU Orbit

DTU Library
Technical Information Center of Denmark

Entrained Flow Gasification of Biomass

Ke Qin

Ph.D. Thesis

2012

Department of Chemical and Biochemical Engineering

Technical University of Denmark

2800 Kgs.Lyngby

Denmark

Preface

The present dissertation is written in accordance with the partial requirements of obtaining a Ph. D. degree in the Technical University of Denmark (DTU). The work has been performed between September 2008 and August 2012 in the Combustion and Harmful Emission Control (CHEC) Research Center, Department of Chemical and Biochemical Engineering (KT). The work was funded by the Technical University of Denmark, the Danish Research Council for Technology and Production, and the Danish Energy Agency. The supervisors were Professor Anker Degn Jensen, Associate Professor Peter Arendt Jensen, and Associate Professor Weigang Lin.

I would like to express my sincere gratitude to my supervisors for their supervision and encouragement during my study. In the past four years, they were patient and took great trouble to make valuable discussion, give constructive suggestion, and read my manuscripts. I would also like to express my thanks to Professor Peter Glarborg for providing fruitful inputs to my project.

I am grateful to the technical staff in CHEC and KT-Workshop for their assistance in my experimental work, particularly Nikolaj Vinterberg Nissen and Carsten Nørby. I am grateful to my colleagues, Jacob Brix, Hao Wu, Hamid Hashemi, Jakob Munkholt Christensen, Brian Brun Hansen, Peter Mølgaard Mortensen, Qiongxiao Wu, and Martin Høj, for their kind help in my work. I am grateful to the members at CHEC for creating a very friendly and enjoyable working environment. I am also grateful to my best friend, Xiaomin Liu, who let me have precious friendship and not feel lonely any more during pursuing my studies away from home.

Finally, and most important I owe special thanks to my grandparents, my parents, and my husband for their supporting and encouraging during my study and caring and understanding through the years. I wish to dedicate this thesis to them.

Kgs. Lyngby, September 2012

Ke Qin

Summary

The present Ph. D. thesis describes experimental and modeling investigations on entrained flow gasification of biomass and an experimental investigation on entrained flow co-gasification of biomass and coal. A review of the current knowledge of biomass entrained flow gasification is presented.

Biomass gasification experiments were performed in a laboratory-scale atmospheric pressure entrained flow reactor with the aim to investigate the effects of operating parameters and biomass types on syngas products. A wide range of operating parameters was involved: reactor temperature, steam/carbon ratio, excess air ratio, oxygen concentration, feeder gas flow, and residence time. Wood, straw, and lignin were used as biomass fuels. In general, the carbon conversion was higher than 90 % in the biomass gasification experiments conducted at high temperatures (> 1200 °C). The biomass carbon that was not converted to gas in the gasification process only appeared as soot particles in the syngas in all experiments, except for two experiments conducted at 1000 °C without steam addition where a very small amount of char was also left. The effects of reactor temperature, steam/carbon ratio, and excess air ratio on the yields of H_2 and CO were noticeable, while the effects of oxygen concentration, feeder gas flow, and residence time on the yields of H_2 and CO were negligible. The yield of soot could be reduced by a higher reactor temperature, higher steam/carbon ratio, higher excess air ratio, lower oxygen concentration, larger feeder gas flow, and longer residence time. Wood, straw, and lignin had similar gasification behavior except with regard to soot formation. The soot yield was lowest during straw gasification possibly because of its high potassium content. The equilibrium product compositions under the experimental conditions were calculated by using the FactSage Program. At high temperature with steam addition, the experimental product compositions were close to the calculated equilibrium gas compositions. Besides a comprehensive experimental investigation on biomass gasification, a few experiments of biomass pyrolysis were also performed with the aim to obtain a better understanding of the whole gasification process. In comparison to gasification, higher yields of H_2, CO, and soot were produced during pyrolysis.

During wood gasification, the major part of the filter sample was soot on the basis of simultaneous thermal analysis (STA). Soot appeared as agglomerated nano-size spherical particles (< 100 nm) which are very rich in carbon on the basis of scanning electron microscopy (SEM) images coupled with energy dispersive spectroscopy (EDS). In

comparison to wood gasification, the filter sample obtained from straw gasification had quite low content of soot while high contents of volatilizable KCl and K_2SO_4, and thereby appeared as irregular crystals (> 100 nm). During lignin gasification, the filter sample mainly consisted of soot and nonvolatilizable inorganic matter. The parent wood particles and the derived wood char samples obtained from the gasification experiment conducted at 1000 °C had similar structure, size, and shape according to SEM images, but the derived wood char particle surface looked smoother indicating some degree of melting. In STA analysis, the wood char was more reactive than the wood soot with respect to both oxidation and CO_2 gasification. Besides, the wood soot produced at higher temperature was more reactive than the soot produced at lower temperature.

Biomass and coal co-gasification experiments were performed in the same entrained flow reactor. The effect of mixing ratio of different fuels on syngas products was investigated at 1400 °C with steam addition. The yields of residual particulates (char and/or soot) decreased with increasing straw fraction during straw/wood co-gasification and with increasing biomass fraction (straw or wood) during biomass/coal co-gasification. Besides, their yields in the co-gasification experiments were lower than the calculated values from their weighted yields in the individual fuel gasification experiments, indicating a synergistic effect on lowering the yields of residual particulates during co-gasification. The yields of H_2, CO, and CO_2 remained nearly unchanged with varying mixing ratio during straw/wood co-gasification, while increased gradually with increasing biomass mixing ratio during biomass/coal co-gasification.

A mathematic model of biomass entrained flow gasification was developed. The model included mixing, drying and pyrolysis, char-gas and soot-gas reactions, detailed gas-phase reactions, and mass and heat transfer. The model could reasonable predict the yields of syngas products obtained in the biomass gasification experiments. Moreover, the simulation results suggest that the soot can be completely converted and thereby the H_2 and CO yields can reach the maximum values if the reactor length is increased to 2.5 – 3 m under a reasonable condition (high temperature with steam addition).

Dansk Resumé

Denne Ph.D.-afhandling beskriver et eksperimentelt og modelbaseret studium af forgasning af biomasse og biomasse-kul samforgasning i en atmosfærisk tryk laboratorieskala entrained flow reaktor.

Procesbetingelsernes og biomassetypens indflydelse på syntesegasproduktet blev undersøgt systematisk. Kulstofomsætningen var typisk højere end 90 % ved biomasseforgasning ved høj temperatur (> 1200 °C). Reaktortemperaturen, damp/kulstof-forholdet og luftoverskudstallet havde stor betydning for H_2 og CO udbytterne, mens iltkoncentrationen, fødegasflowet og opholdstiden havde mindre betydning. Sodudbyttet kunne reduceres ved at anvende høj reaktortemperatur, højt damp/kulstof-forhold, højt luftoverskudstal, lav iltkoncentration, højt fødegasflow og lang opholdstid. Forgasning af træ, halm og lignin gav ens produktgassammensætning, med undtagelse af sodudbyttet. Halm havde det laveste sodudbytte, muligvis pga. det høje kaliumindhold i halm. Ved høj temperatur og med vanddamp i gassen var produktgassen tæt på ligevægtssammensætningen. Ud over et systematisk eksperimentelt studie af biomasseforgasning, blev der udført nogle få eksperimenter om biomassepyrolyse for at opnå en bedre forståelse af hele forgasningsprocessen. Sammenlignet med forgasning blev der opnået højere udbytter af H_2, CO og sod ved pyrolyse.

Ved træforgasning var størstedelen af filterprøven sod, hvilket blev bestemt ved simultan termisk analyse (STA). Soden bestod af agglomerater af sfæriske nanopartikler (< 100 nm), med et højt indhold af kulstof, hvilket blev undersøgt med skanning elektron mikroskopi (SEM) koblet med energidispersiv spektroskopi (EDS). Sammenlignet med træforgasning indeholdt filterprøven fra halmforgasning små mængder sod, men store mængder KCl og K_2SO_4, hvilket fremstod som irregulære krystaller (> 100 nm). Ved ligninforgasning indeholdt filterprøven hovedsageligt sod og ikke-flygtige uorganiske forbindelser.

Træpartiklerne og de afledte kokspartikler, der blev dannet ved forgasning ved 1000 °C, havde samme struktur, størrelse og facon, men overfladen af kokspartiklerne var mere glat, hvilket indikerer at træet delvist var smeltet. Forsøg med STA analyse viste at koks dannet fra træ var mere reaktivt end sod dannet fra træ, både ved oxidation og ved CO_2 forgasning. Desuden var sod dannet fra træ fremstillet ved højere temperatur mere reaktivt end tilsvarende sod fremstillet ved lavere temperatur. Dette er en umiddelbart overraskende observation.

Sam-forgasning af biomasse og kul blev undersøgt i den samme reaktor. Forgasningsproduktets sammensætning blev undersøgt ved 1400 °C og med tilsætning af vanddamp som funktion af blandingsforholdet mellem biomasse og kul. Udbyttet af faste produkter (koks og/eller sod) faldt når halmmængden øgedes i halm/træ sam-forgasning og når biomassemængden (halm eller træ) øgedes i biomasse/kul sam-forgasning. Desuden var udbyttet af faste produkter lavere ved sam-forgasning end det forventede udbytte, beregnet ud fra forgasningsforsøgene med de enkelte komponenter, vægtet med mængden af komponenterne. Dette indikerer en positiv effekt der reducerer udbyttet af faste partikler ved sam-forgasning. Udbyttet af H_2, CO og CO_2 var stort set det samme ved forskellige halmmængder i halm/træ sam-forgasning, mens gasudbyttet øgedes gradvist når biomassemængden øgedes i biomasse/kul sam-forgasning.

En detaljeret matematisk model for entrained flow forgasning af biomasse er blevet udviklet. Modellen inkluderer blanding, tørring og pyrolyse, koks-gas og sod-gas reaktioner, detaljerede gasfase reaktioner og masse- og energioverførsel. Modellen kunne tilfredsstillende beregne udbyttet af syntesegas ved biomasseforgasning.

Introduction to this thesis

Under environmental and sociopolitical considerations, there is an increasing world-wide interest in the use of biomass resources for energy and chemicals. It is estimated that by 2050 biomass could supply 10 – 20 % of the global primary energy requirements. Gasification is one of the effective thermochemical conversion processes for biomass unitization, which provides a syngas that can be used to synthesize liquid fuels and chemicals or produce heat and power. Entrained flow gasification operates at high temperatures (> 1200 °C) with rather small particles to achieve a high carbon conversion within a few seconds and may provide a high-quality syngas especially without tar. Currently, coal gasification is the most commercially available technology in large scale. Biomass is an important alternative to coal but differs from coal in many important aspects, including lower carbon content, higher oxygen content, higher volatile content, lower heating value, and lower bulk density. Therefore, knowledge on biomass gasification is needed to support the development of commercial biomass entrained flow gasifiers.

Most of the chapters of this thesis are written as manuscripts to scientific journals. A general introduction to the field of biomass entrained flow gasification is given through a literature study in Chapter 1. Chapter 2 and Chapter 3 concern biomass gasification experiments performed in an entrained flow reactor with the aim of testing the effects of operating parameters and biomass types on syngas products. Chapter 4 deals with the morphology, composition, and kinetics of residual particulates, char and soot, obtained from biomass entrained flow gasification. Chapter 5 concerns biomass and coal co-gasification experiments performed in the same entrained flow reactor with the aim of testing the effects of mixing ratio on syngas products. In order to predict gasification product and optimize gasification process, Chapter 6 presents the model work of biomass entrained flow gasification on the basis of the obtained experimental results. Finally, conclusions and suggestions for further work are given in Chapter 7.

Chapter 2 has been published in Fuel: Ke Qin, Weigang Lin, Peter Arendt Jensen, and Anker Degn Jensen, High temperature entrained flow gasification of biomass, volume 93 (2012), 589 – 600.

Chapter 3 has been published in Energy and Fuels: Ke Qin, Peter Arendt Jensen, Weigang Lin, and Anker Degn Jensen, Biomass gasification behavior in an entrained flow reactor: gas product distribution and soot formation, volume 26 (2012), 5992 – 6002.

Chapter 4 has been published in Energy and Fuels: Ke Qin, Weigang Lin, Søren Fæster, Peter Arendt Jensen, Hao Wu, and Anker Degn Jensen, Characterization of residual particulates from biomass entrained flow gasification, volume 27 (2013), 262 – 270.

Content

Chapter 1 Literature study

Abstract

In the present literature study, gasification technology including main processes and reactions, different fuel types (coal and biomass), and different gasifier types (moving bed, fluidized bed, and entrained flow gasifier) were discussed and summarized. Further, attention has been paid to the effects of operating conditions on products distribution during biomass entrained flow pyrolysis and gasification respectively. H_2 and CO are the main gas products during pyrolysis and gasification, and CO_2 is also the main gas product during gasification. On the whole, from a viewpoint of syngas utilization for fuels and chemicals, high temperature is desirable for providing high yields of H_2 and CO and achieving a high carbon conversion. Besides, at high temperature, a suitable excess air ratio, longer residence time, increased reactor length, and smaller particles are also favored for improving the carbon conversion.

1.1 Introduction

Gasification is in one sense an old technology, which was firstly investigated by Thomas Shirley in 1659 [1,2]. Some of the important milestones in gasification development are depicted in Figure 1.1. More than a century ago, gasification was commercially applied for the production of both fuels and chemicals [3]. In accordance with the current developing trends in the power generation and refinery industry, the advanced stages of gasification technology continue to be applied toward the syngas, with an increasing number of applications in power, heat, fuels, and chemicals [3]. The worldwide historical growth in the gasification capacity since 1960s, as well as the future addition through 2010s, is illustrated in Figure 1.2. Today, gasification is widely deployed throughout the world in many industrial settings.

Gasification is a thermochemical solid fuel conversion process by which a combustible gas is produced. In conventional combustion technology fuel is burned using excess air to ensure complete combustion. In gasification the amount of oxygen is generally one-fifth to one-third of the amount theoretically required for complete combustion [4]. H_2 and CO are the main desired components of the syngas. Gasification, as a possibility of more environmentally friendly use of solid fuel, has been advancing in the past 25 years [1]. The focus on the environmental benefits of gasification can partly be contributed to the increased focus on the

impact of CO_2, SO_x, and NO_x on the climate. Major environmental benefits in gasification can be found in Integrated Gasification Combined Cycles (IGCC) [1].
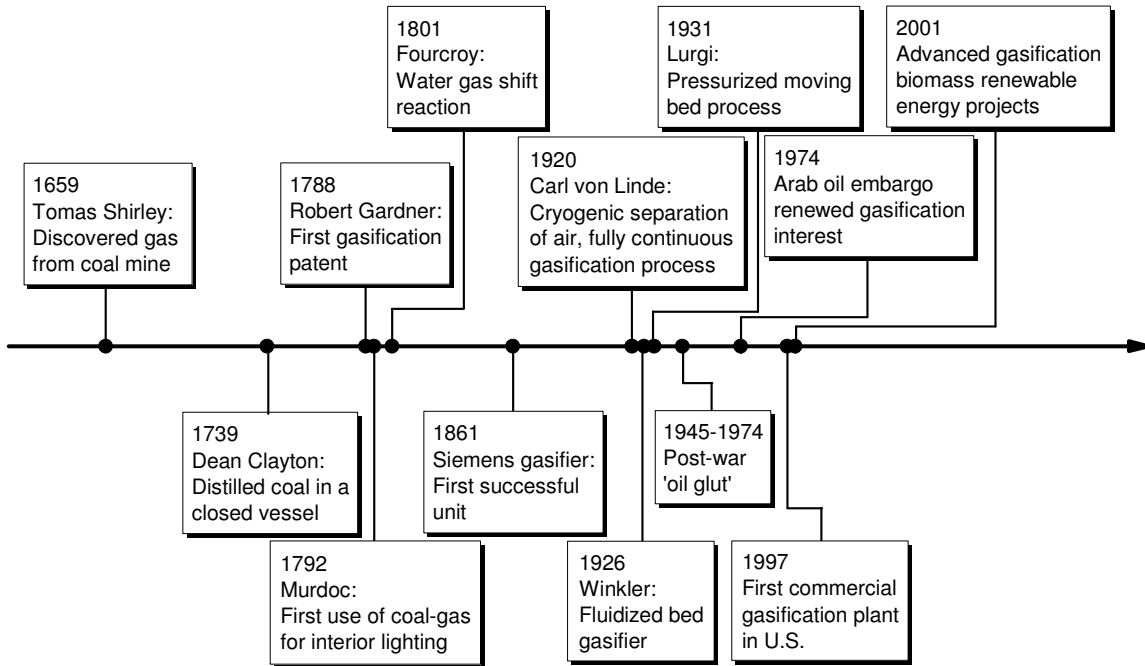
Figure 1.1 Milestones in gasification development [2]
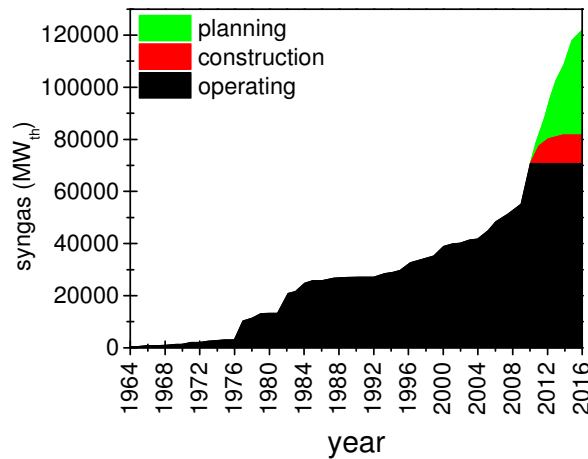
Figure 1.2 Worldwide gasification capacity and planned growth (cumulative by year) [5]

Now, after oil, coal, and gas, biomass has become the fourth largest energy resource in the world [6,7]. Biomass resources are a major component of strategies to mitigate global climate change since they are considered as sustainable CO_2-neutral energy sources [8]. In recent years, taking into consideration the environmental and sociopolitical issues, biomass resources are regarded as priority resources to substitute fossil fuels in the energy and transport sectors, and thereby their utilization for energy and chemicals have attracted growing worldwide interest [6,9-11]. Among the various thermochemical conversion

technologies for biomass utilization, gasification is currently considered as a flexible and effective technology [12].

1.2 Gasification Technologies

1.2.1 Gasification process and reaction

Gasification is a thermochemical process for converting carbonaceous material, such as coal and biomass, to a combustible or synthetic gas by partial oxidation at elevated temperatures [3,13]. The gasification of solid fuel involves a series of heterogeneous and homogeneous reactions, for example, the reactions of carbon with O_2, CO_2, H_2O, or their mixtures, O_2 with H_2 and CO, and CO with H_2O. Generally the final desired components in the syngas are H_2, CO, and CH_4. Mixtures of H_2 and CO at various ratios in the syngas are necessary for many syntheses. The primary CH_4 formation is of great significance for the substitute natural gas (SNG) production [3]. The produced syngas can be used to provide electric power and heat or synthesize liquid fuels and chemicals. As fuel enters a gasifier, the following physical, chemical, and thermal processes may take place sequentially or simultaneously, depending on fuel and gasifier types and operating conditions.

1.2.1.1 Drying and pyrolysis

As the fuel is heated by the hot gases in the gasifier, moisture is the first component to evolve with increasing temperature.

$$fuel + heat = dry\ fuel + H_2O \tag{1.1}$$

As the temperature of the dry fuel continuously increases to approximately 300 – 400 °C, pyrolysis takes place and the dry fuel is converted to char and volatiles.

$$dry\ fuel + heat = volatiles + char \tag{1.2}$$
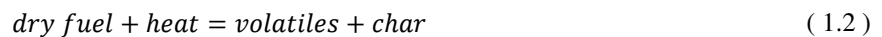
Depending on the properties of fuel and gasifier, the volatiles may include H_2, CO, CO_2, H_2O, CH_4, C_2H_6, H_2S, NH_3, some olefins, aromatics, and tar, and certain amounts of soot. Char is solid particles consisting of organic (e.g. carbon) and inorganic (e.g. ash) materials. Sometimes, due to the high heating rate in the gasifier, drying and pyrolysis take place simultaneously and complete almost instantaneously.

1.2.1.2 Oxidation and gasification

In general, some limited oxygen is injected into the gasifier as oxidant, thus the thermal energy for gasification reactions are provided by oxidizing some of the pyrolysis products. The following main reactions may take place when the pyrolysis products are burned.

$$C + 1/2\,O_2 = CO + heat\ (123.1 kJ/mol) \tag{1.3}$$

$$CO + 1/2\,O_2 = CO_2 + heat\ (282.8 kJ/mol) \tag{1.4}$$

$$H_2 + 1/2\,O_2 = H_2O + heat\ (241.1 kJ/mol) \tag{1.5}$$

$$CH_4 + 2O_2 = CO_2 + 2H_2O + heat\ (801.1 kJ/mol) \tag{1.6}$$
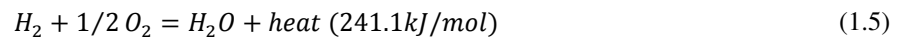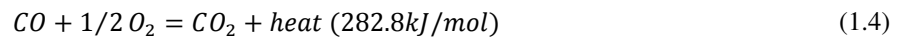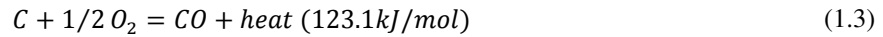
When the temperature of the remaining particles (e.g. char and soot) exceeds approximately 600 – 700 °C, they can be gasified by H_2O and CO_2. At elevated pressure, they also can be gasified by H_2. Compared with pyrolysis and oxidation, the heterogeneous gasification reactions are much slower, so they are the rate controlling step. Thus, the design and construction of gasifiers should be primarily dependent on these reactions. Besides, some homogeneous gasification reactions between the gases products also may take place. The main possible gasification reactions are shown below.

$$C + H_2O + heat\ (118.9 kJ/mol) = CO + H_2 \tag{1.7}$$

$$C + CO_2 + heat\ (159.7 kJ/mol) = 2CO_2 \tag{1.8}$$

$$C + 2H_2 = CH_4 + heat\ (87.4 kJ/mol) \tag{1.9}$$

$$CO + H_2O = CO_2 + H_2 + heat\ (40.9 kJ/mol) \tag{1.10}$$

$$CO + 3H_2 = CH_4 + H_2O + heat\ (206.3 kJ/mol) \tag{1.11}$$
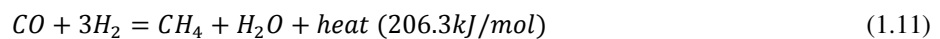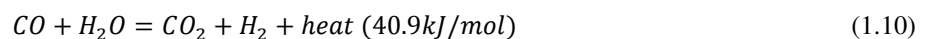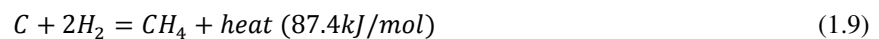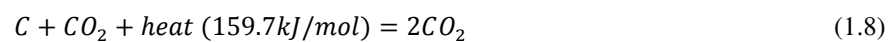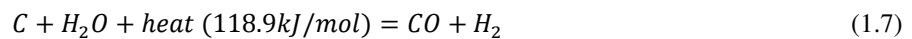
Reaction (1.10) is the water gas shift reaction, which is important because it can be used to shift the H_2/CO ratio, and reaction (1.11) is the methanation reaction, which is important if methane is the desired product. In these two exothermic reactions, low temperature is favorable. However, the reactions proceed very slowly at low temperature in the absence of catalysts. At high temperature, the reactions may follow their reverse directions. In addition, reaction (1.11) also prefers higher pressure.

1.2.2 Types of fuels

Historically the fuel mostly used for gasification is coal [14,15]. In recent years, using a renewable energy resource, biomass, as fuel in gasification, has an increased interest [1]. Comparing coal with biomass, there are some general differences that could affect their behaviors during gasification [16]. One of the principal differences is that coal is predominantly an aromatic fuel, while the aromatic component is a relatively minor constituent for most biomass. Besides, biomass has much high oxygen content, and the oxygen is present as ether, hydroxyl, carboxyl, aldehyde, and ketone functionalities [17]. Biomass usually has a higher volatile content. In the gasification process, ash properties of a fuel must be taken into consideration. The ash softening and melting temperatures are important variables for all gasifiers, since some gasifiers should operate above the ash melting temperature and some should operate below. Therefore fuels with high ash melting temperature are preferred in dry ash gasifiers, while fuels with low ash melting temperature are preferred in slagging gasifiers.

1.2.2.1 Coal

Worldwide, coal plays a significant direct role as energy resource, which accounted for approximate 28 % of world energy consumption [18]. The global proven coal reserves are estimated at 860 billion tons, and at current combustion rates the world's coal reserves will last 155 years [1,19]. All coal has been formed from biomass. Over time, this biomass has been turned into peat. As covered under a layer of overburden, the influence of time, pressure and temperature converts this material into lignite. Subsequently, lignite further turns into subbituminous coal, then into bituminous coal, and finally into anthracite. Coal is often classified in terms of its rank, which increases from lignite to anthracite. Lignite and subbituminous coals are called low-rank coals, whereas bituminous coals and anthracite are called high-rank coals.

The coal composition is very complex, and the types of coal differ considerably. The important coal properties for gasification are its rank, water content, caking properties, and ash properties [1]. The composition of selected coal in different ranks is list in Table 1.1. It can be seen in the table that comparing with high rank coals, low rank coals usually have high moisture and volatile contents but low fixed carbon content and heating value. In addition, low rank coals tend to be more reactive because of their less ordered structure and higher content of heteroatoms (particularly oxygen). Coal ash is generally very high in silicon and

aluminum, which lead to a high ash melting point. Some coal ash is also rich in calcium and iron, which can decrease the ash melting point to some extent. On the whole, the relationship between ash melting characteristics and ash composition is complicated and is dependent largely on the quaternary SiO_2-Al_2O_3-CaO-FeO system [1]. Apart from the major ash components listed in Table 1.1, the presence of many trace components does not contribute much to the ash melting characteristics but has a major effect on environment associated with coal use, for example, mercury, arsenic, zinc, lead, cadmium, chromium, chlorine, and fluorine.

1.2.2.2 Biomass

Biomass as a term covers a wide range of materials, encompassing all kinds of plants, animals, and their wastes and residues, especially utilized to produce energy and chemicals [20]. As the fourth largest energy resource in the world and the largest and most important renewable energy resource now, biomass is widely recognized to have a high potential to meet the increased world energy demand [21]. In the present review, the biomass scope is limited to plants including agricultural and forestry wastes. The benefits of biomass utilization are its widespread availability, renewable nature, and potential CO_2 neutrality [22]. In Denmark, the most abundant biomasses used for power and heat production are wood and straw [23] .

The composition of selected biomass from different origins is list in Table 1.2. The biomass fuels are divided into four primary classes: wood, straw, grass, and residues. Their properties are as diverse as the sources from which they come. However, compared with coal, biomass usually has high volatile and oxygen contents, but low carbon content and heating value. Additionally, the sulfur content in biomass is much low, mostly less than 0.5 wt %. Major components of biomass ash are calcium, potassium, and phosphorous, and further sodium, magnesium, iron, silicon, and trace elements. The main difference between biomass and coal ash is that the ash mainly consists of salts (e.g. KCl and NaCl) in the majority of biomass. Therefore, biomass ash usually has a low melting temperature.

Table 1.1 Composition of selected coal [24,25]

fuel[a]	M[b] wt % (ar)	V[b]	FC[b]	A[b]	C wt % (db)	H	O	N	S	HHV[c] MJ/kg (db)	LHV[d]	SiO$_2$	Al$_2$O$_3$	Fe$_2$O$_3$	MgO	CaO wt %[e] (db)	K$_2$O	Na$_2$O	TiO$_2$	SO$_3$
lignite																				
min value	8.3	28.0	24.4	9.2	30.2	2.7	10.5	0.5	0.2	12.3	11.7	32.0	11.3	6.8	2.0	5.2	1.2	0.3	0.6	3.2
max value	12.5	50.8	40.0	52.0	58.3	4.7	27.1	1.0	5.5	22.7	21.7	57.0	20.9	13.2	2.9	27.8	2.1	0.7	1.1	13.2
elhovo-bg	8.3	32.1	24.4	43.5	36.3	3.2	10.5	1.0	5.5	15.3	14.6	48.7	19.6	13.2	2.7	6.0	1.6	0.3	0.9	7.1
maritza East-bg	8.6	32.7	27.6	39.7	39.5	3.4	12.7	0.6	4.1	16.3	15.6	57.0	18.3	10.2	2.6	5.2	2.1	0.7	0.7	3.2
maritza west-bg	10.7	28.0	20.0	52.0	30.2	2.7	10.5	0.5	4.1	12.3	11.7	40.9	15.7	13.2	2.0	14.1	1.1	0.5	0.6	11.8
sofia-bg	12.5	40.7	31.8	27.5	45.6	4.0	19.6	0.7	2.5	18.3	17.5	32.0	11.3	10.7	2.9	27.8	1.2	0.2	0.8	13.2
usibelli-us	12.4	50.8	40.0	9.2	58.3	4.7	27.1	0.5	0.2	22.7	21.7	46.2	20.9	6.8	2.4	12.5	1.5	0.7	1.1	8.0
subbituminous coal																				
min value	2.4	22.0	24.5	6.3	36.8	2.6	8.0	0.3	0.2	14.2	13.7	38.5	16.3	1.6	1.4	2.4	0.7	0.3	0.8	0.7
max value	20.2	51.8	53.1	50.4	72.8	4.8	20.1	1.8	2.1	29.3	28.2	64.4	29.9	8.4	4.0	18.4	2.7	2.9	1.2	14.4
akabira-jp	2.7	25.3	24.5	50.3	38.0	3.0	8.0	0.5	0.2	15.2	14.6	63.0	21.2	5.6	2.1	2.4	2.3	1.4	0.8	1.3
beluga-us	18.9	51.8	33.8	14.4	60.1	4.6	19.7	1.0	0.2	24.0	23.0	48.5	29.9	6.0	1.5	9.8	0.9	0.5	0.9	1.9
black Thunder-us	20.2	45.6	48.1	6.3	68.0	4.7	20.1	0.7	0.4	26.9	25.9	38.5	16.3	5.7	4.0	18.4	0.7	0.8	1.2	14.4
bobov Dol-bg	6.3	31.7	37.1	31.2	50.9	4.2	9.8	1.8	2.1	21.4	20.5	59.8	22.1	8.4	2.2	2.0	2.7	0.3	1.0	1.6
colowyo-us	9.1	41.1	53.1	5.7	72.8	4.8	14.8	1.5	0.4	29.3	28.2	46.9	24.6	8.0	1.8	8.9	1.0	2.9	1.0	4.9
horonai-jp	2.6	34.5	32.5	33.0	51.4	4.0	10.6	0.3	0.7	21.1	20.3	64.4	23.0	3.2	1.4	3.3	2.1	0.7	1.1	0.7
montana-us	8.4	40.7	46.4	12.9	61.5	4.3	20.0	0.6	0.8	24.2	23.2	44.5	20.3	1.6	3.5	15.7	1.1	1.3	0.8	11.1
pernik-bg	6.0	22.0	27.6	50.4	36.8	2.6	8.0	1.4	0.7	14.2	13.7	63.9	21.9	6.0	1.5	1.5	2.4	0.3	1.1	1.4
sunagawa-jp	2.4	32.8	37.1	30.1	54.7	4.4	9.2	0.9	0.6	22.9	22.0	60.7	23.4	5.0	2.0	2.7	2.3	1.4	0.9	1.6
taiheiyo-jp	5.3	42.4	34.3	23.2	56.7	4.8	14.4	0.7	0.2	23.6	22.6	57.8	26.1	3.5	1.4	5.9	1.3	1.2	1.2	1.8
bituminous coal																				
min value	0.4	12.4	36.1	8.2	52.9	2.5	2.8	0.6	0.3	21.3	20.6	44.1	18.5	2.6	0.3	0.4	0.3	0.1	0.6	0.4
max value	7.8	43.1	68.1	38.3	76.7	5.6	13.2	2.0	2.9	31.4	30.8	68.4	35.2	16.4	3.2	22.2	3.8	2.2	1.6	5.5
ashibetsu-jp	2.1	31.8	36.1	32.2	54.8	4.1	8.0	0.7	0.3	22.7	21.8	62.4	19.8	4.8	2.0	4.7	1.6	2.2	0.8	1.6
asturias-es	1.7	17.7	52.5	29.8	61.0	2.5	4.8	0.9	1.0	23.2	22.6	52.7	26.0	7.2	2.8	3.8	3.8	1.0	1.0	1.8
balkan-bg	0.4	14.8	47.0	38.3	52.9	2.9	2.8	0.6	2.5	21.3	20.6	57.8	22.9	7.3	1.4	2.7	4.2	0.3	0.8	2.7
coal Mountain-ca	1.2	26.5	56.2	17.3	70.3	4.0	7.1	1.0	0.3	28.1	27.3	39.9	27.3	2.6	3.2	22.2	0.6	0.7	1.5	2.0
coal Valley-ca	3.3	32.5	57.3	10.2	73.2	4.3	9.3	1.9	1.0	29.3	28.4	59.4	20.0	4.8	1.2	9.2	0.6	0.6	0.8	3.4
datong-cn	2.6	28.5	58.2	13.2	71.4	4.0	10.0	0.7	0.7	28.3	27.4	63.3	19.7	9.6	0.5	2.1	1.6	0.2	0.9	2.0
donbass-ua	1.8	17.3	68.1	14.6	74.0	3.7	3.8	1.3	2.7	29.7	28.9	53.8	20.4	15.1	1.3	2.8	3.1	0.7	0.9	2.1
ebenezer-au	3.4	39.9	47.4	12.7	69.7	5.2	10.9	1.0	0.4	29.1	28.0	62.8	22.7	5.8	1.1	3.2	0.9	0.8	1.4	1.3
entham-au	7.8	30.6	58.5	11.0	76.2	4.3	6.9	1.2	0.4	30.7	29.7	51.7	29.2	10.7	1.4	3.7	0.3	0.3	1.2	1.5
ermelo-za	6.6	36.2	53.1	10.7	70.4	4.5	13.2	1.0	0.3	28.2	27.2	44.1	31.8	6.7	2.9	8.7	0.8	0.4	1.3	3.2

fuel[a]	M[b] wt % (ar)	V[b]	FC[b]	A[b]	C wt % (db)	H	O	N	S	HHV[c] MJ/kg (db)	LHV[d]	SiO$_2$	Al$_2$O$_3$	Fe$_2$O$_3$	MgO	CaO wt %[e] (db)	K$_2$O	Na$_2$O	TiO$_2$	SO$_3$
fording River-ca	3.3	30.4	59.3	10.3	74.8	4.5	9.1	0.9	0.4	30.2	29.3	62.4	24.1	4.7	1.0	3.1	2.0	0.2	1.4	1.3
illinois-us	3.8	40.6	47.7	11.6	69.1	5.1	10.6	0.6	2.9	29.2	28.1	49.7	19.1	16.4	1.1	5.6	2.0	1.1	0.9	4.1
lithgow-au	1.8	29.2	49.5	21.3	66.0	3.8	7.2	1.1	0.6	26.4	25.5	68.3	25.6	0.8	0.3	0.4	2.8	0.1	1.3	0.4
moura-au	1.2	31.9	57.8	10.3	76.7	4.7	6.6	1.3	0.4	31.4	30.4	54.6	24.0	6.1	2.1	5.5	1.9	1.3	1.3	3.3
natal-za	1.9	12.4	71.8	15.8	69.3	4.5	8.1	1.7	0.7	28.3	27.4	50.5	30.8	6.0	1.8	4.3	1.7	1.3	1.6	2.1
newlands-au	1.7	27.9	57.1	15.1	71.4	4.1	8.1	0.9	0.4	28.6	27.7	52.2	35.2	6.6	0.6	2.2	0.5	0.1	1.6	0.9
plateau-us	6.0	42.4	47.8	9.8	71.9	5.1	10.9	1.4	0.8	29.8	28.7	65.0	19.1	3.7	1.3	4.8	1.1	0.8	1.0	3.2
takashima-jp	1.7	43.1	48.6	8.2	75.4	5.6	8.8	1.1	0.8	32.0	30.8	46.6	27.3	7.1	2.0	7.4	1.0	1.6	1.5	5.5
wallarah-au	1.3	30.2	55.8	14.0	72.3	4.2	8.3	0.9	0.3	29.0	28.1	57.9	29.6	5.2	1.1	2.5	0.9	0.5	1.3	1.0
wambo-au	3.5	35.4	52.3	12.2	71.9	4.7	9.7	1.3	0.3	29.3	28.3	68.4	18.5	4.1	1.7	3.2	0.9	1.1	0.6	1.5
witbank-za	2.5	34.5	53.1	12.4	75.8	3.6	4.9	2.0	1.3	29.8	29.1	55.1	22.1	7.9	3.0	5.1	2.2	1.2	0.8	2.6
anthracite																				
min value	1.9	4.6	86.3	5.5	85.5	2.6	0.7	1.2	0.5	32.3	31.7	48.3	28.2	4.6	1.6	2.3	1.4	0.8	1.8	1.0
max value	3.6	8.3	86.9	8.5	87.3	2.6	1.6	3.5	0.5	32.8	32.2	56.9	30.6	6.9	1.8	5.1	1.7	1.8	2.0	3.3
mt. Klappan-ca	1.9	8.2	86.3	5.5	87.3	2.6	0.7	3.5	0.5	32.8	32.2	56.9	28.2	4.6	1.8	2.3	1.4	1.8	2.0	1.0
pencilvania-us	3.6	4.6	86.9	8.5	85.5	2.6	1.6	1.2	0.5	32.3	31.7	48.3	30.6	6.9	1.6	5.1	1.7	0.8	1.8	3.3

a: us - United States, ca - Canada, au - Australia, es - Spain, ua - Ukraine, bg - Bulgaria, cn - China, jp - Janpan, za - South Africa

b: M - moisture, VM - volatile matter, FC - fixed carbon, A - ash

c: $HHV_{dry} = 0.342 \times C_{dry} + 1.322 \times H_{dry} - 0.120 \times O_{dry} - 0.120 \times N_{dry} + 0.123 \times S_{dry} - 0.015 \times Ash_{dry}$ [26]

d: $LHV_{dry} = HHV_{dry} - 2.326 \times 9.270 \times H_{dry} / 100$ [27]

e: Normalized to 100 %

Table 1.2 Composition of selected biomass [28-41]

fuel	M^a wt % (ar)	V^a	FC^a	A^a	C wt % (db)	H	O	N	S	HHV MJ/kg (db)	LHV	SiO_2	CaO	K_2O	P_2O_5	Al_2O_3	MgO wt %^{b} (db)	Fe_2O_3	SO_3	Na_2O	TiO_2
wood																					
min value	2.4	72.4	12.3	0.1	47.4	5.3	38.0	0.03	0.01	18.5	17.3	0.1	7.9	4.5	0.2	0.1	2.4	0.2	1.2	0.3	0.00
max value	15.3	86.2	25.3	6.0	52.5	6.4	44.8	0.70	0.08	21.0	19.7	68.3	65.2	36.1	14.7	7.9	20.5	5.5	5.3	3.7	0.55
beech sawdust	7.4	84.2	14.9	0.9	49.5	6.1	43.4	0.13	0.01	19.6	18.3	21.8	43.0	18.5	1.8	1.1	7.8	1.0	4.4	0.4	0.16
beech wood	14.2	75.2	24.2	0.6	48.1	6.4	44.8	0.08	0.01	19.5^c	18.1^d	2.7	36.8	35.5	4.8	0.3	12.4	2.7	2.0	2.8	0.05
birch wood	11.1	78.7	20.9	0.4	48.7	6.4	44.5	0.08	0.01	19.7^c	18.3^d	0.1	44.9	36.1	8.3	0.1	8.6	0.3	1.7	0.1	0.01
eucalyptus bark	12.0	78.1	17.1	4.8	47.4	5.5	42.0	0.30	0.05	18.5	17.3	10.0	57.7	9.3	2.4	3.1	10.9	1.1	3.5	1.9	0.12
hybrid poplar	6.9	84.8	12.5	2.7	50.2	6.1	40.4	0.60	0.02	19.0	17.7^d	6.6	55.5	10.7	1.5	0.9	20.5	1.6	2.3	0.1	0.33
red oak sawdust	11.5	86.2	13.5	0.3	50.0	5.9	43.8	0.03	0.01	19.5	18.2^d	29.9	15.6	32.0	1.9	4.3	5.9	4.2	3.8	2.0	0.39
olive wood	3.7	79.6	18.9	1.5	48.2	5.3	44.3	0.70	0.03	19.1	17.9^d	10.4	41.5	25.2	10.8	2.0	3.0	0.9	2.7	3.7	0.00
pine bark	4.7	73.0	25.3	1.7	52.5	5.7	39.7	0.40	0.03	21.0	19.7	1.9	60.6	11.3	7.2	7.9	6.7	0.5	3.0	0.8	0.18
pine sawdust	15.3	83.1	16.8	0.1	51.0	6.0	42.8	0.08	0.02	20.3^d	19.0	9.7	48.9	14.4	6.1	2.3	13.8	2.1	2.2	0.4	0.14
pine wood	7.6	72.4	21.6	6.0	49.7	5.7	38.0	0.51	0.08	19.8	18.6	68.3	7.9	4.5	1.6	7.0	2.4	5.5	1.2	1.2	0.55
poplar wood	6.7	86.1	12.3	1.6	50.8	5.9	41.1	0.59	0.02	18.9	17.6^d	1.27	59.2	26.8	0.2	0.4	5.8	0.8	5.3	0.3	0.21
spruce bark	5.3	75.2	22.5	2.3	49.9	5.9	41.5	0.40	0.03	19.8	18.5	2.5	65.2	12.7	6.8	1.8	8.5	0.2	1.7	0.7	0.00
willow wood	2.4	79.9	18.9	1.2	49.7	6.1	42.6	0.40	0.03	19.8	18.4	0.5	39.4	33.9	14.7	0.4	6.5	0.3	3.8	0.4	0.00
straw																					
min value	7.4	65.5	13.6	4.7	38.2	5.2	35.8	0.46	0.07	17.7	16.4	7.9	3.1	12.6	1.5	0.1	1.8	0.2	1.2	0.2	0.02
max value	16.8	80.5	19.4	10.8	47.6	6.1	42.4	2.68	0.25	18.9	17.7	66.8	30.7	38.1	10.4	5.6	14.1	2.8	4.9	2.0	0.33
alfalfa straw	9.3	78.9	15.8	5.3	47.2	6.0	38.6	2.68	0.20	18.7	17.4^d	7.9	24.9	38.1	10.4	0.1	14.1	0.4	2.6	1.5	0.02
barley straw	11.5	76.1	18.0	5.9	46.2	5.7	41.5	0.60	0.08	18.7	17.4	66.8	4.9	20.8	2.7	0.2	2.4	0.2	1.5	0.5	0.02
corn straw	7.4	73.2	19.1	7.7	44.7	5.9	41.0	0.60	0.07	17.7	16.4	50.0	14.7	18.5	2.4	5.1	4.5	2.5	1.8	0.2	0.29
mint straw	16.8	69.8	19.4	10.8	45.2	5.5	35.8	2.47	0.25	17.7	16.5^d	23.5	17.6	32.0	5.8	5.6	6.9	2.8	3.5	2.0	0.33
oat straw	8.2	80.5	13.6	5.9	47.6	5.8	40.1	0.50	0.08	19.0	17.7	37.8	12.0	26.8	6.1	4.7	4.5	2.2	4.9	0.7	0.24
rape straw	8.7	76.5	17.8	4.7	46.2	6.1	42.4	0.46	0.10	18.3	17.0	40.8	30.7	13.5	2.2	5.5	2.0	2.0	2.7	0.4	0.29
rice straw	7.9	65.5	15.8	18.7	38.2	5.2	36.9	0.87	0.18	18.9	17.8^d	76.7	3.1	12.6	1.5	1.1	1.8	0.9	1.3	1.0	0.09
wheat straw	10.3	77.7	17.6	4.7	47.3	5.9	41.4	0.60	0.07	18.9	17.7	65.7	8.0	18.5	2.5	0.9	2.0	0.6	1.2	0.6	0.04
grass																					
min value	4.5	73.4	14.3	3.3	45.0	5.4	37.5	0.32	0.04	17.5	16.3	9.5	3.3	2.9	3.1	0.6	1.4	0.5	0.5	0.1	0.02
max value	11.3	81.7	18.2	9.9	47.9	6.0	42.9	1.00	0.55	19.0	17.7	84.9	44.3	49.1	5.9	4.6	8.6	2.1	8.2	1.9	0.25
bana grass	4.5	73.4	16.7	9.9	45.1	5.4	38.7	0.84	0.11	17.5	16.3^d	38.6	4.1	49.1	3.1	0.9	2.0	0.7	1.0	0.4	0.08
kenaf grass	7.5	79.4	17.0	3.6	46.6	5.8	42.9	1.00	0.14	18.6	17.3	9.5	44.3	19.1	3.9	2.6	8.6	1.7	8.2	1.9	0.12
miscanthus grass	5.7	78.5	18.2	3.3	47.9	6.0	41.7	0.60	0.55	19.0	17.7	47.8	8.5	28.3	5.9	0.6	5.4	0.5	2.4	0.8	0.03
reed canary grass	7.7	73.5	17.7	8.9	45.0	5.7	38.9	1.40	0.14	18.4	17.1	84.9	3.3	2.9	3.9	1.3	1.4	1.0	1.0	0.1	0.05

fuel	M^a wt % (ar)	V^a	FC^a	A^a	C wt % (db)	H	O	N	S	HHV MJ/kg (db)	LHV	SiO_2	CaO	K_2O	P_2O_5	Al_2O_3 wt %^{b} (db)	MgO	Fe_2O_3	SO_3	Na_2O	TiO_2
sorghum grass	11.3	81.7	18.1	4.2	47.3	6.0	42.1	0.32	0.04	18.7	17.4^d	73.2	7.0	9.0	4.4	1.8	2.2	1.0	1.1	0.3	0.02
sweet sorghum	7.0	77.2	18.1	4.7	47.3	5.8	41.7	0.40	0.09	18.9	17.7	66.9	10.4	9.5	3.5	0.8	3.1	0.6	3.5	1.7	0.06
switchgrass	9.8	76.7	14.3	9.0	46.7	5.8	37.5	0.77	0.19	18.1	16.8^d	66.7	5.7	11.9	4.6	4.6	3.1	2.1	0.5	0.6	0.25
residues																					
max value	3.7	59.3	12.0	1.4	36.1	4.3	34.6	0.00	0.00	14.4	13.4	2.0	2.4	3.7	1.5	0.8	0.1	0.1	0.1	0.1	0.01
min value	11.4	85.6	37.9	20.3	53.5	8.8	47.3	2.72	0.49	22.5	20.7	90.8	44.1	58.6	31.1	14.6	13.5	36.3	14.7	27.6	2.02
almond shell	6.9	76.0	20.7	3.3	49.3	6.0	40.6	0.76	0.04	19.5	18.2^d	10.5	12.6	58.6	5.4	3.3	3.8	2.8	1.1	1.9	0.11
coconut shell	4.4	73.7	23.0	3.2	49.5	5.4	41.7	0.00	0.10	19.0^c	17.8^d	66.8	2.4	8.5	1.5	8.5	1.5	6.2	0.1	4.6	0.01
coffee husk	11.4	72.9	22.5	4.6	41.9	4.6	47.3	1.53	0.10	14.4^c	13.4^d	17.5	13.9	49.4	4.8	5.1	5.2	2.9	0.5	0.5	0.26
corn cob	3.7	80.7	16.4	2.9	46.3	4.6	45.9	0.29	0.01	16.3^c	15.3^d	29.8	3.2	50.7	5.3	1.8	3.5	2.4	2.4	0.9	0.09
cotton husk	6.9	78.4	18.2	3.4	48.7	8.1	38.4	1.35	0.00	22.5^c	20.7^d	10.9	21.0	50.2	4.1	1.3	7.6	1.9	1.7	1.3	0.01
grape marc	7.8	65.8	26.4	7.8	49.7	5.6	34.6	2.20	0.14	20.7^d	19.5	9.5	28.5	36.8	8.8	2.6	4.8	1.8	6.3	0.7	0.18
groundnut shell	7.9	73.9	22.7	3.4	49.2	7.2	39.0	1.16	0.02	21.5^c	19.9^d	27.7	24.8	8.5	3.7	8.3	5.4	10.3	10.4	0.8	0.10
hazelnut shell	7.2	70.3	28.3	1.4	51.6	6.2	39.2	1.60	0.04	20.2	18.8^d	29.2	16.5	32.5	3.4	3.3	8.4	4.1	1.2	1.4	0.11
mustard husk	5.6	72.7	23.2	4.1	44.2	8.8	42.3	0.38	0.19	21.6^c	19.6^d	17.4	44.1	7.6	2.1	1.6	9.5	0.8	14.7	2.1	0.10
olive husk	6.8	63.9	32.8	3.3	52.8	6.7	36.7	0.50	0.05	20.9	19.4^b	30.4	15.0	4.5	2.6	8.7	4.3	6.5	0.6	27.1	0.31
olive kernel	4.8	72.0	23.7	4.3	49.7	6.1	38.2	1.60	0.08	21.2	19.9^d	12.4	25.4	28.5	17.0	3.1	3.5	2.0	4.0	3.9	0.23
olive pits	6.1	82.0	16.3	1.7	52.8	6.7	38.3	0.45	0.05	21.6	20.1^d	30.6	14.6	4.4	2.4	8.8	4.2	6.5	0.6	27.6	0.34
palm kernels	11.0	77.3	17.6	5.1	48.3	6.2	37.5	2.62	0.26	20.7	19.4	18.3	9.3	16.5	31.1	6.2	6.6	9.2	2.5	0.1	0.12
pPepper plant	6.5	64.7	20.9	14.4	36.1	4.3	42.0	2.72	0.49	15.4	14.5	12.6	32.2	24.6	5.2	4.9	7.4	2.0	9.7	0.9	0.50
pistachio shell	7.5	81.6	17.0	1.4	50.2	6.3	41.2	0.69	0.22	18.2	16.8^d	8.4	10.3	18.7	12.1	2.2	3.3	36.3	3.9	4.6	0.21
rice husk	10.9	63.5	16.2	20.3	38.8	4.8	35.5	0.52	0.05	15.8	14.8^d	90.8	3.2	3.7	0.4	0.8	0.1	0.1	0.7	0.2	0.02
soya husk	6.3	74.3	20.3	5.4	42.9	6.3	44.3	0.85	0.09	17.5^c	16.1^d	2.0	25.3	36.0	5.8	8.7	8.4	3.0	4.4	6.3	0.24
sugar cane bagasse	10.4	85.6	12.0	2.4	48.6	5.9	42.9	0.16	0.04	19.0	17.7^d	46.8	4.9	7.0	3.9	14.6	4.6	11.1	3.5	1.6	2.02
sunflower husk	9.1	76.0	21.9	2.1	50.3	4.9	42.1	0.59	0.00	18.5^c	17.4^d	17.9	14.7	21.2	9.5	14.6	8.6	6.4	6.8	0.1	0.20
walnut shell	6.8	59.3	37.9	2.8	53.5	6.6	35.5	1.50	0.10	22.5^c	21.1^d	23.3	16.7	33.0	6.2	2.4	13.5	1.5	2.2	1.0	0.10

a: M - moisture, VM - volatile matter, FC - fixed carbon, A - ash

b: Normalized to 100 %

c: $HHV_{dry} = 0.341 \times C_{dry} + 1.322 \times H_{dry} - 0.120 \times O_{dry} - 0.120 \times N_{dry} + 0.069 \times S_{dry} - 0.015 \times Ash_{dry}$ [42]

d: $LHV_{dry} = HHV_{dry} - 2.442 \times 8.936 \times H_{dry} / 100$ [42]

1.2.3 Types of gasifiers

All the types of gasifiers used today can be divided into three categories [1,43]: moving bed, fluidized bed, and entrained flow gasifiers. Figure 1.3 shows the schematic representation of the three types of gasifiers [44]. Their characteristics are summarized in Table 1.3.
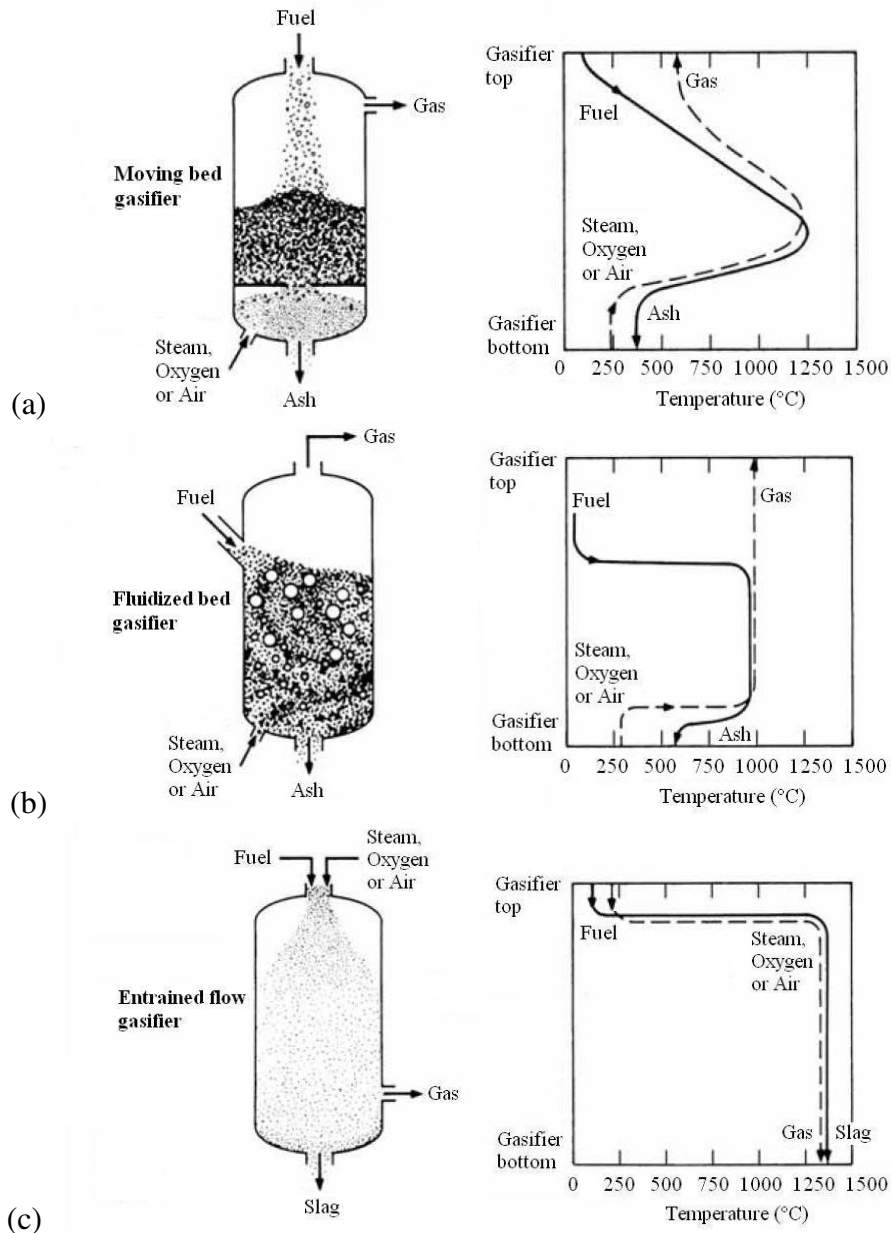

Figure 1.3 Three types of gasifiers [44]

Table 1.3 Characteristics of different gasification process [1,3,15,43,45-47]

gasifer type	moving bed		fluidized bed		entrained flow	
classification						
fuel feeding	dry	dry	dry	dry	dry	slurry
ash condition	dry ash	slagging	dry ash	agglomerating	slagging	slagging
typical process	Lurgi	BGL	Winkler, HTW, HRL, CFB, KBR,	KRW, U-Gas	KT, Shell, Siemens, MHI, EAGLE, PWR	GEE, E-Gas, ICCT OMB
fuel characteristics						
preferred fuel	lignite, reactive bituminous coal, anthracite, wastes	bituminous coal, anthracite, coke, wastes	lignite, reactive bituminous coal, anthracite, wastes	lignite, bituminous coal, anthracite, coke, biomass, wastes	lignite, reactive bituminous coal, anthracite, cokes	lignite, reactive bituminous coal, anthracite, cokes
fuel size limits	5 - 80 mm	5 - 80 mm	< 6 mm	< 6 mm	< 0.1 mm	< 0.1 mm
acceptability of fines	limited	better than dry ash	good	better	unlimited	unlimited
acceptability of caking	yes (with stirrer)	yes	possibly	possibly	yes	yes
ash content limits	unlimited	<25% preferred	unlimited	unlimited	<25% preferred	<25% preferred
preferred ash melting temperature	> 1200 °C	< 1300 °C	> 1100 °C	> 1100 °C	< 1300 °C	< 1300 °C
operating characteristics						
operating temperature	~ 1000 °C	> 1000 °C	800 - 1100 °C	800 - 1100 °C	> 1200 °C	> 1200 °C
operating pressure	> 20 bar	> 20 bar	1 - 35 bar	1 - 35 bar	1 - 85 bar	1 - 85 bar
oxidant demand	low	low	moderate	moderate	high	high
steam demand	high	low	moderate	moderate	low	low
product gas temperature	400 – 650 °C	400 – 650 °C	900 – 1050 °C	900 – 1050 °C	1250 – 1600 °C	1250 – 1600 °C
product gas purity	low: by-products are tar, dust, oils and phenols	low: by-products are tar, dust, oils and phenols	moderate-high: some tar and particulates can be carried in the product gas depending on the temperature and gas velocity	moderate-high: some tar and particulates can be carried in the product gas depending on the temperature and gas velocity	high: almost tar free gas but with soot	high: almost tar free gas but with soot
unit capacity	10 - 350 MW	10 - 350 MW	100 – 700 MW	20 – 150 MW	up to 700 MW	up to 700 MW
key distinguishing characteristics	tar in product gas		large char recycle		large amount of sensible heat in product gas	
key technical issue	fines and tar utilization		carbon conversion		raw gas cooling	

1.2.3.1 Moving bed gasifiers

Historically, the moving bed gasifier is the oldest gasifier. In a moving bed gasifier, shown in Figure 1.3 (a), fuel particles enter at the top and move slowly downward through several process zones in the reactor vessel while reacting with gases generally from the opposite direction going upward [43]. In the first zone (drying zone), the introduced fuel particles are heated and dried, while they can cool the product gas before it leaves the gasifier. In the second zone (pyrolysis zone), as the fuel particles descend, they are further heated and pyrolyzed owing to the gas with higher temperature. In the third zone (gasification zone), the produced char particles from pyrolysis are gasified by steam and carbon dioxide. In the fourth zone (combustion zone), near the bottom of the vessel, the remaining char particles react with oxygen in the highest temperature area. According to different ash conditions, moving bed gasifiers operate in two different modes. In the dry-ash mode of operation (e.g., Lurgi dry ash gasifier), sufficient steam is injected to the bottom of the gasifiers to keep the temperature lower than the ash melting temperature, so the ash below the combustion zone is cooled and still in the form of dry ash [3]. In the slagging mode of operation (e.g., British Gas/Lurgi slagging gasifier), much less steam is used, and therefore in the combustion zone a much higher temperature is achieved causing the ash melting and forming slag [45]. In addition, according to the way that fuel particles and gases are introduced into the reactor vessel, moving bed gasifiers can also be classified into downdraft, updraft, and cross draft [3]. Moving bed gasifiers commonly use large fuel particles to ensure good bed permeability and efficient heat and mass transfer, and to avoid excess pressure drop. Hence, they need less complex fuel preparation but have limited ability to handle fine particles [1,48]. Their oxygen consumption is low, but a large amount of byproducts from pyrolysis, such as tar, is present in the product gas, which requires more comprehensive gas cleaning [1,43]. Anthracite or coke is preferred in the moving bed gasification due to the low tar formation. The outlet temperature of the product gas is low, thus there is no need for expensive heat recovery equipment.

1.2.3.2 Fluidized bed gasifiers

The history and development of coal gasification and fluidized bed technology have been intimately linked. In a fluidized bed gasifier, shown in Figure 1.3 (b), fuel particles enter at the side of the reactor vessel, and are fluidized by steam and oxidant injected near the bottom with enough velocity. Larger particles are consumed slowly and recycle internally in the

reactor vessel until they are small enough for external recycling. Smaller particles are converted in one pass, or are entrained by the product gas when it leaves the top of the vessel. The product gas passes through a cyclone to separate the small particles that could return to the reactor vessel via the external recycling. Ash is removed at the bottom of the reactor vessel. To sustain fluidization, small fuel particles are normally used. However, too fine particles are not employed, because they leave the reactor vessel together with the product gas and are only partially captured in a cyclone and returned to the vessel, which obviously lower the carbon conversion [1]. Depending on the degree of fluidization, three types of fluidized bed gasifiers are named as bubbling fluidized bed gasifiers (2 – 3 m/s gas velocity), circulating fluidized bed gasifiers (5 – 10 m/s gas velocity), and transport gasifiers (11 – 18 m/s gas velocity) [1,45], which are compared in Figure 1.4. Fluidized bed gasifiers offer extremely good mixing between fuel and gas due to the high levels of back-mixing, which promotes both heat and mass transfer. Thereby a uniform temperature can be obtained in the reactor vessel, which is always below the ash melting temperature, typically in the range of 950 – 1100 °C for coal and 800 – 950 °C for biomass, to avoid clinker formation and bed defluidization [1,46,48]. Fluidized bed gasifiers can operate in dry ash mode (e.g., High-Temperature Winkler gasifier) or in agglomerating mode (Kellogg-Rust Westinghouse agglomerating gasifier) [1,3]. The dry ash gasifiers operate at relatively low temperatures that are below the ash softening point, which are suited to gasifying reactive fuels, such as low rank coals and biomass. The agglomerating gasifiers operate at slightly higher temperatures, which are suitable to gasifying high rank coals. In the agglomerating gasifiers, some small ash particles soften sufficiently to stick together to form larger and denser agglomerates, which eventually become large enough to defluidize and sink down through the reactor vessel to a suitable extractor. Fluidized bed gasifiers offer load flexibility [46]. Compared with moving bed gasifiers, fluidized bed gasifiers have higher fuel throughput but their high gas velocity may cause equipment erosion [45]. In the product gas, a certain amount of tar is present due to the moderately high temperatures. However, the bed material, sand, makes it possible to use in-bed tar catalytic process. Besides, the product gas is rich in particulates. When biomass is used as fuel, there is a risk for bed agglomeration due to its ash composition being rich in alkali metals. To overcome the agglomeration problem, three methods are usually employed: decreasing gasification temperature, exchanging bed material with proper intervals, and using some proven mineral binding additives [45].
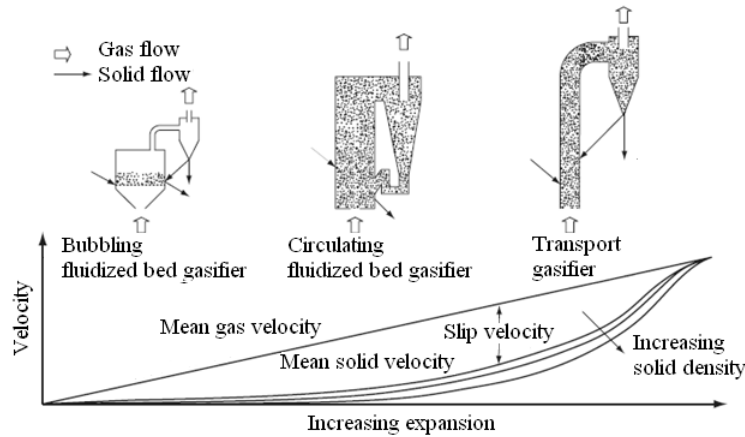
Figure 1.4 Sketches of different types of fluidized bed gasifiers [49]

1.2.3.3 Entrained flow gasifiers

The entrained flow slagging gasifiers have been developed after 1950 and have been selected for the majority of commercial-sized IGCC application. In an entrained flow gasifier, shown in Figure 1.3 (c), fuel and gases are introduced at the top of the reactor vessel, and fuel is entrained by the gases in the vessel. The gasification reactions take place at very high reaction rate because of the high operating temperature (1200 – 1600 °C) and pressure (2 – 8 MPa), and after a few seconds (0.5 – 4.0 s) the product gas leaves the reactor vessel at the bottom together with the molten slag [1,46]. Then, the product gas can be cooled by two main methods: quenching the gas with water or using a high temperature radiant cooler, while the molten slag falls to a quench chamber for solidifying and leaves it via a lock hopper [46]. Fine fuel particles, such as sizes of about 100 μm for coal, which are employed to promote mass transfer and allow transport in the gas, can be fed in either a dry form (e.g., Shell gasifier) or slurry form (e.g., GE Energy gasifier) [1]. Entrained flow gasifiers have the ability to gasify practically any fuels, but fuel with lower moisture and ash content are favored to reduce oxygen consumption [1,3]. Due to the short residence time, high temperatures are required to ensure a good carbon conversion, and therefore entrained flow gasifiers have a high oxygen demand and operate in a slagging mode. Sometimes, it may be necessary to add fluxes to achieve good slagging characteristics. Compared with moving bed gasifiers and fluidized bed gasifiers, entrained flow gasifiers operating at very high temperatures, can produce a clean, almost tar-free, product gas and in short residence time can achieve a high load throughput [1]. However, the high operating temperature could shorten the lifetime of system components. Using biomass powder as fuel during entrained flow gasification may give an extra cost due to its low bulk density, which might be reduced by an initial torrefaction process [45].

1.2.4 Gasification application

The composition of the syngas produced from solid fuel gasification can be varied by changing some factors, such as gasifier types, fuel types, and operating conditions (e.g. temperature, pressure. oxidizer, and gasifying agent). Based on the different composition, the syngas is applied in many different ways. Figure 1.5 shows the main applications of the syngas with different composition. All these applications can be divided into two main aspects: synthesis that is applied to produce fuels and chemicals, and combustion that is applied to produce power and heat. In general, the required quality of syngas is more critical for synthesis than for combustion, because purifying syngas can substantially increase the cost of downstream equipment used for fuels and chemicals synthesis [50].
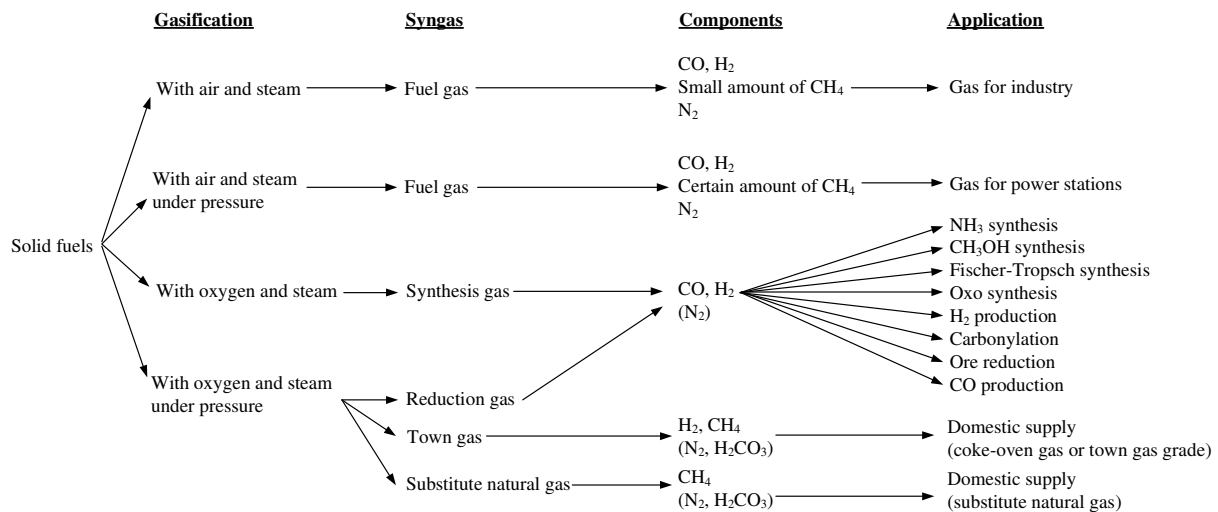
Figure 1.5 Applications of syngas with different composition [51]

1.3 Entrained flow gasification of biomass

The effects of operating conditions on both pyrolysis and gasification were investigated in the following sections due to the close relationship between the initial pyrolysis and further gasification steps during gasification, which could provide a clear understanding of the whole gasification process

1.3.1 Effects of operating condition on pyrolysis

In this section, the effects of temperature, particle size, reactor length, and steam addition on the pyrolysis products, char, tar, soot, H_2O, and gas including H_2, CO, CO_2, and C_xH_y (light hydrocarbons including C_1 and C_2 species) are discussed.

1.3.1.1 Effect of temperature on pyrolysis

The effect of temperature on the char yield during pyrolysis is shown in Figure 1.6. The char yield decreased quickly with increasing temperature from 600 to 900 °C, and then decreased slowly with further increasing temperature to 1400 °C. This indicates that the primary pyrolysis of biomass is almost completed at around 900 °C and the gradually decreased char yield after 900 °C is related to the enhanced reactions of char with CO_2 and H_2O at higher temperature in an entrained flow reactor where the gas stays around the particles. The char yield from rice husk was much higher than that from other selected biomass due to the very high ash content in the rice husk. Owing to the same reason, a little higher char yields from straw and olive waste were observed. The char yield from biomass with a low ash content (< 1 wt %) was generally less than 0.05 kg/kg used biomass when the pyrolysis temperature was higher than 1000 °C.
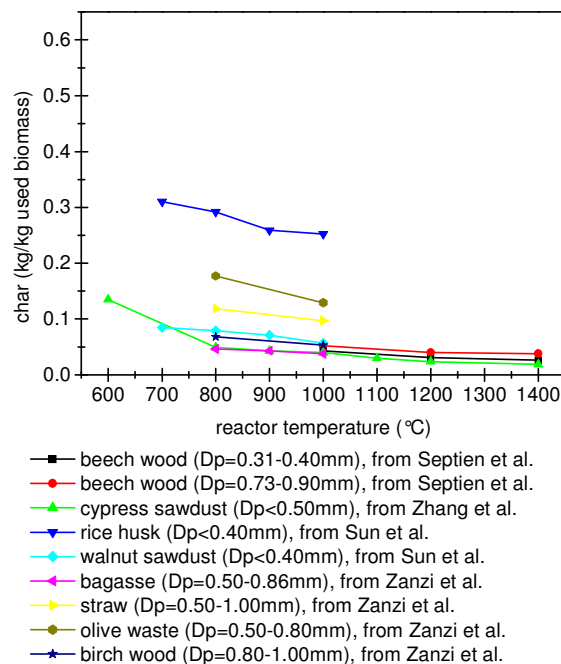

Figure 1.6 Effect of temperature on the char yield during biomass pyrolysis [52-57]

The effect of temperature on the H_2O/tar/soot yield during pyrolysis is shown in Figure 1.7. In the temperature range of 600 – 1400 °C, the total yields of H_2O, tar, and soot decreased steadily, especially from 600 to 900 °C. Figure 1.7 (b) shows the H_2O yield at different pyrolysis temperatures. The H_2O not only came from the moisture in the biomass but also formed by dehydration during pyrolysis [58]. The yield of H_2O decreased with increasing temperature, which might be related to the steam gasification and reforming reactions and water gas shift reaction during pyrolysis. Figure 1.7 (c) and (d) show the tar and soot yields

respectively. The tar yield decreased with increasing temperature from 600 to 1100 °C and disappeared at 1200 °C due to its cracking and reforming reactions and soot formation. It has been reported that the tar produced at elevated temperature is mainly composed by volatile compounds and benzene is the most abundant species in them [54]. Soot was not observed until the temperature was higher than 800 °C. Its yield increased as the temperature further increased to 1100 °C. These observations reveal that there is a tradeoff between tar and soot formation, which may be due to soot formation by tar and hydrocarbon polymerization. When the temperature was higher than 1100 °C, the soot yield stopped increasing or started declining probably because all tar was consumed and due to soot gasification reactions.

Figure 1.8 shows the effect of temperature on the total yields of gas products (as a sum of H_2, CO, CO_2, and light hydrocarbons, C_xH_y, up C_3 species) during pyrolysis. The total yields of gas products increased as the temperature increased from 600 to 1400 °C due to the breaking of long-chain macromolecules and the cracking of aromatic rings [59-61]. Particularly, the total yields of gas products increased sharply in the temperature range of 600 – 900 °C, which was probably related to the primary pyrolysis. The effect of temperature on the individual gas yields on volume basis is shown in Figure 1.9. The H_2 and CO yields increased obviously with increasing temperature from 600 to 1400 °C, while the yield of CO_2 was almost unchanged and stayed at a low value (around 0.1 Nm^3/kg used biomass). This is because H_2 mainly comes from the direct dehydrogenation of char and the rearranging and condensing of aromatic clusters in primary pyrolysis [55,62-64] and from tar cracking and soot formation in secondary pyrolysis [65,66], both of which prefer higher temperatures. CO is mainly evolved by the dehydrogenation of hydroxyl groups in primary pyrolysis [55,61,67-70] and by tar cracking in secondary pyrolysis [65,71,72], both of which prefer higher temperatures as well. Formation of CO_2 is mainly caused by cross linking reactions in the evolving char and direct decomposition of carboxyl groups in primary pyrolysis, which are rather easily broken even at relatively low temperatures [55,61,67-70], and almost no CO_2 is generated and converted in secondary pyrolysis [65,71,72]. Therefore a rise of temperature does not affect its yield notably. The C_xH_y increased from 600 to 900 °C and then decreased from 900 to 1400 °C. This is because in primary pyrolysis the formation of light hydrocarbons is due to the release of the methoxyl groups, the charring processes, and the long-chain polymethylene structures, which could be promoted by higher temperatures to some degree [55,68,73,74]. However, in secondary pyrolysis the light hydrocarbons are formed by the tar cracking and simultaneously are consumed by the soot formation, however their consumption become dominant at elevated

temperatures [61,71,75,76]. At high temperatures, gasification and reforming reactions also could affect the gas yields slightly. Besides, the corresponding individual gas yields on mass basis are listed in Table 1.4 as supplementary information.
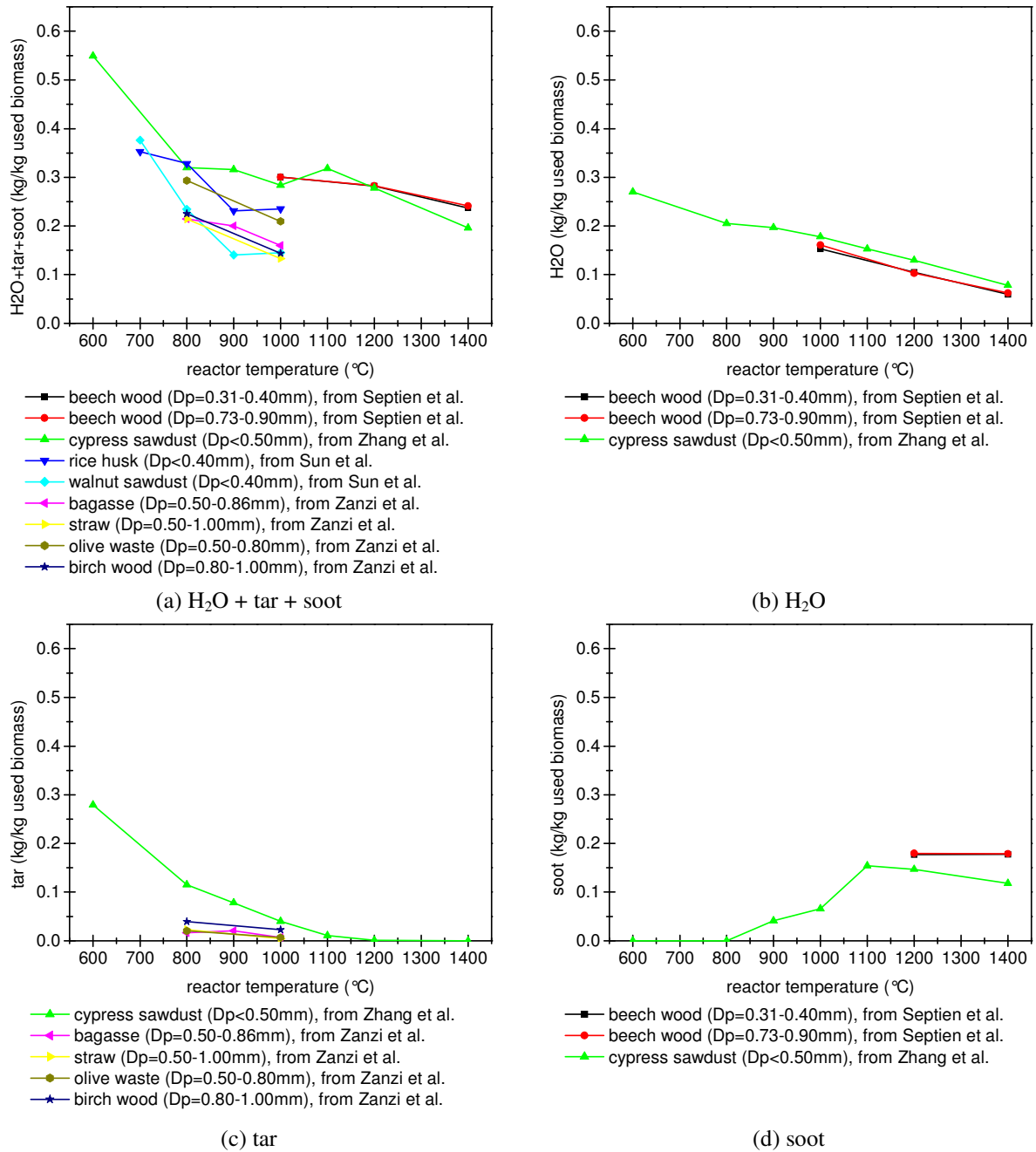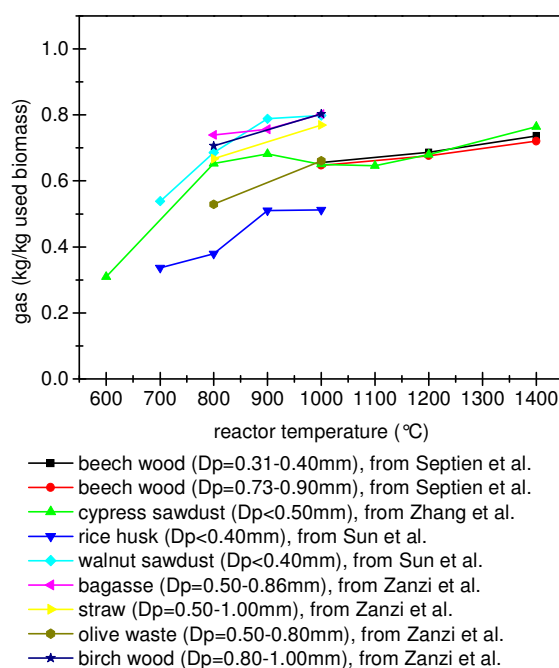

(a) H_2O + tar + soot

(b) H_2O

(c) tar

(d) soot

Figure 1.7 Effect of temperature on the H_2O/tar/soot yield during biomass pyrolysis [52-57]

Table 1.4 Effect of temperature on the individual gas yields (mass) during biomass pyrolysis [52-57]

fuel	T	H_2	CO	CO_2	C_xH_y
-	°C		kg/kg used biomass		
weech wood	1000	0.020	0.415	0.118	0.103
(Dp = 0.31 - 0.40 mm)	1200	0.043	0.477	0.130	0.037
	1400	0.052	0.614	0.062	0.009
beech wood	1000	0.021	0.415	0.111	0.101
(Dp = 0.73 - 0.90 mm)	1200	0.041	0.458	0.140	0.038
	1400	0.050	0.596	0.062	0.012
cypress sawdust	600	0.003	0.210	0.046	0.044
(Dp < 0.50 mm)	800	0.010	0.462	0.068	0.113
	900	0.016	0.478	0.071	0.118
	1000	0.021	0.478	0.073	0.078
	1100	0.032	0.486	0.083	0.046
	1200	0.040	0.546	0.066	0.028
	1400	0.047	0.701	0.015	0.002
rice husk	700	0.005	0.209	0.095	0.028
(Dp < 0.40 mm)	800	0.006	0.235	0.105	0.034
	900	0.011	0.303	0.132	0.064
	1000	0.019	0.327	0.133	0.034
walnut sawdust	700	0.007	0.346	0.141	0.046
(Dp < 0.40 mm)	800	0.009	0.439	0.145	0.093
	900	0.017	0.528	0.174	0.068
	1000	0.024	0.569	0.158	0.047
bagasse	800	0.029	0.408	0.217	0.085
(Dp = 0.50 - 0.86 mm)	900	0.031	0.515	0.153	0.058
	1000	0.051	0.717	0.009	0.025
straw	800	0.022	0.245	0.326	0.075
(Dp = 0.50 – 1.00 mm)	1000	0.040	0.593	0.101	0.035
olive waste	800	0.007	0.251	0.158	0.114
(Dp = 0.50 - 0.80 mm)	1000	0.022	0.432	0.129	0.078
birch wood	800	0.011	0.445	0.114	0.137
(Dp = 0.80 – 1.00 mm)	1000	0.030	0.571	0.112	0.090

- ■ beech wood (Dp=0.31-0.40mm), from Septien et al.
- ● beech wood (Dp=0.73-0.90mm), from Septien et al.
- ▲ cypress sawdust (Dp<0.50mm), from Zhang et al.
- ▼ rice husk (Dp<0.40mm), from Sun et al.
- ◆ walnut sawdust (Dp<0.40mm), from Sun et al.
- ◀ bagasse (Dp=0.50-0.86mm), from Zanzi et al.
- straw (Dp=0.50-1.00mm), from Zanzi et al.
- olive waste (Dp=0.50-0.80mm), from Zanzi et al.
- ★ birch wood (Dp=0.80-1.00mm), from Zanzi et al.

Figure 1.8 Effect of temperature on the total yields of gas products (mass) during biomass pyrolysis [52-57]

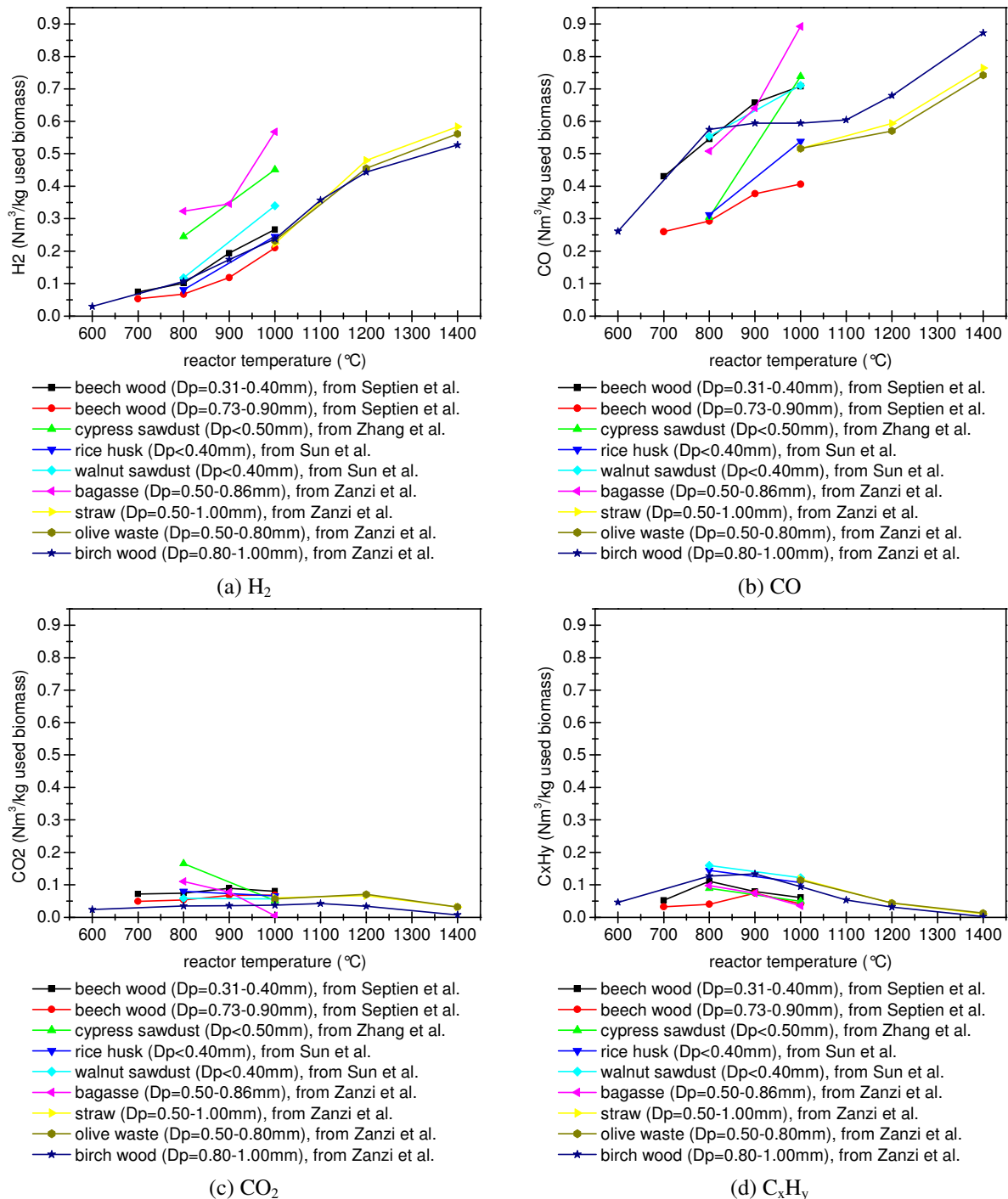(a) H$_2$

(b) CO

(c) CO$_2$

(d) C$_x$H$_y$

Figure 1.9 Effect of temperature on the individual gas yields (volume) during biomass pyrolysis [52-57]

1.3.1.2 Effect of particle size on pyrolysis

The effect of particle size on the char yield during pyrolysis is shown in Figure 1.10. The char yield increased slightly with increasing particle size. This is probably because the particle size affects the heating rate. The heating rate was lower in large particles than in small particles, resulting in less gas releasing and more char producing in large particles [56].

21
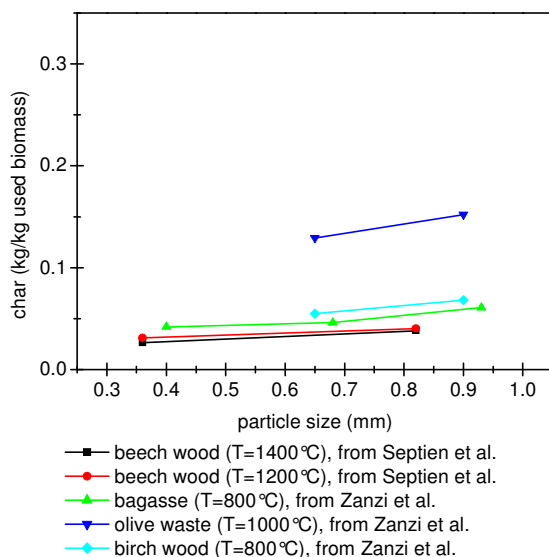
Figure 1.10 Effect of particle size on the char yield during biomass pyrolysis [52,53,56,57]

The effect of particle size on the H_2O/tar/soot yield during pyrolysis is shown Figure 1.11. With increasing particles size, the total yields of H_2O, tar, and soot almost kept constant or increased a little. The increased total yields of H_2O, tar, and soot during pyrolysis of bagasse, olive waste and birch wood were mainly from the higher moisture content in their larger particles [56,57,77]. The yield of H_2O also almost kept constant or increased a little with increasing particle size, which still might be mainly related to the different moisture content in the different size of particles. The tar and soot yields were nearly unchanged, which probably indicates that particle size could not affect the tar and soot formation.

Figure 1.12 shows the effect of particle size on the total yields of gas products during pyrolysis. The total yields of gas products decreased with increasing particle size. This is because higher heating rate is obtained in the small particles leading to more gas releasing from the smaller particles [56]. The effect of particle size on the individual gas yields on volume basis is shown in Figure 1.13. Generally, the yields of H_2, CO, and CO_2 decreased with increasing particle size due to less gas releasing from primary pyrolysis caused by the lower heating rate in the large particles. The C_xH_y yield increased a little with increasing particle size. This is probably because in the small particles the produced gas leaves the particles faster and the residence time of the produced gas thereby is longer, which lead to more hydrocarbons cracking [56]. Besides, the corresponding individual gas yields on mass basis are listed in Table 1.5 as supplementary information. On the whole, when the biomass particle size was less than 1.0 mm, no large limitation on pyrolysis was observed.
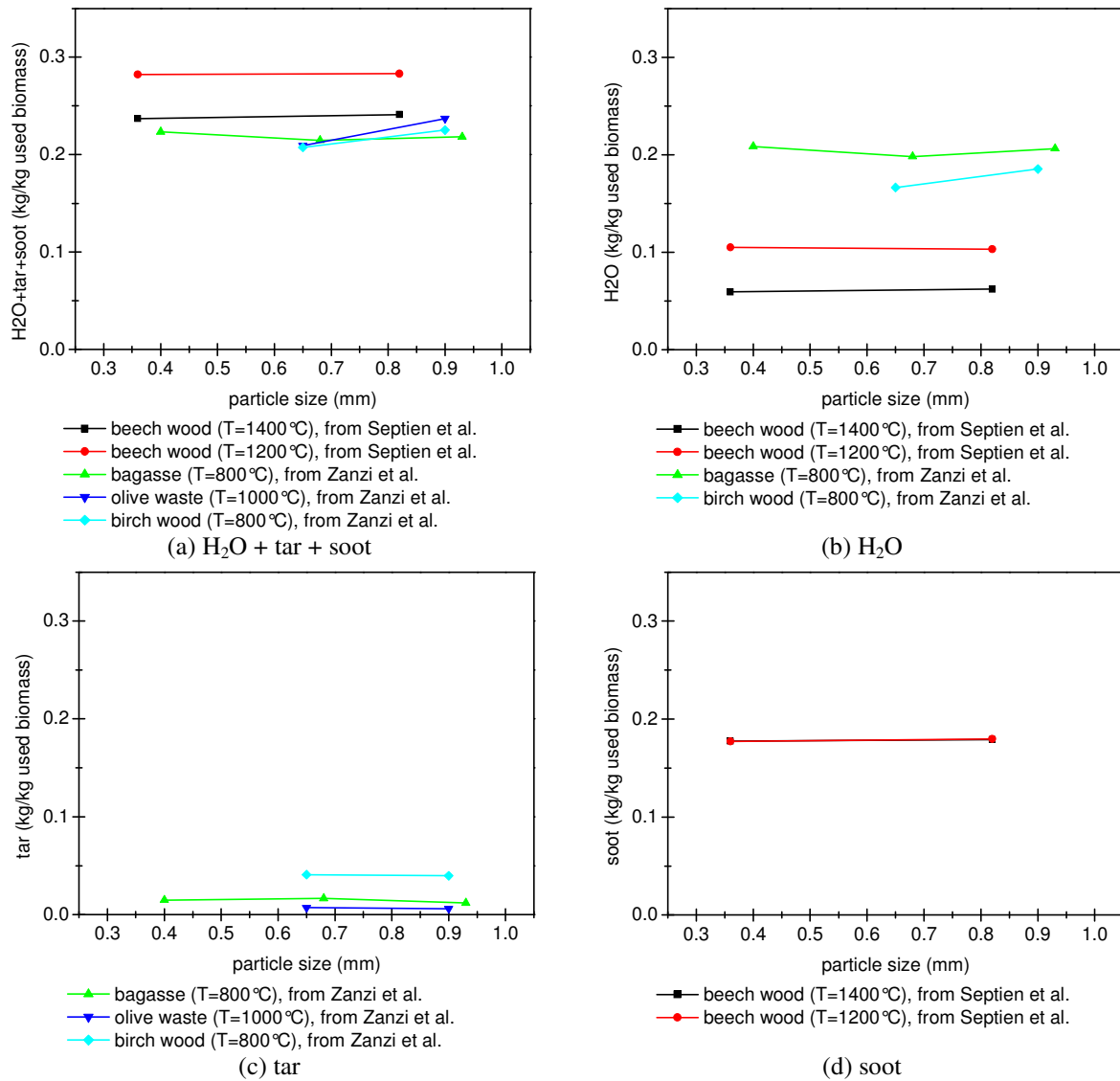
(a) H_2O + tar + soot

(b) H_2O

(c) tar

(d) soot

Figure 1.11 Effect of particle size on the H_2O/tar/soot yield during biomass pyrolysis [52,53,56,57]

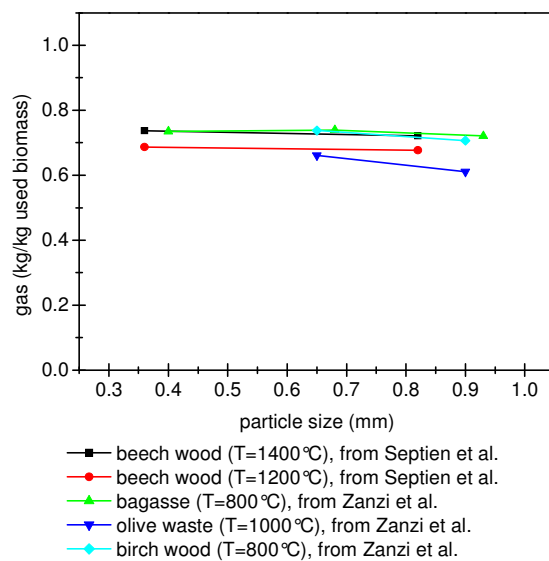**Figure 1.12 Effect of particle size on the total yields of gas products (mass) during biomass pyrolysis**
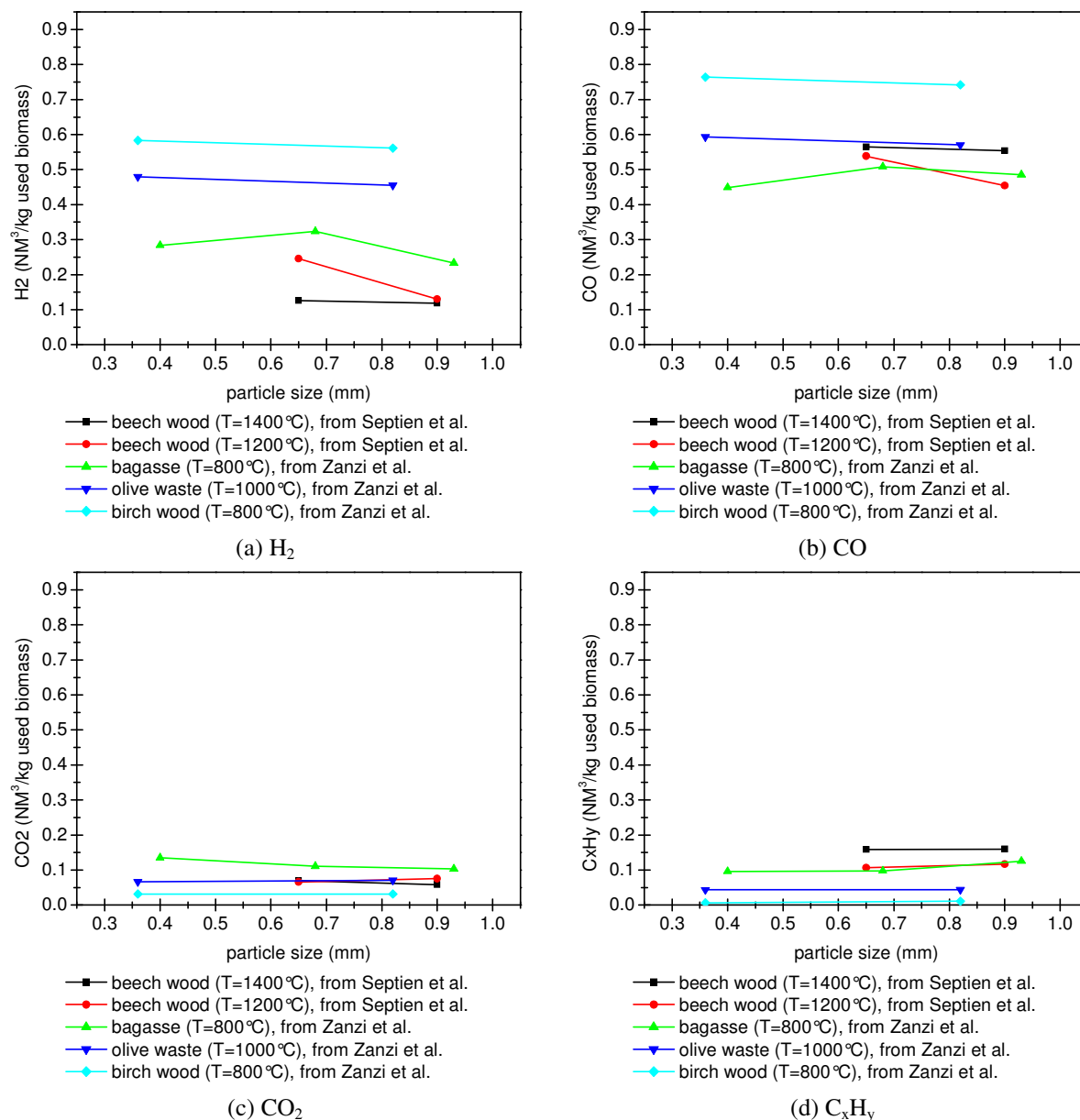
[52,53,56,57]

23

(a) H_2

(b) CO

(c) CO_2

(d) C_xH_y

Figure 1.13 Effect of particle size on the individual gas yields (volume) during biomass pyrolysis

[52,53,56,57]

Table 1.5 Effect of particle size on the individual gas yields (mass) during biomass pyrolysis [52,53,56,57]

fuel	Dp	H_2	CO	CO_2	C_xH_y
-	mm	kg/kg used biomass			
beech wood	0.36 (0.31 – 0.40)	0.052	0.614	0.062	0.009
(T = 1400 °C)	0.82 (0.73 – 0.90)	0.050	0.596	0.062	0.012
beech wood	0.36 (0.31 – 0.40)	0.043	0.477	0.130	0.037
(T = 1200 °C)	0.82 (0.73 – 0.90)	0.041	0.458	0.140	0.038
bagasse	0.40 (0.30 – 0.50)	0.025	0.361	0.265	0.083
(T = 800 °C)	0.68 (0.50 – 0.86)	0.029	0.408	0.217	0.085
	0.93 (0.86 – 1.00)	0.021	0.390	0.202	0.108
olive waste	0.65 (0.50 – 0.80)	0.022	0.432	0.129	0.078
(T = 1000 °C)	0.90 (0.80 – 1.00)	0.012	0.365	0.149	0.086
birch wood	0.65 (0.50 – 0.80)	0.011	0.454	0.137	0.135
(T = 800 °C)	0.90 (0.80 – 1.00)	0.011	0.445	0.114	0.137

1.3.1.3 Effect of reactor length on pyrolysis

The effect of reactor length on the char yield during pyrolysis is shown in Figure 1.14. Along with the axial direction of the reactor, pyrolysis products were obtained at 5 different sampling points. The distance between the fuel injector and the product sampling point increased from 410 to 1530 mm. At 800 and 1000 °C, the char yield decreased with increasing reactor length, particularly from 410 to 690 mm, probably indicating the primary pyrolysis was complete before 690 mm and after 690mm gasification reactions of the char led to its yield decreasing slightly.
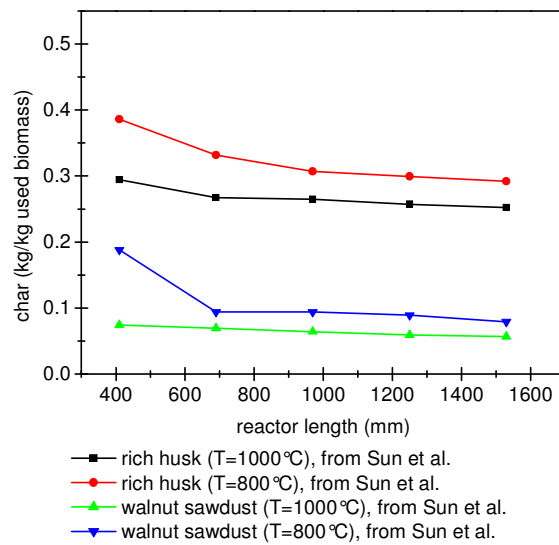
Figure 1.14 Effect of reactor length on the char yield during biomass pyrolysis [55]
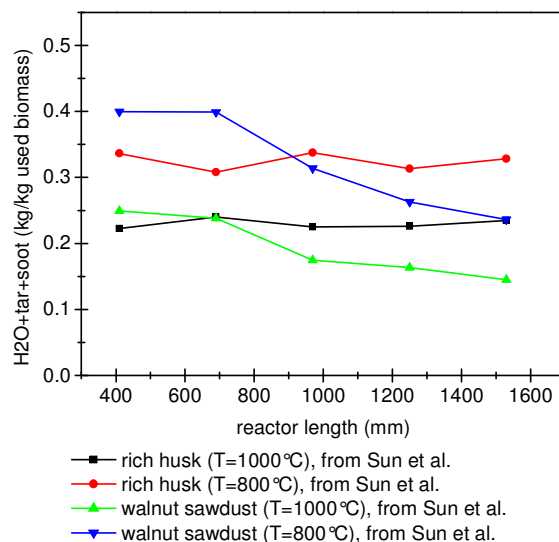
Figure 1.15 Effect of reactor length on the H$_2$O/tar/soot yield during biomass pyrolysis [55]

The effect of reactor length on the H$_2$O/tar/soot yield during pyrolysis is shown in Figure 1.15. Along with the reactor, in general, the total yields of H$_2$O, tar, and soot decrease gradually or

almost kept constant at 800 and 1000 °C. This is probably because more H_2O, tar, and soot were consumed by cracking, reforming and gasification reactions as the reactor length increased.

Figure 1.16 shows the total yields of gas products along with reactor during pyrolysis. In generally, at 800 and 1000 °C, the total yields of gas products increased with increasing reactor length. Before 690 mm, the increase of the total yields was probably related to the degree of the primary pyrolysis, and after 690 mm, the increase might be due to cracking and reforming of tar and gasification of char and soot. The individual gas yields on volume basis are shown as function of the reactor length in Figure 1.17. The yields of H_2 and CO increased with increasing reactor length, which was caused by the primary pyrolysis evolution, tar cracking and reforming, and char and soot gasification. The CO_2 yield was very low compared with the H_2 and CO yields, and was nearly unchanged, probably indicating that CO_2 was mainly released in the early stage of the pyrolysis process [55]. The yield of C_xH_y generally increased slightly with increasing reactor length probably due to further tar cracking at 800 and 1000 °C. Besides, the corresponding individual gas yields on mass basis are listed in Table 1.6 as supplementary information.

Table 1.6 Effect of reactor length on the individual gas yields (mass) during biomass pyrolysis [55]

fuel	L	H_2	CO	CO_2	C_xH_y
-	mm		kg/kg used biomass		
rice husk	410	0.012	0.296	0.150	0.025
(T = 1000 °C)	690	0.014	0.300	0.150	0.029
	970	0.016	0.313	0.145	0.037
	1250	0.017	0.320	0.145	0.035
	1530	0.019	0.327	0.133	0.034
rice husk	410	0.006	0.149	0.109	0.013
(T = 800 °C)	690	0.006	0.204	0.122	0.028
	970	0.006	0.215	0.105	0.030
	1250	0.006	0.232	0.114	0.035
	1530	0.006	0.235	0.105	0.034
walnut sawdust	410	0.017	0.465	0.165	0.030
(T = 1000 °C)	690	0.017	0.468	0.164	0.044
	970	0.018	0.526	0.164	0.052
	1250	0.021	0.550	0.157	0.048
	1530	0.024	0.569	0.158	0.047
walnut sawdust	410	0.010	0.264	0.120	0.021
(T = 800 °C)	690	0.009	0.334	0.118	0.044
	970	0.009	0.399	0.124	0.060
	1250	0.010	0.433	0.130	0.076
	1530	0.009	0.439	0.143	0.093
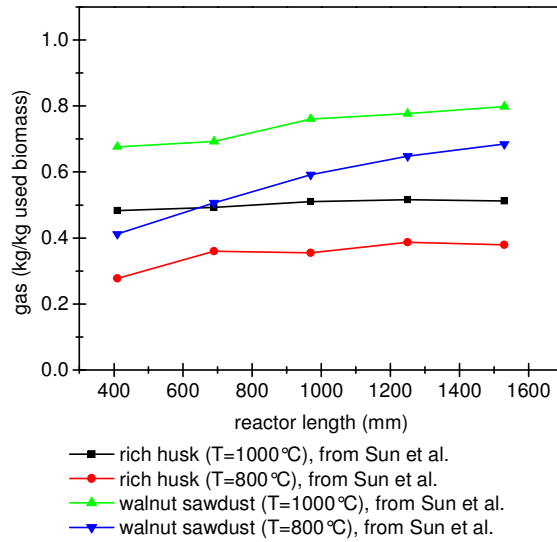
Figure 1.16 Effect of reactor length on the total yields of gas products (mass) during biomass pyrolysis [55]

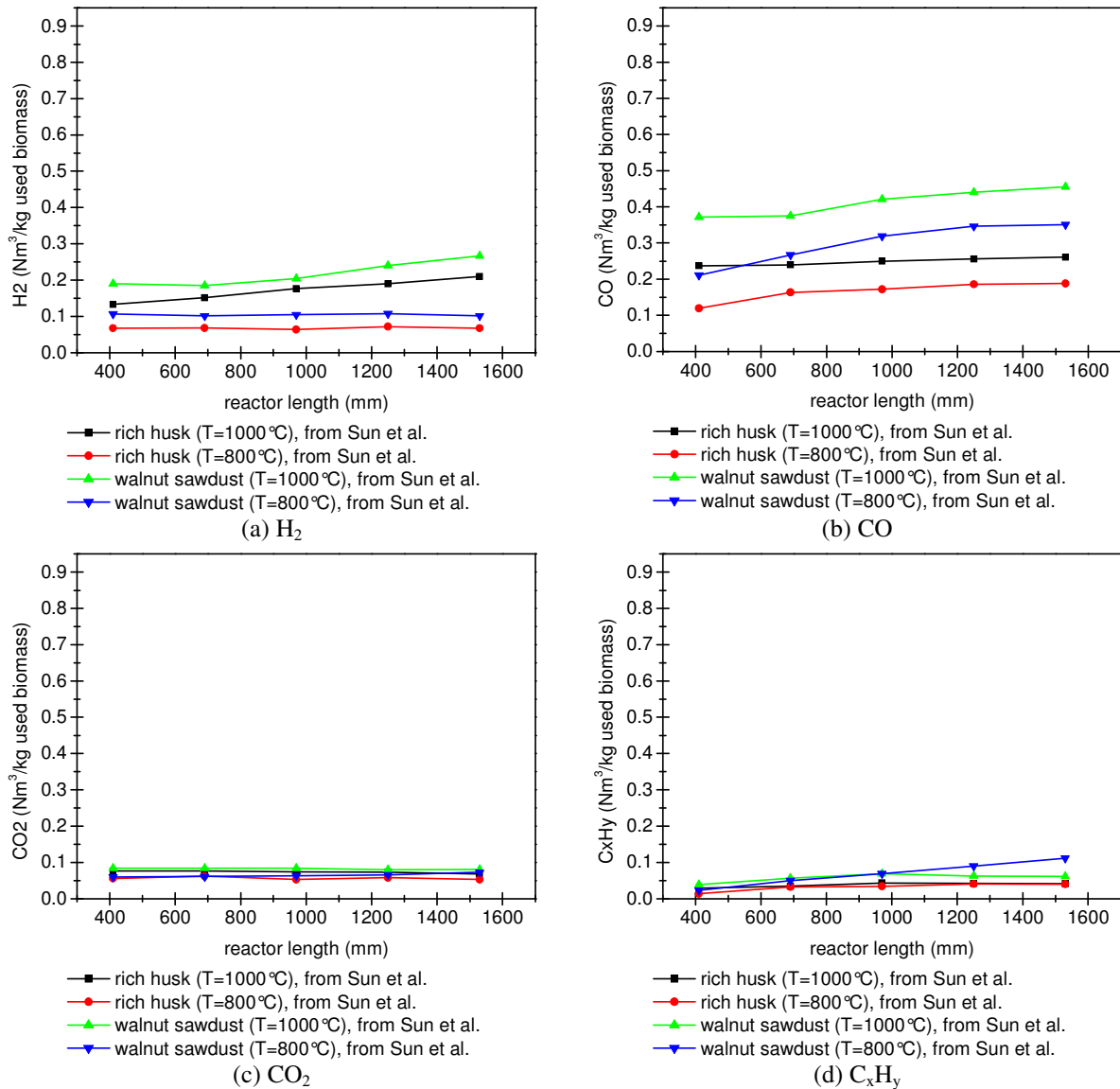

(a) H_2

(b) CO

(c) CO_2

(d) C_xH_y

Figure 1.17 Effect of reactor length on the individual gas yields (volume) during biomass pyrolysis [55]

1.3.1.4 Effect of steam addition on pyrolysis

The effect of steam addition on the char yield during pyrolysis is shown in Figure 1.18. The char yield decreased obviously as the steam/carbon molar ratio was increased from 0.00 to 2.85 in the studied temperature range of 800 – 1400 °C. This is probably because steam addition is beneficial to promoting the gasification reaction of char and steam.
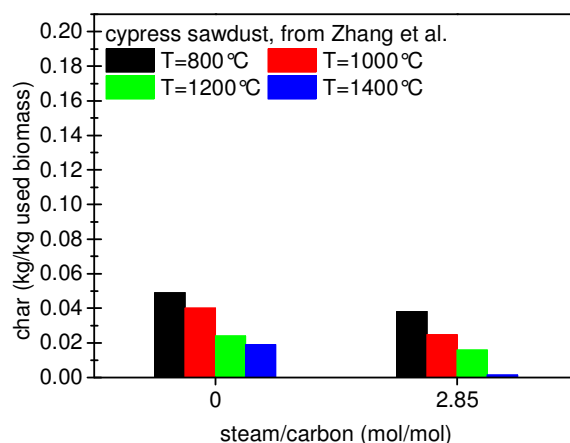
Figure 1.18 Effect of steam addition on the char yield during biomass pyrolysis [78]

The effect of steam addition on the tar and soot yields during pyrolysis is shown in Figure 1.19. The yield of H_2O cannot be compared in these experiments owing to the extra steam addition in half of these experiments. Tar was observed only at 800 and 1000 °C, and its yield decreased with steam addition mainly because of the enhanced tar reforming reaction. Soot was observed when the temperature was higher than 1000 °C. The lower soot yield was obtained as the steam was added. It is most likely both because more tar was reformed leading to less soot formation and because more soot was gasified by steam. However, at very high temperature (1400 °C) with a large amount of steam addition (H_2O/C = 2.85), soot was still present and cannot be completely removed possibly due to its low reactivity.

Figure 1.20 shows the effect of steam addition on the total yields of gas products during pyrolysis. The total yields of gas products increased with steam addition in the studied temperature range of 800 – 1400 °C. This is partly due to the enhanced conversion of char, tar, soot, and hydrocarbons by gasification and reforming reactions and partly due to the promoted water gas shift reaction (consuming 1 mole CO but producing 2 mole gases, CO_2 and H_2). The effect of steam addition on the individual gas yields on volume basis is shown in Figure 1.21. The H_2 yield increased with steam addition, because more char and soot were gasified, more tar and hydrocarbons were reformed, and the water gas shift reaction was promoted. With steam addition, the CO yield almost kept constant when the temperature was

lower than 1200 °C but increases at 1400 °C. This is because the CO yield is affected by two sets of reactions. The first set of reactions, such as the steam gasification reactions of char and soot and the steam reforming reactions of tar and hydrocarbons, is helpful to produce more CO, while the second type of reactions, such as the water gas shift reaction, tend to consume more CO. When the temperature was lower than 1200 °C, these two sets of reactions may compete with each other, resulting in the produced amount of CO being almost equal to the consumed amount with steam addition and thereby the CO yield was nearly unchanged. However, at 1400 °C, the first type of endothermic reactions predominated while the second type of exothermic reactions were repressed, thus the produced amount of CO was more than the consumed amount with steam addition, leading to an increasing CO yield. The CO_2 yield increased with steam addition probably due to the promoted water gas shift reaction. The C_xH_y yield decreased with steam addition mainly because of the enhanced steam reforming reactions of them. Besides, the corresponding individual gas yields on mass basis are listed in Table 1.7 as supplementary information.
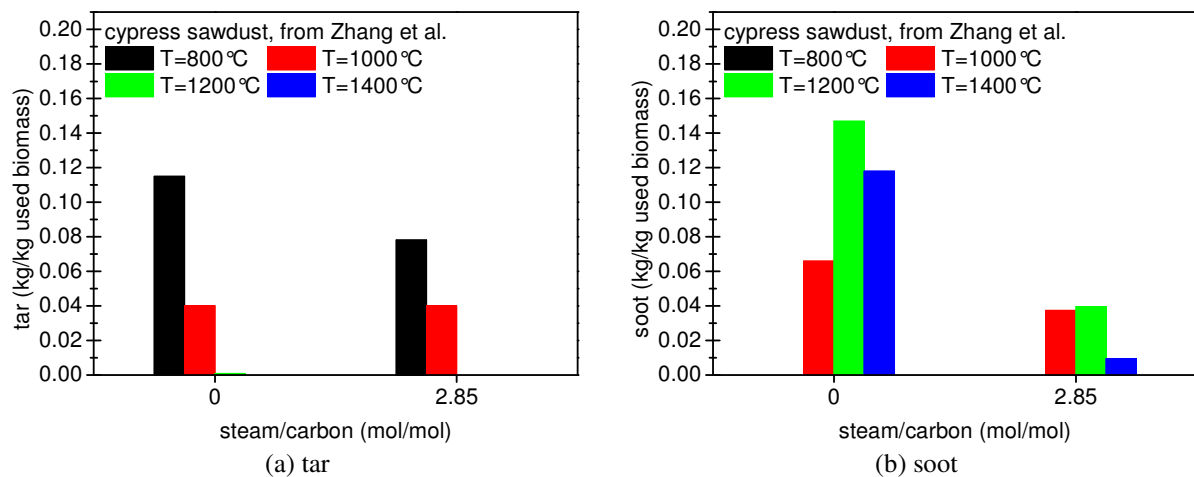

| (a) tar | (b) soot |

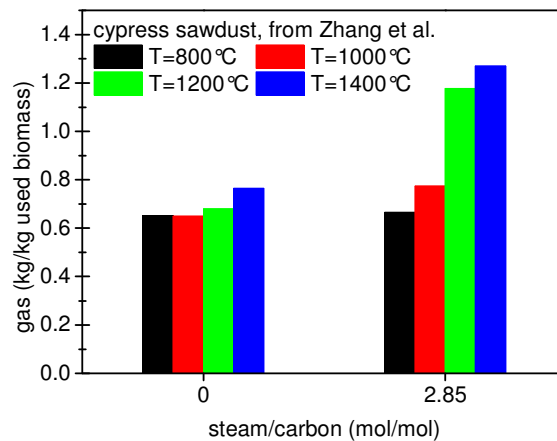**Figure 1.19 Effect of steam addition on the tar/soot yield during biomass pyrolysis** [78]

Figure 1.20 Effect of steam addition on the total yields of gas products (mass) during biomass pyrolysis [78]
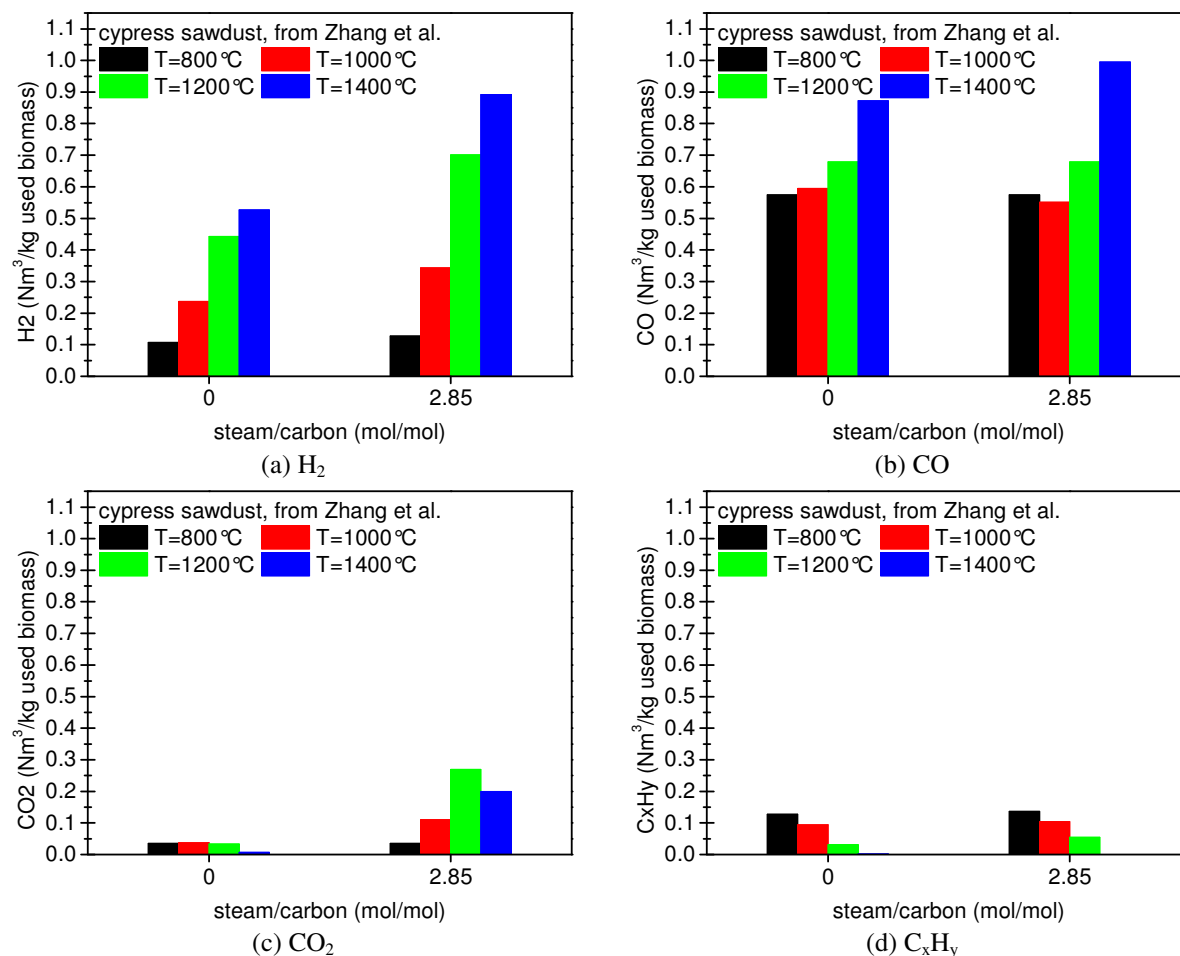
29

Figure 1.21 Effect of steam addition on the individual gas yields (volume) during biomass pyrolysis [78]

Table 1.7 Effect of steam addition on the individual gas yields (mass) during biomass pyrolysis [78]

fuel	H_2O/C	H_2	CO	CO_2	C_xH_y
-	mol/mol	kg/kg used biomass			
cypress sawdust	0	0.010	0.462	0.068	0.113
(T = 800 °C)	2.85	0.011	0.462	0.068	0.123
cypress sawdust	0	0.021	0.478	0.073	0.078
(T = 1000 °C)	2.85	0.031	0.444	0.216	0.084
cypress sawdust	0	0.040	0.546	0.066	0.028
(T = 1200 °C)	2.85	0.063	0.546	0.529	0.039
cypress sawdust	0	0.047	0.701	0.015	0.002
(T = 1400 °C)	2.85	0.080	0.800	0.391	0.000

1.3.2 Effects of operating condition on gasification

In this section, the effects of temperature, excess air ratio, residence time, particle size, and reactor length on the individual gas yields were discussed. Besides, the two important factors in the gasification process, the producer gas yield that was defined as the total amount of H_2, CO, CO_2, and C_xH_y (light hydrocarbons including C_1 and C_2 species), and the carbon conversion that was defined as the ratio of carbon in the producer gas to carbon from the fuel, were also investigated.

1.3.2.1 Effect of temperature on gasification

The effect of temperature on biomass gasification process is shown in Figure 1.22 and Figure 1.23. In these experiments, different oxidants were fed: Zhang et al. [78] and Zhou et al. [80] used oxygen, while Lapuerta et al. [35], Hernandez et al. [81], and Zhao et al. [82,83] used air. In general, the yields of H_2 and CO increased with increasing temperature, while the yields of CO_2 and C_xH_y decreased. At elevated temperature, the formed amounts of H_2 and CO increased obviously in the pyrolysis step, while the produced amounts of CO_2 and C_xH_y increased slightly or kept constant, because they were from different structures, functional groups, and cross linking reactions [55,61,63,64,67-70,73,74,79]. In the following gasification step, char, tar and hydrocarbons reforming reactions with CO_2 favored at higher temperature, resulting in more H_2 and CO were generated but more CO_2 and C_xH_y were consumed with increasing temperature. At very high temperature (> 1200 °C), the water gas shift reaction was reversed, which also led to a lower CO_2 yield. In the lower temperature range of 700 – 900 °C, the decreased CO yield and increased CO_2 yield may be related to the accelerated water gas shift reaction owing to the increased temperature. More C_xH_y was produced from 700 to 800 °C during walnut sawdust gasification, which is probably because of the promoted tar cracking. In generally, the producer gas yield, especially the H_2 and CO_2 content, and carbon conversion increased as the temperature increased, thus the syngas quality was upgraded and gasification efficiency was increased.

1.3.2.2 Effect of excess air ratio on gasification

The effect of excess air ratio on biomass gasification process is shown in Figure 1.24 and Figure 1.25. The varied excess air ratio was obtained by changing the fuel feeding rate and keeping the gas flow, which led to the other operating parameters nearly remaining the same. In these experiments, different oxidants were employed: Zhou et al. [80,84] used oxygen and Hernandez et al. [81] used air. With increasing excess air ratio, the yields of H_2, CO, and C_xH_y decreased obviously owing to their oxidation reactions, while the yield of CO_2 increased quickly because of both carbonaceous gas and char oxidation. The decreased producer gas yield was mainly caused by the conversation of H_2 to water. These results indicate that increasing excess air ratio tends to reduce the syngas quality, particularly the amounts of H_2 and CO. However, the carbon conversion was increased at higher excess air ratio due to more converted char and tar, which could improve the fuel conversion.
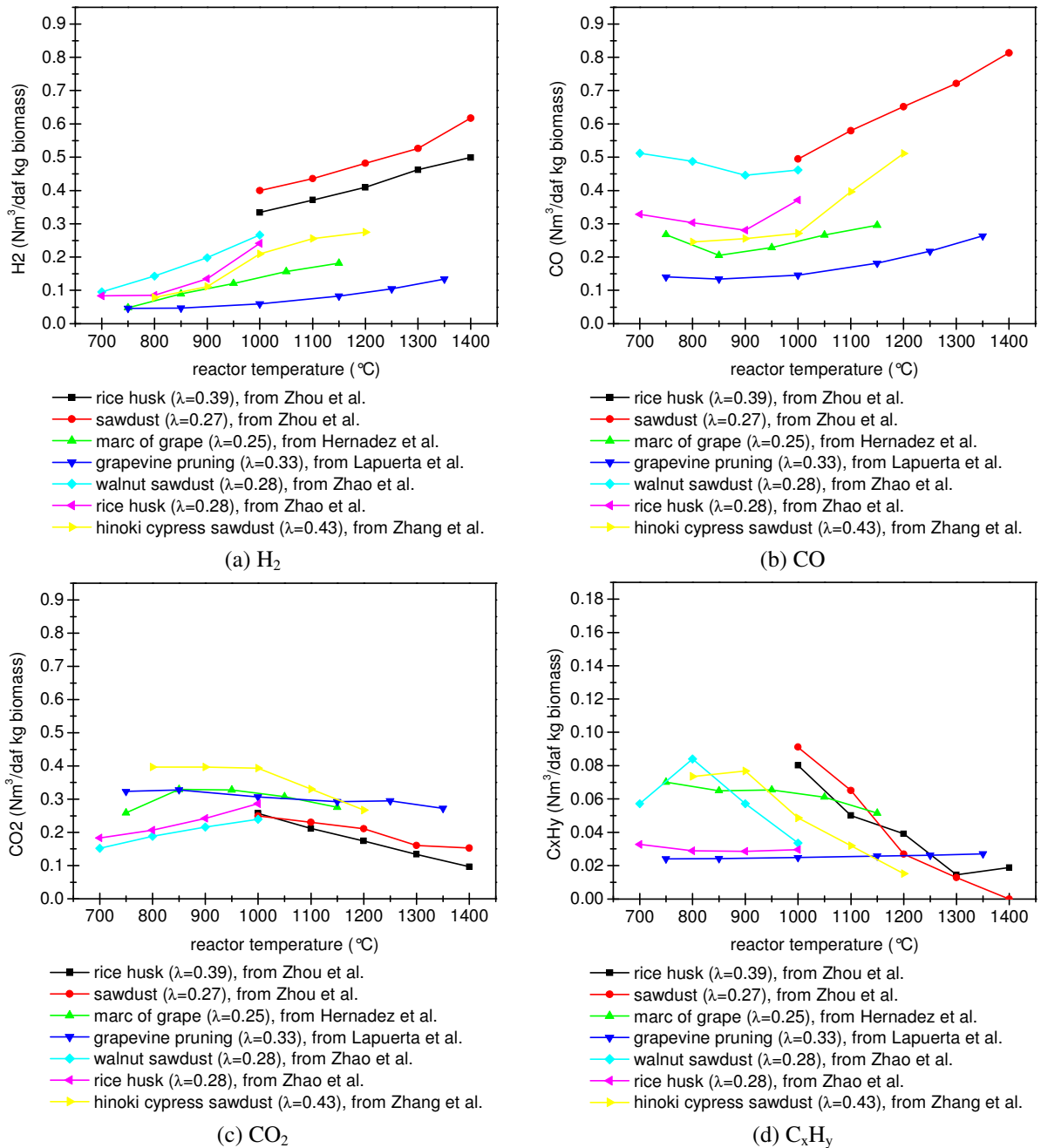
(a) H$_2$

(b) CO

(c) CO$_2$

(d) C$_x$H$_y$

Figure 1.22 Effect of temperature on the syngas yield during biomass gasification [35,78,80-83]

(a) producer gas

(b) carbon conversion
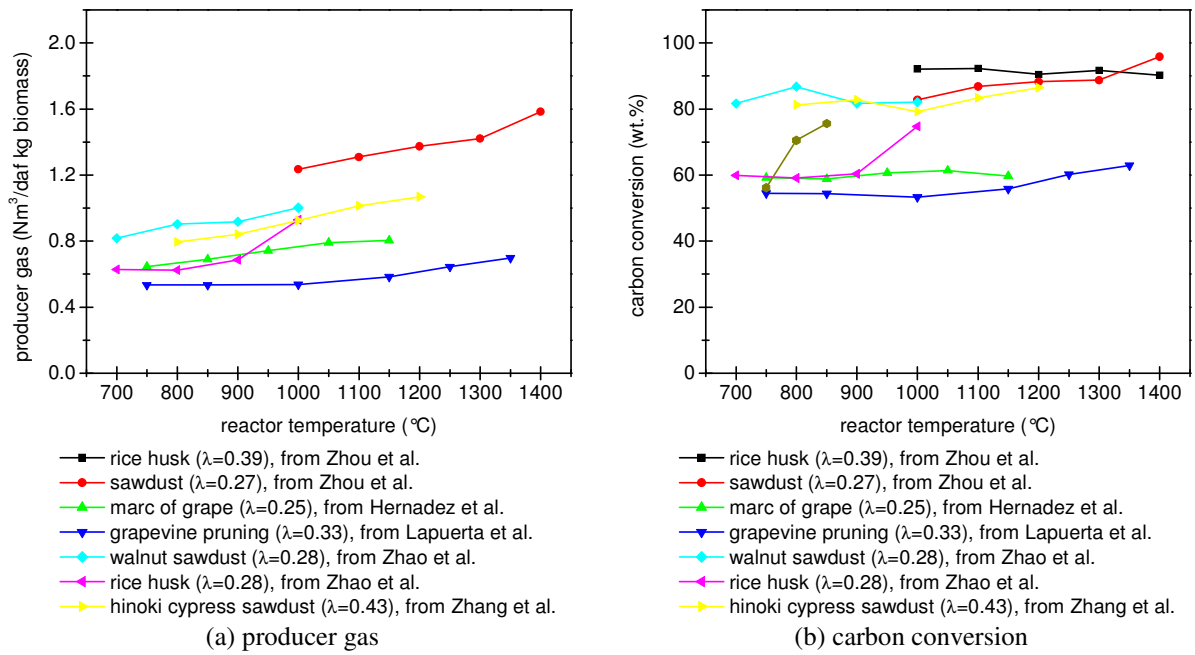
Figure 1.23 Effect of temperature on the performance of biomass gasification process [35,78,80-83]

(a) H_2

(b) CO

(c) CO_2

(d) C_xH_y
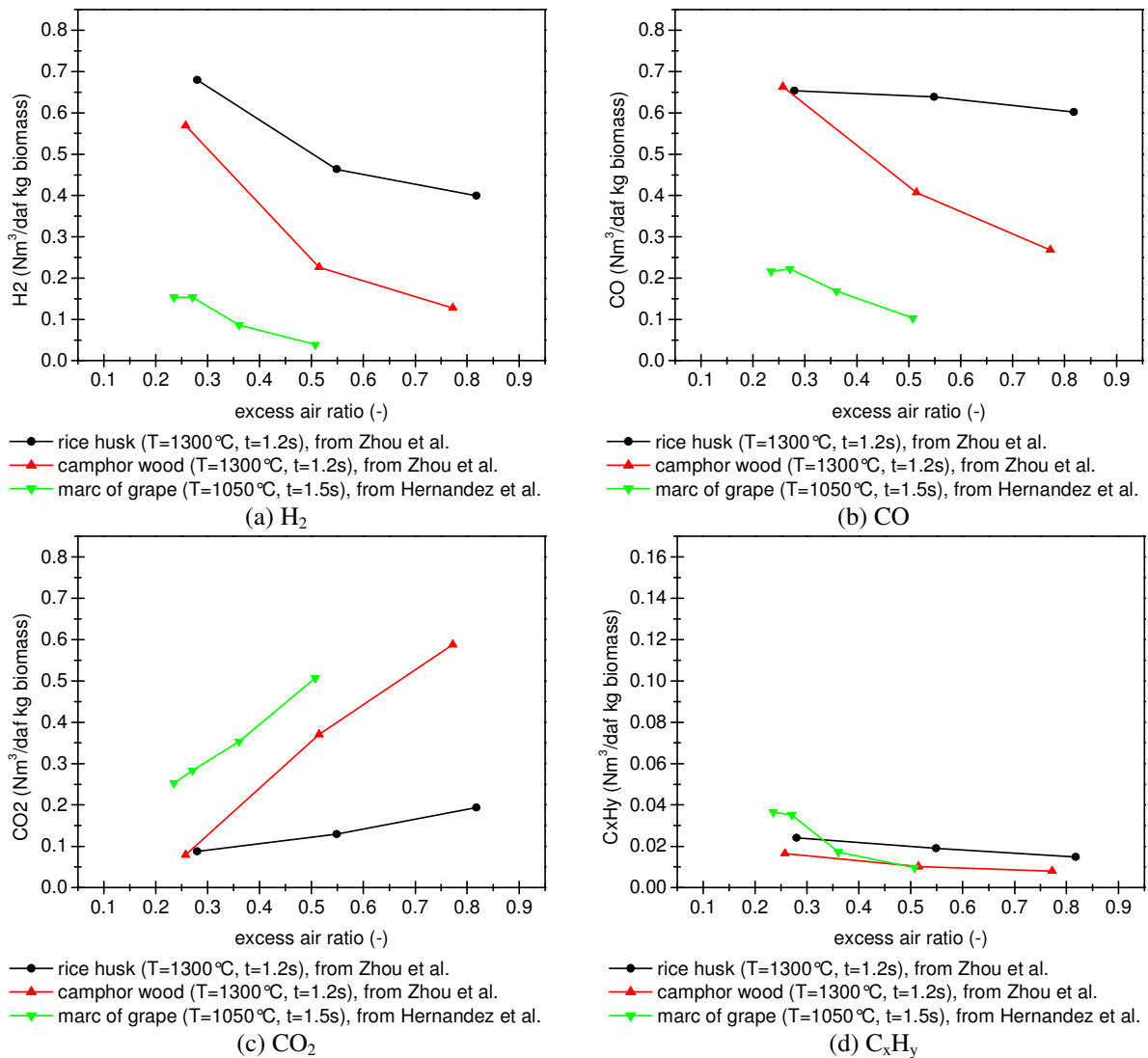
Figure 1.24 Effect of excess air ratio on the gas product yield during biomass gasification [80,81,84]

33

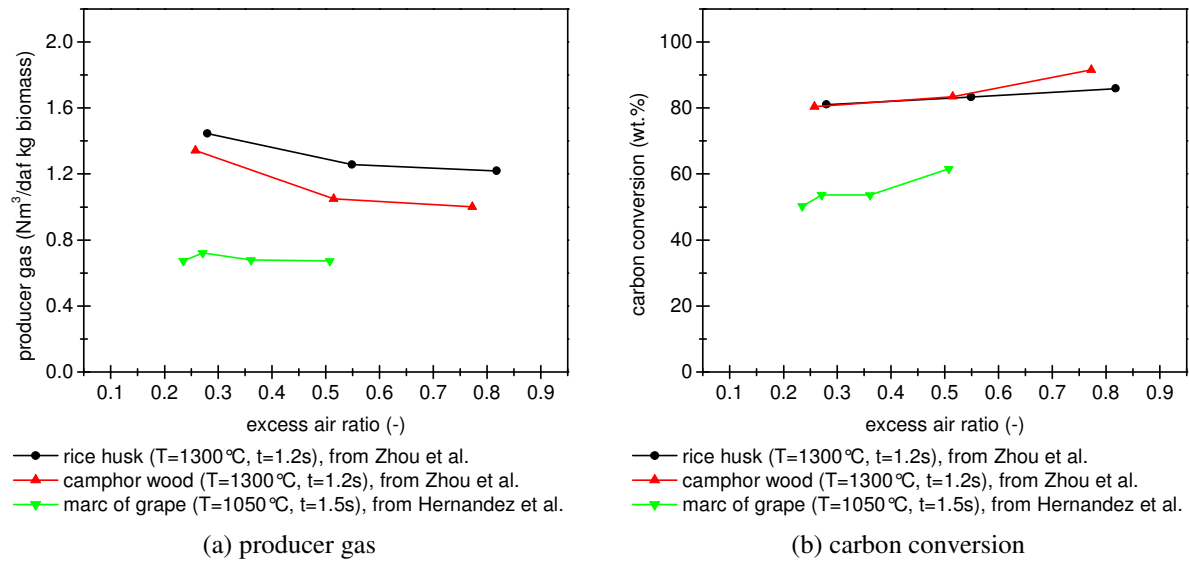(a) producer gas   (b) carbon conversion

Figure 1.25 Effect of excess air ratio on the performance of biomass gasification process [80,81,84]

1.3.2.3 Effect of residence time on gasification

The effect of residence time on biomass gasification process is shown in Figure 1.26 and Figure 1.27. In order to keep other operating parameters constant, the varied residence time was obtained by changing both the fuel feeding rate and gas flow. As the residence time increased from 1.36 to 1.92 s at 1050 °C, the yields of H_2, CO, and C_xH_y increased, whereas the CO_2 yield reduced slightly. This is because more remaining tar can be cracked to generate more gaseous species, such as H_2, CO, and C_xH_y, in a longer reaction time. Also, more produced char can reacted with CO_2, which leads to an increase and decrease amounts of CO and CO_2 respectively. The producer gas yield and the carbon conversion increased with increasing residence time, which is helpful to increasing gasification efficiency.

1.3.2.4 Effect of particle size on gasification

The effect of particle size on biomass gasification process is shown in Figure 1.28. It can be observed that the yields of all the gas species, the producer gas yield, and the carbon conversion increased with decreasing particle size from 0.5 to 8 mm. As the particle size decreases, the particle external surface area/volume increases. Thus in a limited time more volatile tends to release during pyrolysis and the produced char particles become more porous [85], which lead to the char reactivity increasing and thereby the char gasification reactions taking place to a higher extent. Besides, mass and heat transfer are improved (lower diffusion resistance coefficients) as the particle size diminishes, hence an increased reaction rate can be obtained and more char particles can be converted to gas products. Therefore, from a viewpoint of fuel conversion efficiency, smaller particles should be fed. However, from

technical and economic points of view, using small biomass particles may increase the difficulty and cost in comminuting or grinding [86]. As a result, the pros and cons should be under consideration when smaller biomass particles are employed.
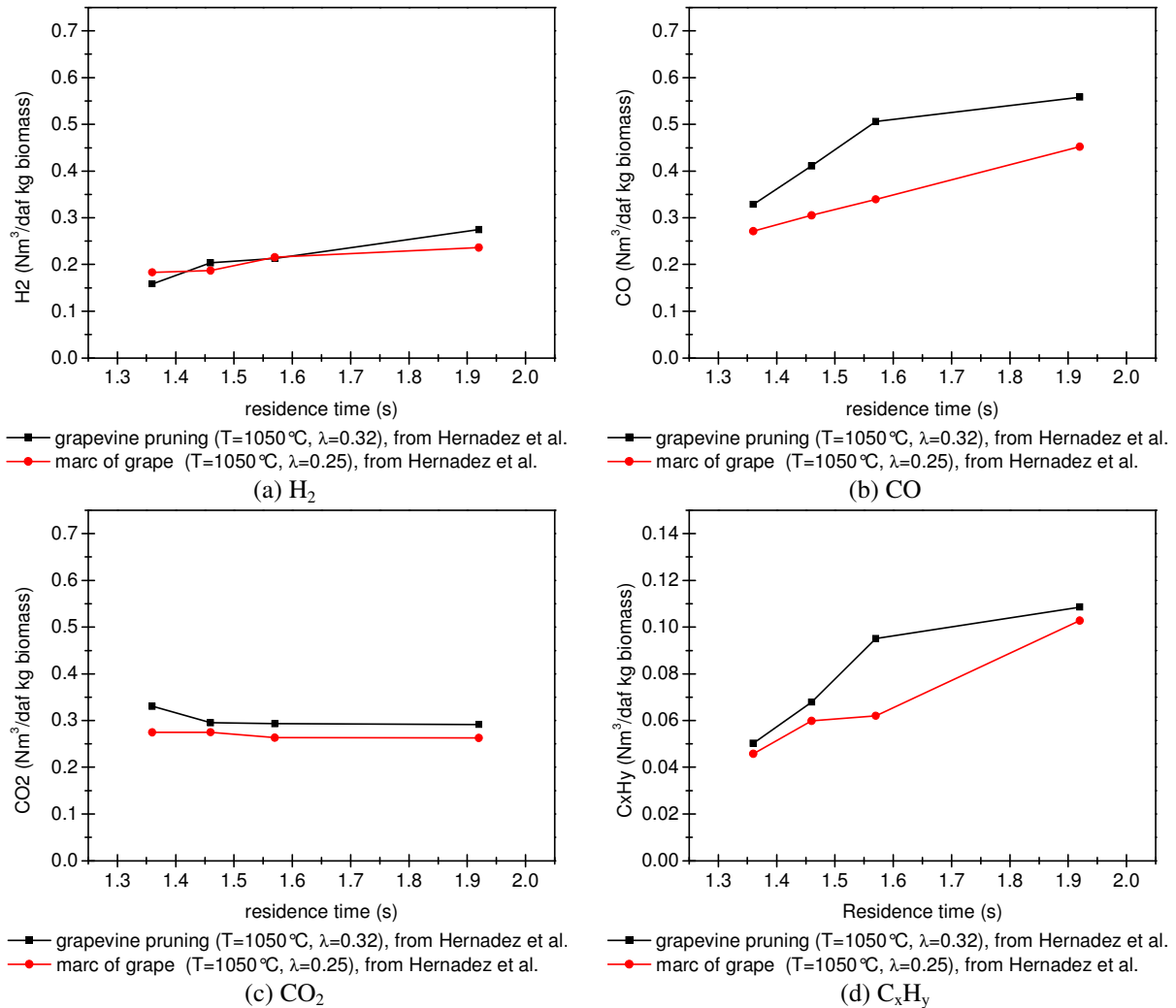

(a) H₂   (b) CO

(c) CO₂   (d) CₓHᵧ

Figure 1.26 Effect of residence time on the gas product yield during biomass gasification [36]

(a) producer gas   (b) carbon conversion
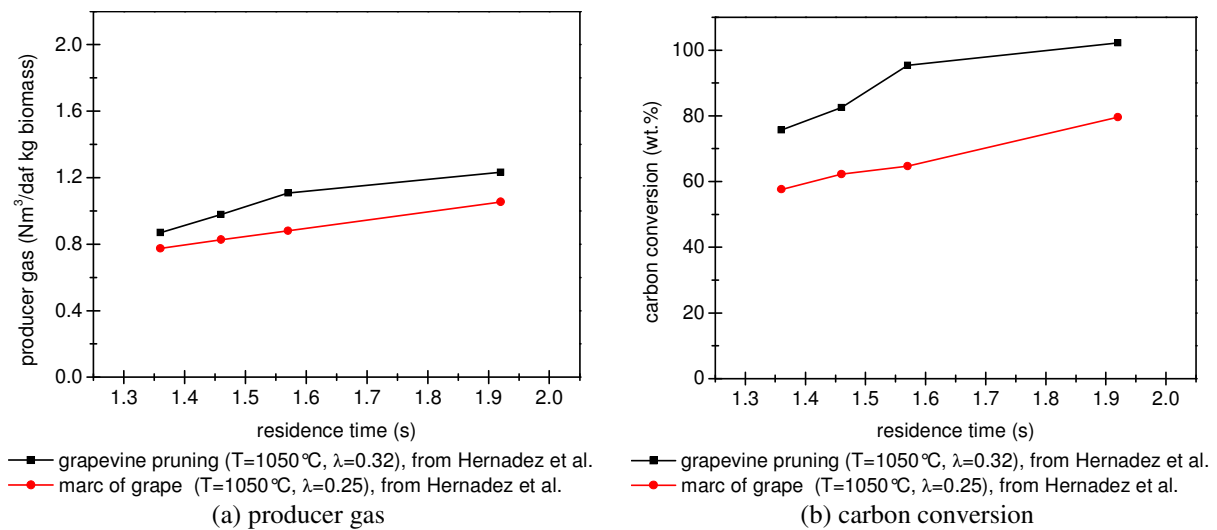
Figure 1.27 Effect of residence time on the performance of biomass gasification process [36]

35

(a) individual gas product
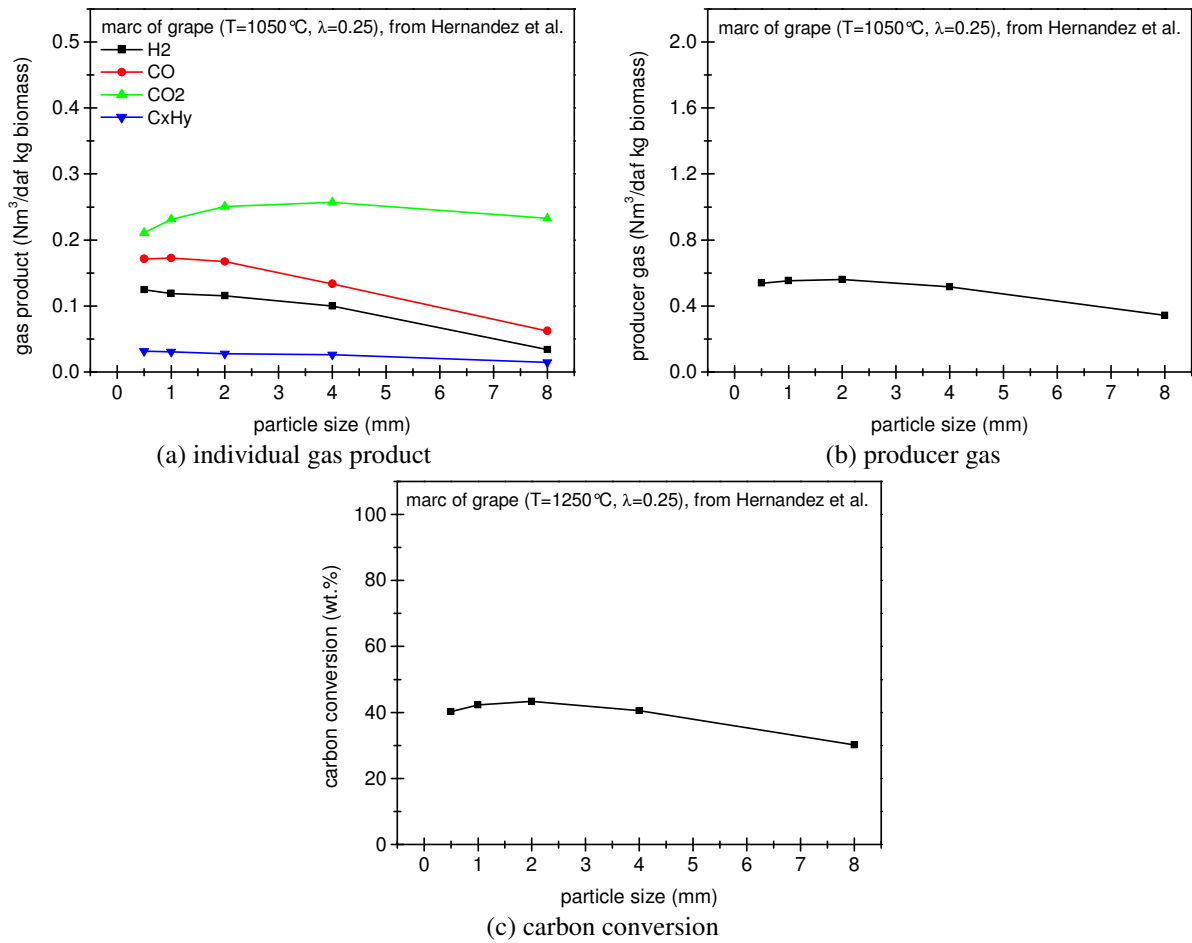
(b) producer gas

(c) carbon conversion

Figure 1.28 Effect of particle size on the gasification process [36]

1.3.2.5 Effect of reactor length on gasification

The effect of reactor length on biomass gasification process is shown in Figure 1.29 and Figure 1.30. At the applied temperature range of 700 – 900 °C, as the distance between the fuel injector and the product sampling point increased from 410 to 1530 mm, the yields of H_2, CO, and C_xH_y increased while the CO_2 yield decreased. Along with the axial direction of the reactor, the produced char during pyrolysis can be gasified with CO_2, resulting in the increased amount of CO at the expense of CO_2. Besides, the released tar during pyrolysis might gradually undergo cracking reactions to produce more light gases, resulting in the higher yields of H_2, CO, and C_xH_y. With increasing reactor length, both the producer gas yield and the carbon conversion increased steadily, which is always preferred in the gasification process.
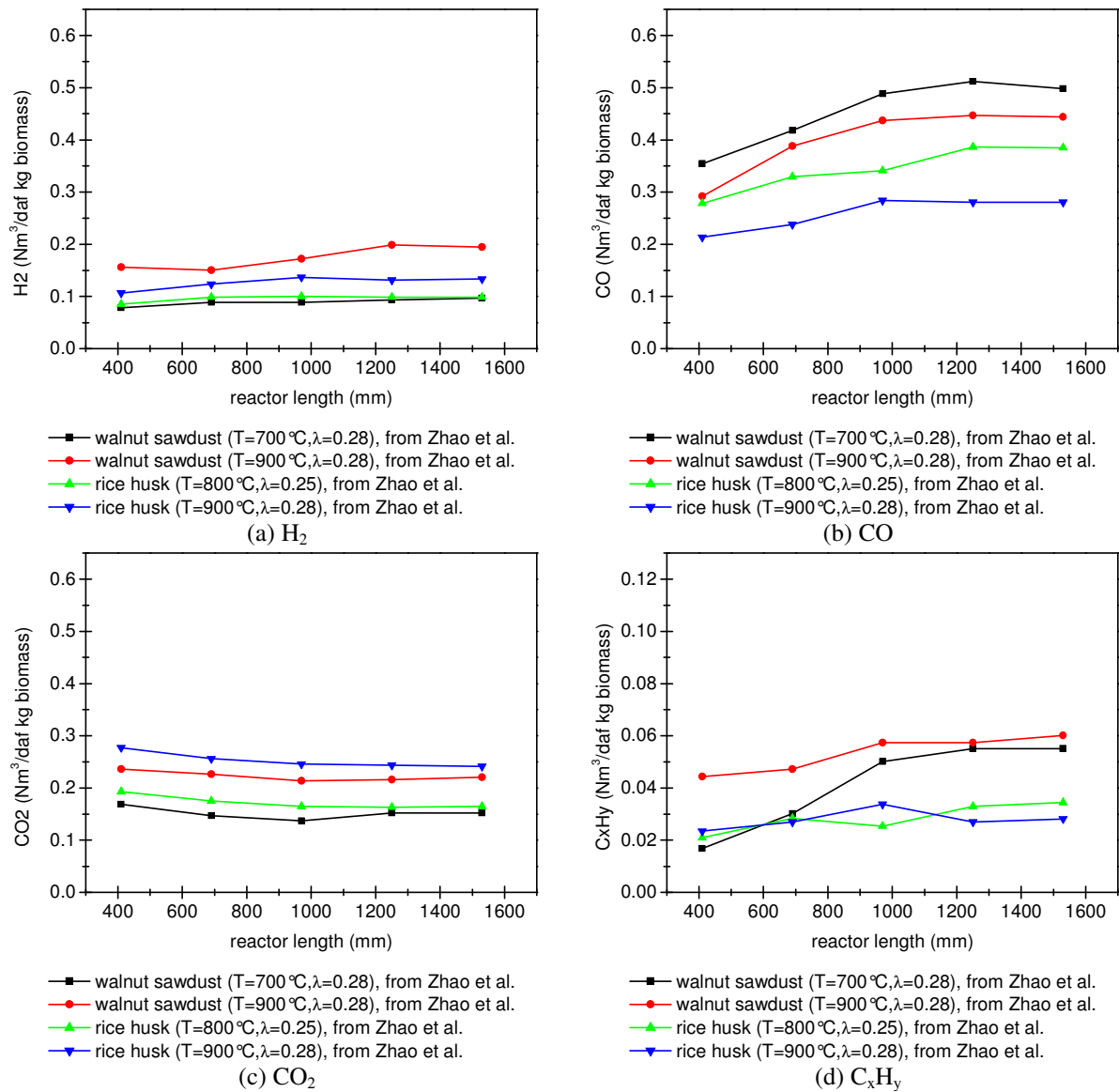
(a) H_2

(b) CO

(c) CO_2

(d) C_xH_y

Figure 1.29 Effect of reactor length on the gas product yield during biomass gasification [82,83]

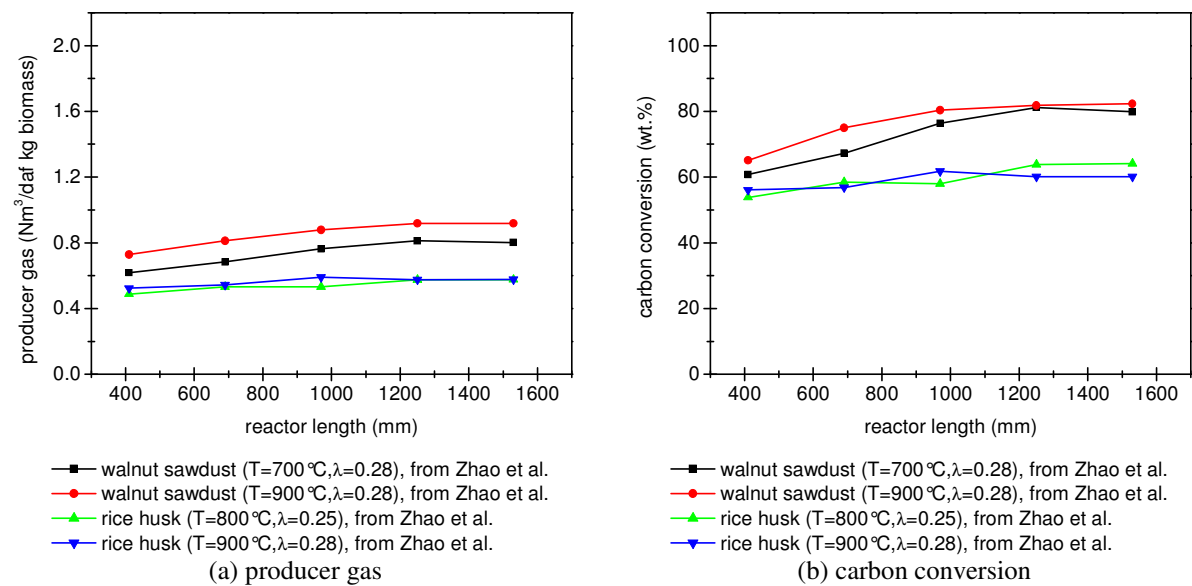(a) producer gas

(b) carbon conversion

Figure 1.30 Effect of reactor length on the performance of gasification process [82,83]

1.4 Conclusions

Gasification is a flexible and effective thermochemical conversion technology available for biomass utilization, which is gaining more and more global attention now. Compared with coal gasification which is a mature and most commercially available technology in large scale, biomass gasification is a young and less mature technology. Therefore, more comprehensive fundamental research and further pilot and demonstration scale testing on biomass gasification are still needed.

The basic physical, chemical, and thermal processes and major heterogeneous and homogeneous reactions during gasification are described and summarized in the present literature review, which could provide some general information and knowledge of gasification and be helpful to understanding the entire technology. In the gasification process, the properties of the most common fuel - coal, and an important alternative fuel – biomass, are summarized and compared. The coal rank, water content, caking properties and ash properties are the important properties for gasification. Compared with high rank coals, low rank coals usually have high moisture and volatile contents but low fixed carbon content and heating value, and are more reactive. The coal ash generally has a high melting point due to the high contents of silicon and aluminum. Overall, the ash melting characteristics is dependent largely on the quaternary SiO_2-Al_2O_3-CaO-FeO system in the ash composition. The properties of biomass are as diverse as the source origins (for example from wood, straw, grass, or residues). However, compared with coal, biomass usually has high volatile and oxygen contents, but low carbon content, heating value, and bulk density. It is worth to note that generally the sulfur content in biomass is low, typically less than 0.5 wt %. For the majority of biomass the ash has high contents of salts, such as KCl and NaCl, which is the main difference between biomass ash and coal ash, thus biomass ash has relatively low melting temperature. The knowledge of biomass properties is beneficial to applying biomass in the gasification plants originally designed to use coal and supporting the development of commercial biomass gasifiers. Moving bed gasifiers, fluidized bed gasifiers, and entrained flow gasifiers are three different types of gasifiers used today. Their characteristics are summarized and discussed. On the whole, compared with fixed bed and fluidized bed gasifiers, entrained flow gasifiers operate at higher temperatures with smaller particles to achieve a high carbon conversion within a few seconds and provide a high-quality syngas without tar. The produced syngas in the gasification process can be used for synthesis, which is applied to produce fuels and chemicals, and for combustion, which is applied to produce

power and heat. Moreover, the syngas characteristics and conditioning are usually more critical for synthesis than for combustion.

Besides the above summary and comparison of gasification technology, the present literature review mainly focuses on the effects of operating conditions on product distribution during biomass entrained flow pyrolysis and gasification respectively due to the close relationship between the initial pyrolysis step and further gasification step in the whole gasification process. During biomass pyrolysis, H_2 and CO are the main gas products. Higher temperature decreased the char and tar yields during pyrolysis. When the temperature was higher than 1100 °C, the soot yield also decreased with increasing temperature due to the faster reaction rate than the formation rate. The total yields of gas products increased as the temperatures increased, and the yields of the desired products, H_2 and CO, also increased. Increasing reactor length and steam addition during pyrolysis reduced the yields of char, tar, and soot mainly due to the improved conversion, and increased the total yields of gas products and the yields of H_2 and CO. When the particle size was less than 1.0 mm, generally no large influence of particle size on pyrolysis was observed. During biomass gasification, not only H_2 and CO but also CO_2 were the main gas products owing to the partial oxidation condition. Increasing temperature during gasification improved the carbon conversion and increased the producer gas yield. In generally, the H_2 and CO yields increased while the CO_2 and C_xH_y decreased as the temperature increased. Although increasing the excess air ratio improved the carbon conversion, the producer gas yield and especially the H_2 and CO yields decreased. In the studied temperature range of 700 – 1050 °C, a certain amount of char must be left in the syngas during gasification, and thus increasing residence time and reactor length could clearly increase the carbon conversion and the yields of producer gas, H_2, and CO. At 1050 °C, increasing the size of particles from 0.5 to 8.0 mm during gasification, the carbon conversion, the producer gas yield, and the yield of all the gas species decreased obviously due to the worse char conversion. On the whole, from a viewpoint of syngas utilization for fuels and chemicals, high temperature is desirable for providing high yields of H_2 and CO and achieving high carbon conversion. In addition, at high temperature, suitable excess air ratio, increased residence time, increased reactor length, and smaller particles are also favored for improving the carbon conversion.

1.5 References

[1] Higman C, Van der Burgt M. Gasification. Burlington: Gulf Professional Publishing. 2008.

[2] Basu P. Biomass gasification and pyrolysis: Practical design and theory. Oxford: Academic Press. 2010.

[3] Rezaiyan J, Cheremisinoff NP. Gasification technologies: a primer for engineers and scientists. Boca Raton: Taylor & Francis. 2005.

[4] Collet AG. Matching gasifiers to coal. IEA Clean Coal Centre. 2002.

[5] Gasification 2010 worldwide database. 2011. Available from: http://www.netl.doe.gov/technologies/coalpower/gasification/worlddatabase/2010_Worldwide_Gasification_Database.pdf.

[6] World energy outlook. 2008.

[7] Johansson TB, Kelly H, Reddy AKN, Williams R, Drennen TE. Renewable energy: sources for fuels and electricity. Washington, D.C.: Island Press, 1992:593-651.

[8] Stevens DJ. Hot gas conditioning: recent progress with larger-scale biomass gasification systems. NREL Subcontractor Report: NREL/SR-510-29952. 2001.

[9] Hamelinck CN, Faaij APC, den Uil H, Boerrigter H. Production of FT transportation fuels from biomass; technical options, process analysis and optimisation, and development potential. Energy 2004;29:1743-71.

[10] Savolainen K. Co-firing of biomass in coal-fired utility boilers. Appl Energy 2003;74:369-81.

[11] McLendon TR, Lui AP, Pineault RL, Beer SK, Richardson SW. High-pressure co-gasification of coal and biomass in a fluidized bed. Biomass Bioenergy 2004;26:377-88.

[12] McKendry P. Energy production from biomass (part 2): conversion technologies. Bioresour Technol 2002;83:47-54.

[13] Sheth PN, Babu B. Experimental studies on producer gas generation from wood waste in a downdraft biomass gasifier. Bioresour Technol 2009;100:3127-33.

[14] Hobbs M, Radulovic P, Smoot L. Combustion and gasification of coals in fixed-beds. Progress in Energy and Combustion Science 1993;19:505-86.

[15] Schilling HD, Bonn B, Krauss U. Coal gasification: existing processes and new developments. London: Graham & Trotman. 1981.

[16] Chen Y, Charpenay S, Jensen A, Wójtowicz MA, Serio MA. Modeling of biomass pyrolysis kinetics. Symposium (International) on Combustion 1998;27:1327-1334.

[17] Biagini E, Falcitelli M, Tognotti L. Devolatilisation and pyrolysis of biomasses: development and validation of structural models 2007.

[18] U.S. Energy Information Administration. International Energy Outlook. 2011.

[19] World Energy Council. Survey of Energy Resources. 2010.

[20] Twidell J, Weir AD. Renewable energy resources. London: Taylor & Francis. 2006.

[21] Ladanai S,Vinterbäck J. Global potential of sustainable biomass for energy. Report ISSN 1654-9406. 2009.

[22] Bridgwater AV, Czernik S, Piskorz J. Progress in biomass gasification: an overview. Progress in thermochemical biomass conversion. Cornwall: MPG Books Ltd, 2001:1-31.

[23] Sander B. Properties of Danish biofuels and the requirements for power production. Biomass Bioenergy 1997;12:177-83.

[24] Vassilev SV, Vassileva CG. A new approach for the combined chemical and mineral classification of the inorganic matter in coal. 1. Chemical and mineral classification systems. Fuel 2009;88:235-45.

[25] Vassilev SV, Kitano K, Takeda S, Tsurue T. Influence of mineral and chemical composition of coal ashes on their fusibility. Fuel Process Technol 1995;45:27-51.

[26] Institute of gas technology. Coal conversion systems technical data book. Virginia: Springfield. 1978.

[27] Speight JG. Handbook of coal analysis. New Jersey: John Wiley and Sons. 2005.

[28] Theis M, Skrifvars BJ, Zevenhoven M, Hupa M, Tran H. Fouling tendency of ash resulting from burning mixtures of biofuels. Part 2: Deposit chemistry. Fuel 2006;85:1992-2001.

[29] MILES T, BAXTER L, BRYERS R, JENKINS B, ODEN L. Alkali deposits found in biomass power plants: a preliminary investigation of their extent and nature. National Renewable Energy Laboratory: summary report. 1995.

[30] Vamvuka D, Zografos D. Predicting the behaviour of ash from agricultural wastes during combustion. Fuel 2004;83:2051-7.

[31] Vamvuka D, Zografos D, Alevizos G. Control methods for mitigating biomass ash-related problems in fluidized beds. Bioresour Technol 2008;99:3534-44.

[32] Moilanen A. Thermogravimetric Characterisations of Biomass and Waste for Gasification Processes. VIT Technical Research Center of Finland: report no. 607. 2007.

[33] Tortosa Masiá A, Buhre B, Gupta R, Wall T. Characterising ash of biomass and waste. Fuel Process Technol 2007;88:1071-81.

[34] Werther J, Saenger M, Hartge EU, Ogada T, Siagi Z. Combustion of agricultural residues. Progress in energy and combustion science 2000;26:1-27.

[35] Lapuerta M, Hernández JJ, Pazo A, López J. Gasification and co-gasification of biomass wastes: Effect of the biomass origin and the gasifier operating conditions. Fuel Process Technol 2008;89:828-37.

[36] Hernández JJ, Aranda-Almansa G, Bula A. Gasification of biomass wastes in an entrained flow gasifier: Effect of the particle size and the residence time. Fuel Process Technol 2010;91:681-92.

[37] Demirbaş A. Fuel characteristics of olive husk and walnut, hazelnut, sunflower, and almond shells. Energy Sources 2002;24:215-21.

[38] Demirbas A. Potential applications of renewable energy sources, biomass combustion problems in boiler power systems and combustion related environmental issues. Progress in energy and combustion science 2005;31:171-92.

[39] Demirbas A. Combustion characteristics of different biomass fuels. Progress in energy and combustion science 2004;30:219-30.

[40] Vassilev SV, Baxter D, Andersen LK, Vassileva CG. An overview of the chemical composition of biomass. Fuel 2010;89:913-33.

[41] Barrio M, Gøbel B, Rimes H, Henriksen U, Hustad J, Sørensen L. Steam gasification of wood char and the effect of hydrogen inhibition on the chemical kinetics. Progress in Thermochemical Biomass Conversion. Cornwall: MPG Books Ltd, 2001:32-46.

[42] ECN Phyllis: the composition of biomass and waste. 2002. Available from: http://www.ecn.nl/phyllis/.

[43] Moulijn JA, Makkee M, van Diepen A. Chemical process technology. New York: John Wiley & Sons. 2001.

[44] Simbeck DR, Korens N, Biasca FE, Vejtasa S, Dickenson RL. Coal gasification guidebook: status, applications, and technologies. Electric Power Research Institute Report TR-102034. 1993.

[45] Olofsson I, Nordin A, Söderlind U. Initial review and evaluation of process technologies and systems suitable for cost-efficient medium-scale gasification for biomass to liquid fuels. 1653-0551 ETPC Report 05-02. 2005.

[46] Collot AG. Matching gasification technologies to coal properties. International Journal of Coal Geology 2006;65:191-212.

[47] Collot AG. Matching gasifiers to coals. London: IEA Clean Coal Centre. 2002.

[48] Ratafia-Brown J, Manfredo L, Hoffmann J, Ramezan M. Major environmental aspects of gasification-based power generation technologies. U.S. Department of Energy Final Report. 2002.

[49] Greil C, Hirschfelder H. Biomass integrated CFB gasification combined cycle plants. Gasification: Gateway to a Cleaner Future (IChemE Conference) 1998.

[50] Ciferno JP,Marano JJ. Benchmarking biomass gasification technologies for fuels, chemicals and hydrogen production. U.S. Department of Energy and National Energy Technology Laboratory Report. 2002.

[51] Falbe J, Ahland E, Baron G. Gasification of coal. Chemical feedstocks from coal. New York: John Wiley and Sons, 1982:164-247.

[52] Septien S, Valin S, Dupont C, Peyrot M, Salvador S. Effect of particle size and temperature on woody biomass fast pyrolysis at high temperature (1000–1400° C). Fuel 2012;97:202-10.

[53] Septien Stringel S. High temperature gasification of millimetric wood particles between 800° C and 1400° C. Ph.D Thesis, National Polytechnic Institute of Toulouse. 2011.

[54] Zhang Y, Kajitani S, Ashizawa M, Miura K. Peculiarities of rapid pyrolysis of biomass covering medium-and high-temperature ranges. Energy Fuels 2006;20:2705-12.

[55] Sun S, Tian H, Zhao Y, Sun R, Zhou H. Experimental and numerical study of biomass flash pyrolysis in an entrained flow reactor. Bioresour Technol 2010;101:3678-84.

[56] Zanzi R, Sjostrom K, Bjornbom E. Rapid pyrolysis of bagasse at high temperature. Proceedings of the 3rd Asia-Pacific International Symposium on Combustion and Energy Utilization, Hong Kong 1995:211-215.

[57] Zanzi R, Sjöström K, Björnbom E. Rapid pyrolysis of agricultural residues at high temperature. Biomass Bioenergy 2002;23:357-66.

[58] Shafizadeh F. Introduction to pyrolysis of biomass. J Anal Appl Pyrolysis 1982;3:283-305.

[59] Zhang L, Xu S, Zhao W, Liu S. Co-pyrolysis of biomass and coal in a free fall reactor. Fuel 2007;86:353-9.

[60] Fagbemi L, Khezami L, Capart R. Pyrolysis products from different biomasses: application to the thermal cracking of tar. Appl Energy 2001;69:293-306.

[61] Wei L, Xu S, Zhang L, Zhang H, Liu C, Zhu H, et al. Characteristics of fast pyrolysis of biomass in a free fall reactor. Fuel Process Technol 2006;87:863-71.

[62] Porada S. The reactions of formation of selected gas products during coal pyrolysis. Fuel 2004;83:1191-6.

[63] Sharma R, Wooten J, Baliga V, Hajaligol M. Characterization of chars from biomass-derived materials: pectin chars. Fuel 2001;80:1825-36.

[64] Williams PT, Besler S. The pyrolysis of rice husks in a thermogravimetric analyser and static batch reactor. Fuel 1993;72:151-9.

[65] Cho S, Marlow D, Niksa S. Burning velocities of multicomponent organic fuel mixtures derived from various coals. Combust Flame 1995;101:399-410.

[66] Xu WC, Tomita A. The effects of temperature and residence time on the secondary reactions of volatiles from coal pyrolysis. Fuel Process Technol 1989;21:25-37.

[67] Xu WC, Tomita A. Effect of temperature on the flash pyrolysis of various coals. Fuel 1987;66:632-6.

[68] Xu WC, Tomita A. Effect of coal type on the flash pyrolysis of various coals. Fuel 1987;66:627-31.

[69] Lopez B, Blanco C, Martinez-Alonso A, Tascon J. Composition of gases released during olive stones pyrolysis. J Anal Appl Pyrolysis 2002;65:313-22.

[70] Uzun BB, Putun AE, Putun E. Composition of products obtained via fast pyrolysis of olive-oil residue: Effect of pyrolysis temperature. J Anal Appl Pyrolysis 2007;79:147-53.

[71] Chen JC, Castagnoli C, Niksa S. Coal devolatilization during rapid transient heating. 2. Secondary pyrolysis. Energy Fuels 1992;6:264-71.

[72] Doolan KR, Mackie JC, Tyler RJ. Coal flash pyrolysis: secondary cracking of tar vapours in the range 870–2000 K. Fuel 1987;66:572-8.

[73] Van Heek K, Hodek W. Structure and pyrolysis behaviour of different coals and relevant model substances. Fuel 1994;73:886-96.

[74] Jakab E, Faix O, Till F. Thermal decomposition of milled wood lignins studied by thermogravimetry/mass spectrometry. J Anal Appl Pyrolysis 1997;40:171-86.

[75] Neves D, Thunman H, Matos A, Tarelho L, Gomez-Barea A. Characterization and prediction of biomass pyrolysis products. Progress in Energy and Combustion Science 2011;37:611-30.

[76] Zhang H. Nitrogen evolution and soot formation during secondary coal pyrolysis. Ph.D Thesis, Department of Chemical Engineering, Brigham Young University. 2001.

[77] Budinova T, Ekinci E, Yardim F, Grimm A, Björnbom E, Minkova V, et al. Characterization and application of activated carbon produced by H_3PO_4 and water vapor activation. Fuel Process Technol 2006;87:899-905.

[78] Zhang Y, Kajitani S, Ashizawa M, Oki Y. Tar destruction and coke formation during rapid pyrolysis and gasification of biomass in a drop-tube furnace. Fuel 2010;89:302-9.

[79] Zhou J, Chen Q, Zhao H, Cao X, Mei Q, Luo Z, et al. Biomass-oxygen gasification in a high-temperature entrained-flow gasifier. Biotechnol Adv 2009;27:606-11.

[80] Hernández JJ, Aranda-Almansa G, Serrano C. Co-Gasification of Biomass Wastes and Coal– Coke Blends in an Entrained Flow Gasifier: An Experimental Study. Energy Fuels 2010;24:2479-88.

[81] Zhao Y, Sun S, Zhou H, Sun R, Tian H, Luan J, et al. Experimental study on sawdust air gasification in an entrained-flow reactor. Fuel Process Technol 2010;91:910-4.

[82] Zhao Y, Sun S, Tian H, Qian J, Su F, Ling F. Characteristics of rice husk gasification in an entrained flow reactor. Bioresour Technol 2009;100:6040-4.

[83] Zhou J, Zhao H, Cao X, Luo Z, Cen K. Syngas production with biomass entrained flow gasifciation. Acta Energiae Solaris Sinica 2008;29:1406-13.

[84] Niksa S, Kerstein AR. FLASHCHAIN theory for rapid coal devolatilization kinetics. 1. Formulation. Energy Fuels 1991;5:647-65.

[85] Babu B, Chaurasia A. Modeling for pyrolysis of solid particle: kinetics and heat transfer effects. Energy Conversion and Management 2003;44:2251-75.

[86] Bridgwater A. The technical and economic feasibility of biomass gasification for power generation. Fuel 1995;74:631-53.

Chapter 2 Biomass gasification behavior I

Abstract

Wood gasification was studied in a laboratory-scale atmospheric pressure entrained flow reactor. Effects of reactor temperature, steam/carbon ratio, excess air ratio, and biomass type on the solid, liquid and gas products were investigated. The biomass was completely converted at all investigated operating conditions and the syngas contained nearly no tar but some soot at the highest applied reactor temperature of 1350 °C. With a rise of reactor temperature from 1000 to 1350 °C, the yield of producer gas (defined as the sum of H_2, CO, CO_2, and light hydrocarbons up to C_3 species) increased dramatically by 72 %. The H_2/CO molar ratio in syngas was close to 1.0 at reactor temperature above 1200 °C with steam addition. Higher temperature was beneficial to lower the amount of tar while the soot yield showed a peak of 56.7 g/kg fuel (daf basis) at 1200 °C. With steam addition, the producer gas yield and in particular the H_2 yield increased gradually, while the CO yield decreased slowly. The molar ratio of H_2/CO was equal to 1.0 with the largest supplied amount of steam addition (H_2O/C = 1.0). Steam addition gave an obvious reduction in the soot yield, but it was not possible to completely avoid soot. Increasing excess air ratio from 0.25 to 0.50 gave no significant change in the producer gas yield, but the yields of H_2, CO, and soot decreased, the CO_2 yield increased, and the molar ratio of H_2/CO decreased. At 1350 °C with steam addition, the syngas composition is close to equilibrium as verified by calculation.

2.1 Introduction

Biofuels play an important role in helping to address some global challenges, such as energy supply security, and environment and climate protection [1-6]. Governments, particularly those in the OECD (Organization for Economic Cooperation and Development) are striving to become less dependent on imported oil and are seeking diversified sources of energy supply. Biofuels can contribute to a more secure and diverse energy supply [5,6]. Furthermore, biofuels are CO_2 neutral because the growth of new plants will absorb CO_2 through photosynthesis even though the production and consumption of biofuels emit CO_2 as well. Therefore, utilization of biofuels can reduce dependence on imported oil, reduce CO_2 emission, and provide a growing market for the farming community.

Gasification is a thermochemical process currently available for biofuel production, and converts solid carbonaceous materials to a synthesis gas, a mixture rich in H_2, CO, CO_2, and

CH_4, by partial oxidation at elevated temperature [7,8]. The syngas produced by gasification can be used to synthesize liquid fuels and chemicals or to produce power in a combined cycle plant. However, some challenges of the gasification technology still exist, such as the utilization of biomass in entrained flow gasifiers originally designed for coal, as well as ash behavior and formation of soot and tar.

Compared with fixed bed and fluidized bed gasification, entrained flow gasification operates at higher temperature with smaller particles, often achieves a high carbon conversion, and produces a high quality syngas with low methane and tar content [9,10]. Coal gasification in entrained flow gasifiers has been studied to some extent [11-16]. However, systematic studies on gasification of biomass in entrained flow gasifiers are scarce, and these studies mainly focus on the gas compositions [17-21] and are performed at relatively low temperatures (700 – 1050 °C) [10,17,20]. Steam addition has a significant influence on the coal gasification [13], but there are no studies of the effect of steam addition on biomass gasification in an entrained flow reactor. Entrained flow gasifiers usually operate at high temperature (> 1200 °C) to produce a syngas with low or no tar content, however soot produced at higher temperature is another serious issue, especially for biomass because of its high volatile content. Nevertheless, according to the authors' best knowledge, there is no literature considering soot formation in biomass entrained flow gasification. Therefore, a systematic study of biomass gasification in an entrained flow reactor is of great practical and scientific interest.

In the present study, a gasification system including a laboratory-scale entrained flow reactor (5 kW) and other auxiliary facilities were developed. Biomass gasification was investigated concentrating on the effects of operating parameters, such as reactor temperature (T), steam/carbon ratio (H_2O/C), excess air ratio (λ) on the product yield (soot, tar, and $H_2/CO/CO_2$/light hydrocarbons). The objective is to provide valuable insights into the biomass gasification in an entrained flow reactor and especially to fill in a gap on knowledge of soot formation and yield in this process.

2.2 Experimental

2.2.1 Setup

The experimental setup used for the present work is shown schematically in Figure 2.1. The entrained flow gasification system is comprised of a gas preheater, vertical reactor, fuel feeding system, gas supply system, gas sampling and analysis system, and solid particle

sampling system. The 0.8 m long gas preheater is located on the top of the reactor and consists of two electrical heating elements. The SiC reaction tube inside the reactor has a length of 2 m with an inner diameter of 0.08 m and is externally heated by seven independent electrical heating elements to obtain a maximum temperature of 1500 °C. In the present work, one heating element at the top of the gas preheater and two heating elements at the bottom of the reactor were broken. Thus, the effective heating length of gas preheater and reactor are approximate 0.4 m and 1.4 m respectively.
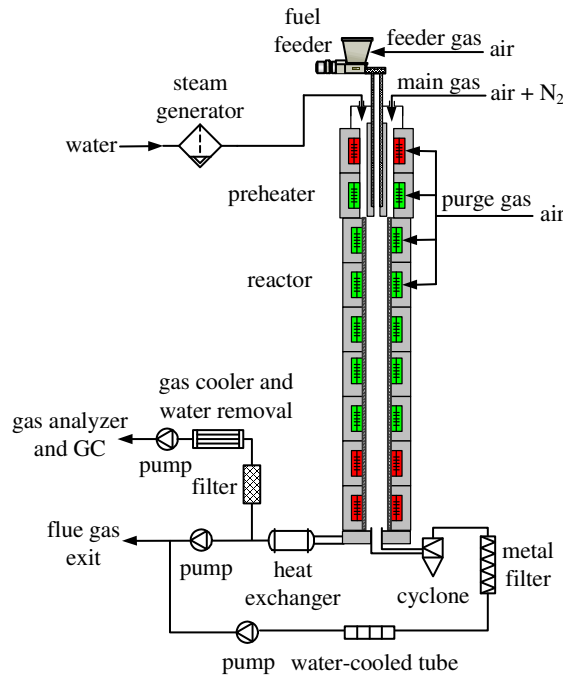

Figure 2.1 Sketch of experimental setup

The fuel feeder is located in a pressure tight container so that the flow of feeding gas can be controlled accurately. The fuel feeding rate is measured by weighing the silo and the strew feeder. In order to obtain a steady fuel feeding rate, a vibration table is employed between the screw feeder and the water-cooled feeding probe.

The gas supply system is composed by mass flow meters and magnetic valves, which make it possible to mix gases and direct them to various purposes: to the fuel feeder (as feeder gas), to the preheater and reactor (as main gas), and to the heating elements of the preheater and reactor (as purge gas). The fuel and feeder gas are kept cold by using the water-cooled feeding probe inside the gas preheater, and the main gas is heated to the desired temperature by the gas preheater. Besides, the steam is produced by a steam generator and injected into the gas preheater together with the main gas. The feeder gas entrained with fuel particles is mixed

with the steam, main gas, and purge gas at the inlet of the reaction tube and subsequently they reacted in the reaction tube.

After the heat exchanger and before the gas cooler, the gas sampling line is heated to 100 °C in order to prevent water condensation. The gas products are continuously sampled and are cleaned and dried by a filter and a gas cooler. The composition of gas samples (mainly H_2, CO, CO_2, and light hydrocarbons) without dust and water was measured online by a nondispersive infrared (NDIR) gas analyzer and a gas chromatograph (Agilent 6890N). The analytical error from these two equipment is less than 5 %.

When the measured gas composition reached a stable state, a certain amount of syngas was drawn to a solid sampling system through a bottom sampling probe according to the principle of isokinetic sampling. In the solid sampling system, the larger particles (e.g. char) were collected by a cyclone and the smaller particles (e.g. soot) passing the cyclone were captured by a metal filter. The designed cut size of the cyclone was 2.5 µm and the size of pore in the metal filter is 1 µm. The bottom sampling probe, cyclone and filter were heated to 400 °C to avoid liquid condensation. The solid particles were sampled for 10 min during each experiment that lasted approximately 60 min. After each experiment, when the solid sampling system was cooled to room temperature, the solid particles in the cyclone and metal filter were gathered, weighed, and preserved for further analysis.

2.2.2 Materials

Wood (beech sawdust) was used as fuel in all experiments. The results of ultimate and proximate analysis are listed in Table 2.1. It is shown that wood has a high volatile content while low fixed carbon content and heating value. The particle size distribution of wood is shown in Figure 2.2. The median diameter (d_{50}) of the wood particles is 310 µm.

Table 2.1 Properties of wood

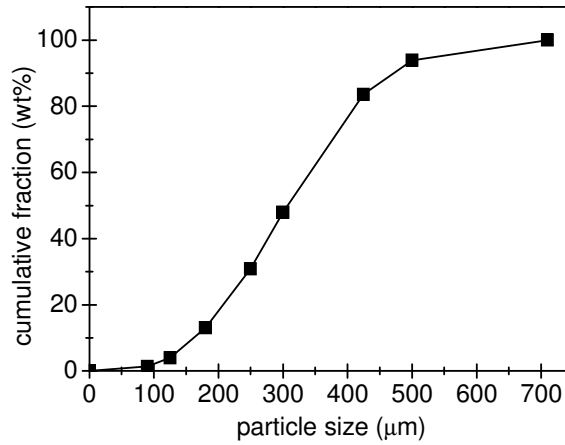| properties		wood (as-received basis)
moisture	wt %	9.04
ash	wt %	0.61
volatile	wt %	76.70
fixed carbon	wt % (by diff.)	13.65
lower heating value	MJ/kg	16.44
C	wt %	45.05
H	wt %	5.76
O	wt % (by diff.)	39.41
N	wt %	0.13
S	wt %	0.01

Figure 2.2 Particle size distribution of wood

2.2.3 Conditions

The applied experiments are listed in Table 2.2. In this study, three reactor temperatures (T) were selected: 1000, 1200, and 1350 °C. The steam/carbon ratio (H_2O/C) was varied between 0 and 1. The excess air ratio (λ) was changed in the range of 0.25 – 0.50. In order to obtain an isothermal condition in the entrained flow reactor, besides air used as reaction gas, a large amount of nitrogen was used as balance gas which led to a low oxygen concentration (O_2) in the combined reaction gas (5 – 10 %). Keeping the fuel feeding rate and total flows of air and nitrogen constant, the effects of reactor temperature, steam/carbon ratio, and excess air ratio were studied. In the present work, the steam/carbon ratio, excess air ratio, and oxygen concentration were calculated as below:

$$\text{steam/carbon ratio (mol/mol)} = \frac{\text{the amount of supplied steam(mol/min)}}{\text{the amount of carbon in fuel(mol/min)}} \qquad (2.1)$$

$$\text{excess air ratio }(-) = \frac{\text{the amount of supplied air for fuel gasifciation(NL/min)}}{\text{the amount of required air for complete fuel oxidation(NL/min)}} \qquad (2.2)$$

$$\text{oxygen concentration }(\%) = \frac{\text{the amount of supplied oxygen in feeder and main gas(NL/min)}}{\text{the amount of feeder and main gas(NL/min)}} \times 100\ \% \qquad (2.3)$$

The particle residence time (t) in the reactor was approximately 2 – 3 s, which was determined by the gas mean residence time assuming no relative velocity between the solid phase and gas phase. It was not possible to measure the total gas flow directly. Thus the total flow was calculated by using N_2 as a tracer, from which the gas product yield per kilogram fuel (Nm^3/kg fuel, dry and ash-free basis) can be calculated. Also, the solid product yield can be expressed by the similar unit (g/kg fuel, dry and ash-free basis).

Table 2.2 List of conducted experiments

NO.	fuel feeding rate g/min	air flow NL/min	nitrogen flow NL/min	steam flow g/min	T °C	H_2O/C mol/mol	λ -	O_2 %	t s
1	9.2	10	30	3.3	1000	0.5	0.25	5	2.98
2	9.2	10	30	0	1200	0.0	0.25	5	2.49
3	9.2	10	30	3.3	1200	0.5	0.25	5	2.51
4[a]	9.2	10	30	0	1350	0.0	0.25	5	2.21
5	9.2	13	26	0	1350	0.0	0.35	7	2.21
6	9.2	19	21	0	1350	0.0	0.50	10	2.24
7	9.2	10	30	3.3	1350	0.5	0.25	5	2.15
8	9.2	13	26	3.3	1350	0.5	0.35	7	2.17
9	9.2	19	21	3.3	1350	0.5	0.50	10	2.23
10[a]	9.2	10	30	6.7	1350	1.0	0.25	5	2.15
11	9.2	13	26	6.7	1350	1.0	0.35	7	2.17

[a] Repetition experiments were performed

2.3 Results and discussion
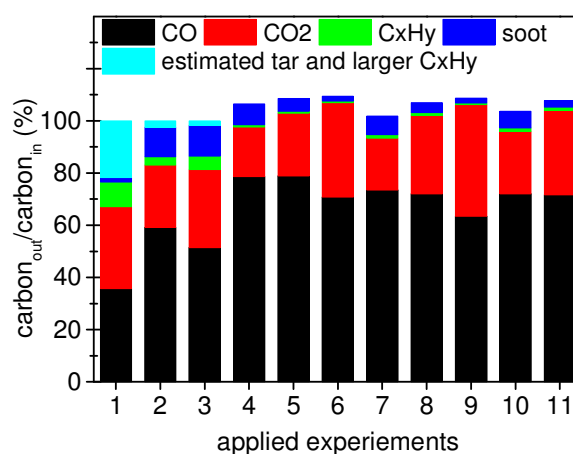
2.3.1 Carbon mass balance

Figure 2.3 Carbon balances for all applied experiments: the carbon contents in CO, CO_2, C_xH_y, and soot are calculated based on the experimental measurement, while the carbon content in tar and larger C_xH_y is determined by the gap of the carbon mass balance

In all applied experiments, no converted char was left in the cyclone, while soot was always observed in the metal filter. Based on the measured data of soot (filter sample, defined as pure carbon) and gas products, carbon mass balances were calculated for all applied experiments listed in Table 2.2, and the results are shown in Figure 2.3. In the figure, the contents of CO, CO_2, C_xH_y (lighter hydrocarbons including CH_4, C_2H_4, and C_3H_8), and soot were calculated by the measured products, while the tar and larger hydrocarbons contents were estimated by the gap of the carbon mass balance. In the experiment, NO. 1 (at 1000 °C) listed in Table 2.2, the carbon mass balance has a large deviation (22 wt %) probably due to the high contents of tar and larger hydrocarbons in the syngas. At higher temperatures (at 1200 and 1350 °C), the carbon mass balance closure was better, typically within ± 9 %. The hydrogen and oxygen

mass balance could not be closed since the water yield were not determined, so they are not shown in the present study.

2.3.2 Effects of gasification parameters

2.3.2.1 Reactor temperature

In high temperature entrained flow gasification, unburned char, soot and ash are normally the solid products. However, in the present study, biomass was completely converted and no unburned char was left, while soot often was observed. Very low amounts of ash were collected in the cyclone, because the ash mainly melted and deposited on the wall of the reactor due to the high temperature and the remaining small amount probably was mixed with soot. Figure 2.4 (a) shows the effect of reactor temperature on the soot yield during wood gasification at $\lambda = 0.25$. A sharp increase from 8.5 to 58.7 g/daf kg fuel (kg fuel on a dry and ash-free basis) in the soot yield was observed when the reactor temperature was increased from 1000 to 1200 °C at $H_2O/C = 0.5$. Then it declined to 35.3 g/daf kg fuel as the reactor temperature further increased to 1350 °C. It is widely observed that soot is produced in high temperature processes (1000 – 2500 °C), such as pyrolysis and gasification [22-27]. Thus increasing the reactor temperature favors soot formation. However, at higher temperature, soot or its precursors probably have higher gasification reactivity. As a result of the competition between soot formation and destruction [27-30], its yield starts to drop down after reaching a peak value at 1200 °C. As shown in Figure 4, the same trend was observed for the experiments without steam addition ($H_2O/C = 0.0$) at higher temperature (1200 – 1350 °C).

Comparing Figure 2.4 (a) to Figure 2.3, it is found that the soot yield was lowest at 1000 °C, whereas the amount of tar in the syngas was highest. However, at 1350 °C a significant yield of soot was produced, while there was nearly no tar in the syngas due to cracking and the reaction with steam of the heavy hydrocarbon chains to form H_2, CO, and CO_2 [31]. This shows that there is a tradeoff between soot and tar formation, which may result from soot formation by tar and hydrocarbon polymerization competing with soot gasification by CO_2 and H_2O at high temperature.
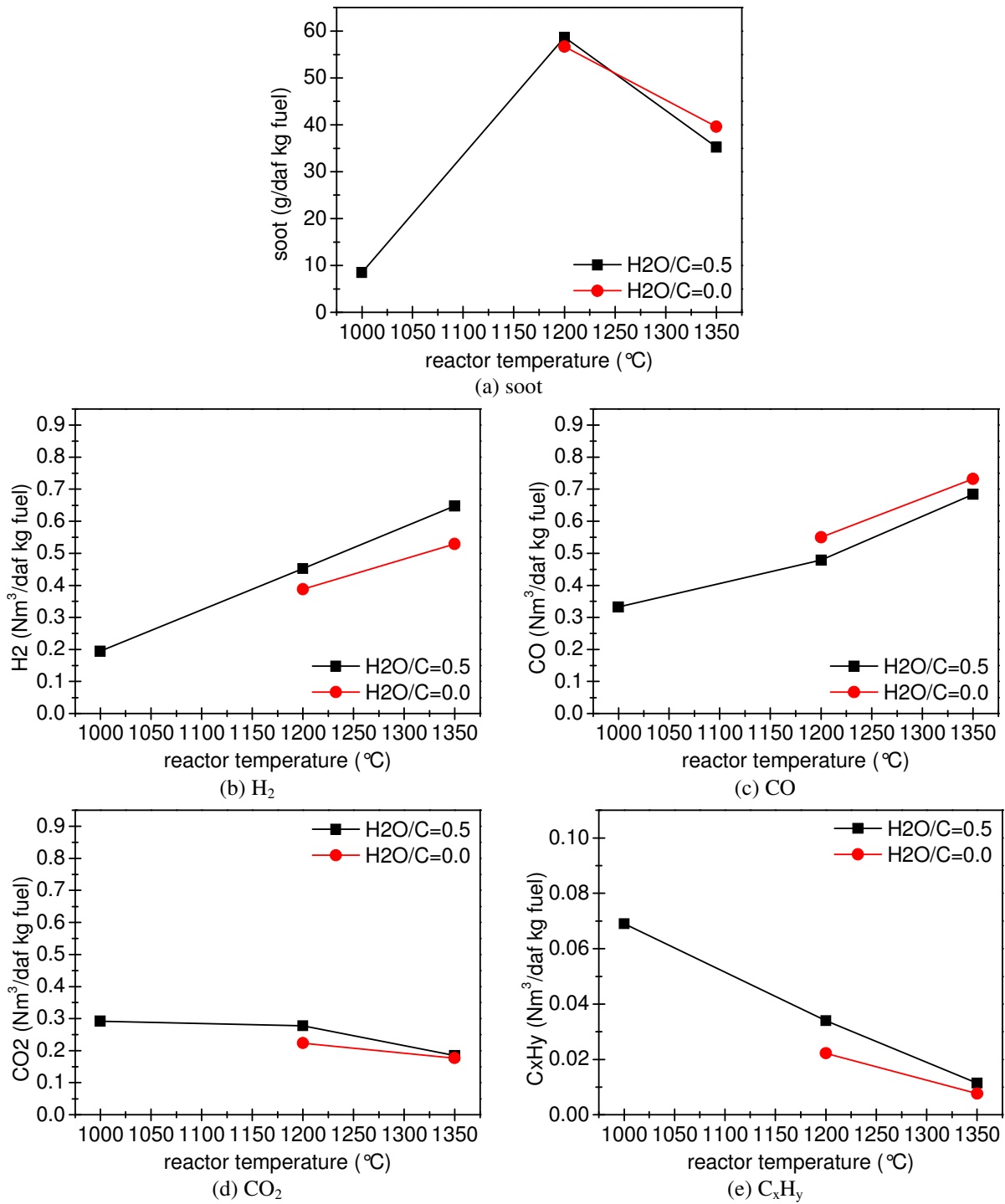
(a) soot

(b) H_2

(c) CO

(d) CO_2

(e) C_xH_y

Figure 2.4 Effect of reactor temperature on the product yield during wood gasification at λ = 0.25

The yields of H_2, CO, CO_2, and C_xH_y (total amount of light hydrocarbons up to C_3 species) at different reactor temperatures during wood gasification at λ = 0.25 are shown in Figure 2.4 (b) – (e). The yields of H_2 and CO increased from 0.19 to 0.65 Nm^3/daf kg fuel (kg fuel on a dry and ash-free basis) and 0.33 to 0.68 Nm^3/daf kg fuel respectively when the reactor temperature increased from 1000 to 1350 °C at H_2O/C = 0.5, while the yields of CO_2 and C_xH_y decreased from 0.29 to 0.19 Nm^3/daf kg fuel and 0.069 to 0.011 Nm^3/daf kg fuel

respectively. The yields of measured hydrocarbons at different temperatures are shown in Figure 2.5. CH_4 is the major product in hydrocarbons, which decreased quickly with a rise of temperature. The yields of C_2H_4 and C_3H_8 are very low in the whole temperature range, and especially at higher temperatures, there is almost no formation of C_2H_4 and C_3H_8. As thermodynamically predicted, the declining yield of CO_2 may be explained as being due to the consumption of CO_2 by dry reforming reactions of hydrocarbons. These reactions increase with temperature and cause the yield of C_xH_y to decrease and the yields of H_2 and CO to increase [31,32]. The steam reforming reactions of hydrocarbons increase with temperature as well. These reactions also lead to the decreasing yield of C_xH_y and the increasing yields of H_2 and CO. Meanwhile, higher temperature (> 1200 °C) reverses the exothermic water gas shift reaction, which also reduces the yield of CO_2. Besides, the soot produced at higher temperature probably could be partly gasified by CO_2, which causes the reduction of the CO_2 yield too. The gas product distribution displayed similar trends when no steam was introduced ($H_2O/C = 0.0$).
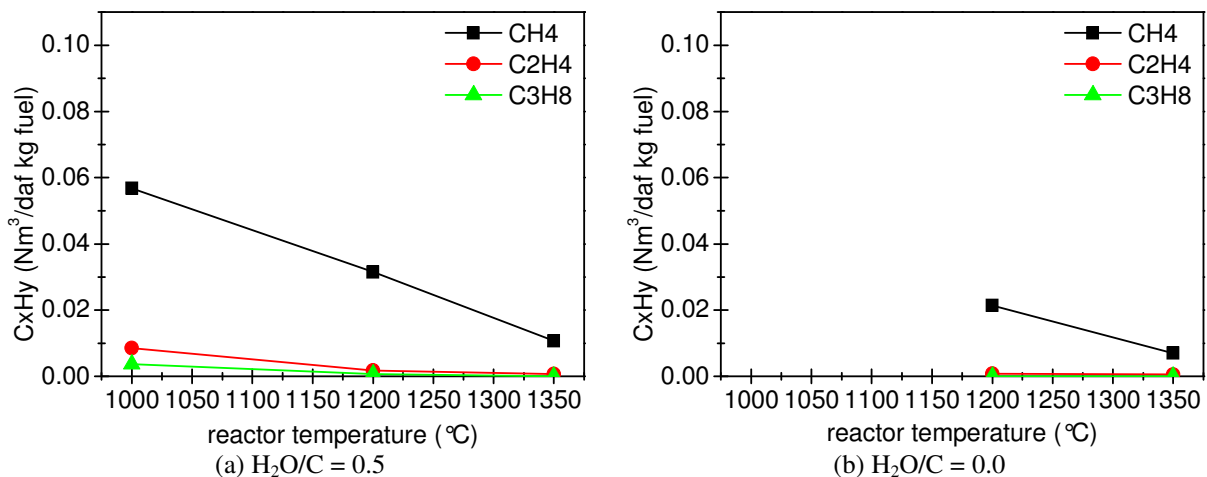

Figure 2.5 Effect of reactor temperature on the individual C_xH_y yields during wood gasification at λ = 0.25

The producer gas yield is an important indicator to evaluate the gasification process. As much gas as possible produced per unit fuel is desired, especially the yields of H_2 and CO. The effect of reactor temperature (1000, 1200, and 1350 °C) on the producer gas yield during wood gasification at λ = 0.25 is shown in Figure 2.6 (a). It can be seen that the producer gas yield, which is defined as the sum of H_2, CO, CO_2, and C_xH_y, increased from 0.89 to 1.53 Nm^3/daf kg fuel with an increase of the reactor temperature from 1000 to 1350 °C at $H_2O/C = 0.5$. The increased gas formation is mainly for two reasons: the steam cracking and reforming of tar and heavier hydrocarbons, which increase with temperature [33,34], and also soot gasification is promoted at higher temperature. Biomass was completely converted and no

unburned char was collected in the present study, so there is no direct relation between the increased yield of producer gas with reactor temperature and char gasification reactions. The yield of producer gas also increased from 1.18 to 1.45 Nm^3/daf kg fuel (daf basis) with increased reactor temperature from 1200 to 1350 °C at $H_2O/C = 0.0$. The molar ratio of H_2/CO in the producer gas is another important indicator for gasification. For different chemical utilization of syngas, different ratio is required. In higher alcohols synthesis, a molar ratio of H_2/CO close to 1.0 is favored [35]. The molar ratio of H_2/CO as a function of the reactor temperature is shown in Figure 2.6 (b). This ratio increased from 0.6 to 1.0 when the reactor temperature was increased from 1000 to 1200 °C at $H_2O/C = 0.5$, and was then nearly constant even when the temperature increased to 1350 °C. The molar ratio of H_2/CO also can be kept around 0.7 in the temperature range of 1200 – 1350 °C at $H_2O/C = 0.0$. Consequently, it can be concluded that at $\lambda = 0.25$, the molar ratio of H_2/CO can approximately keep constant at higher temperatures (> 1200 °C), particularly with steam addition, it can stay close to 1 due to the water gas shift reaction.
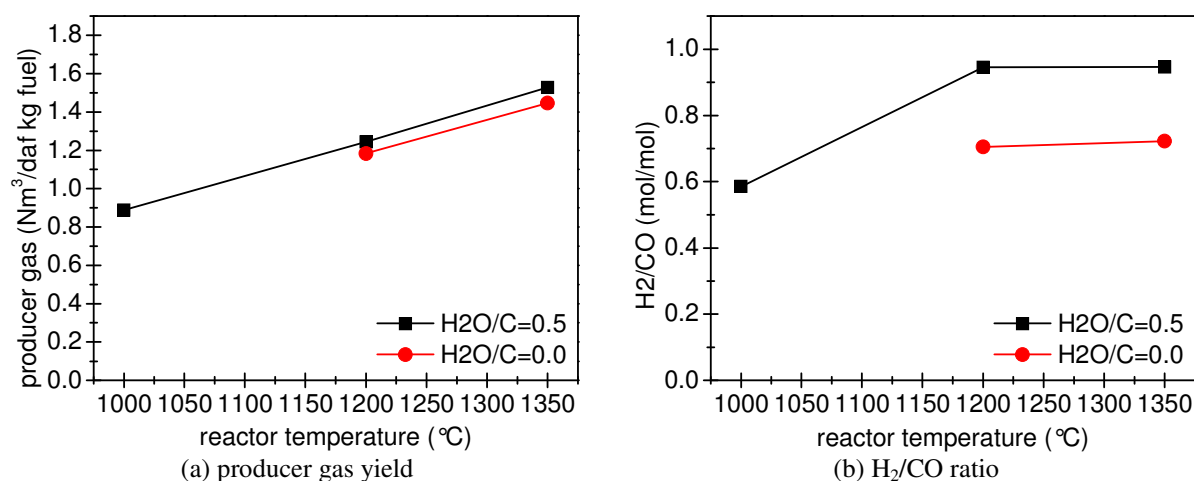

(a) producer gas yield   (b) H_2/CO ratio

Figure 2.6 Effect of reactor temperature on the indicators during wood gasification at λ = 0.25

2.3.2.2 Steam/carbon ratio

Figure 2.7 (a) shows the effect of steam/carbon ratio on the soot yield during wood gasification at 1350 °C. As the steam/carbon ratio was increased from 0.0 to 1.0, the soot yield decreased from 39.6 to 31.3 g/daf kg fuel at $\lambda = 0.25$ and from 24.6 to 12.2 g/daf kg fuel at $\lambda = 0.35$. Clearly, the steam addition is helpful to reduce the soot yield, but it is not possible to completely remove soot in the syngas.

The effect of steam/carbon ratio on the gas yield during wood gasification at 1350 °C is depicted in Figure 2.7 (b) – (e). When the steam/carbon ratio increased from 0.0 to 1.0, the H_2 and CO_2 yields increased gradually from 0.53 to 0.65 Nm^3/daf kg fuel and from 0.18 to 0.22

Nm^3/daf kg fuel respectively at $\lambda = 0.25$, accompanied with a little decrease of the CO yield from 0.73 to 0.67 Nm^3/daf kg fuel. The probable reason is that steam addition promotes the soot-steam gasification reaction and the water gas shift reaction [16,36]. When the steam/carbon ratio was increased from 0.0 to 1.0, the C_xH_y yield only had a small rise of 0.004 Nm^3/daf kg fuel at $\lambda = 0.25$, which might be caused by the cracking and reforming of larger hydrocarbons and tar. Similar trends were observed at $\lambda = 0.35$.
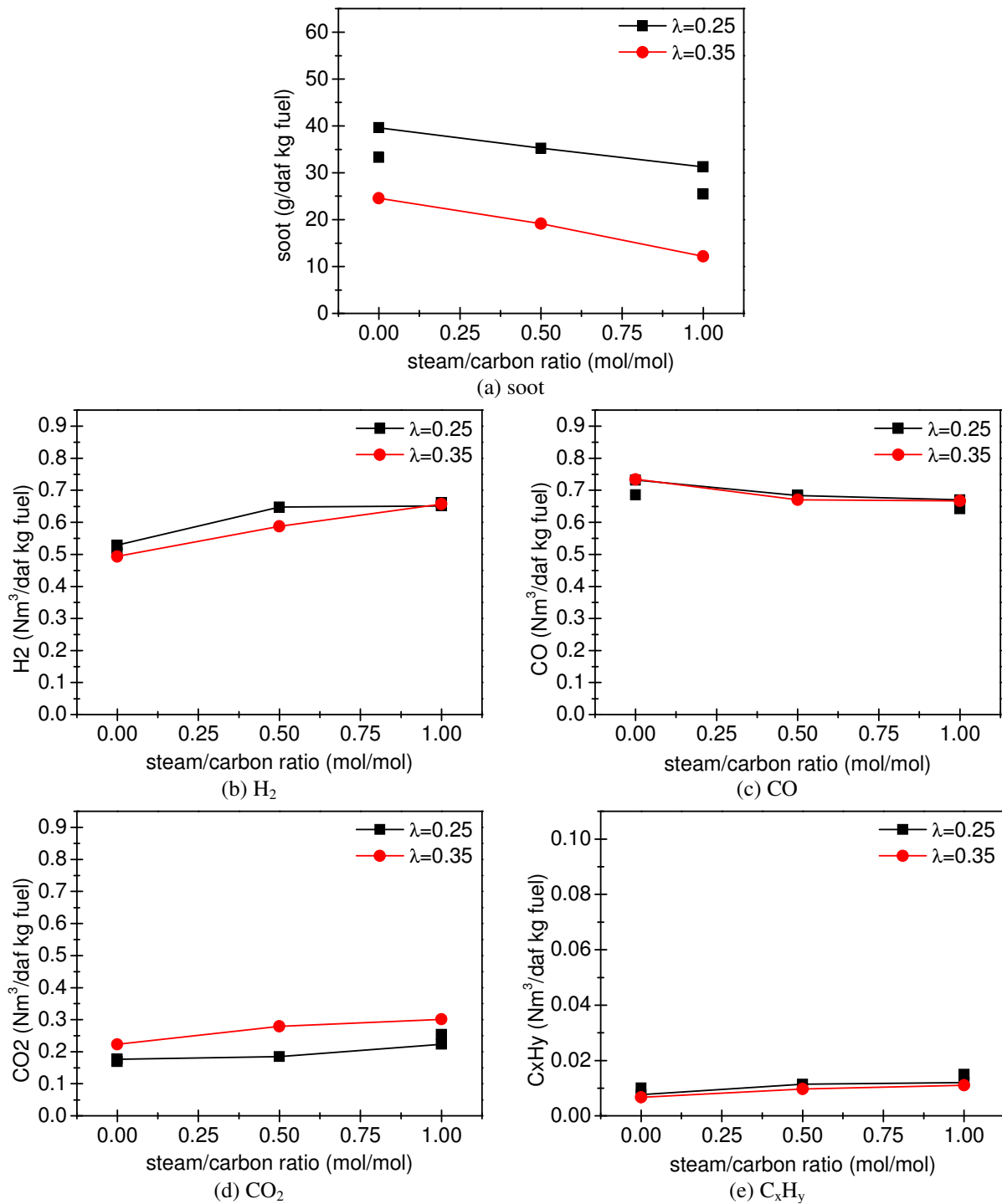

(a) soot

(b) H$_2$

(c) CO

(d) CO$_2$

(e) C$_x$H$_y$

Figure 2.7 Effect of steam/carbon ratio on the product yield during wood gasification at 1350 °C

The variation of the producer gas yield with the steam/carbon ratio during wood gasification at 1350 °C is shown in Figure 2.8 (a). With addition of steam, the producer gas yield increased about 0.11 – 0.18 Nm^3/daf kg fuel, most likely due to the promotion of steam gasification of soot and the increase of steam cracking and reforming of larger hydrocarbons and tar. According to Figure 2.7 (b) – (e) and Figure 2.8 (a), it can be concluded that even a high amount of steam injection ($H_2O/C = 1.0$) only makes small changes of the gas yields. The effect of steam/carbon ratio on the molar ratio of H_2/CO during wood gasification at 1350 °C is shown in Figure 2.8 (b). This ratio increased from 0.7 to 1.0 with the increased steam/carbon ratio from 0.0 to 0.5 at $\lambda = 0.25$, and was then nearly constant at steam/carbon ratio larger than 0.5. At $\lambda = 0.35$, the molar ratio of H_2/CO kept increasing continually with the steam/carbon ratio in the range of 0.0 – 1.0, and its maximum value was also 1. The molar ratio of H_2/CO is equal to 1 with the largest supplied amount of steam addition ($H_2O/C = 1.0$). The repeated experimental results are also shown in Figure 2.7 and Figure 2.8, which have a good repeatability.
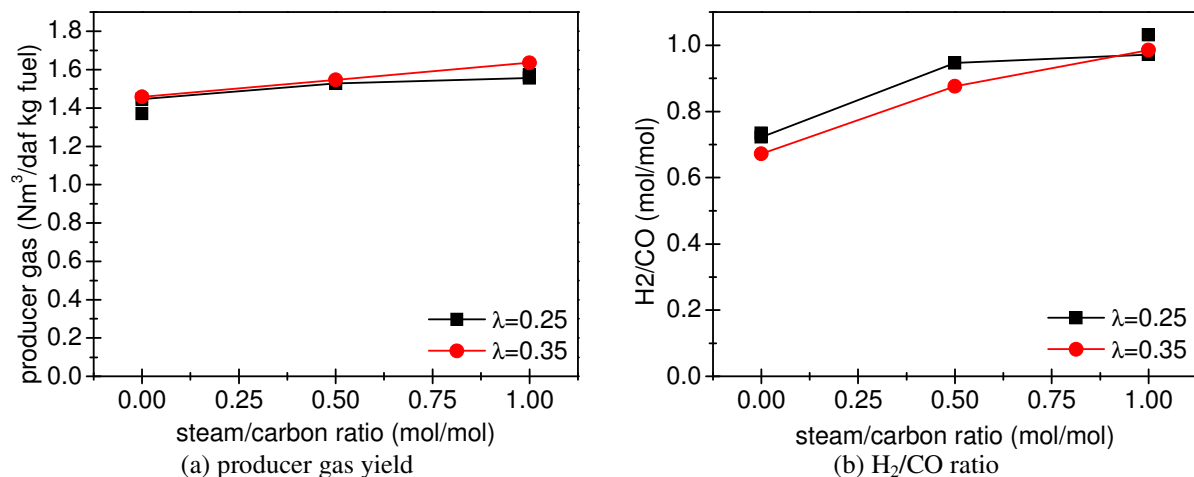

Figure 2.8 Effect of steam/carbon ratio on the indicators during wood gasification at 1350 °C

2.3.2.3 Excess air ratio

The varied excess air ratio was obtained by changing the gas composition but fixing the fuel feeding rate and total gas flow. It was increased from 0.25 to 0.50 accompanying with a little rise of the oxygen concentration from 5 to 10 %. Figure 2.9 (a) presents the effect of excess air ratio on the soot yield during wood gasification at 1350 °C. The amount of soot decreased significantly from 35.3 to 9.4 g/daf kg fuel at $H_2O/C = 0.5$ and from 39.6 to 9.3 g/daf kg fuel at $H_2O/C = 0.0$ respectively with increasing excess air ratio from 0.25 to 0.50. This is because a larger part of the soot or soot precursors are combusted with increasing excess air ratio.
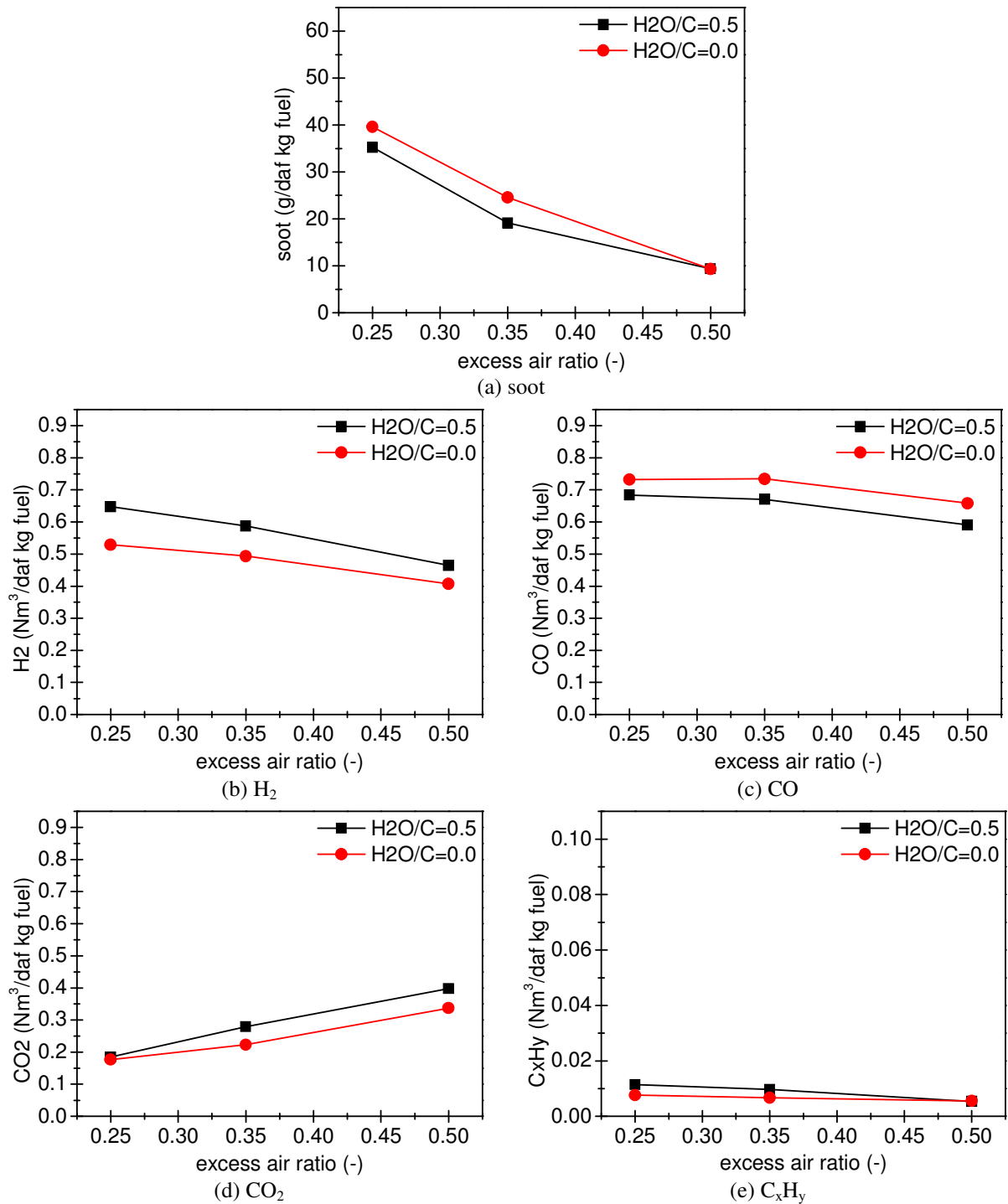
(a) soot

(b) H_2

(c) CO

(d) CO_2

(e) C_xH_y

Figure 2.9 Effect of excess air ratio on the product yield during wood gasification at 1350 °C

The effect of excess air ratio on the gas yield during wood gasification at 1350 °C is shown in Figure 2.9 (b) – (e). When the excess air ratio was increased from 0.25 to 0.50, the yields of H_2 and CO decreased from 0.65 to 0.47 Nm^3/daf kg fuel and 0.68 to 0.59 Nm^3/daf kg fuel respectively at $H_2O/C = 0.5$, and the C_xH_y yield reduced from 0.011 to 0.005 Nm^3/daf kg fuel, whereas the CO_2 yield increased from 0.19 to 0.40 Nm^3/daf kg fuel. This is due to the oxidation of soot, H_2, CO, and other gaseous species [13,16,19,37]. There was no large drop

in the CO yield when the excess air ratio increased from 0.25 to 0.35, probably because the partial combustion of hydrocarbons and soot could produce a certain amount of CO and then a part of them might be further oxidized to CO_2, which nearly keeps the CO yield constant. However, when the excess air ratio was increased to 0.50, the CO yield decreased. With and without steam addition, the gas yield had the same variation tendency as the excess air ratio increased.
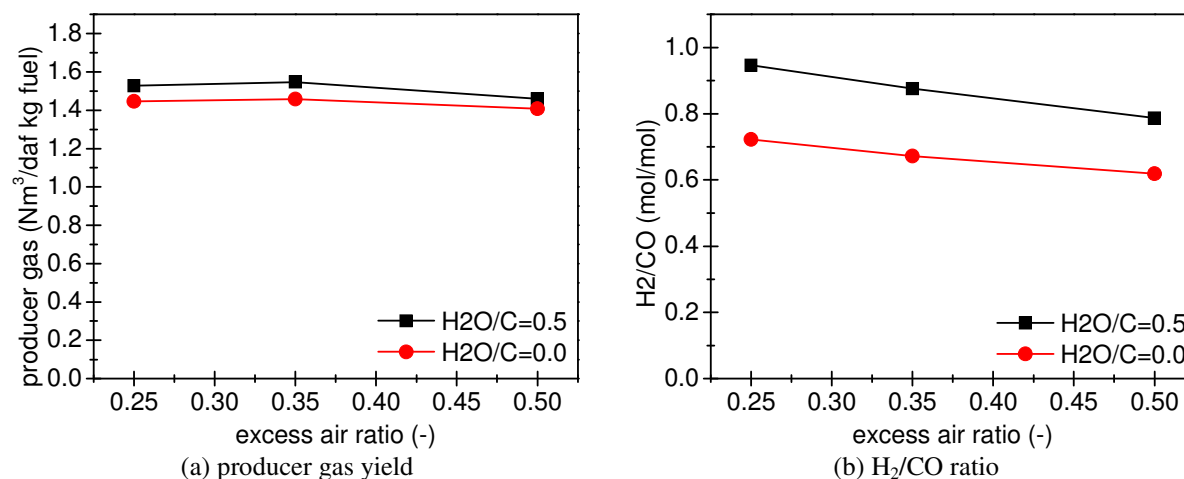

(a) producer gas yield (b) H_2/CO ratio

Figure 2.10 Effect of excess air ratio on the indicators during wood gasification at 1350 °C

The producer gas yield shown in Figure 2.10 (a) is obtained at different excess air ratios in the range of 0.25 – 0.50 during wood gasification at 1350 °C. The amount of producer gas nearly kept constant with an increase of excess air ratio especially between 0.25 and 0.35. The soot oxidation forms gas while the H_2 combustion consumes gas, so based on an overall consideration of formation and consumption, the increased excess air ratio does not influence the producer gas yield a lot. The molar ratio H_2/CO as a function of excess air ratio during wood gasification at 1350 °C is depicted in Figure 2.10 (b). This ratio decreased from 1.0 to 0.8 when the excess air ratio increased from 0.25 to 0.50 at $H_2O/C = 0.5$. The yields of H_2 and CO also decreased with a rise of excess air ratio. Thus, these observations reveal that the H_2 yield decreases faster than the CO yield with the increased excess air ratio. A small excess air ratio is required if a high molar ratio of H_2/CO is preferred. Without steam addition, the same trends can be observed.

2.3.3 Comparison between experimental and equilibrium calculations results

The equilibrium product composition is calculated by using the FactSage Program at the experimental conditions. There was not observed any carbon and hydrocarbons formation in

the equilibrium calculation, so the products are H_2, CO, CO_2, and H_2O. The product distributions of experiments and calculations are compared in Figure 2.11. In Figure 2.11 (a), the product distributions are based on the carbon mass balances. The estimated tar and larger hydrocarbons contents (experiments NO. 1, 2, and 3 listed in Table 2.2) are determined by the gap of the carbon mass balance. In Figure 2.11 (b), the product distributions are based on the hydrogen mass balances. Since water, tar, and larger hydrocarbons yields were not measured in the experiments, the estimated products contents are shown as a gap in the hydrogen mass balance. At 1350 °C, the unmeasured products are mostly water, while at lower temperatures (1000 and 1200 °C), the unmeasured products are a mixture of water, tar and larger hydrocarbons. From the Figure 2.11 (a) and (b), it is observed that at 1350 °C and with steam addition (experiments NO. 7, 8, 9, 10, and 11 listed in Table 2.2), the experimental results are reasonably similar to the calculation results indicating that chemical equilibrium is obtained in the experiments. Addition of steam promotes the conversion of soot and hydrocarbons because the rate of reaction with steam is faster than with CO_2 [38] and thereby equilibrium conditions are obtained in the limited residence time.

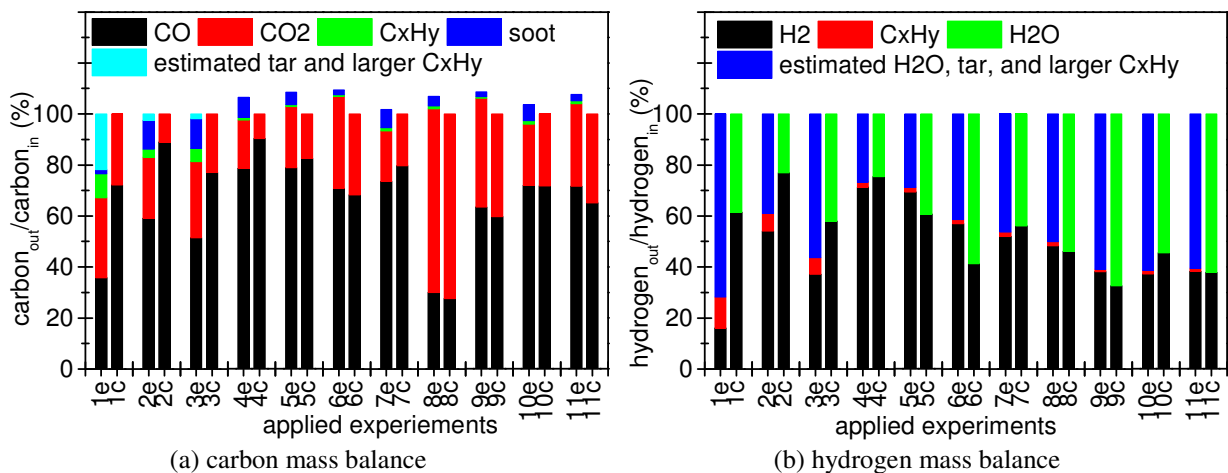(a) carbon mass balance   (b) hydrogen mass balance

Figure 2.11 Comparison of the results between experiment and equilibrium calculation: e means experimental results and c means equilibrium calculation results

Recalculated experimental results at the operating conditions without steam addition (e.g. experiments NO. 4 listed in Table 2.2) are presented in Figure 2.12. Assuming that all the soot and hydrocarbons react with CO_2 to produce CO, the recalculated and normalized experimental results can be compared with equilibrium calculations in Figure 2.12. It is observed that the recalculated and normalized experimental results are nearly similar to the equilibrium calculation results. Therefore, at 1350 °C without steam addition, the main difference between the experimental condition and the equilibrium condition is the limited reactions of CO_2 with soot and hydrocarbons.
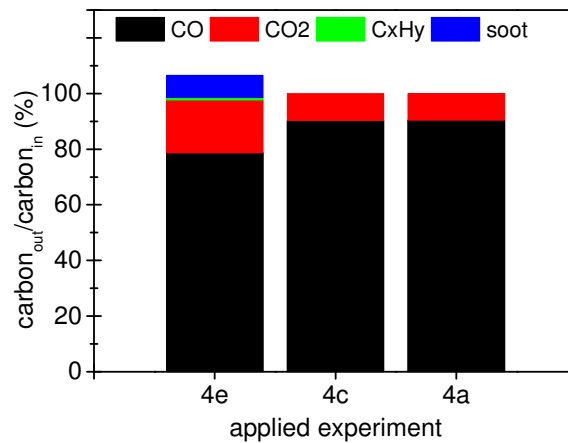
Figure 2.12 Comparison of the results among experiment, equilibrium calculation and assumption at 1350 °C with $H_2O/C = 0.0$ and $\lambda = 0.25$: e means experimental results, c means equilibrium calculation results and a means recalculated and normalized experimental results assuming soot and hydrocarbons are gasified by CO_2
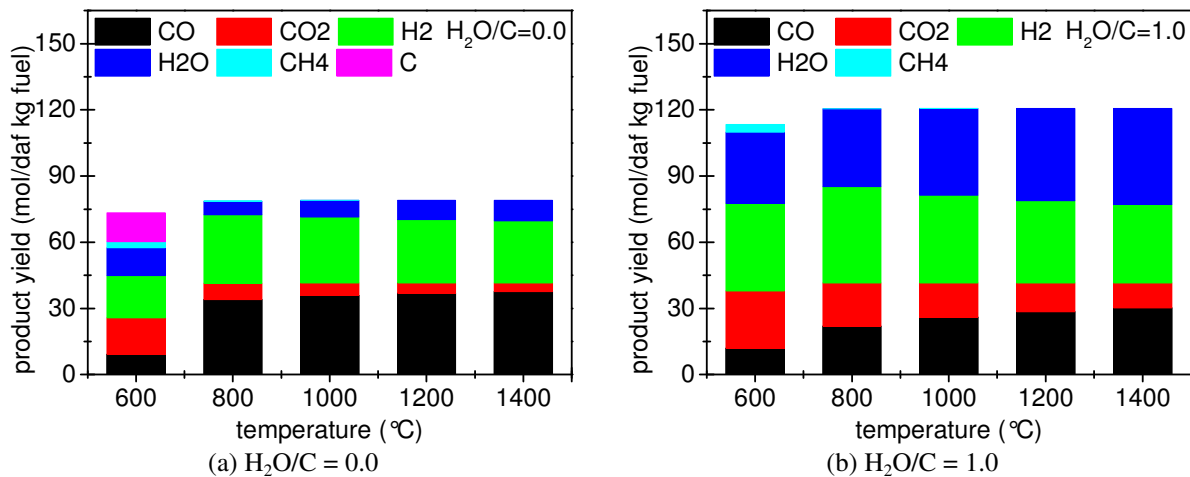

Figure 2.13 Effects of temperature and steam/carbon ratio on the product distribution with $\lambda = 0.25$ at equilibrium conditions

Both the experimental results and the equilibrium calculations indicate that reactor temperature and steam /carbon ratio strongly influence the product distribution. Therefore, the effects of temperature (T = 600 – 1400 °C) and steam/carbon ratio ($H_2O/C = 0.0 – 1.0$) on the product distribution with $\lambda = 0.25$ were studied by equilibrium calculation and the results are shown in Figure 2.13. It is observed that at 600 °C without steam addition ($H_2O/C = 0.0$), unreacted carbon exists in the products, while with steam addition ($H_2O/C = 1.0$), there is no carbon left. CH_4, the only hydrocarbon product, can be observed at 600 °C. The producer gas only contains CO, CO_2, H_2, and H_2O at 800 °C and above. The influence of steam addition and increased temperature can be related to the water gas shift reaction. Steam addition pushes the water gas shift reaction towards higher H_2 and CO_2 formation levels and increased temperature increases the CO and H_2O production.

Overall, comparing the experimental results to the equilibrium calculation, a reasonably good agreement is observed at 1350 °C, while at lower temperatures, soot and hydrocarbons appear in the syngas that are not seen in the equilibrium calculation. The largest deviation between experiments and equilibrium calculations conducted at 1350 °C is observed at λ = 0.25 without steam addition. In this case, the syngas has a high CO_2 and a low H_2O content, and reactions between CO_2 and soot and hydrocarbons have not reached equilibrium.

2.4 Conclusions

Wood gasification was investigated in a laboratory scale atmospheric pressure entrained flow reactor at low oxygen concentration to ensure isothermal conditions. In all experiments, the char was completely converted. At 1200 and 1350 °C, all calculated carbon mass balance closures were reasonable, typically within ± 9 %, but at 1000 °C, the carbon mass balance has a large deviation (22 wt %) probably due to the high contents of unmeasured tar and larger hydrocarbons in the syngas. The yields of producer gas (defined as the sum of H_2, CO, CO_2, and light hydrocarbons up to C_3 species) increased by 72 % when the reactor temperature was increased from 1000 to 1350 °C because of steam reforming of tar and heavier hydrocarbons. The H_2/CO molar ratio in syngas was close to 1.0 at high temperatures (> 1200 °C) with steam addition. At 1350 °C, a significant yield of soot was produced, while there was nearly no tar formation. Conversely, at 1000 °C, the soot yield was lowest, whereas the amount of tar was highest. Thus, there is a tradeoff between soot and tar formation. When steam was introduced, the yields of producer gas and H_2 increased slightly while the CO yield decreased a little. The molar ratio of H_2/CO was equal to 1.0 with the largest addition amount of steam (H_2O/C = 1.0). The soot yield can be reduced approximately by 20 – 50 % with H_2O/C = 1.0. The amount of producer gas nearly kept constant with an increase of excess air ratio from 0.25 to 0.50 especially in the range of 0.25 – 0.35. Increasing excess air ratio from 0.25 to 0.50 decreased the yields of H_2 and CO by about 25 and 12 % respectively, increased the yield of CO_2 by 89 – 111 %, and decreased the H_2/CO molar ratio. Increasing excess air ratio also led to a sharp drop of the soot yield by about 75 %. At 1350 °C and with steam addition, the experimental results are close to the gas composition obtained by equilibrium calculation.

From an energy efficiency point of view, a relatively low reactor temperature and a minimum of oxygen and water should be employed. However from a viewpoint of utilizing the syngas as a fuel, the highest temperature (T = 1350 °C), the largest amount of steam addition (H_2O/C = 1.0), and a suitable excess air ratio (λ = 0.35) are desirable providing high yields of H_2 and

CO with low yield of soot and almost without tar, and a suitable molar ratio of H_2/CO (close to 1.0) for synthesis of higher alcohols.

2.5 References

[1] World Energy Council. Survey of energy resources: bioenergy. 2007.

[2] World Energy Council. Deciding the future: energy policy scenarios to 2050. 2007.

[3] Biofuel. 2010. Available from: http://en.wikipedia.org/wiki/Biofuel.

[4] International Energy Agency. World energy outlook: executive summary. 2009.

[5] BP Back to a bio future. 2007. Available from: http://www.bp.com/liveassets/bp_internet/globalbp/globalbp_uk_english/reports_and_publications/frontiers/STAGING/local_assets/pdf/bpf18_01-05_newspatsbriefs.pdf.

[6] BP Biofuels: a growing alternative. 2008. Available from: http://www.bp.com/genericarticle.do?categoryId=9025016&contentId=7057129.

[7] Rezaiyan J, Cheremisinoff NP. Gasification technologies: a primer for engineers and scientists. Boca Raton: Taylor & Francis. 2005.

[8] Sheth PN, Babu BV. Experimental studies on producer gas generation from wood waste in a downdraft biomass gasifier. Bioresour Technol 2009;100:3127-33.

[9] Higman C, Van der Burgt M. Gasification processes. Gasification. Burlington: Gulf Professional Publishing, 2008:91-3.

[10] Henrich E, Weirich F. Pressurized entrained flow gasifiers for biomass. Environ Eng Sci 2004;21:53-64.

[11] Azuhata S, Hedman PO, Smoot LD, Sowa WA. Effects of flame type and pressure on entrained coal gasification. Fuel 1986;65:1511-5.

[12] Brown BW, Smoot LD, Hedman PO. Effect of coal type on entrained gasification. Fuel 1986;65:673-8.

[13] Crnomarkovic N, Repic B, Mladenovic R, Neskovic O, Veljkovic M. Experimental investigation of role of steam in entrained flow coal gasification. Fuel 2007;86:194-202.

[14] Guo X, Dai Z, Gong X, Chen X, Liu H, Wang F, et al. Performance of an entrained-flow gasification technology of pulverized coal in pilot-scale plant. Fuel Process Technol 2007;88:451-9.

[15] Harris D, Roberts D, Henderson D. Gasification behaviour of Australian coals at high temperature and pressure. Fuel 2006;85:134-42.

[16] Lee JG, Kim JH, Lee HJ, Park TJ, Kim SD. Characteristics of entrained flow coal gasification in a drop tube reactor. Fuel 1996;75:1035-42.

[17] Hernández JJ, Aranda-Almansa G, Serrano C. Co-gasification of biomass wastes and coal-coke blends in an entrained flow gasifier: an experimental study. Energy Fuels 2010;24:2479-88.

[18] Hernández JJ, Aranda-Almansa G, Bula A. Gasification of biomass wastes in an entrained flow gasifier: effect of the particle size and the residence time. Fuel Process Technol 2010;91:681-92.

[19] Lapuerta M, Hernández JJ, Pazo A, López J. Gasification and co-gasification of biomass wastes: effect of the biomass origin and the gasifier operating conditions. Fuel Process Technol 2008;89:828-37.

[20] Zhao Y, Sun S, Tian H, Qian J, Su F, Ling F. Characteristics of rice husk gasification in an entrained flow reactor. Bioresour Technol 2009;100:6040-4.

[21] Zhou J, Chen Q, Zhao H, Cao X, Mei Q, Luo Z, et al. Biomass–oxygen gasification in a high-temperature entrained-flow gasifier. Biotechnol Adv 2009;27:606-11.

[22] Wagner H. Soot formation in combustion. Proc Combust Inst 1979;17:3-19.

[23] Fletcher TH, Ma J, Rigby JR, Brown AL, Webb BW. Soot in coal combustion systems. Progress in Energy and Combustion Science 1997;23:283-301.

[24] Ruiz MP, de Villoria RG, Millera A, Alzueta MU, Bilbao R. Influence of the temperature on the properties of the soot formed from C_2H_2 pyrolysis. Chem Eng J 2007;127:1-9.

[25] Frenklach M. Reaction mechanism of soot formation in flames. Physical Chemistry Chemical Physics 2002;4:2028-37.

[26] Indarto A. Soot growth mechanisms from polyynes. Environ Eng Sci 2009;26:1685-91.

[27] Kennedy IM. Models of soot formation and oxidation. Progress in Energy and Combustion Science 1997;23:95-132.

[28] Glassman I. Soot formation in combustion processes. Symposium (International) on Combustion 1989;22:295-311.

[29] Koziski JA, Saade R. Effect of biomass burning on the formation of soot particles and heavy hydrocarbons: an experimental study. Fuel 1998;77:225-37.

[30] Stanmore B, Brilhac J, Gilot P. The oxidation of soot: a review of experiments, mechanisms and models. Carbon 2001;39:2247-68.

[31] Kriengsak SN, Buczynski R, Gmurczyk J, Gupta AK. Hydrogen production by high-temperature steam gasification of biomass and coal. Environ Eng Sci 2009;26:739-44.

[32] Pinto F, Franco C, Andre RN, Tavares C, Dias M, Gulyurtlu I, et al. Effect of experimental conditions on co-gasification of coal, biomass and plastics wastes with air/steam mixtures in a fluidized bed system. Fuel 2003;82:1967-76.

[33] Xu B, Wu C, Luo Z, Zhou X. Kinetic study on biomass gasification. Solar Energy 1992;49:199-204.

[34] Herguido J, Corella J, Gonzalez-Saiz J. Steam gasification of lignocellulosic residues in a fluidized bed at a small pilot scale: effect of the type of feedstock. Ind Eng Chem Res 1992;31:1274-82.

[35] Christensen JM, Jensen PA, Jensen A. Effects of feed composition and feed impurities in the catalytic conversion of syngas to higher alcohols over alkali-promoted cobalt-molybdenum sulfide. Ind Eng Chem Res 2011;50:7949-63.

[36] Gil J, Corella J, Aznar MP, Caballero MA. Biomass gasification in atmospheric and bubbling fluidized bed: effect of the type of gasifying agent on the product distribution. Biomass Bioenergy 1999;17:389-403.

[37] Lv Y, Ji C, Guo L. Experimental investigation on hydrogen production by agricultural biomass gasification in supercritical water. Journal of Xi'an Jiaotong University 2005;3:238-42. Chinese.

[38] Klose W, Wölki M. On the intrinsic reaction rate of biomass char gasification with carbon dioxide and steam. Fuel 2005;84:885-92.

Chapter 3 Biomass gasification behavior II

Abstract

Biomass gasification and pyrolysis were studied in a laboratory-scale atmospheric pressure entrained flow reactor. Effects of operating parameters and biomass types on the syngas composition were investigated. In general, the carbon conversion during biomass gasification was higher than 90 % at the optimal conditions of 1400 °C with steam addition. The biomass carbon that was not converted to gas in the gasification process only appeared as soot particles in the syngas in all of the experiments except for the two experiments performed at 1000 °C where a very small amount of char was also left. In comparison to pyrolysis, lower yields of soot, H_2 and CO were produced during gasification. The yield of soot could be reduced by a longer residence time, larger feeder air flow, lower oxygen concentration, higher excess air ratio, higher steam/carbon ratio, and higher reactor temperature. Changes in residence time, feeder air flow and oxygen concentration did not show a noticeable influence on H_2 and CO. Increasing the excess air ratio decreased both the H_2 and CO yields, increasing the steam/carbon ratio increased the H_2 yield but decreased the CO yield, and increasing the reactor temperature increased both the H_2 and CO yields. Wood, straw, and dried lignin had similar gasification behavior except with regard to soot formation. The soot yield was lowest during straw gasification possibly because of its high potassium content.

3.1 Introduction

Worldwide, biomass is the fourth largest energy resource after oil, coal, and gas [1,2]. It is estimated that by 2050 biomass could supply 10 – 20 % of the global primary energy requirements [1-3]. Biomass is CO_2-neutral and can thereby reduce the global greenhouse gas emission. Three thermochemical conversion processes are available for biomass use: combustion, pyrolysis, and gasification [4]. Gasification using pressurized fluidized bed or entrained flow gasifiers provides a syngas that can be used to synthesize liquid fuels and chemicals or produce heat and power by efficient combined-cycle power plants [5-7].

Currently, coal gasification is the most commercially available technology in large scale. Biomass is an important alternative to coal but differs from coal in many important aspects, including lower carbon content, higher oxygen content, higher volatile content, lower heating value, and lower bulk density [8-10]. Therefore, knowledge on biomass gasification is needed to support the development of commercial entrained flow biomass gasifiers. Entrained flow

gasification operates at high temperatures (> 1200 °C) with rather small particles to achieve a high carbon conversion within a few seconds and may provide a high-quality syngas especially without tar. However, only a few experimental investigations [11-15] are published on entrained flow gasification of biomass. These studies were mainly performed at relatively low temperatures (< 1200 °C) and investigated the effects of the reaction temperature, excess air ratio, residence time, particle size, and biomass type on gas composition. Steam addition and oxygen concentration, which might give a large influence on gasification behavior [16], were not studied in these references. Additionally, when biomass is pyrolyzed at high temperatures, secondary reactions occur in the gas phase, which converts tar compounds into light hydrocarbons, aromatics, oxygenates olefins, soot precursors, and soot [17-19]. Unconverted soot in the syngas reduces the efficiency of the gasification process. In Chapter 2, we investigated the influence of operating conditions on syngas composition during biomass gasification in an atmospheric pressure entrained flow reactor at high temperatures (1000 – 1350 °C) with low oxygen concentrations (5 – 10 %). We found that a significant yield of soot was obtained at 1350 °C, but there was nearly no yield of tar probably because the heavy hydrocarbon chains were cracked and reacted with steam to form H_2, CO, and CO_2 [20]. A higher temperature was beneficial to lower the amount of tar, while the soot yield showed a peak at 1200 °C, which may result from soot formation by tar and hydrocarbon polymerization competing with soot gasification by CO_2 and H_2O at high temperatures. Thus, high temperature and steam addition are helpful to provide a syngas product rich in H_2 and CO with a low content of soot.

As a continuation of the previous study, the main objective of the present work is to comprehensively investigate the effects of operating parameters and biomass types on gas product distribution and soot formation in air/steam entrained flow gasification and to determine favorable conditions for achieving complete biomass conversion. The investigated reactor temperature is up to 1400 °C, and the oxygen concentration is 21 % in most of the experiments. Six gasification parameters (residence time, feeder air flow, oxygen concentration, excess air ratio, steam/carbon ratio, and reactor temperature) and three biomasses (wood, straw, and lignin, a waste product from bioethanol production) are investigated in the present study. Besides a systematic study on biomass gasification, biomass pyrolysis is also investigated to support a deeper understanding of the whole gasification process.

3.2 Experimental

3.2.1 Setup

The experimental setup, an entrained flow gasification system, used for the present work is shown schematically in Figure 3.1. It consists of a gas preheater, vertical reactor, fuel feeding system, gas supply system, gas sampling and analysis system, solid particle sampling system, tar sampling system, and flue gas treatment system. It is very similar to the old set up used in Chapter 2, but some following modifications are made. Due to the broken of one heating element at the top of the gas preheater and two heating elements at the bottom of the reactor in the old setup, a new gas preheater and vertical reactor are installed to replace the old ones. In addition, two more flows of purge gas to the two heating elements at the bottom of the reactor are added in the present setup. For safety consideration, a blue shell with ventilation system is installed outside the reactor. An open burner supporting by Natural gas are employed for syngas treatment before emission, owing to the high contents of H_2 and CO in the syngas in the present study. A micro gas chromatograph (Agilent 3000) is used instead of the gas chromatograph (Agilent 6890N) used in the old setup, which can measure the gas composition in a shorter time. A Petersen column [21], locating after the metal filter, is employed for tar sampling during low-temperature (< 1200 °C) gasification experiments. It is cooled to 0 °C and filled with acetone as the solvent to capture tar compounds.

3.2.2 Materials

Wood (beech sawdust) and straw (pulverized wheat straw pellets) were the main biomass fuels used in this study, while dried lignin gasification was tested in a single experiment for comparison. The wood used in the present study is same as that used in the Chapter 2. The lignin, which was obtained as a byproduct from a straw ethanol plant, had a high content of moisture (69.2 wt %, as-received basis). In the pretreatment process, most of the moisture was removed by suction filtration and the solid residues were dried at 105 °C for 24 h. In order to attain a stable feeding, the dried lignin was sieved to the desired particle size (< 1 mm). The properties of wood, straw, and dried lignin are listed in Table 3.1. It can be seen that the compositions of wood and straw are quite similar, except for the ash content. The potassium content in straw is high. In comparison to wood and straw, the dried lignin has a higher heating value, higher fixed carbon content, lower volatile content, and higher ash content being rich in silica. The particle size distributions, shown in Figure 3.2, were determined by

sieve classification. The median diameters (d_{50}) of wood, straw, and dried lignin were 310, 130, and 280 µm, respectively.
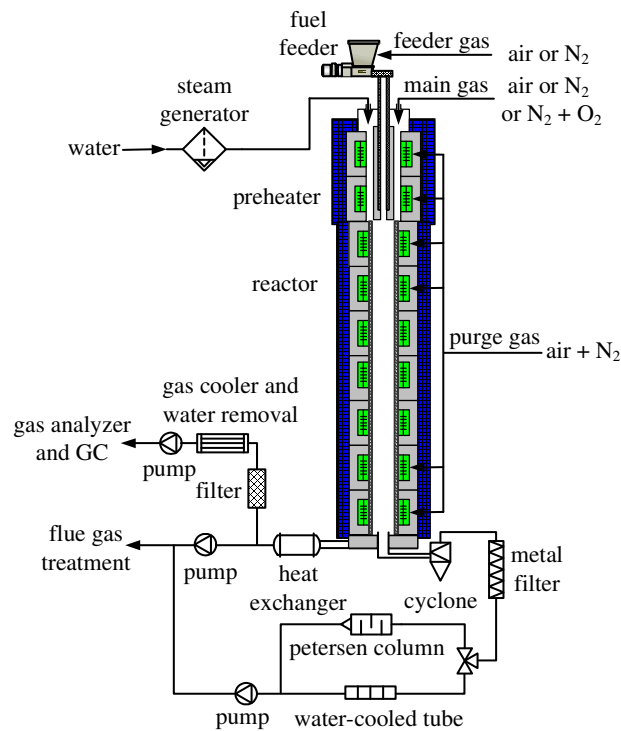

Figure 3.1 Sketch of experimental setup

Table 3.1 Properties of fuels

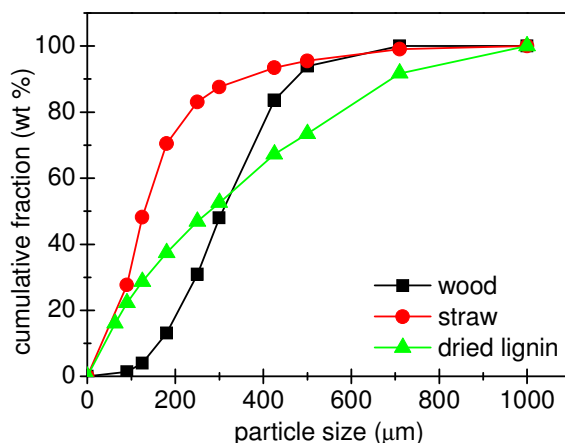| properties		wood (as-received basis)	straw (as-received basis)	dried lignin (dry basis)
moisture	wt %	9.04	5.40	0.00
ash	wt %	0.61	4.54	11.10
volatile	wt %	76.70	72.27	63.10
fixed carbon	wt % (by diff.)	13.65	17.79	25.80
lower heating value	MJ/kg	16.44	16.35	21.42
C	wt %	45.05	43.42	53.80
H	wt %	5.76	5.58	5.70
O	wt % (by diff.)	39.41	40.60	28.10
N	wt %	0.13	0.37	1.18
S	wt %	0.01	0.09	0.12
Si	wt %	-	1.23	4.18
K	wt %	-	0.76	0.13
Cl	wt %	-	0.25	0.02
Ca	wt %	-	0.23	0.43
Mg	wt %	-	0.06	0.02
P	wt %	-	0.03	0.06
Na	wt %	-	0.01	0.28
Al	wt %	-	0.01	0.07
Fe	wt %	-	0.01	0.30

Figure 3.2 Particle size distributions of fuels

3.2.3 Conditions

The applied experiments are listed in Table 3.2. In the present study, the effects of six operating parameters (residence time, feeder air flow, oxygen concentration, excess air ratio, steam/carbon ratio, and reactor temperature) and three fuel types (wood, straw, and dried lignin) on the gasification process were investigated. Besides, biomass pyrolysis was also investigated and compared with biomass gasification. The definitions of residence time, oxygen concentration, excess air ratio, steam/carbon ratio were presented in Chapter 2.

To determine the char and soot content, the solid samples from the cyclone and metal filter were analyzed by a thermogravimetric apparatus (Netzsch STA-449C). In these experiments, 5 mg samples were loaded in a platinum crucible and heated at 10 °C/min to the final setting temperature. The temperature program and applied gas environment for the simultaneous thermal analysis (STA) is shown in Figure 3.3. In the analysis, different fractions of the sample, such as moisture, organic matter, volatilizable inorganic compounds, and residual ash, can be successfully separated and detected. The organic matters in the cyclone and filter samples are defined as char and soot respectively. To determine the tar content in the solvent (acetone), the solvent of the liquid sample was evaporated by two different ways, at 60 °C for 1.5 h and at room temperature for 5.5 h respectively, and then the residues were considered as the tar compounds.

Table 3.2 List of conducted experiments

(a) pyrolysis experiments

parameter	NO.	fuel	fuel feeding rate	t	feeder N_2 flow	H_2O/C	T
-	-	-	g/min	s	NL/min	mol/mol	°C
steam/carbon ratio (H_2O/C)	wP1	wood	12.8	2.8	10	1.0	1400
	wP2	wood	12.8	2.7	10	0.5	1400
	wP3[a]	wood	12.8	2.6	10	0.0	1400

(b) gasification experiments

| parameter	NO.	fuel	fuel feeding rate	t	FAL	O_2	λ	H_2O/C	T
-	-	-	g/min	s	NL/min	%	-	mol/mol	°C
residence time (t)	wR1	wood	10.7	3.7	10	21	0.30	0.5	1400
	wR2[a]	wood	12.8	3.1	10	21	0.30	0.5	1400
	wR3	wood	15.9	2.5	10	21	0.30	0.5	1400
	wR4	wood	6.4	5.9	6	21	0.30	0.5	1400
	wR5	wood	12.8	3.1	6	21	0.30	0.5	1400
feeder air flow (FAL)	wF1	wood	12.8	3.1	14	21	0.30	0.5	1400
	wF2[a]	wood	12.8	3.1	10	21	0.30	0.5	1400
	wF3	wood	12.8	3.1	6	21	0.30	0.5	1400
	wF4	wood	15.9	2.5	18	21	0.30	0.5	1400
	wF5	wood	15.9	2.5	10	21	0.30	0.5	1400
oxygen concentration (O_2)	wO1	wood	15.8	2.8	10	26	0.30	0.5	1400
	wO2[a]	wood	12.8	3.1	10	21	0.30	0.5	1400
	wO3	wood	9.7	3.4	10	16	0.30	0.5	1400
	wO4	wood	12.8	3.1	6	21	0.30	0.5	1400
	wO5	wood	6.7	3.7	6	11	0.30	0.5	1400
	sO1	straw	15.9	2.8	10	26	0.30	0.5	1400
	sO2	straw	12.8	3.1	10	21	0.30	0.5	1400
	sO3	straw	9.8	3.4	10	16	0.30	0.5	1400
excess air ratio (λ)	wL1	wood	10.9	3.4	10	21	0.35	0.5	1400
	wL2[a]	wood	12.8	3.1	10	21	0.30	0.5	1400
	wL3	wood	15.3	2.8	10	21	0.25	0.5	1400
	sL1	straw	11.0	3.4	10	21	0.35	0.5	1400
	sL2	straw	12.8	3.1	10	21	0.30	0.5	1400
	sL3	straw	15.4	2.8	10	21	0.25	0.5	1400
steam/carbon ratio (H_2O/C)	wH1	wood	12.8	3.0	10	21	0.30	1.0	1400
	wH2[a]	wood	12.8	3.1	10	21	0.30	0.5	1400
	wH3	wood	12.8	3.2	10	21	0.30	0.0	1400
	sH1	straw	12.8	3.0	10	21	0.30	1.0	1400
	sH2	straw	12.8	3.1	10	21	0.30	0.5	1400
	sH3	straw	12.8	3.2	10	21	0.30	0.0	1400
reactor temperature (T)	wT1[a]	wood	12.8	3.1	10	21	0.30	0.5	1400
	wT2	wood	12.8	3.4	10	21	0.30	0.5	1300
	wT3	wood	12.8	3.8	10	21	0.30	0.5	1200
	wT4	wood	12.8	4.2	10	21	0.30	0.5	1100
	wT5	wood	12.8	4.7	10	21	0.30	0.5	1000
	sT1	straw	12.8	3.1	10	21	0.30	0.5	1400
	sT2	straw	12.8	3.4	10	21	0.30	0.5	1300
	sT3	straw	12.8	3.8	10	21	0.30	0.5	1200
	sT4	straw	12.8	4.4	10	21	0.30	0.5	1100
	sT5	straw	12.8	5.0	10	21	0.30	0.5	1000
-	dl	lignin	9.8	3.1	10	21	0.30	0.5	1400

[a] Repetition experiments were performed
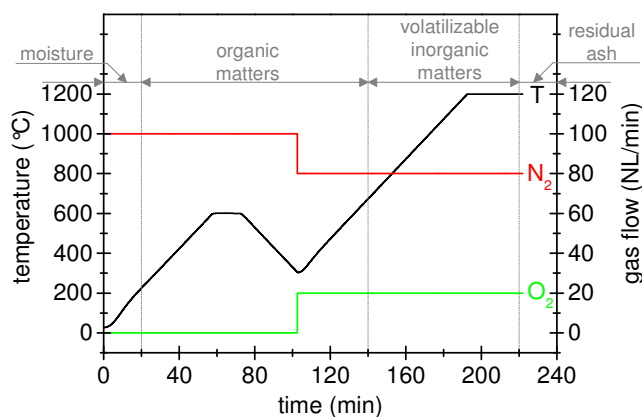
Figure 3.3 Temperature program and gas environment used for solid particles analysis

3.3 Results and discussion

3.3.1 Carbon mass balance

In all conducted experiments, listed in Table 3.2, soot was always observed but no unreacted char was collected, except in two experiments conducted at 1000 °C. Hardly any ash was found in the cyclone but small amounts of ash were collected with the soot captured by the metal filter. The small amount of ash collected is probably because, at high temperatures, most ash melted and deposited on the reactor walls and that cannot be collected by the solid sampling system. After both of the two ways of evaporating the solvent, no tar was found in the liquid sample collected at 1000 °C, maybe partly because some light compounds in the tar were not captured during the liquid sampling process and maybe partly because the light compounds escaped during the solvent evaporation process. The carbon mass balance is depicted in Figure 3.4. It was calculated on the basis of the fuel composition, fuel feeding rate, and yields of CO, CO_2, C_xH_y, and soot. At 1000 °C, a very small amount of char was observed, and it could contribute 0.1 – 0.2 % to the overall carbon mass balance, thus this insignificant contribution was not shown in Figure 3.4. In all conducted experiments, most fuel carbon was partitioned to CO and CO_2. When the temperature was decreased, the contribution of C_xH_y increased gradually. Soot also gave a significant contribution to the closure of the carbon mass balance in the pyrolysis experiments. The carbon mass balance closure was reasonable and, in most cases, higher than 95 %, except for a few experiments conducted at 1000 and 1100 °C (13 – 21 % gap). The most likely reason is that, at lower temperatures, some carbonaceous products, for instance unreacted char, soot, and tar, were deposited on the reactor walls and were not totally oxidized and gasified and, thereby, were not included in the carbon mass balance calculation. The water yields in the syngas were not

determined, and therefore the hydrogen and oxygen mass balance could not be done. To compare the experimental results for dried lignin, wood, and straw gasification with equilibrium conditions, equilibrium calculations were conducted using the FactSage Program for experiments NO. wT1, sT1, and dl, listed in Table 3.2. There was no carbon left in the equilibrium calculation, therefore the equilibrium syngas consisted of CO, CO_2, H_2, and H_2O. The product distributions of experiments and equilibrium calculations are compared in Figure 3.5. The majority of the undetermined product is water in these experiments (highest temperature with steam addition). Generally, the experimental results were reasonably similar to the equilibrium calculation results.
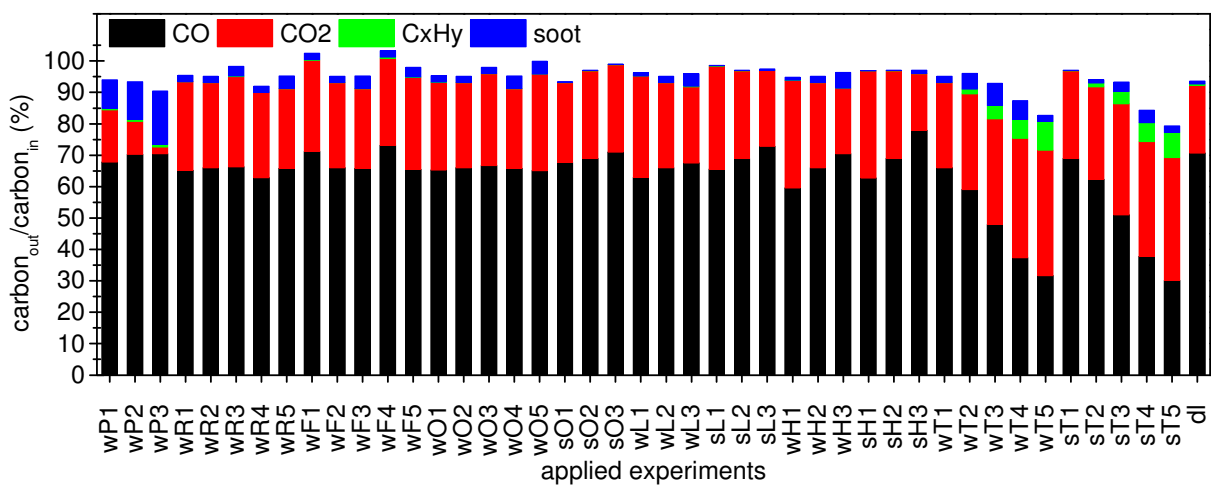
Figure 3.4 Carbon balances for all conducted experiments
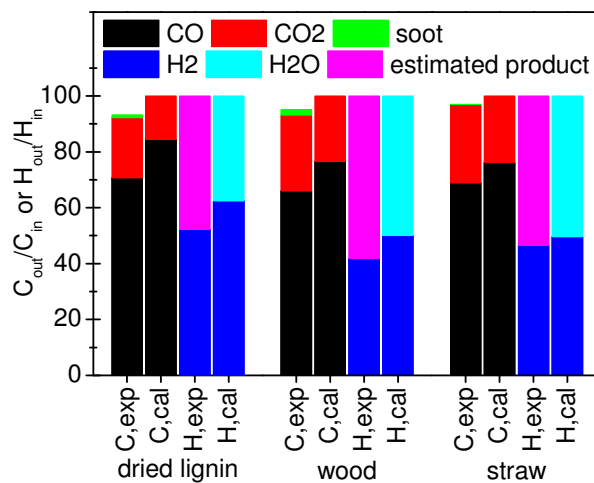
Figure 3.5 Comparison between the results of experiment and equilibrium calculation: the selected experiments are No. wT1, sT1, and dl, listed in Table 3.2, with fixed operating parameters (FAL = 10 NL/min, O_2 = 21 %, λ = 0.3, H_2O/C = 0.5, and T = 1400 °C); C,exp and H,exp are the carbon and hydrogen balance in the experiment; C,cal and H,cal are the carbon and hydrogen balance in the equilibrium calculation

3.3.2 Comparison between pyrolysis and gasification

(a) soot

(b) H_2

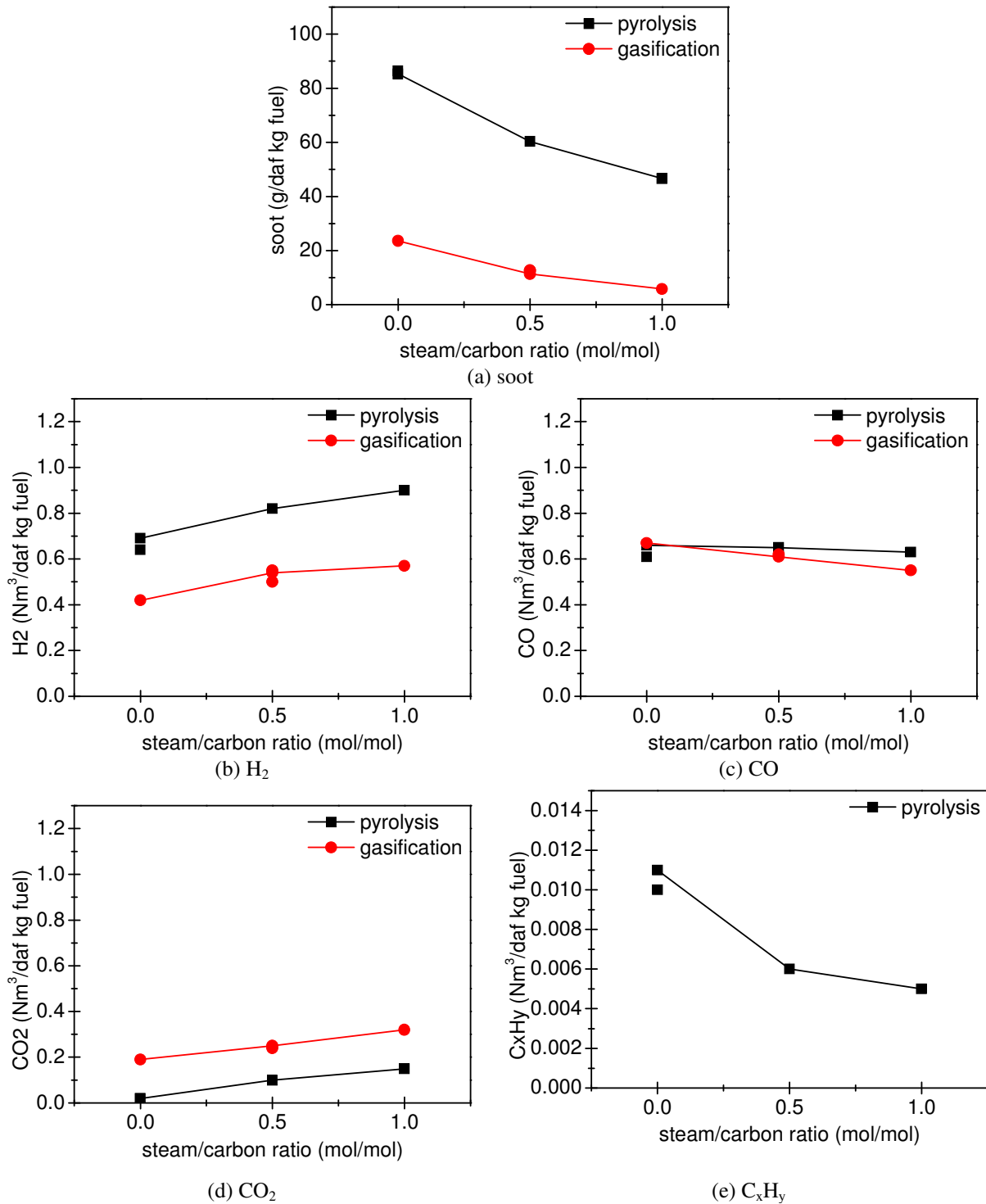(c) CO

(d) CO_2

(e) C_xH_y

Figure 3.6 Comparison between wood pyrolysis and gasification at 1400 °C: during pyrolysis, N_2 was employed as the inlet gas and 10 NL/min N_2 was used as feeder gas; during gasification, air was employed as the inlet gas, 10 NL/min air was used as feeder gas and the oxygen concentration and the excess air ratio was 21 % and 0.3, respectively

Figure 3.6 shows the soot and gas yields during wood pyrolysis and gasification at 1400 °C with different steam addition levels. 10 NL/min N_2 and air were employed as feeder gas in the pyrolysis and gasification experiments, respectively. During gasification, the applied oxygen concentration was 21 % and the excess air ratio was 0.3. Without steam addition, the soot yield was 85.3 g/daf kg fuel (kg fuel on a dry and ash-free basis) during pyrolysis and 23.6 g/daf kg fuel during gasification. The lower soot yield during gasification is most likely both because of more oxidizing conditions at the top of the reactor, leading to oxidation of the tar to lighter molecules, and because more soot was oxidized and gasified. The relative importance of these two contributions however could not be determined by these experiments. With steam addition, the same tendency of the soot yield was observed in Figure 3.6. As a result, the soot yield was approximately 70 – 90 % lower in gasification experiments than in pyrolysis experiments. During gasification the H_2 and CO yields were lower and no C_xH_y was produced, while the CO_2 yield was higher because of the more oxidizing conditions. It should be noted that during pyrolysis without steam addition the CO_2 yield, 0.02 Nm^3/daf kg fuel (kg fuel on a dry and ash-free basis), was very low, probably because the CO_2 was consumed by char and soot gasification reactions.

3.3.3 Effects of gasification parameters

3.3.3.1 Residence time

Figure 3.7 shows the effect of the residence time on the product yield during wood gasification. The two studied ranges of residence time are 2.5 – 3.7 s with a feeder air flow of 10 NL/min and 3.1 – 5.9 s with a feeder air flow of 6 NL/min with otherwise fixed operating parameters (oxygen concentration = 21 %, excess air ratio = 0.3, steam/carbon ratio = 0.5, and reactor temperature = 1400 °C). The longer residence time was achieved by decreasing the fuel feeding rate and the total inlet gas flow. The estimated residence time was calculated on the basis of the reactor size and the total flow of the syngas. In Figure 3.7 (a), the soot yield decreased slightly from 15.5 to 9.8 g/daf kg fuel as the residence time increased from 2.5 to 3.7 s, because more soot was gasified at the longer residence time. However, the individual gas yields were almost kept constant, probably because the experimental conditions were close to the equilibrium conditions [11,12,22-25]. In Figure 3.7 (b), similar trends of soot and gas product yields were obtained when the residence time was further increased from 3.1 to 5.9 s with a feeder air flow of 6 NL/min.
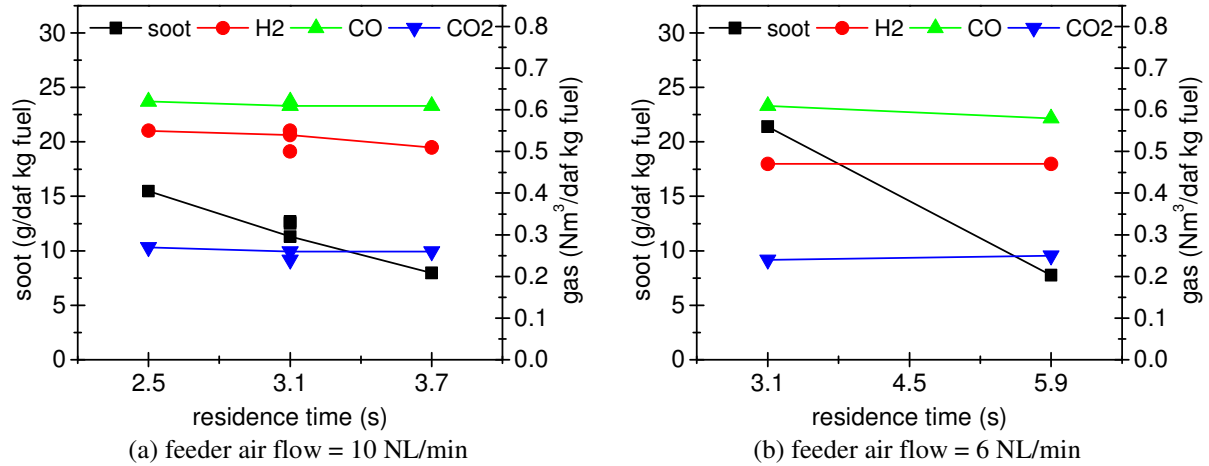
(a) feeder air flow = 10 NL/min   (b) feeder air flow = 6 NL/min

Figure 3.7 Effect of the residence time on the product yield during wood gasification: $O_2 = 21$ %, $\lambda = 0.3$, $H_2O/C = 0.5$, and $T = 1400$ °C

3.3.3.2 Feeder air flow

The effect of the feeder air flow on the product yield during wood gasification is depicted in Figure 3.8. The applied feeder air flow was increased from 6 to 14 NL/min at a residence time of 3.1 s and from 10 to 18 NL/min at a residence time of 2.5 s, while all other operating parameters were fixed (oxygen concentration = 21 %, excess air ratio = 0.3, steam/carbon ratio = 0.5, and reactor temperature = 1400 °C). Figure 3.8 (a) shows that the soot yield decreased from 21.4 to 10.2 g/daf kg fuel when the feeder air flow was increased from 6 to 14 NL/min, while the yield of the individual gas species increased a little. It is probably because the increasing feeder air flow improved the mixing at the top of the reactor, which enhanced tar being converted to light gases instead of soot. The results show that mixing is very important for the formation of soot. Similar results in another range of applied feeder air flow from 10 to 18 NL/min is shown in Figure 3.8 (b).
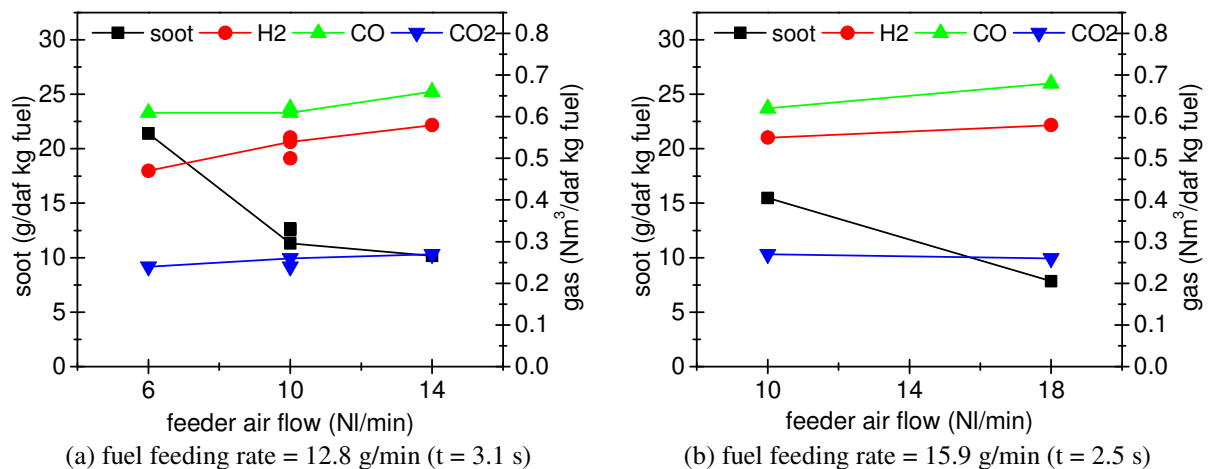

(a) fuel feeding rate = 12.8 g/min (t = 3.1 s)   (b) fuel feeding rate = 15.9 g/min (t = 2.5 s)

Figure 3.8 Effect of the feeder air flow on the product yield during wood gasification: $O_2 = 21$ %, $\lambda = 0.3$, $H_2O/C = 0.5$, and $T = 1400$ °C

The obtained mixing condition during combustion and gasification can be revealed by flame observation. The condition at the top part of the reactor could be visually observed by removing the bottom probe. Figure 3.9 shows the flame structures of wood combustion (excess air ratio = 1.1) at 1000 °C with different feeder air flows. A central flame can be observed clearly in Figure 3.9 (a) with the feeder air flow of 5 NL/min. This figure shows that the released volatiles from single fuel particles did not mix with oxygen instantly but accumulated together to form volatile clouds, which delayed the gas oxidation and formed a central flame. Figure 3.9 (b) shows that a smaller central flame surrounded by many single burning particles was obtained by increasing the feeder air flow to 10 NL/min, which represented an improved mixing compared to Figure 3.9 (a). Many single particle flames, without an overall flame envelope, were observed with a feeder air flow of 15 NL/min in Figure 3.9 (c), meaning that the released volatile gases were immediately oxidized. Therefore, it can be concluded that faster mixing can be obtained by increasing the feeder air flow. Moreover, the flame behavior during wood gasification (excess air ratio = 0.7) at 1000 °C with different feeder air flows is exhibited in Figure 3.10. A comparison between Figure 3.10 (a) and (b) shows that, with the lower feeder air flow, more soot was generated, which was consistent with the experimental results. As a result, these observations reinforce the conclusion that a larger feeder air flow could improve the mixing condition and thereby decrease the soot formation.
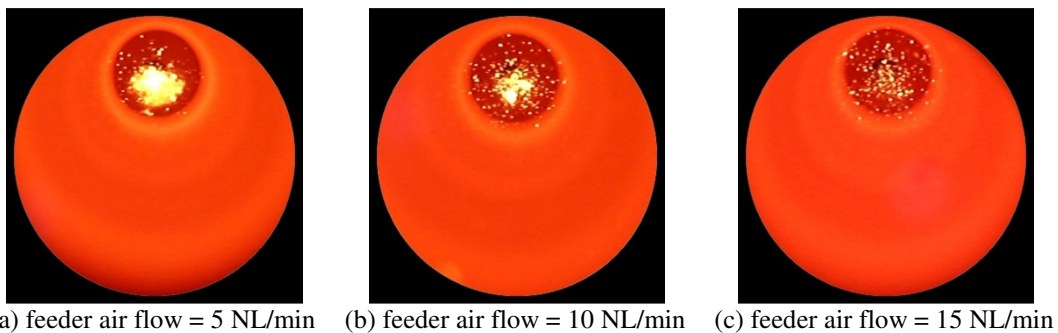

(a) feeder air flow = 5 NL/min   (b) feeder air flow = 10 NL/min   (c) feeder air flow = 15 NL/min

Figure 3.9 Flame structure at 1000 °C with an excess air ratio of 1.1 during wood combustion

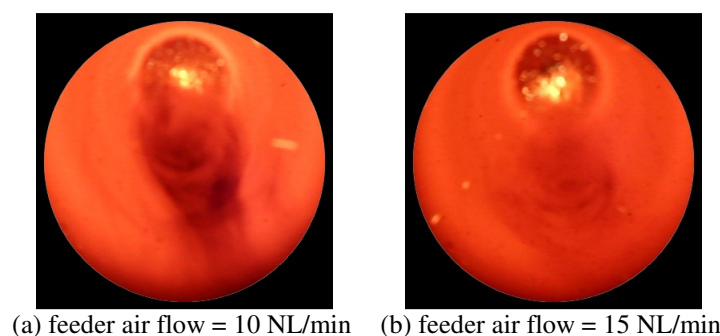(a) feeder air flow = 10 NL/min   (b) feeder air flow = 15 NL/min

Figure 3.10 Flame structure at 1000 °C with an excess air ratio of 0.7 during wood gasification

3.3.3.3 Oxygen concentration and excess air ratio

The combined effects of the oxygen concentration and excess air ratio on the product yield during wood gasification at 1350 °C with a steam/carbon ratio of 0.5 and a feeder air flow of 10 NL/min were investigated in Chapter 2, depicted in Figure 3.11. It was found that increasing the excess air ratio by increasing the oxygen concentration decreased the soot, H_2, and CO yields but increased the CO_2 yield. The effects of the oxygen concentration and excess air ratio on syngas product yields during wood and straw gasification were studied independently in the present study. The effect of the oxygen concentration on the product yield during wood and straw gasification is depicted in Figure 3.12. The studied ranges of the oxygen concentration were 16 – 26 % with a feeder air flow of 10 NL/min and 11 – 21 % with a feeder air flow of 6 NL/min, while all other operating parameters were fixed (excess air ratio = 0.3, steam/carbon ratio = 0.5 and reactor temperature = 1400 °C). The soot yield increased from 9.6 to 12.4 g/daf kg fuel during wood gasification and from 0.5 to 1.0 g/daf kg fuel during straw gasification when the oxygen concentration was increased from 16 to 26 % with a feeder air flow of 10 NL/min. The increasing oxygen concentration could raise the flame temperature, which may cause more soot formation [26]. The H_2, CO, and CO_2 yields were almost constant, independent of the oxygen concentration during both wood and straw gasification and close to equilibrium at the nominal reactor temperature. During wood gasification, similar trends of soot and gas product yields were observed when the oxygen concentration was increased from 11 to 21 % with a feeder air flow of 6 NL/min.
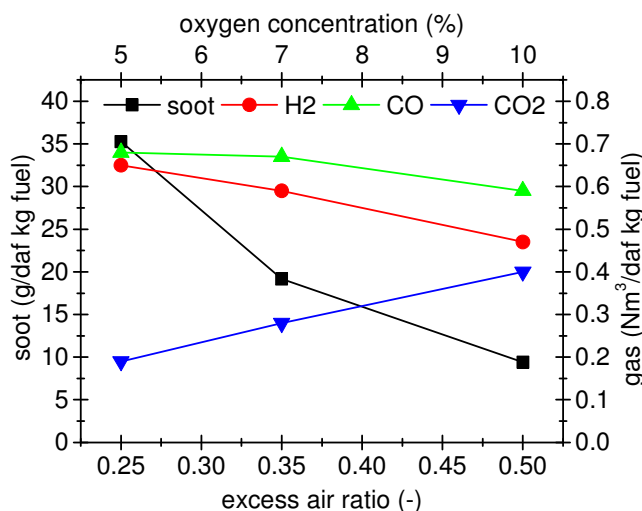

Figure 3.11 Combined effects of the oxygen concentration and excess air ratio on the product yield during wood gasification (FAL = 10 NL/min, H_2O/C = 0.5, and T = 1350 °C)
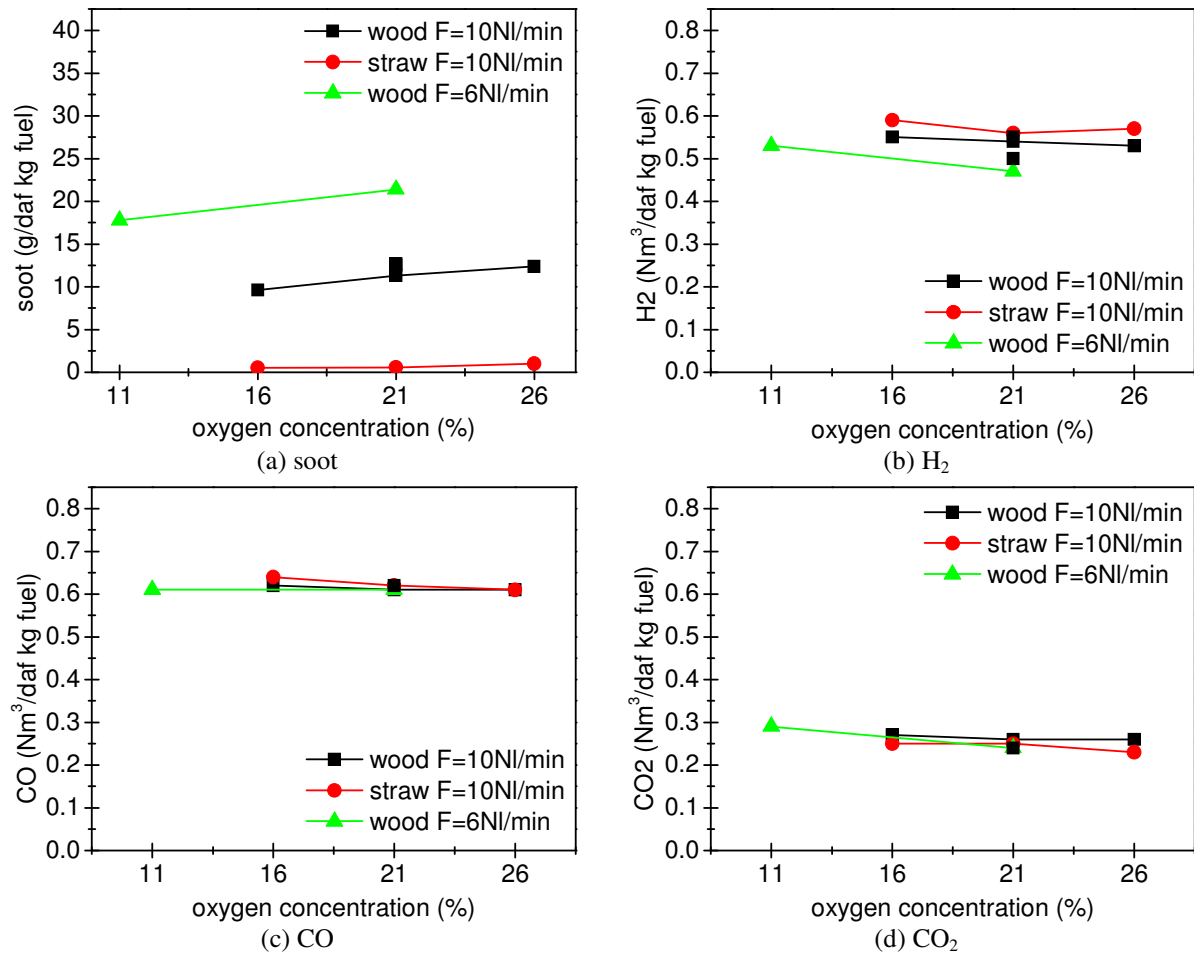
Figure 3.12 Effect of the oxygen concentration on the product yield during wood and straw gasification: FAL = 6 – 10 NL/min, λ = 0.3, H_2O/C = 0.5, and T = 1400 °C

The effect of the excess air ratio on the product yield during wood and straw gasification is shown in Figure 3.13. The applied excess air ratio was increased from 0.25 to 0.35 by lowering the fuel feeding rate with otherwise fixed operating parameters (feeder air flow = 10 NL/min, oxygen concentration = 21 %, steam/carbon ratio = 0.5, and reactor temperature = 1400 °C). The soot yield decreased obviously from 21.8 to 5.8 g/daf kg fuel and from 2.0 to 0.3 g/daf kg fuel during wood and straw gasification, respectively, with an increasing excess air ratio from 0.25 to 0.35. This is because more soot was oxidized and gasified. Also, it is likely that the initially generated soot was lower at the higher excess air ratio because of the lower fuel feeding rate and the higher oxygen content that could produce less and destroy more tar and soot precursors in the gas phase [27-29]. The H_2 yield decreased from 0.56 to 0.47 Nm^3/kg fuel during wood gasification and from 0.63 to 0.53 Nm^3/kg fuel during straw gasification, and the CO yield decreased from 0.63 to 0.59 Nm^3/kg fuel during wood gasification and from 0.66 to 0.59 Nm^3/kg fuel during straw gasification. However, the CO_2 yield increased approximately from 0.23 to 0.30 Nm^3/kg fuel during both wood and straw

gasification because of the oxidation of CO and soot. Therefore, it can be summarized that increasing the excess air ratio by increasing the oxygen concentration noticeably affected the product yields, and increasing the excess air ratio with a fixed oxygen concentration clearly decreased the yields of soot, H_2, and CO while increased the CO_2 yield, while increasing the oxygen concentration with a fixed excess air ratio only slightly increased the soot yield and nearly retained the yields of gas products. We can conclude that the effect of the excess air ratio on the syngas composition is much stronger than the effect of the oxygen concentration.
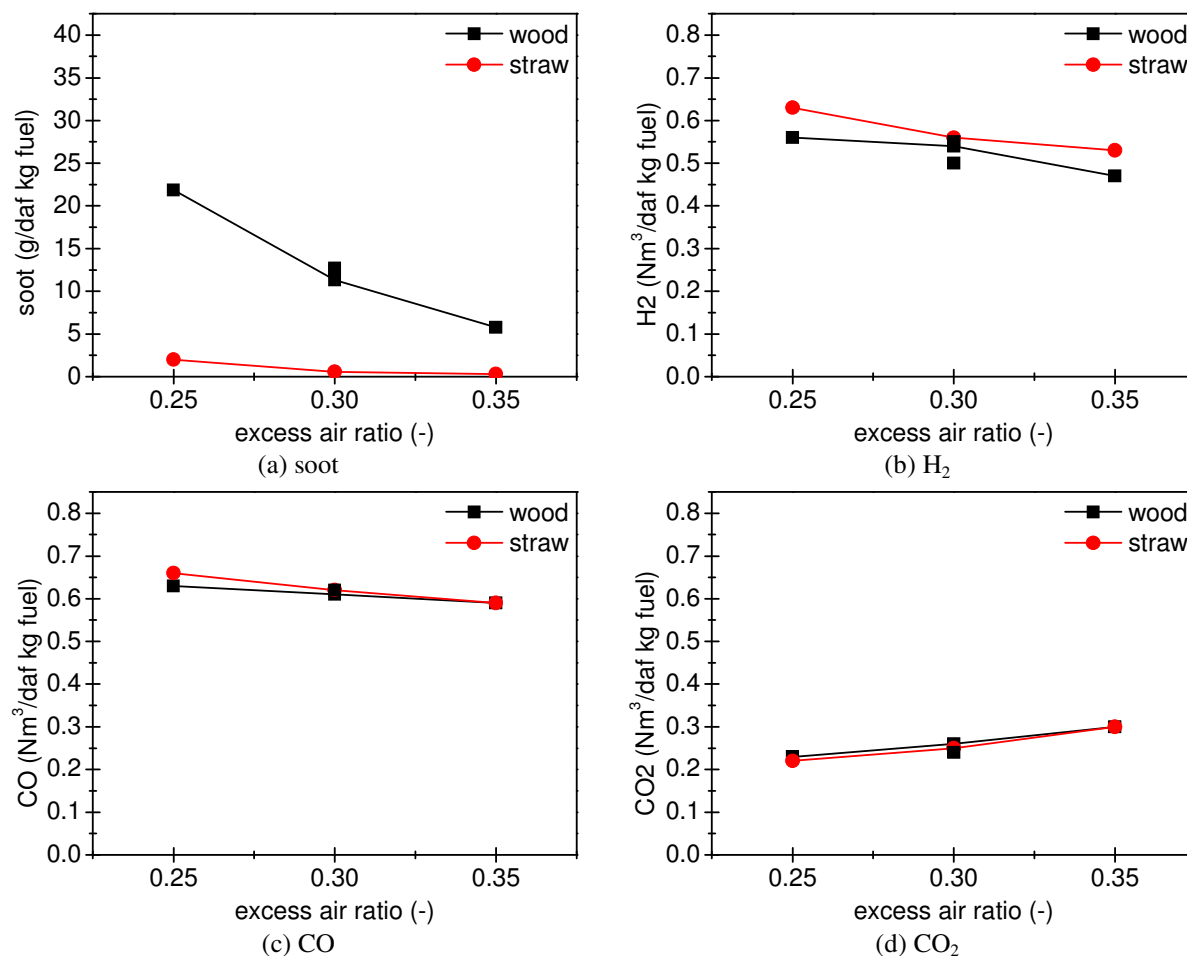

(a) soot

(b) H_2

(c) CO

(d) CO_2

Figure 3.13 Effect of the excess air ratio on the product yield during wood and straw gasification: FAL = 10 NL/min, O_2 = 21 %, H_2O/C = 0.5, and T = 1400 °C

In Figure 3.9 (b) and Figure 3.10 (a), at 1000 °C with a feeder air flow of 10 NL/min, the flame structures during wood combustion (excess air ratio = 1.1) and gasification (excess air ratio = 0.7) are shown, respectively. Clearly, no soot was observed during combustion in Figure 3.9 (b) while soot was formed and escaped the flame during gasification in Figure 3.10 (a). In addition, a comparison between Figure 3.9 (c) (combustion, excess air ratio = 1.1) and Figure 3.10 (b) (gasification, excess air ratio = 0.7) shows similar results at 1000 °C with a feeder air flow of 15 NL/min. The observations are quite in accordance with the experimental

results shown in Figure 3.13 (a) that the more oxidizing condition is employed, the less soot forms.

3.3.3.4 Steam/carbon ratio and reactor temperature

In Chapter 2, the effects of the steam/carbon ratio and reactor temperature on syngas composition during wood gasification with low oxygen concentration (5 %) were studied. To reveal the effects of the two parameters on syngas composition with a higher oxygen concentration, more experiments were carried out in the present study. Figure 3.14 shows the effect of the steam/carbon ratio on the product yield during wood and straw gasification with an oxygen concentration of 21 %. The steam/carbon ratio was increased from 0.0 to 1.0 with otherwise fixed operating parameters (feeder air flow = 10 NL/min, excess air ratio = 0.3 and reactor temperature = 1400 °C). The soot yield decreased from 23.6 to 5.4 g/daf kg fuel and from 5.4 to 0.3 g/daf kg fuel during wood and straw gasification, respectively, by increasing the steam/carbon ratio from 0.0 to 1.0. During wood gasification, the H_2 and CO_2 yields increased steadily from 0.42 to 0.57 Nm^3/daf kg fuel and from 0.19 to 0.32 Nm^3/daf kg fuel respectively, while the CO yield gradually decreased from 0.66 to 0.55 Nm^3/daf kg fuel. During straw gasification, a similar variation of the gas compositions was found. These results were consistent with the obtained results in Chapter 2 also shown in Figure 3.14. During wood gasification, more soot was produced in the previous study shown in Chapter 2 than in the present study because the applied reactor temperature (T = 1350 °C) and excess air ratio (λ = 0.25) were lower and the residence time (t = 2.2 s) was shorter in the previous study. For the same reason, C_xH_y was produced only in the previous study shown in Chapter 2. Thus, we can conclude that the effect of the steam/carbon ratio on syngas product distribution with different oxygen concentrations is consistent.
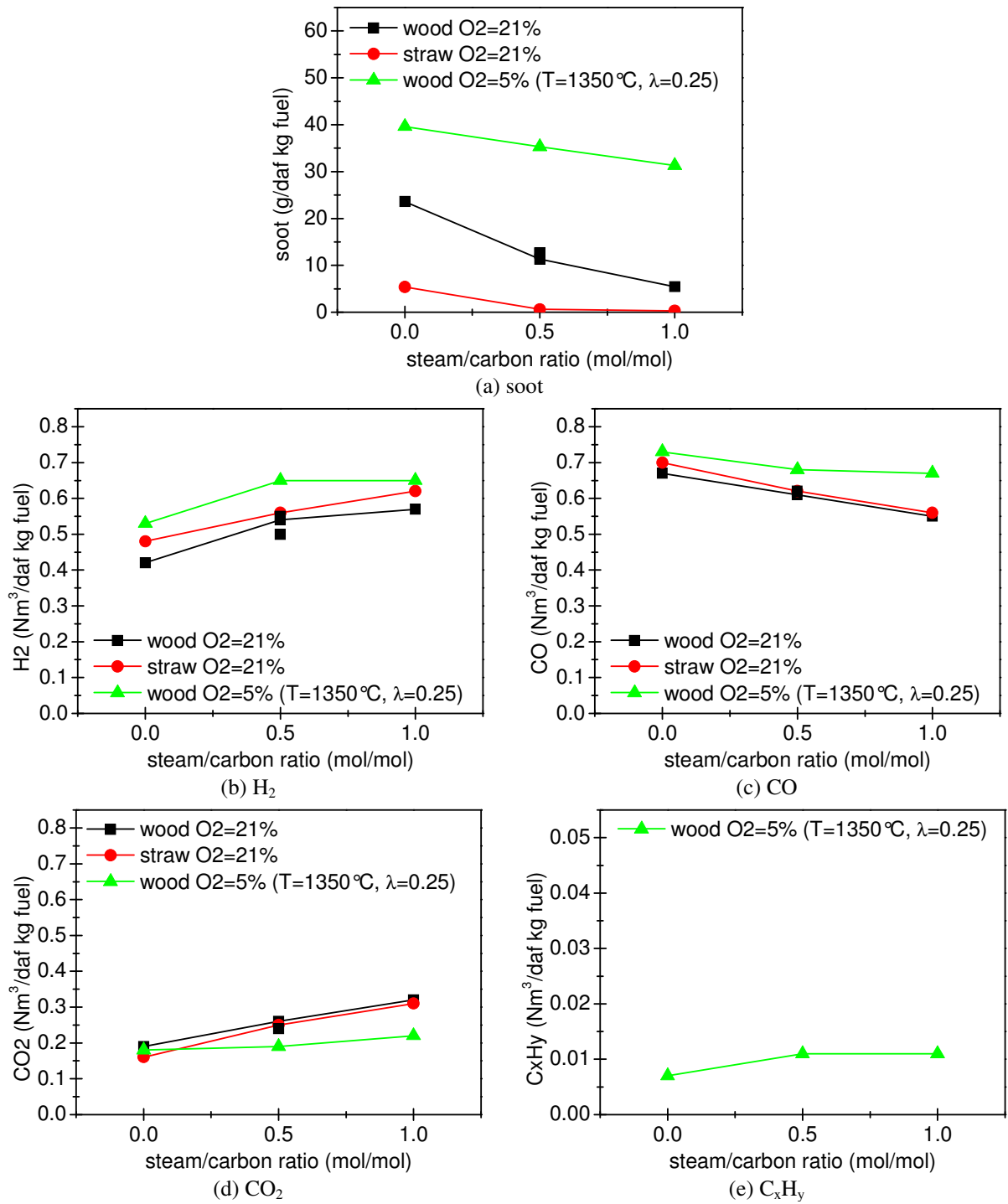
(a) soot

(b) H$_2$

(c) CO

(d) CO$_2$

(e) C$_x$H$_y$

Figure 3.14 Effect of the steam/carbon ratio on the product yield during wood and straw gasification: FAL = 10 NL/min, in the present study λ = 0.3 and T = 1400 °C; in the previous study λ = 0.25 and T = 1350 °C
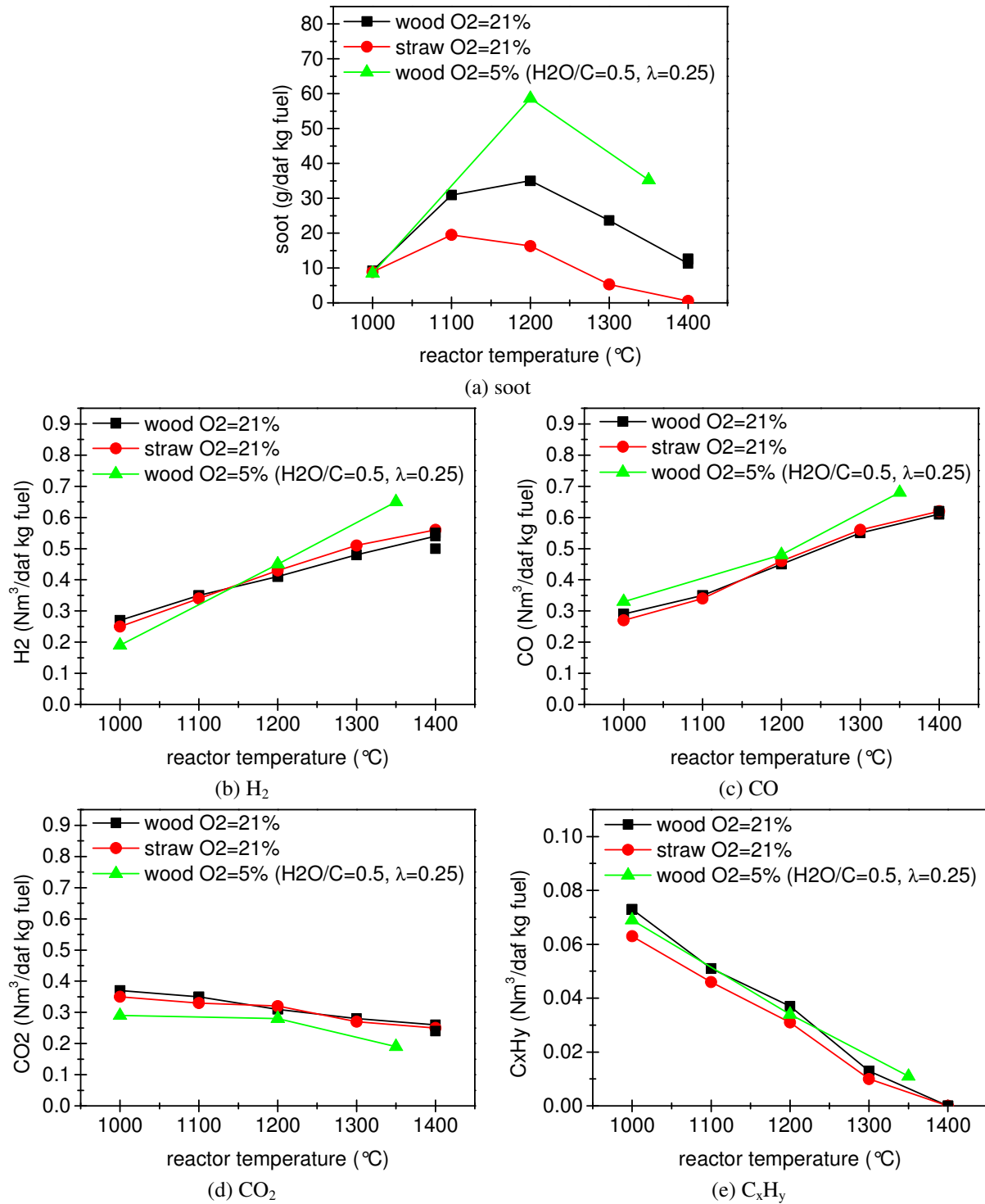
(a) soot

(b) H$_2$

(c) CO

(d) CO$_2$

(e) C$_x$H$_y$

Figure 3.15 Effect of the reactor temperature on the product yield during wood and straw gasification: FAL = 10 NL/min and H$_2$O/C = 0.5, in the present study λ = 0.3; in the previous study λ = 0.25

Figure 3.15 shows the effect of the reactor temperature on the product yield during wood and straw gasification with an oxygen concentration of 21 %. The applied reactor temperature range was between 1000 and 1400 °C with otherwise fixed operating parameters (feeder air flow = 10 NL/min, excess air ratio = 0.3 and steam/carbon ratio = 0.5). During wood gasification, the soot yield had a low value of 9.2 g/daf kg fuel at 1000 °C, increased to a

maximum of 35.0 g/daf kg fuel at 1200 °C, and then started to decline and finally reached 11.3 g/daf kg fuel at 1400 °C. During straw gasification, the soot yield had a similar trend, except that the peak value of 19.5 g/daf kg fuel was achieved at 1100 °C. From 1000 to 1400 °C, during both wood and straw gasification, the yields of H_2 and CO monotonically increased from about 0.26 to about 0.56 Nm^3/daf kg fuel and from about 0.28 to about 0.62 Nm^3/daf kg fuel, respectively. Simultaneously, the CO_2 yield monotonically decreased from about 0.36 to about 0.26 Nm^3/daf kg fuel, and the C_xH_y yield had a steady decline from about 0.07 Nm^3/daf kg fuel at 1000 °C to disappearance at 1400 °C. It should be remarked that no C_xH_y was produced at 1400 °C. CH_4 was the most abundant component of C_xH_y, corresponding to a level of 85 – 100 %. The CH_4 yield also decreased steadily with the increasing temperature. The results from this work were in good agreement with the results obtained in Chapter 2, also shown in Figure 3.15. In comparison to the present study, the soot yield was higher in the previous study shown in Chapter 2, where the applied excess air ratio ($\lambda = 0.25$) was lower and the residence time (t = 2.2 – 3.0 s) was shorter at each temperature, as explained above.

3.3.4 Effects of biomass types

The gasification behaviors of wood and straw are compared in Figure 3.12 – Figure 3.15. It can be observed that the soot yield is significantly lower during straw gasification. This could be due to the high potassium content in straw that might catalyze char formation during pyrolysis at the expense of volatiles, which then lead to less soot formation. Besides, the potassium species, which must be present in the gas phase during the high-temperature gasification process, could adsorb and deposit on the surface of the soot particles in the reactor. Thus, another reason for the low soot yield during straw gasification might be that the potassium has a catalytic effect on the soot gasification reactions [30-34]. The oxidation and gasification rates of the soot that was produced in wood and straw gasification experiments, respectively, were analyzed by a thermogravimetric apparatus (Netzsch STA-449C). In the analysis, 5 mg filter samples (almost pure soot during wood gasification, while mixtures of soot, KCl, and K_2SO_4 during straw gasification) were loaded in an alumina crucible and heated at 10 °C/min from room temperature to 1400 °C. The applied gas environment was 20 % O_2 or CO_2 in N_2. We found that the initial oxidation temperature of wood soot was about 11 °C lower than that of straw soot, while the initial gasification temperature of straw soot was about 115 °C lower than that of wood soot probably because of the presence of potassium in straw. These observations might confirm the catalytic effect of potassium on soot with

respect to CO_2 gasification. Wood and straw gasification provided quite similar gas compositions, which was in agreement with other studies [15,35]. The gasification behaviors of the three fuels, dried lignin, wood, and straw, are compared in Figure 3.16. The three gasification experiments were carried out at the same operating conditions (feeder air flow = 10 NL/min, oxygen concentration = 21 %, excess air ratio = 0.3, steam/carbon ratio = 0.5, and reactor temperature = 1400 °C). The soot yield was 8.6 g/daf kg fuel during dried lignin gasification, which was a little lower than that during wood gasification (11.3 g/daf kg fuel) but much higher than that during straw gasification (0.3 g/daf kg fuel). Besides, in comparison to wood and straw gasification, the dried lignin gasification exhibited higher H_2 and CO yields, a lower CO_2 yield, and no C_xH_y as well.
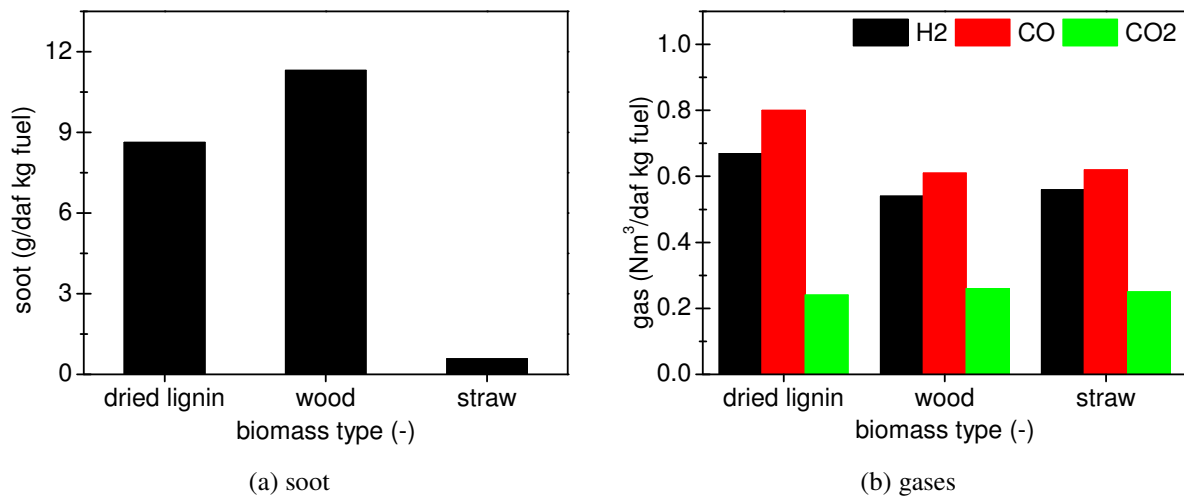

(a) soot   (b) gases

Figure 3.16 Effect of the biomass type on the product yield during biomass gasification: FAL = 10 NL/min, O_2 = 21 %, λ = 0.3, H_2O/C = 0.5, and T = 1400 °C

3.4 Conclusions

Biomass gasification has been investigated in a laboratory-scale atmospheric pressure entrained flow reactor with the purpose of obtaining insight into the effects of operating parameters and biomass types on gas product distribution and soot formation. In the present study, the effects of six operating parameters (residence time, feeder air flow, oxygen concentration, excess air ratio, steam/carbon ratio, and reactor temperature) were investigated. Wood, straw, and dried lignin, were used as fuels. Besides a comprehensive experimental study on biomass gasification, biomass pyrolysis was also investigated to obtain a better understanding of the whole gasification process.

During entrained flow gasification, H_2 and CO are the desired products, while soot is the main byproduct and is required to be removed or minimized. In comparison to pyrolysis, the soot

yield during gasification was lower, probably partly because of lower initially generated soot amounts and partly because of soot gasification with CO_2 and H_2O. A longer residence time and larger feeder air flow (better mixing) reduced the soot yield, while the yields of H_2 and CO were nearly unchanged. The effects of the oxygen concentration and excess air ratio on syngas products were investigated. When the oxygen concentration was increased but the excess air ratio was fixed, the soot yield increased slightly and the yields of gas products were almost kept constant. When the excess air ratio was increased but the oxygen concentration was fixed, the yields of soot, H_2, and CO decreased, while the CO_2 yield increased. Both the previous study shown in Chapter 2 and the present study, with oxygen concentrations of 5 and 21 %, respectively, revealed that high temperature and steam addition reduced the soot yield and increased the H_2 yield, and high temperature also increased the CO yield. Wood, straw, and dried lignin gasification exhibited similar gas compositions. However, the soot yield was much lower during straw gasification than that during both wood and dried lignin gasification. It may be due to the high potassium content in straw that might catalyze char formation during pyrolysis at the expense of volatiles, which then lead to less soot formation or, alternatively, that potassium has a catalytic effect on the soot gasification reactions. On the basis of our work, it can be concluded that high-temperature (> 1200 °C) entrained flow air/steam gasification of biomass can achieve a high carbon conversion within a few seconds of residence time and a high-quality syngas with a low but not negligible soot yield and very low hydrocarbons content and, in particular, without tar. Increasing the residence time, feeder air flow, and excess air ratio can further reduce the amount of soot in syngas.

3.5 References

[1] World energy outlook. 2008.

[2] Johansson TB, Kelly H, Reddy AKN, Williams R, Drennen TE. Renewable energy: sources for fuels and electricity. Washington, D.C.: Island Press, 1992:593-651.

[3] Biomass: the fourth energy source. 2012. Available from: www.draxpower.com/files/page/84635/Biomass___the_fourth_energy_source_FINAL.pdf.

[4] McKendry P. Energy production from biomass (part 2): conversion technologies. Bioresour Technol 2002;83:47-54.

[5] Demirbas A. Yields of hydrogen-rich gaseous products via pyrolysis from selected biomass samples. Fuel 2001;80:1885-91.

[6] Rabah MA, Eldighidy SM. Low cost hydrogen production from waste. Int J Hydrogen Energy 1989;14:221-7.

[7] McKendry P. Energy production from biomass (part 3): gasification technologies. Bioresour Technol 2002;83:55-63.

[8] Demirbas A. Combustion characteristics of different biomass fuels. Progress in Energy and Combustion Science 2004;30:219-30.

[9] McKendry P. Energy production from biomass (part 1): overview of biomass. Bioresour Technol 2002;83:37-46.

[10] Basu P. Biomass gasification and pyrolysis: Practical design and theory. Oxford: Academic Press. 2010.

[11] Hernández JJ, Aranda-Almansa G, Bula A. Gasification of biomass wastes in an entrained flow gasifier: Effect of the particle size and the residence time. Fuel Process Technol 2010;91:681-92.

[12] Zhao Y, Sun S, Zhou H, Sun R, Tian H, Luan J, et al. Experimental study on sawdust air gasification in an entrained-flow reactor. Fuel Process Technol 2010;91:910-4.

[13] Zhao Y, Sun S, Tian H, Qian J, Su F, Ling F. Characteristics of rice husk gasification in an entrained flow reactor. Bioresour Technol 2009;100:6040-4.

[14] Zhou J, Chen Q, Zhao H, Cao X, Mei Q, Luo Z, et al. Biomass–oxygen gasification in a high-temperature entrained-flow gasifier. Biotechnol Adv 2009;27:606-11.

[15] Lapuerta M, Hernández JJ, Pazo A, López J. Gasification and co-gasification of biomass wastes: effect of the biomass origin and the gasifier operating conditions. Fuel Process Technol 2008;89:828-37.

[16] Crnomarkovic N, Repic B, Mladenovic R, Neskovic O, Veljkovic M. Experimental investigation of role of steam in entrained flow coal gasification. Fuel 2007;86:194-202.

[17] Milne TA, Abatzoglou N, Evans RJ. Biomass gasifier 'tars' : their nature, formation, and conversion. National Renewable Energy Laboratory. 1998.

[18] Morf P, Hasler P, Nussbaumer T. Mechanisms and kinetics of homogeneous secondary reactions of tar from continuous pyrolysis of wood chips. Fuel 2002;81:843-53.

[19] Evans RJ, Milne TA. Molecular characterization of the pyrolysis of biomass. Energy Fuels 1987;1:123-37.

[20] Kriengsak SN, Buczynski R, Gmurczyk J, Gupta AK. Hydrogen production by high-temperature steam gasification of biomass and coal. Environ Eng Sci 2009;26:739-44.

[21] Van Paasen SVB, Kiel JHA, Neeft JPA, Knoef HAM, Buffinga GJ, Zielke U. Guideline for sampling and analysis of tars and particles in biomass producer gases (report). 2002.

[22] Wang Y, Kinoshita C. Experimental analysis of biomass gasification with steam and oxygen. Solar Energy 1992;49:153-8.

[23] Chen G, Andries J, Luo Z, Spliethoff H. Biomass pyrolysis/gasification for product gas production: the overall investigation of parametric effects. Energy conversion and management 2003;44:1875-84.

[24] Zhao Y, Sun S, Tian H, Qian J, Su F, Ling F. Characteristics of rice husk gasification in an entrained flow reactor. Bioresour Technol 2009;100:6040-4.

[25] Qin K, Lin W, Jensen PA, Jensen AD. High-temperature entrained flow gasification of biomass. Fuel 2012;93:589-600.

[26] Glassman I, Yaccarino P. The effect of oxygen concentration on sooting diffusion flames. Combustion Sci Technol 1980;24:107-14.

[27] Glassman I. Soot formation in combustion processes. Symposium (International) on Combustion 1989;22:295-311.

[28] Fletcher TH, Ma J, Rigby JR, Brown AL, Webb BW. Soot in coal combustion systems. Progress in Energy and Combustion Science 1997;23:283-301.

[29] Stanmore BR, Brilhac JF, Gilot P. The oxidation of soot: a review of experiments, mechanisms and models. Carbon 2001;39:2247-68.

[30] Howard JB, Kausch Jr WJ. Soot control by fuel additives. Progress in Energy and Combustion Science 1980;6:263-76.

[31] Haynes BS, Jander H, Wagner H. The effect of metal additives on the formation of soot in premixed flames. Symposium (International) on Combustion 1979;17:1365-74.

[32] Tappe M, Haynes B, Kent J. The effect of alkali metals on a laminar ethylene diffusion flame. Combust Flame 1993;92:266-73.

[33] Bulewicz EM, Evans DG, Padley PJ. Effect of metallic additives on soot formation processes in flames. Symposium (International) on Combustion 1975;15:1461-70.

[34] Glarborg P. Hidden interactions - Trace species governing combustion and emissions. Proceedings of the combustion institute 2007;31:77-98.

[35] Lv Y, Ji C, Guo L. Experimental investigation on hydrogen production by agricultural biomass gasification in supercritical water. Journal of Xi'an Jiaotong University 2005;39:238-42.

Chapter 4 Characterization of residual particulates from biomass gasification

Abstract

Biomass gasification experiments were carried out in a bench scale entrained flow reactor, and the produced solid particles were collected by a cyclone and a metal filter for subsequent characterization. During wood gasification, the major part of the solid material collected in the filter is soot. Scanning electron microscopy (SEM) images coupled with energy dispersive spectroscopy (EDS) show agglomerated nano-size spherical soot particles (< 100 nm) that are very rich in carbon. In comparison to wood gasification, the soot content in the filter sample from straw gasification is quite low, while the contents of KCl and K_2SO_4 in the filter sample are high. SEM images of the straw filter samples show that with steam addition during gasification, where the soot yield is lower, the filter sample becomes richer in KCl and K_2SO_4 and appears as irregular crystals, and the typical particle size increases from below 100 nm to above 100 nm. During gasification of dried lignin, the filter sample mainly consists of soot and non-volatilizable inorganic matter. SEM images of the parent wood particles and the derived char samples show that they have similar structure, size, and shape but the derived char particle surface looks smoother indicating some degree of melting. The reactivity of the organic fraction of the samples was determined by thermogravimetry, and it was found that char was more reactive than soot with respect to both oxidation and CO_2 gasification. The activation energy for the soot conversion is higher than for the char conversion. These results support the observation from gasification experiments that char is more easily converted than soot. Surprisingly, the soot produced at a higher temperature is more reactive than the soot produced at a lower temperature.

4.1 Introduction

Gasification of solid fuels, such as coal and biomass, is a way of producing synthesis gas that can be used to make a range of products such as hydrogen, methanol, dimethyl ether, and synthetic natural gas, as well as heat and power [1]. Generally, the various gasifiers used can be grouped in three main classes: fixed bed, fluidized bed, and entrained flow [2]. The majority of the coal gasification processes that have been developed after 1950 are based on entrained flow gasifiers, and the majority of commercial-sized IGCC plants also use entrained

flow gasifiers [3]. The main advantages of entrained flow gasification are fuel flexibility [4], large capacity [5,6], high carbon conversion [7,8], and high-quality syngas [2,9]. In many countries, biomass represents a domestic energy source that can ensure a secure supply of raw material to the energy system. In addition, the use of biomass as a fuel can reduce the CO_2 emission. Owing to the high volatile content in biomass, a potential problem in biomass gasification is the large amount of tar formed that is an undesired by-product [10-13]. However, entrained flow gasification operates at high temperature, thus a tar-free gas can be obtained.

In entrained flow gasification, the fuel conversion includes pyrolysis, char and soot oxidation and gasification by CO_2 and H_2O, and gas phase reactions. Among these, char and soot gasification are the conversion limiting steps because the heterogeneous reactions are slower than the initial pyrolysis and the gas phase reactions [14,15]. In previous experiments of biomass (wood and straw) entrained flow gasification, shown in Chapter 3, we found a low yield of char (< 0.1 wt %) at 1000 °C while no char was left at higher reactor temperatures. On the other hand, soot was always observed in the syngas in the temperature range of 1000 – 1400 °C [16]. Thus, in comparison to char gasification, soot gasification appears to be a slower process and hence determines the overall fuel conversion of the gasification process and influences the syngas quality [17]. Therefore, the knowledge on soot conversion is needed, but presently little is known about the properties of soot particles emitted from biomass entrained flow gasification [16,18].

The objective of the present work was to characterize the residual solid particles obtained from biomass entrained flow gasification and, particularly, to determine the reactivity of the soot and char particles. Simultaneous thermal analysis (STA) was employed to determine the sample composition and reactivity with respect to oxidation and CO_2 gasification of the particles. Scanning electron microscopy (SEM) with energy dispersive X-ray spectrometry (EDS) was used to examine the size, morphology, and elemental composition of the solid particles.

4.2 Experimental

4.2.1 Property analysis of residual particulates

The setup, materials, and conditions used in the biomass gasification experiments are described in Chapter 3. The solid particles collected by the cyclone and metal filter during

entrained flow gasification were analyzed by various analytical techniques. Simultaneous thermal analysis (STA) was employed to determine different fractions of the samples. The detailed analysis method is described in Chapter 3. Based on the STA analysis, different fractions of the solid particles, such as moisture, organic matters, volatilizable inorganic compounds, and residual ash, can be identified. The organic matters in the cyclone and filter samples are defined as char and soot respectively. For volatilizable inorganic compounds, different species, such as KCl and K_2SO_4, can be identified on the basis of their evaporating temperatures. The amount of organic matters in the filter sample is defined as soot. Scanning electron microscopy (SEM) with energy dispersive X-ray spectroscopy (EDS) was employed to obtain the size, morphology, and elemental distribution of the solid particles. The used apparatus was a Zeiss Supra 35 FEGSEM equipped with an X-ray analysis tool by Noran Instruments for filter sample analysis and a Quanta FEGSEM 200F for cyclone sample and parent fuel analysis.

4.2.2 Reaction kinetics of residual particulates

The kinetics of the soot and char collected during wood entrained flow gasification were also derived by non-isothermal experiments in the thermogravimetric apparatus. In a measurement, approximate 1 mg sample was loaded in an alumina crucible and heated at 5 – 10 °C/min from room temperature to 800 °C during oxidation or to 1100 °C during gasification. The total gas flow was 100 mL/min. Three different O_2 and CO_2 concentrations were selected. The O_2 concentrations in N_2 were 10, 15, and 20 vol %, and the CO_2 concentrations in N_2 were 10, 50, and 90 vol %.

The sample conversion in the temperature range of oxidation or gasification was defined as

$$\alpha = \frac{w_i - w}{w_i - w_f} \tag{4.1}$$

where w was the sample weight at a certain temperature T (or at a certain time t), w_i was the initial sample weight at the start of oxidation or gasification, and w_f was the final sample weight at the end of oxidation or gasification. The non-isothermal fuel conversion can be described by using an nth order reaction model with the rate constant given by the Arrhenius equation

$$k = P_g^m A_0 e^{\left(-\frac{E}{RT}\right)} \tag{4.2}$$

$$\frac{d\alpha}{dT} = \frac{1}{\beta}k(1-\alpha)^n = \frac{1}{\beta}P_g^m A_0 e^{\left(-\frac{E}{RT}\right)}(1-\alpha)^n \tag{4.3}$$

where T is the reaction temperature, β is the heating rate, P_g is the O_2 or CO_2 partial pressure, A_0 is the pre-exponential factor, E is the activation energy, R is the ideal gas constant, and m and n are the reaction order with respect to gas phase and solid phase respectively. There was no change of the O_2 or CO_2 partial pressure during an experiment, so an apparent pre-exponential factor A can be used as below:

$$A = P_g^m A_0 \tag{4.4}$$

Thus, the equation (4.3) can be expressed as

$$\frac{d\alpha}{dT} = \frac{1}{\beta}A e^{\left(-\frac{E}{RT}\right)}(1-\alpha)^n \tag{4.5}$$

In the present study, a common integral method presented by Coats and Redfern [19,20] was used to determine the kinetic parameters used in equation (4.5). Through integral transformation and mathematic approximation, equation (4.5) can be expressed in a linear form as [19]:

$$ln[\frac{g(\alpha)}{T^2}] = -\frac{E}{R}\cdot\frac{1}{T} + ln\left(\frac{AR}{\beta E}\right) \tag{4.6}$$

here if

$$n=1, g(\alpha) = -\ln(1-\alpha) \tag{4.7}$$

otherwise,

$$n\neq1, g(\alpha) = [(1-\alpha)^{1-n} - 1]/(n-1) \tag{4.8}$$

A plot of $ln[g(\alpha)/T^2]$ versus 1/T should give a straight line whose slope and intercept determine the values of the activation energy E and the apparent pre-exponential factor A respectively. Three different values, 1/2, 2/3, and 1, of the reaction order n were tested to determine which value provided the best fit.

In addition, equation (4.4) can be linearized by taking the natural log of both sides, shown below:

$$lnA = mlnP_g + lnA_0 \tag{4.9}$$

94

For each sample, measurements at three concentrations of oxidant and gasification agent were performed. Thus based on equation (4.9), a plot of lnA versus lnP$_g$ should give a straight line, from which the gas phase reaction order m and pre-exponential factor A$_0$ are obtained from the slope and the intercept separately.

Arrhenius plots can be obtained by using a linear form of the Arrhenius equation, shown below:

$$lnk = -\frac{E}{R} \cdot \frac{1}{T} + \ln(P_g^m A_0) \tag{4.10}$$

4.3 Results and discussion

4.3.1 Composition and morphology of residual particulates

The weight loss curves (TG) of filter samples obtained from the entrained flow gasification of wood, straw, and dried lignin are shown in Figure 4.1 and the determined compositions of the three samples are listed in Table 4.1. In the three entrained flow gasification experiments, the operating parameters were fixed (reactor temperature = 1400 °C; steam/carbon molar ratio = 0.5; excess air ratio = 0.3; and oxygen concentration = 21 %). During wood gasification, soot (92.6 wt %), is the major component in the filter sample. The temperature (about 1050 °C) at which the inorganic matter starts to vaporize indicates that the major part of the volatilizable inorganic matter in the filter sample is K$_2$SO$_4$ (4.2 wt %) [21]. During straw gasification, the soot content (11.1 wt %) in the filter sample is low, while the volatilizable inorganic matter content (sum of KCl and K$_2$SO$_4$ is 47.4 wt %) is high. According to the evaporating temperatures of about 700 and 1050 °C [21,22], the first volatilizable inorganic matter is KCl (38.2 wt %) and the second is K$_2$SO$_4$ (9.2 wt %). KCl and K$_2$SO$_4$ were collected together with soot particles by the metal filter, because they appeared in the gas phase during gasification due to the high reactor temperature and then formed solid aerosols when the syngas was cooled [23-26]. The filter sample obtained from dried lignin gasification mainly consists of soot (44.9 wt %) and residual ash (52.9 wt %). A small amount of volatilizable inorganic matter (1.5 wt %) was mixed with the soot and ash. The lignin ash mainly consists of silica and calcium, which are hard to volatilize.
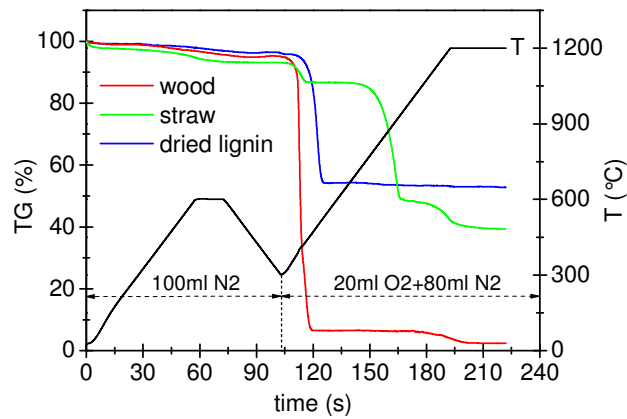
Figure 4.1 STA analysis of the filter samples obtained from biomass entrained flow gasification (operating parameters: T = 1400 °C, H_2O/C = 0.5, λ = 0.3, and O_2 = 21 %)

Table 4.1 Composition of the solid samples obtained from biomass entrained flow gasification

samples	moisture	organic matters	volatilizable inorganic compounds		residual ash	total solid yield
			KCl	K_2SO_4		
			(wt %)			(g/daf kg fuel)
filter samples						
wood, T = 1000 °C, H_2O/C = 0.5	1.0	96.3	0.0	1.0	1.8	9.6
wood, T = 1400 °C, H_2O/C = 0.5	0.9	92.6	0.0	4.2	2.3	12.2
straw, T = 1000 °C, H_2O/C = 0.5	1.6	67.1	14.1	1.0	16.1	13.2
straw, T = 1400 °C, H_2O/C = 0.0	2.7	43.7	21.3	6.0	26.3	12.3
straw, T = 1400 °C, H_2O/C = 0.5	2.2	11.1	38.2	9.2	39.3	5.3
straw, T = 1400 °C, H_2O/C = 1.0	1.6	5.9	40.7	9.9	41.9	5.2
dried lignin, T = 1400 °C, H_2O/C = 0.5	0.8	44.9	0.9	0.6	52.9	19.2
cyclone samples						
wood, T = 1000 °C, H_2O/C = 0.5	4.4	60.9	0.5	2.4	31.8	1.4
straw, T = 1000 °C, H_2O/C = 0.5	5.2	42.6	2.3	1.2	48.7	1.4

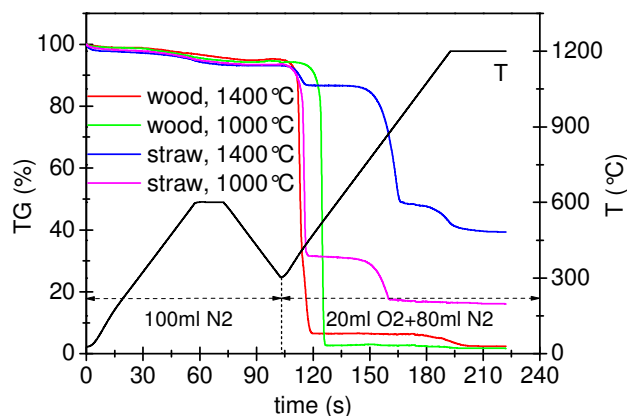**Figure 4.2 STA analysis of the filter samples obtained from wood and straw entrained flow gasification (operating parameters: T = 1000 and 1400 °C, H_2O/C = 0.5, λ = 0.3, and O_2 = 21 %)**

Both gasification temperature and steam addition have an obvious influence on the soot yield [16,18]. The compositions of filter samples obtained from wood entrained flow gasification at reactor temperatures of 1000 and 1400 °C with otherwise fixed operating parameters

96

(steam/carbon ratio = 0.5; excess air ratio = 0.3; and oxygen concentration = 21 %) are listed in Table 4.1 and the corresponding weight loss curves (TG) are shown in Figure 4.2. Soot (92.6 – 96.3 wt %) is the major fraction in the two filter samples obtained at 1000 and 1400 °C. Volatilizable inorganic matter (as K_2SO_4) was present in the filter samples produced at 1400 °C, while it was almost absent in the filter samples produced at 1000 °C probably because a smaller amount of K_2SO_4 aerosols were formed at the low temperature. The compositions of filter samples obtained from straw entrained flow gasification at reactor temperatures of 1000 and 1400 °C with otherwise fixed operating parameters (steam/carbon ratio = 0.5; excess air ratio = 0.3; and oxygen concentration = 21 %) are listed in Table 4.1 and the corresponding weight loss curves (TG) are shown in Figure 4.2. The soot amount in the straw filter sample obtained at 1400 °C was lower than that obtained at 1000 °C. This is most likely because more soot was gasified at higher temperature and possibly catalyzed by potassium species. The amount of volatilizable inorganic matter, KCl and K_2SO_4, in the filter sample obtained at 1400 °C was higher than that obtained at 1000 °C, probably due to the formation of KCl and K_2SO_4 aerosols at the high temperature.

The composition of filter samples obtained from straw entrained flow gasification at different steam/carbon molar ratios of 0.0, 0.5, and 1.0 with otherwise fixed operating parameters (reactor temperature = 1400 °C; excess air ratio = 0.3; and oxygen concentration = 21 %) is listed in Table 4.1 and the corresponding weight loss curves (TG) are shown in Figure 4.3. Without steam addition (H_2O/C = 0.0) the soot content (43.7 wt %) in the filter sample is relatively high, while with steam addition the soot content quickly decreases (11.1 wt % at H_2O/C = 0.5 and 5.9 wt % at H_2O/C = 1.0) owing to the soot and steam gasification reaction. Additionally, when an almost fixed amount of syngas was drawn to the solid sampling system in the gasification experiments, the amount of collected filter sample also decreased with increasing steam/carbon molar ratio. These observations further confirm that steam addition is helpful to reduce soot emission. As a consequence of the lower soot content, the KCl and K_2SO_4 contents increased from 21.3 to 40.7 wt % and from 6.0 to 9.9 wt % respectively with the steam/carbon molar ratio increasing from 0.0 to 1.0. The total amounts of KCl and K_2SO_4 collected in the filter sample, however, were nearly unchanged.
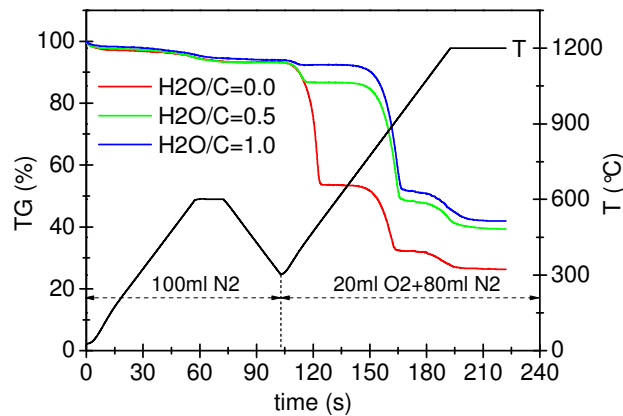
Figure 4.3 STA analysis of the filter samples obtained from straw entrained flow gasification (operating parameters: T = 1400 °C, H₂O/C = 0.0, 0.5, and 1.0, λ = 0.3, and O₂ = 21 %)

During wood and straw entrained flow gasification, char particles were found in the cyclone only at 1000 °C. The composition of cyclone samples obtained from entrained flow gasification of wood and straw respectively with fixed operating parameters (reactor temperature = 1000 °C; steam/carbon ratio = 0.5; excess air ratio = 0.3; and oxygen concentration = 21 %) is listed in Table 4.1 and the corresponding weight loss curves (TG) are shown in Figure 4.4. The cyclone sample from straw gasification has higher ash content than that from wood gasification because of the higher ash content in straw. Besides, compared with the filter sample, we found that the ash content in the cyclone sample was higher.
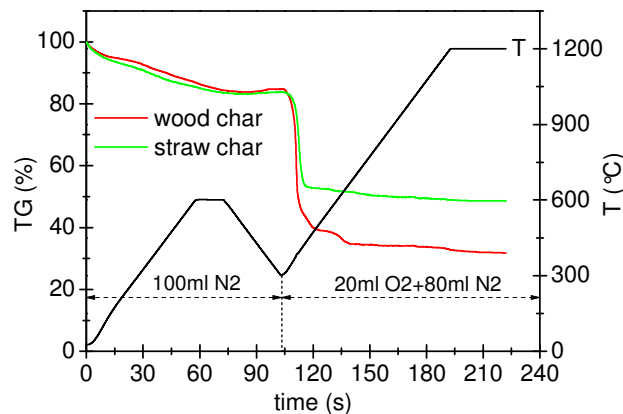

Figure 4.4 STA analysis of the cyclone samples obtained from wood and straw entrained flow gasification respectively (operating parameters: T = 1000 °C, H₂O/C = 0.5, λ = 0.3, and O₂ = 21 %)

Four filter samples, one obtained from wood gasification and the other three obtained from straw gasification, which were already analyzed by STA and listed in Table 4.1, were further investigated by SEM with EDS analysis. Figure 4.5 shows the SEM image with EDS spectrum of the filter sample obtained from wood gasification (reactor temperature = 1400 °C; steam/carbon ratio = 0.5; excess air ratio = 0.3; and oxygen concentration = 21 %). In the

STA analysis, we found soot (92.6 wt %) is the major component in the filter sample. In the SEM image, it can be observed that the single soot particles are nano-sized carbon spheres (< 100 nm) that are agglomerated together to form clusters and chains of spheres. This is agreement with the structure of soot reported in the literature [27], where it was also shown that there was no visual difference observed between soot produced at 1200 and 1400 °C during wood (beech sawdust) pyrolysis in a drop tube furnace. The wood filter sample is almost homogeneous. The EDS spectrum of this sample reveals that it is very rich in carbon because of the very high soot content, and includes traces of oxygen, silica, sulfur, and potassium due to low fractions of K_2SO_4 and SiO_2 being present. The obtained results by SEM with EDS are in qualitative agreement with the results obtained by STA.
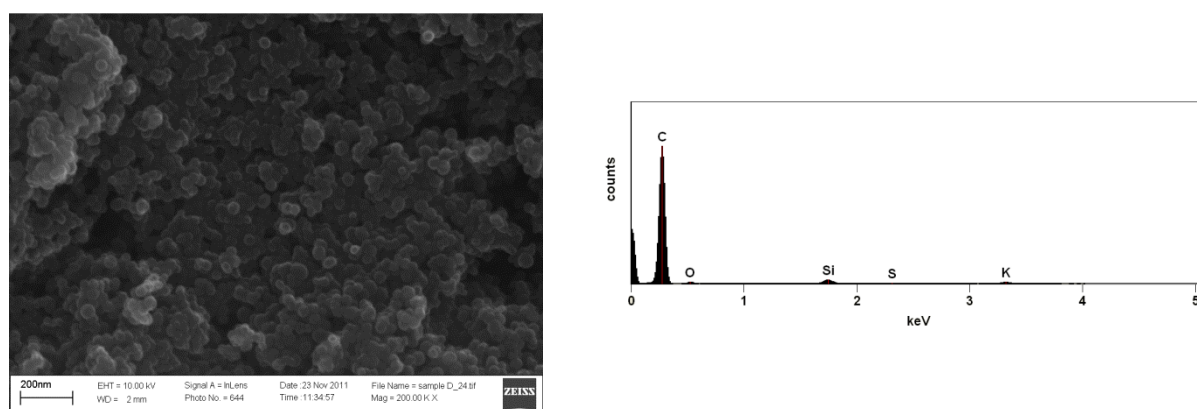

Figure 4.5 SEM image with EDS spectrum of the filter sample obtained from wood entrained flow gasification (operating parameters: T = 1400 °C, H_2O/C = 0.5, λ = 0.3, and O_2 = 21 %)

Figure 4.6 shows the SEM images with EDS spectra of the three filter samples obtained from straw gasification (reactor temperature = 1400 °C; steam/carbon molar ratio = 0.0, 0.5, 1.0; excess air ratio = 0.3; and oxygen concentration = 21 %). The straw filter samples are almost homogenous. In Figure 4.6 (a), without steam addition (H_2O/C = 0.0), the straw filter sample looks similar to the wood filter sample, shown in Figure 4.5, because of the relatively high soot content (43.7 wt %) in the straw filter sample. However, compared with the wood filter sample, the particle size of the straw filter sample looks larger and the shapes of the particles are irregular instead of spherical. This is probably because of the larger amount of KCl and K_2SO_4 present, which adsorbs on the surface of the soot particles. In its EDS spectrum, it can be found that the filter sample is mainly composed of carbon and also includes potassium and chlorine and minor fractions of oxygen, silica, and sulfur. In Figure 4.6 (b), with steam addition (H_2O/C = 0.5), the particle size further increases (> 100 nm) and the irregular particle shape indicates that crystalline materials are present in agreement with the high contents of KCl and K_2SO_4. The EDS spectrum of this filter sample shows that carbon, potassium and

chlorine are present in significant amounts. In Figure 4.6 (c), at $H_2O/C = 1.0$, the particles entirely lost the spherical shape and the boundary of different particles vanished due to their conjunction, probably because of the low soot content and high KCl and K_2SO_4 contents in the filter sample. In the corresponding EDS spectrum, it can be observed that the filter sample is rich in potassium and chlorine and contains additionally carbon, oxygen, sodium, silica, phosphor, and sulfur. The EDS results of the three straw filter samples are all in accordance with their STA results.
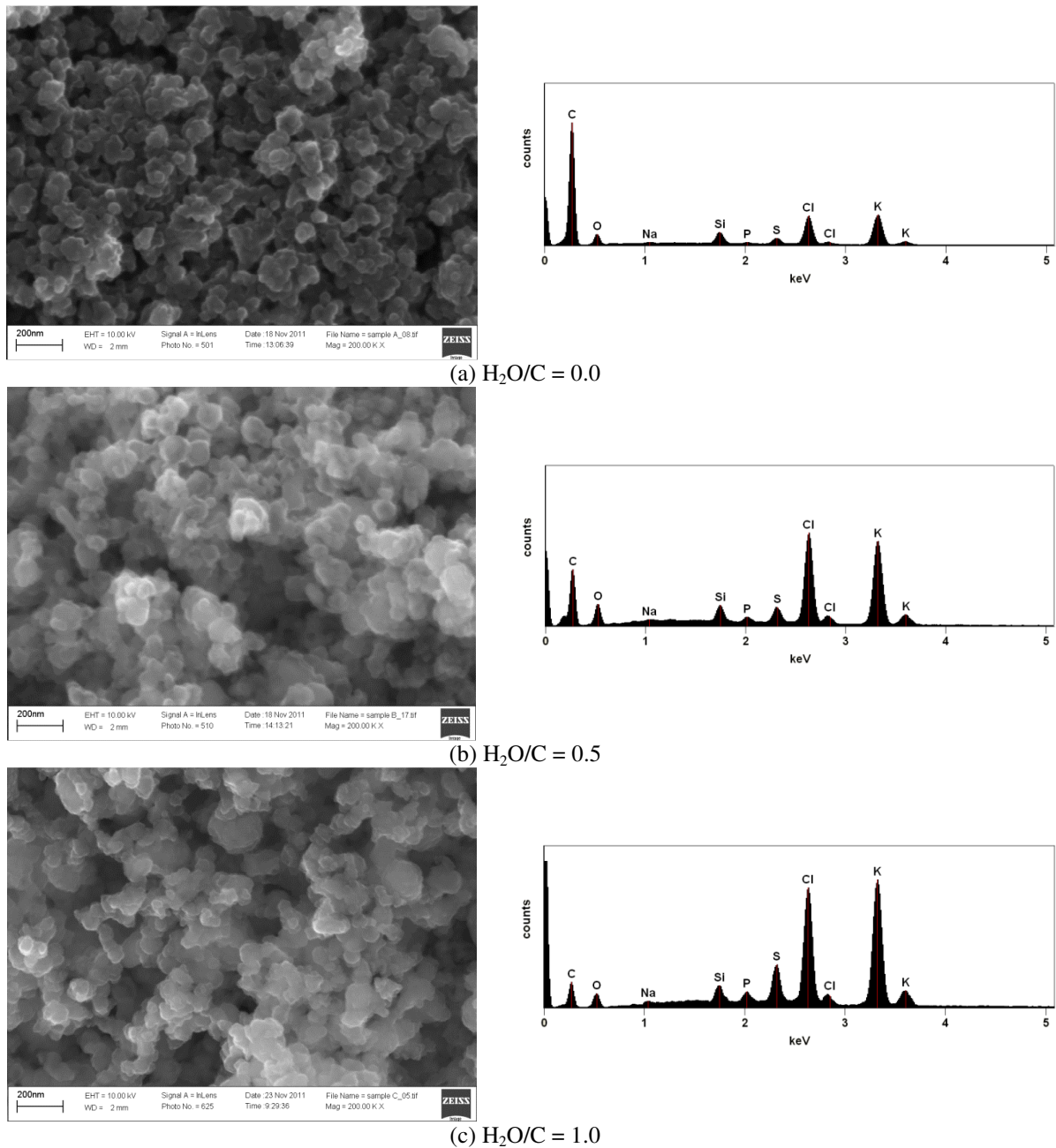

(a) $H_2O/C = 0.0$

(b) $H_2O/C = 0.5$

(c) $H_2O/C = 1.0$

Figure 4.6 SEM images with EDS spectra of the filter samples obtained from straw entrained flow gasification (operating parameters: T = 1400 °C, H_2O/C = 0.0, 0.5, and 1.0, λ = 0.3, and O_2 = 21 %)

The SEM images of the parent wood particle used as fuel and the derived wood char samples collected by the cyclone during entrained flow gasification (reactor temperature = 1000 °C; steam/carbon molar ratio = 0.5; excess air ratio = 0.3; and oxygen concentration = 21 %) are shown in Figure 4.7. Both the parent wood particle and the derived char particle have a layered structure with a loose and porous texture. Furthermore, the size and shape of them are similar, thus complete melting of the char particles does not take place [28,29]. However, in comparison to the wood particle, the surface of the derived char particle looks smoother, which probably indicates partial melting [29,30].

(a) image of the parent wood particle

(b) enlarged image of the parent wood particle

(c) image of the wood char particle

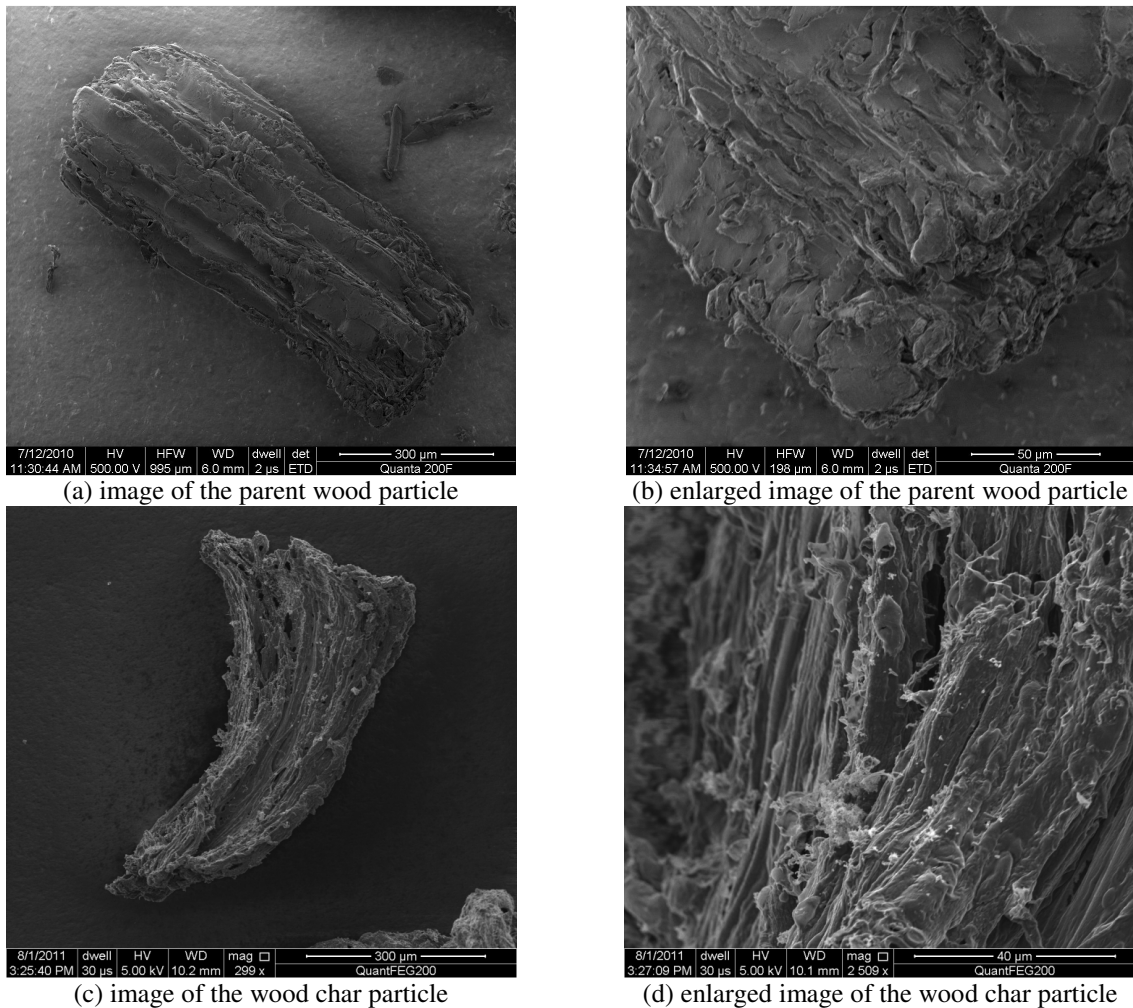(d) enlarged image of the wood char particle

Figure 4.7 SEM image of the parent wood particle and the derived wood char particle (cyclone sample) obtained from entrained flow gasification (operating parameters: T = 1000 °C; H$_2$O/C = 0.5; λ = 0.3; O$_2$ = 21 %)

4.3.2 Kinetics of char and soot particles

The kinetics of oxidation and CO$_2$ gasification of the soot (T = 1400 °C) and char (T = 1000 °C) samples produced during wood entrained flow gasification were determined. The

gasification with H_2O was not investigated since the STA does not allow addition of steam, although this gasification agent would have been most relevant. However, it is generally accepted that the reactivity with respect to H_2O gasification is approximately 2 – 5 times higher than gasification with CO_2 and so the results obtained here for CO_2 may to some extent be generalized [31,32]. The weight loss curves (TG) and the corresponding differential weight loss curves (DTG) for the oxidation and gasification of the soot and char in different O_2 and CO_2 concentrations are shown in Figure 4.8. As expected, the TG and DTG curves are shifted to lower temperatures with increasing O_2 or CO_2 concentration. The soot and char are oxidized approximately between 300 – 600 °C in different O_2 concentrations, while they are gasified at higher temperatures in different CO_2 concentrations, approximately between 600 – 1000 °C. The temperature at the maximum rate of weight loss is commonly used to characterize reactivity [33]. Figure 4.8 (a) shows that the oxidation reaction for char reaches the maximum rate at 400 – 410 °C, which is approximate 50 – 60 °C lower than for soot. As shown in Figure 4.8 (b), the char gasification reaches the maximum rate at 760 – 780 °C, while the soot gasification reaches the maximum rate at 820 – 880 °C. Thus the char is more reactive than soot during both oxidation and gasification.

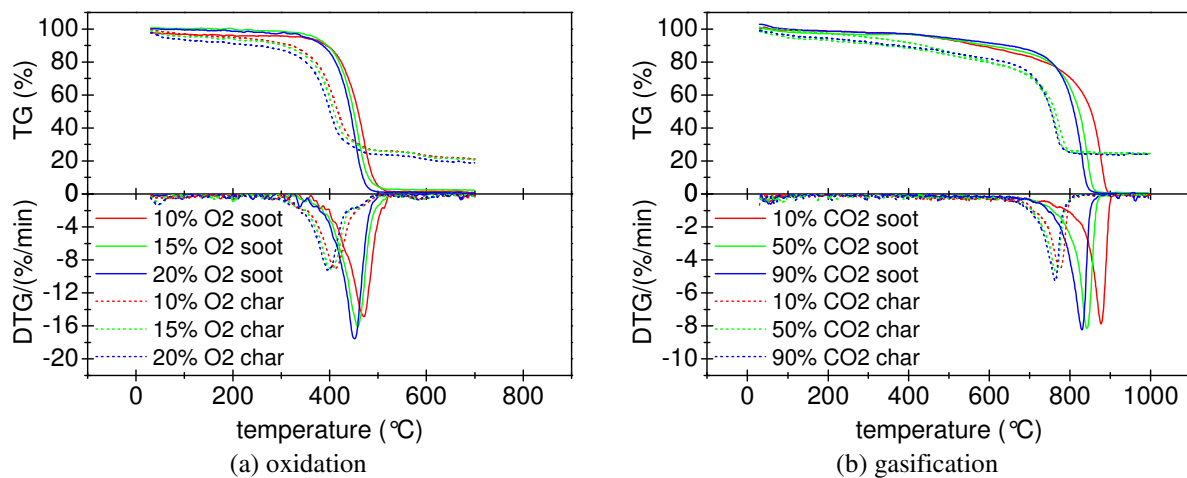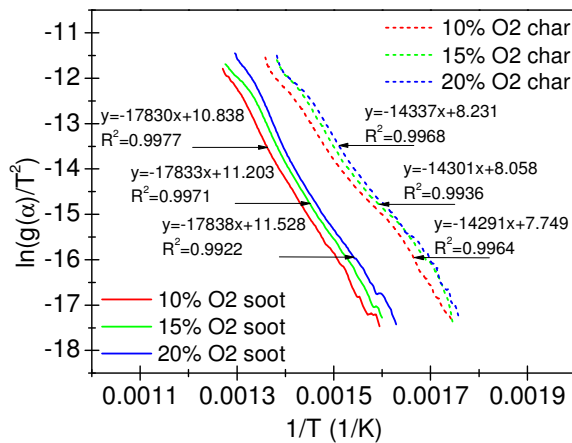(a) oxidation   (b) gasification

Figure 4.8 TG and DTG curves for the wood soot (obtained from entrained flow gasification at 1400 °C) and the wood char (obtained from entrained flow gasification at 1000 °C) oxidation and gasification

The kinetic parameters of the soot and char oxidation and gasification, derived by an integral method, are listed in Table 4.2. The plots of equations (4.6) and (4.9) for char and soot oxidation and gasification are shown in Figure 4.9. We found that good linear fittings can be obtained for n = 1.0 for both soot and char oxidation in different O_2 concentrations and for n = 0.5 for both soot and char gasification in different CO_2 concentrations. It can be seen that the

activation energy is higher for soot conversion than for char conversion. This is probably because the char has a less ordered structure of carbon compared to the more graphitic soot.

Table 4.2 Kinetic parameters of the wood char (obtained from entrained flow gasification at 1000 °C) and the wood soot (obtained from entrained flow gasification at 1400, 1300, 1100, and 1000 °C) oxidation and gasification

samples	char 1000 °C	soot 1400 °C	soot 1300 °C	soot 1100 °C	soot 1000 °C
oxidation in STA	10, 15, and 20 vol % O_2 in N_2	10, 15, and 20 vol % O_2 in N_2	10 vol % O_2 in N_2	10 vol % O_2 in N_2	10 vol % O_2 in N_2
n	1.0	1.0	1.0	1.0	1.0
m	0.71	0.99	0.99	0.99	0.99
A_0 ($s^{-1}MPa^{-m}$)	1.43×10^8	1.43×10^{10}	1.59×10^{10}	7.19×10^{19}	8.59×10^{19}
E (kJ/mol)	119	148	153	315	325
gasification in STA	10, 50, and 90 vol % CO_2 in N_2	10, 50, and 90 vol % CO_2 in N_2	10 vol % CO_2 in N_2	10 vol % CO_2 in N_2	10 vol % CO_2 in N_2
n	0.5	0.5	0.5	0.5	0.5
m	0.12	0.54	0.54	0.54	0.54
A_0 ($s^{-1}MPa^{-m}$)	1.25×10^8	3.61×10^9	4.42×10^9	5.53×10^9	1.16×10^{10}
E (kJ/mol)	213	247	261	279	292

(a) oxidation: linear fitting for equation (4.6)
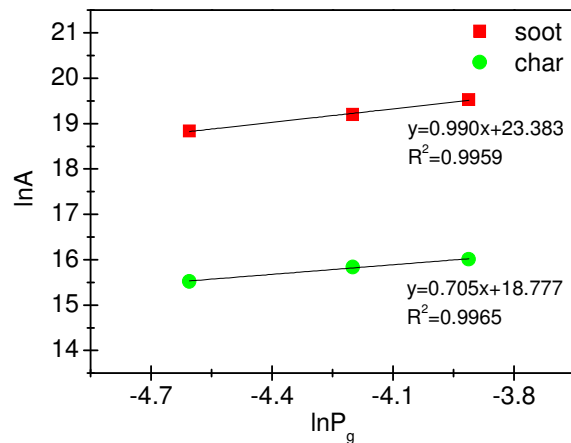
(b) oxidation: linear fitting for equation (4.9)
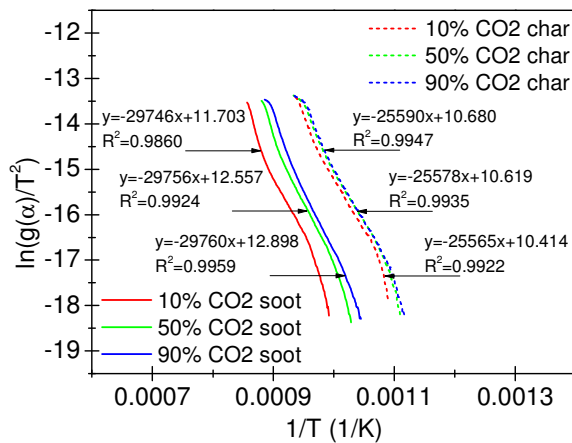
(c) gasification: linear fitting for equation (4.6)
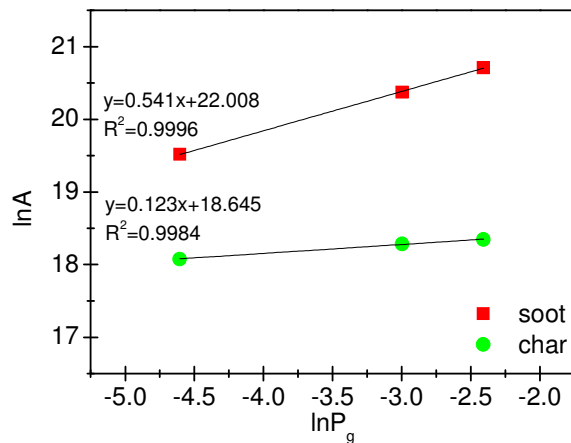
(d) gasification: linear fitting for equation (4.9)

Figure 4.9 Linearized nth order reaction model for oxidation and gasification of the wood soot (obtained from entrained flow gasification at 1400 °C) and the wood char (obtained from entrained flow gasification at 1000 °C): n = 1.0 for oxidation and n = 0.5 for gasification

The obtained kinetic parameters, listed in Table 4.2, were employed in the nth order reaction model, shown in equation (4.3), to simulate the soot and char conversion under oxidation and gasification conditions. Comparison between the experimental measurement and model prediction for soot and char conversion is shown in Figure 4.10. We found that the nth order reaction model can describe the experimental results well with respect to both soot and char oxidation and gasification. Arrhenius plots of the soot and char oxidation and gasification are shown in Figure 4.11. The oxidation rate of the char was about 5 – 10 times faster than that of the soot in the studied temperature range, while the gasification rate of the char was about 5 – 20 times faster than that of the soot. The results show that an important reason for not converting all soot in the available residence time in the entrained flow reactor is the low reactivity of soot.
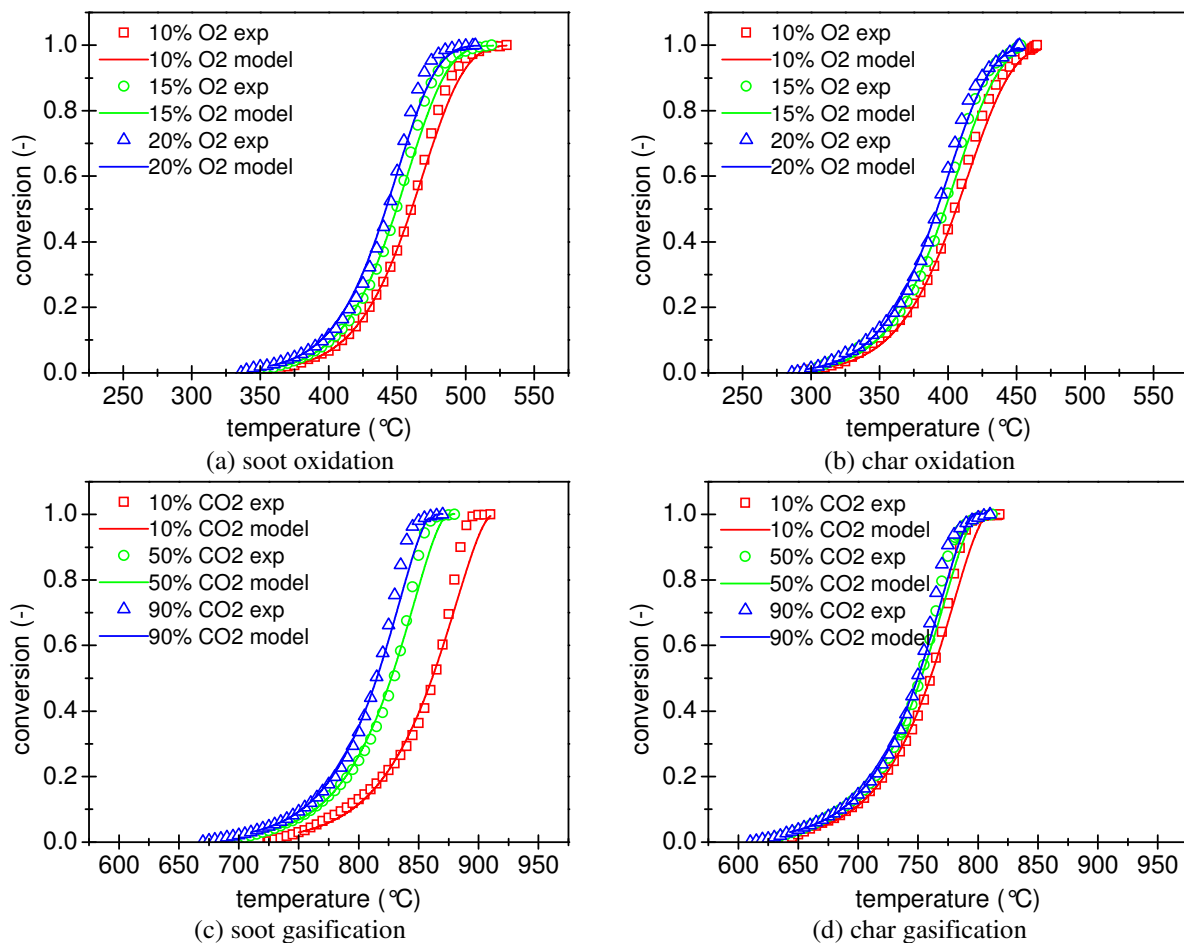

Figure 4.10 Conversion curves of the wood soot (obtained from entrained flow gasification at 1400 °C) and the wood char (obtained from entrained flow gasification at 1000 °C) oxidation and gasification
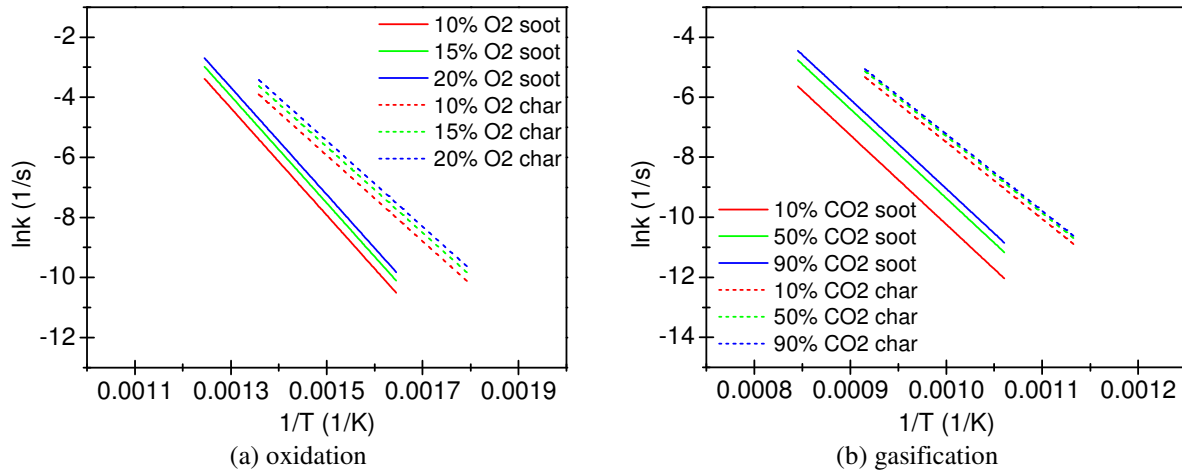
(a) oxidation　　　　　　　　　　　　　　　(b) gasification

Figure 4.11 Arrhenius plots of the wood soot (obtained from entrained flow gasification at 1400 °C) and the wood char (obtained from entrained flow gasification at 1000 °C) oxidation and gasification

As we mentioned, in the experiments of wood gasification at 1000 – 1400 °C, unconverted char was found only at 1000 °C, while soot was always observed in the whole studied temperature range. Thus, the reactivity of the five wood soot samples obtained at 1000 – 1400 °C and the wood char sample produced at 1000 °C were compared. The weight loss curves for the oxidation (10 vol % O_2 in N_2) and gasification (10 vol % CO_2 in N_2) of these samples are shown in Figure 4.12, while the derived kinetic parameters (n and m are fixed) are also shown in Table 4.2. The weight loss curve of the wood soot produced at 1200 °C looks different from the other curves, thus the employed one-step nth order reaction model could not describe its conversion well. Additionally, the kinetic parameters are shown in Arrhenius plots in Figure 4.13. During both oxidation and gasification, the conversion of the soot produced at a higher temperature takes place at a lower temperature in the STA measurements. This reveals that both the oxidation reactivity and gasification reactivity of soot increase when the soot is produced at high temperature. This is surprising since the reactivity of solid carbonaceous fuel normally decreases with increasing pyrolysis temperature [30,34]. However, as listed in Table 4.1, the potassium content is higher in the soot produced at a higher temperature. Therefore the higher reactivity of soot produced at a higher temperature may be related to the presence of potassium, perhaps as intercalated species in the carbon, which is known to catalyze gasification reactions [35,36]. Further experiments would be required to verify this proposal in detail. Moreover, it also can be observed that the char produced at 1000 °C is more reactive than the soot produced at the same temperature as well as the soot produced at higher temperatures.
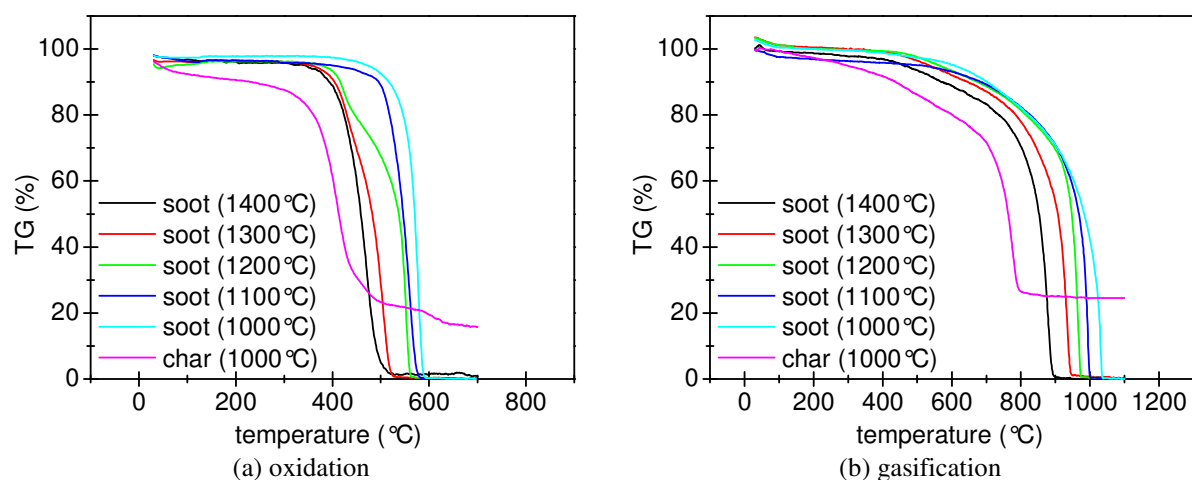
(a) oxidation   (b) gasification

Figure 4.12 Weight loss curves for the oxidation and gasification of the wood soot obtained from entrained flow gasification at 1000 – 1400 °C and the wood char obtained from entrained flow gasification at 1000 °C (10 vol % O_2 or CO_2 in N_2)

(a) oxidation   (b) gasification
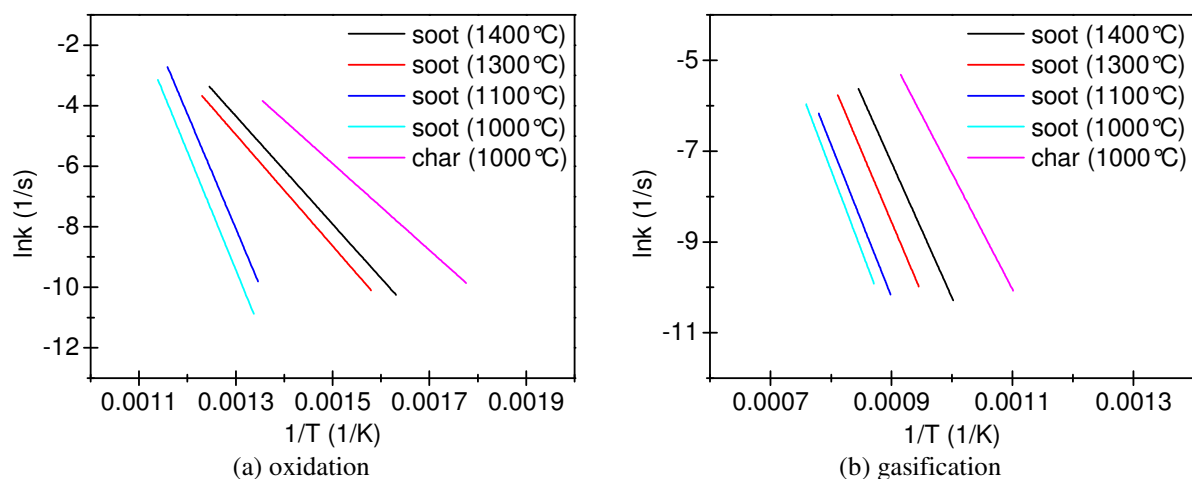
Figure 4.13 Arrhenius plots of the wood soot obtained at 1000, 1100, 1300, and 1400 °C and the wood char obtained at 1000 °C (10 vol % O_2 or CO_2 in N_2)

4.4 Conclusions

Biomass (wood, straw, and dried lignin) gasification was carried out in a lab scale atmospheric pressure entrained flow reactor. In the experiments, the solid products in the syngas were collected successively by a cyclone and a metal filter. In the cyclone, solid particles were collected only in the gasification experiments conducted at 1000 °C, while solid particles were captured in the metal filter in all the gasification experiments conducted at 1000 – 1400 °C. The obtained solid samples were analyzed by STA to determine the composition (moisture, organic matters, volatilizable inorganic compound, and residual ash) and by SEM with EDS to obtain the size, morphology, and elemental distribution.

106

Furthermore, the reactivity and kinetics of the soot and char produced in the wood gasification experiments were assessed by STA.

During wood gasification, the major part of the collected solids on the filter is soot. The SEM image with the EDS spectrum of the wood filter sample obtained at 1400 °C shows that the soot particles appear as agglomerated nano-size carbon spheres (< 100 nm) that are rich in carbon. Under the same operating condition (T = 1400 °C, H_2O/C = 0.5), in comparison to wood gasification, the filter sample obtained from straw gasification has a low soot content and high KCl and K_2SO_4 contents. During straw gasification, increasing the steam/carbon molar ratio from 0.0 to 1.0 leads to decreasing soot content in the solids and thereby an increasing KCl and K_2SO_4 contents. The SEM images show that increasing the steam/carbon molar ratio from 0.0 to 1.0 leads to changes in the shapes of the particles from sphere to irregular crystals and their size increasing from below 100 nm to above 100 nm. This is probably caused by KCl and K_2SO_4 deposited on the surface of soot particles. Their EDS spectra show that with steam addition, the carbon peak obviously decreases while the potassium and chlorine peaks notably increase. The filter sample obtained from the dried lignin gasification experiment mainly consisted of soot and non-volatilizable inorganic matter due to the lignin ash being rich in silica and calcium. The SEM images of the parent wood particle and the derived char samples show that both of them have a layered structure with a loose and porous texture. Their similarity indicates that complete melting of char did not take place in the conducted entrained flow gasification experiment (T = 1000 °C).

In the study on the kinetics and reactivity of the soot and char, we found that the char is more reactive than soot for both oxidation and gasification, probably due to a less ordered structure of carbon in the char compared to the soot. For both the soot and char, the reaction order with respect to the solid phase is found to be 1.0 during oxidation and 0.5 during gasification. The activation energy of the soot conversion is higher than that of the char conversion. This difference in reactivity partly explains why char is generally fully converted in the conducted entrained flow gasification experiments while soot is not. Moreover, the soot produced at a higher temperature is more reactive than the soot produced at a lower temperature, and the char produced at 1000 °C is more reactive than the soot produced at the same temperature as well as the soot produced at higher temperatures.

4.5 References

[1] Balat M, Balat M, Kırtay E, Balat H. Main routes for the thermo-conversion of biomass into fuels and chemicals. Part 2: Gasification systems. Energy Conversion and Management 2009;50:3158-68.

[2] Higman C, Van der Burgt M. Gasification processes. Gasification. Burlington: Gulf Professional Publishing, 2008:91-3.

[3] Syngas production from coal. 2010. Available from: http://www.iea-etsap.org/web/E-TechDS/PDF/S01-Coal%20gasification-GS-gct.pdf.

[4] Crnomarkovic N, Repic B, Mladenovic R, Neskovic O, Veljkovic M. Experimental investigation of role of steam in entrained flow coal gasification. Fuel 2007;86:194-202.

[5] Van der Drift A, Boerrigter H, Coda B, Cieplik M, Hemmes K, van Ree R, Veringa H. Entrained flow gasification of biomass: ash behaviour, feeding issues, and system analyses. ECN. 2004.

[6] Kajitani S, Suzuki N, Ashizawa M, Hara S. CO_2 gasification rate analysis of coal char in entrained flow coal gasifier. Fuel 2006;85:163-9.

[7] Choi Y, Li X, Park T, Kim J, Lee J. Numerical study on the coal gasification characteristics in an entrained flow coal gasifier. Fuel 2001;80:2193-201.

[8] Kristiansen A. Understanding coal gasification. IEA Coal Research. 1996.

[9] Henrich E, Weirich F. Pressurized entrained flow gasifiers for biomass. Environ Eng Sci 2004;21:53-64.

[10] Johansson TB, Kelly H, Reddy AKN, Williams R, Drennen TE. Renewable energy: sources for fuels and electricity. Washington, D.C.: Island Press, 1992:593-651.

[11] Milne TA, Abatzoglou N, Evans RJ. Biomass gasifier 'tars' : their nature, formation, and conversion. National Renewable Energy Laboratory. 1998.

[12] El-Rub ZA, Bramer E, Brem G. Tar removal in an Entrained Flow Cracker (EFC) with application to biomass gasification. Pyrolysis and Gasification of Biomass and Waste, Proceedings of an Expert Meeting, Meeting Date 2002:337-346.

[13] Kirubakaran V, Sivaramakrishnan V, Nalini R, Sekar T, Premalatha M, Subramanian P. A review on gasification of biomass. Renewable and Sustainable Energy Reviews 2009;13:179-86.

[14] Bridgwater A. The technical and economic feasibility of biomass gasification for power generation. Fuel 1995;74:631-53.

[15] Gao C, Vejahati F, Katalambula H, Gupta R. Co-gasification of Biomass with Coal and Oil Sand Coke in a Drop Tube Furnace†. Energy Fuels 2009;24:232-40.

[16] Qin K, Jensen PA, Lin W, Jensen AD. Biomass gasification behavior in entrained flow reactor: gas product distribution and soot formation. Energy & Fuels 2012;26:5992-6002.

[17] Henrich E, Burkle S, Meza-Renken Z, Rumpel S. Combustion and gasification kinetics of pyrolysis chars from waste and biomass. J Anal Appl Pyrolysis 1999;49:221-41.

[18] Qin K, Lin W, Jensen PA, Jensen AD. High-temperature entrained flow gasification of biomass. Fuel 2012;93:589-600.

[19] Coats A, Redfern J. Kinetic parameters from thermogravimetric data. Nature 1964;201:68-9.

[20] Popescu C, Segal E. Critical considerations on the methods for evaluating kinetic parameters from nonisothermal experiments. Int J Chem Kinet 1998;30:313-27.

[21] Arvelakis S, Jensen PA, Dam-Johansen K. Simultaneous thermal analysis (STA) on ash from high-alkali biomass. Energy Fuels 2004;18:1066-76.

[22] Hansen LA, Frandsen FJ, Dam-Johansen K, Sørensen HS. Quantification of fusion in ashes from solid fuel combustion. Thermochimica acta 1999;326:105-17.

[23] Hindiyarti L, Frandsen F, Livbjerg H, Glarborg P, Marshall P. An exploratory study of alkali sulfate aerosol formation during biomass combustion. Fuel 2008;87:1591-600.

[24] Jensen JR, Nielsen LB, Schultz-Møller C, Wedel S, Livbjerg H. The nucleation of aerosols in flue gases with a high content of alkali-A laboratory study. Aerosol Sci Technol 2000;33:490-509.

[25] Christensen KA, Livbjerg H. A plug flow model for chemical reactions and aerosol nucleation and growth in an alkali-containing flue gas. Aerosol Sci Technol 2000;33:470-89.

[26] Glarborg P, Marshall P. Mechanism and modeling of the formation of gaseous alkali sulfates. Combust Flame 2005;141:22-39.

[27] Septien S, Valin S, Dupont C, Peyrot M, Salvador S. Effect of particle size and temperature on woody biomass fast pyrolysis at high temperature (1000–1400° C). Fuel 2012;97:202-10.

[28] Zhang Y, Kajitani S, Ashizawa M, Miura K. Peculiarities of rapid pyrolysis of biomass covering medium-and high-temperature ranges. Energy Fuels 2006;20:2705-12.

[29] Dall'Ora M, Jensen PA, Jensen AD. Suspension combustion of wood: Influence of pyrolysis conditions on char yield, morphology, and reactivity. Energy Fuels 2008;22:2955-62.

[30] Zolin A, Jensen A, Jensen PA, Frandsen F, Dam-Johansen K. The influence of inorganic materials on the thermal deactivation of fuel chars. Energy Fuels 2001;15:1110-22.

[31] Watanabe H, Otaka M. Numerical simulation of coal gasification in entrained flow coal gasifier. Fuel 2006;85:1935-43.

[32] Laurendeau NM. Heterogeneous kinetics of coal char gasification and combustion. Prog Energy Combust Sci 1978;4:221-70.

[33] Cozzani V. Reactivity in oxygen and carbon dioxide of char formed in the pyrolysis of refuse-derived fuel. Ind Eng Chem Res 2000;39:864-72.

[34] Zolin A, Jensen AD, Jensen PA, Dam-Johansen K. Experimental study of char thermal deactivation. Fuel 2002;81:1065-75.

[35] Wen WY. Mechanisms of alkali metal catalysis in the gasification of coal, char, or graphite. Catalysis Reviews—Science and Engineering 1980;22:1-28.

[36] Wigmans T, Hoogland A, Tromp P, Moulijn JA. The influence of potassium carbonate on surface area development and reactivity during gasification of activated carbon by carbon dioxide. Carbon 1983;21:13-22.

Chapter 5 Biomass and coal co-gasification behavior

Abstract

Co-gasification of fuel mixtures, straw/wood, straw/coal, and wood/coal, were investigated at 1400 °C with steam addition in a laboratory-scale atmospheric pressure entrained flow reactor, previously applied for gasification of the individual biomass fuels. The yields of solid products (char and/or soot) decreased with increasing straw fraction during straw/wood co-gasification and with increasing biomass fraction (straw or wood) during biomass/coal co-gasification. The results further indicate a synergistic effect on lowering the solid product yields during co-gasification. The yields of H_2, CO, and CO_2 remained nearly unchanged with changed mixing ratio during straw/wood co-gasification, in agreement with their similar yields during gasification of the individual biomass fuels. On the other hand, the gas yields increased with a rise of biomass mixing ratio during biomass/coal co-gasification.

5.1 Introduction

As a result of environmental and sociopolitical considerations, there is an increasing world-wide interest in the use of biomass resources for energy and chemicals [1]. Biomass resources are one of the major components of strategies to mitigate global climate change since biomass is considered as a sustainable CO_2 neutral energy source [2]. Now, biomass is becoming a priority resource to substitute fossil fuels in the energy sector (heat and power) and is increasingly seen to be so in the transport sector as well [3-5]. In Denmark, wood chips, wood pellets, and straw are increasingly used to substitute fossil fuels for heat and power production. The first step to use biomass can be to apply it together with fossil fuels in the plants originally designed to only use fossil fuels. Thus, co-firing and co-gasification are recognized as a promising technology and is becoming of great importance. Biomass, coal, and their mixtures can be converted into syngas, rich in H_2 and CO, by gasification. The syngas can be used to synthesize storable liquid and gaseous fuels or chemicals in catalytic processes and also be burned to generate heat or electricity in gas engines and gas turbines [6]. Therefore, gasification may be considered as a flexible component in an energy system. Compared with fixed bed and fluidized bed gasifiers, entrained flow gasifiers operate at higher temperature with smaller particle size, hence the carbon conversion and syngas quality (almost free of tar) are high [7]. The syngas composition, most importantly the H_2/CO ratio, may be adjusted by

controlling the operating conditions [8,9] and by changing the feedstock types, such as using different biomass types and biomass/coal mixtures [10].

In order to evaluate possible impacts on the process and the product yields, research activities on co-gasification of biomass/coal have increased in the recent years. Most investigations were carried out in fixed bed gasifiers [11-13] and fluidized bed gasifiers [3,14-20]. However, entrained flow gasification is a most suitable technology for the conversion of biomass and coal mixtures due to high reaction temperature that can compensate for the different reactivity of the fuels and achieve good carbon conversion even with high rank, low reactivity coals. Moreover, because of the commercial large scale availability and potential high efficiency, entrained flow gasification seems to be an interesting technology for syngas production towards XtL processes. To our knowledge, only few studies have been reported on entrained flow gasification of fuel mixtures in the open literatures [21,22]. Among these, the applied temperatures (750 – 1250 °C) were relatively low and steam addition, which has an obvious influence on the gasification behavior, was not studied. Therefore, further studies of entrained flow biomass/coal co-gasification at high temperature (> 1200 °C) with steam addition are of great interest.

The aim of this study is to provide knowledge and experimental data of entrained flow co-gasification. Initially, gasification of the individual fuels (coal, straw, and wood) was investigated at different temperatures (1200 – 1400 °C). Secondly, co-gasification of fuel mixtures (straw/wood, straw/coal, and wood/coal) was investigated at varying mixing ratio at 1400 °C with steam addition.

5.2 Experimental

5.2.1 Materials

The setup used for co-gasification experiments is a laboratory-scale atmospheric pressure entrained flow reactor, shown in Chapter 3. Three fuels were used in the present study: coal (pulverized Columbian bituminous coal), straw (pulverized wheat straw pellets) and wood (beech sawdust). The biomass (straw and wood) used in the present study is same as that used in the previous study, shown in Chapter 3. The properties of coal, straw, and wood are listed in Table 5.1. Compared with straw and wood, coal has lower volatile content, higher carbon content, higher ash content (including high levels of silica, alumina, and iron), and higher heating value. The compositions of the organic fractions of straw and wood are quite similar

but straw has higher ash content and the ash is rich in potassium. Figure 5.1 shows the particle size distributions of the three fuels that were determined by sieve classification. The median diameter (d_{50}) of the coal particles is 60 µm, which is much smaller than that of the straw (130 µm) and wood (310 µm) particles. The fuel mixtures (straw/wood mixtures, or straw/coal mixtures, or wood/coal mixtures) with different mixing ratio were premixed before gasification experiments.

Table 5.1 Properties of fuels

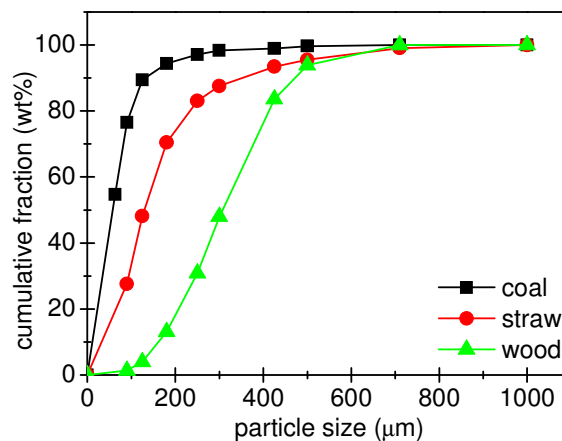| properties		coal (as-received basis)	straw (as-received basis)	wood (as-received basis)
moisture	wt %	5.00	5.40	9.04
ash	wt %	9.60	4.54	0.61
volatile	wt %	34.90	72.27	76.70
fixed carbon	wt % (by diff.)	50.50	17.79	13.65
lower heating value	MJ/kg	27.09	16.35	16.44
C	wt %	68.90	43.42	45.05
H	wt %	4.61	5.58	5.76
O	wt % (by diff.)	9.82	40.60	39.41
N	wt %	1.44	0.37	0.13
S	wt %	0.62	0.09	0.01
Si	wt %	2.57	1.23	-
K	wt %	0.17	0.76	-
Cl	wt %	0.01	0.25	-
Ca	wt %	0.15	0.23	-
Mg	wt %	0.13	0.06	-
P	wt %	0.01	0.03	-
Na	wt %	0.06	0.01	-
Al	wt %	1.05	0.01	-
Fe	wt %	0.49	0.01	-
Ti	wt %	0.05	0.00	-

Figure 5.1 Particle size distributions of fuels

5.2.2 Conditions

All conducted experiments are listed in Table 5.2. The feeding rate of the different fuels was adjusted to ensure the same thermal input (3.5 kW) due to the considerable differences among the heating values of coal, biomass, and their mixtures. The coal, straw, and wood were premixed each other according to the different thermal ratios (th %). The excess air ratio (λ), steam/carbon ratio (H_2O/C), and oxygen concentration (O_2) in all experiments were fixed at 0.3, 0.5, and 21 % respectively. The calculations of thee three operating parameters were described in Chapter 2. The fuel particle residence time (t) in the reactor was approximately 3 – 4 s, which was determined by the gas mean residence time assuming there was no relative velocity between the solid phase and gas phase. Because it was not possible to measure the total flow of gas products directly, the total gas flow was calculated by using N_2 as a tracer, from which the yield of gas product per unit of thermal input (Nm^3/MJ) can be calculated. Also, the yield of solid product can be expressed by the similar unit (g/MJ).

Table 5.2 List of conducted experiments

NO.	Fuel	fuel feeding rate	LHV	feeder gas (air)	main gas (air)	steam	purge gas (N_2+air)	T	t
-	-	g/min	MJ/kg	NL/min	NL/min	g/min	NL/min	°C	s
1	coal	7.8	27.09	10	6.5	4.0	2.7+0.3	1200	4.3
2	coal	7.8	27.09	10	6.5	4.0	2.7+0.3	1300	3.7
3	coal	7.8	27.09	10	6.5	4.0	2.7+0.3	1400	3.3
4	straw	12.8	16.35	10	5.5	4.2	2.7+0.3	1200	3.8
5	straw	12.8	16.35	10	5.5	4.2	2.7+0.3	1300	3.4
6	straw	12.8	16.35	10	5.5	4.2	2.7+0.3	1400	3.1
7	wood	12.8	16.44	10	6.2	4.3	2.7+0.3	1200	3.8
8	wood	12.8	16.44	10	6.2	4.3	2.7+0.3	1300	3.4
9[a]	wood	12.8	16.44	10	6.2	4.3	2.7+0.3	1400	3.1
10	25th % straw + 75th % wood	12.8	16.42	10	6.0	4.3	2.7+0.3	1400	3.1
11	50th % straw + 50th % wood	12.8	16.39	10	5.8	4.2	2.7+0.3	1400	3.1
12	75th % straw + 25th % wood	12.8	16.37	10	5.7	4.2	2.7+0.3	1400	3.1
13	25th % straw + 75th % coal	9.0	23.27	10	6.3	4.1	2.7+0.3	1400	3.2
14	50th % straw + 50th % coal	10.3	20.39	10	6.0	4.1	2.7+0.3	1400	3.1
15	75th % straw + 25th % coal	11.6	18.15	10	5.7	4.1	2.7+0.3	1400	3.1
16	25th % wood + 75th % coal	9.0	23.31	10	6.4	4.1	2.7+0.3	1400	3.2
17	50th % wood + 50th % coal	10.3	20.46	10	6.4	4.2	2.7+0.3	1400	3.1
17	75th % wood + 25th % coal	11.5	18.23	10	6.3	4.2	2.7+0.3	1400	3.0

[a] Repetition experiments were performed

In order to identify different particles and determine the amounts of char and soot, the solid samples were analyzed by scanning electron microscopy (Zeiss Supra 35 FEGSEM) and thermogravimetry (Netzsch STA-449C). The detailed method for STA analysis is described in Chapter 3. Based on the STA analysis, different fractions of the solid particles, such as moisture, organic matters, volatilizable inorganic compounds, and residual ash, can be

identified. The organic matters in the cyclone and filter samples are defined as char and soot respectively.

5.3 Results and discussion

5.3.1 Gasification behaviors of individual fuel

Figure 5.2 depicts the yields of syngas products during coal, straw, and wood gasification. The applied reactor temperature range was between 1200 and 1400 °C with otherwise fixed operating parameters (steam/carbon ratio = 0.5, excess air ratio = 0.3, and oxygen concentration = 21 %). Solid particles were only collected in the cyclone during coal gasification, and according to SEM analysis, the organic matter in these cyclone samples was unconverted char. Solid particles were always collected on the metal filter during coal, straw, and wood gasification. During both straw and wood gasification the organic matter in the filter samples was soot, and during coal gasification it was mainly fine char particles, mixed with a small fraction of soot particles. That char particles bypassed the cyclone and entered the filter is probably because coal particles are rather small and further may undergo fragmentation at the very high heating rate in the reactor. That relatively little soot was produced during coal gasification is probably because the coal has low volatile content, leading to more char but less soot. During coal gasification, the amount of unreacted char and soot decreased when the reactor temperature increased from 1200 to 1400 °C. The H_2 and CO yields increased significantly from 17.1 to 25.8 NL/MJ and from 17.3 to 31.7 NL/MJ respectively, while the CO_2 yield decreased gradually from 12.2 to 9.2 NL/MJ. Besides, CH_4 was the only component of C_xH_y in the coal gasification experiments and it was found only at 1200 °C with a very low value of 0.3 NL/MJ. The H_2, CO, and CO_2 yields are very similar for straw and wood gasification, and are higher than for coal gasification due to the higher amount of unconverted solids during coal gasification. The CH_4 yield was higher during both straw and wood gasification than during coal gasification at low temperature, but declined sharply to disappear at 1400 °C. C_2H_2 was observed only at 1200 °C with a low level of about 0.2 NL/MJ during both straw and wood gasification. Comparing straw and wood gasification, it can be seen that they provided quite similar syngas compositions except for the soot yield. During straw gasification the soot yield was much lower, probably because of the high potassium content in straw that might affect the level of soot precursors and soot formation reactions , as discussed in greater detail elsewhere [23].

The distributions of syngas products are determined by both the initial pyrolysis step and further reactions during the gasification step. The initial pyrolysis step can be divided into two basic stages: primary pyrolysis and secondary pyrolysis [24-28]. During the primary pyrolysis, fuel is converted to light gases (H_2, CO, CO_2, H_2O, and light hydrocarbons), tar, and char [29]. With increasing temperature the yields of H_2 and CO increase obviously while the yields of CO_2 and light hydrocarbons increase slightly or almost keep constant because they come from different structures, functional groups, and cross linking reactions [28,30-39]. The tar release increases with increasing temperature initially, but above a certain temperature (about 500 °C for biomass and about 700 °C for coal) it stays at a steady (maximum) value [24,30,40-43]. Due to the evolution of gas and tar, the char yield decreases as temperature increased. At elevated temperatures under the secondary pyrolysis, tar is converted to lighter gases and soot [24,26,28,29], and so the tar yield declines continuously until all tar is completely converted. Substantial H_2 is released from the tar conversion and soot formation and its yield increases with increasing temperature [44-46]. Significant CO is generated from the tar conversion and its yield also increases with increasing temperature [26,44-46]. A certain amount of CO_2 is also generated from tar conversion while its yield is almost unaltered as temperature is increased [26,45,46]. Light hydrocarbons are formed by the tar cracking but are simultaneously also consumed by the soot formation reactions, particularly at high temperature [24,26,28,29]. Therefore, in the whole pyrolysis step, with an increasing of temperature, the yields of soot, H_2, and CO increase, the CO_2 yield increases slightly or remains at a certain level and the yields of light hydrocarbons and tar decrease gradually. During gasification, high temperature favors endothermic reactions including char and soot gasification and hydrocarbons reforming reactions with CO_2 and H_2O, but suppresses the exothermic water gas shift reaction [47-49]. Thus, more H_2 and CO are generated but CO_2, light hydrocarbons, char, and soot are consumed with increasing temperature. Soot gasification, which competes with soot formation, has higher reactivity at higher temperature (> 1200 °C) [50-52], so the soot yield decreases with increasing temperature. As a result, during the whole gasification process, the final yields of H_2 and CO increase while the yields of CO_2, C_xH_y, char, and soot decrease as the temperature increases, which are consistent with the experimental results shown in Figure 5.2. The results of the repetition experiments conducted at 1400 °C during wood gasification are also shown in Figure 5.2 and good repeatability of the measured values was observed. The average deviations of measurements on main products are listed in Table 5.3.
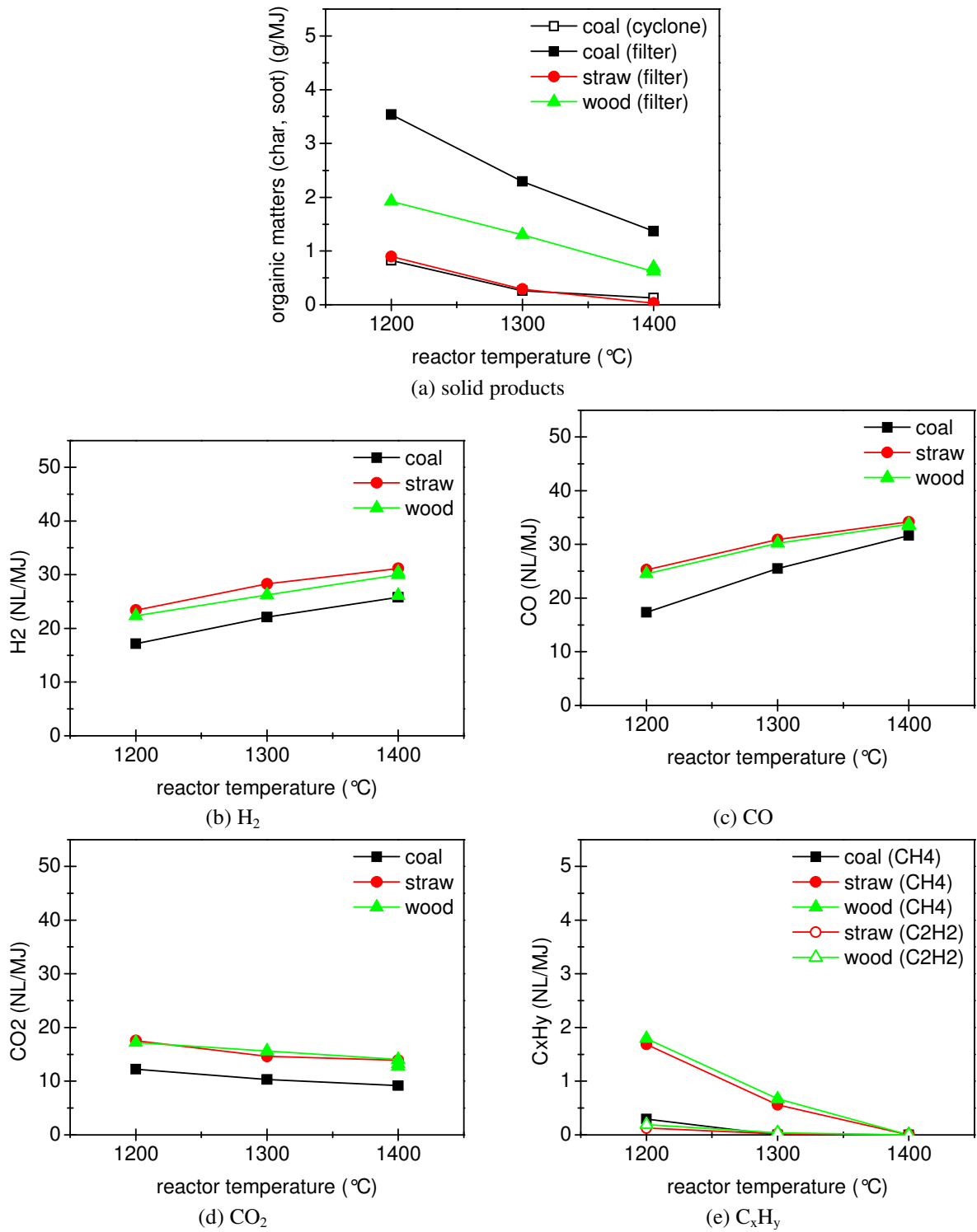
(a) solid products

(b) H$_2$

(c) CO

(d) CO$_2$

(e) C$_x$H$_y$

Figure 5.2 Product yields during coal, straw, and wood gasification: H$_2$O/C = 0.5, λ = 0.3, and O$_2$ = 21 %

Table 5.3 Average deviations of measurements in the experiment NO. 9 listed in Table 5.2

main products	absolute deviation	relative deviation
soot (g/MJ)	± 0.03 g/MJ	± 4.52 %
H$_2$ (NL/MJ)	± 1.81 NL/MJ	± 6.27 %
CO (NL/MJ)	± 0.07 NL/MJ	± 0.21 %
CO$_2$ (NL/MJ)	± 0.45 NL/MJ	± 3.40 %

(a) carbon distribution   (b) carbon conversion
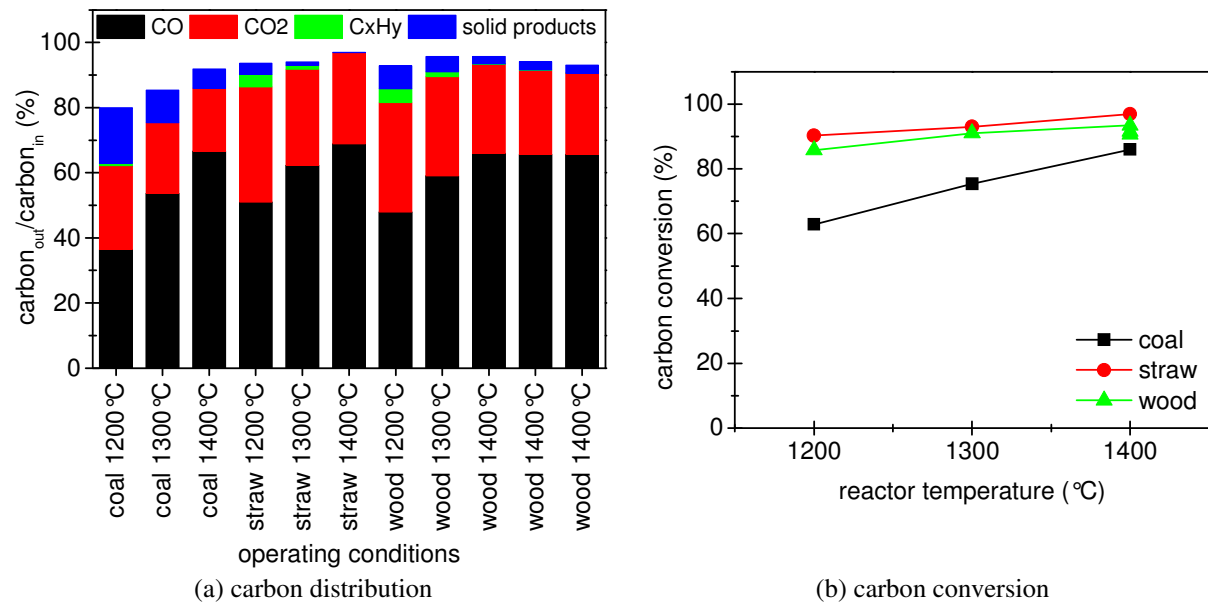
Figure 5.3 Carbon distribution and conversion during coal, straw and wood gasification: $H_2O/C = 0.5$, $\lambda =$ 0.3, and $O_2 = 21$ %

The carbon distribution and conversion in the gasification experiments of coal, straw, and wood is shown in Figure 5.3. The calculation is based on the fuel analysis, the fuel feeding rate, and the yields of carbonaceous products. In Figure 5.3 (a), it can be observed that the carbon in the fuel was mostly partitioned to CO and CO_2. C_xH_y contributes slightly to the overall carbon balance at lower temperature but it decreased gradually with increasing temperature. Carbon in the solid products (char and/or soot) gives an important contribution in all coal gasification experiments and also in biomass gasification experiments at 1200 °C. Overall, the carbon balance closure was reasonable and higher than 90 % except for the two coal gasification experiments that were conducted at 1200 and 1300 °C (15 – 20 % gap). In these two experiments, it is expected that the yields of solid products were higher than measured probably because soot and char deposited on the reactor walls and were not totally converted to gas due to the relatively low temperature. Thereby, they were not included in the carbon balance calculation. The water yields in the syngas were not determined, and therefore the hydrogen and oxygen mass balance could not be done.

The carbon conversion is an important indicator in a gasification process and is defined as [7]:

$$\text{carbon conversion (\%)} = \frac{\text{carbon in gas products}}{\text{carbon in fuel}} \times 100 \text{ \%} \tag{5.1}$$

As shown in Figure 5.3 (b), the carbon conversion increased with increasing temperature which revealed that raising temperature favored fuel conversion to gas products. While this is intuitively expected, it may actually not be the case since in Chapter 2 and 3 we have

previously observed that the soot yield goes through a maximum at intermediate temperature (1100 – 1200 °C). The same operating parameters were used and similar amounts of supplied gas and steam were employed in the coal and biomass gasification experiments, as well as the same thermal input. However, compared with coal gasification (approximate 65 – 85 % at 1200 – 1400 °C), biomass gasification achieved a higher carbon conversion (approximate 85 – 95 % at 1200 – 1400 °C) probably due to higher reactivity of biomass and the lower char mass fraction from biomass pyrolysis. This indicates that biomass gasification can be accomplished at lower oxygen and steam to fuel ratio compared to coal and this is beneficial for the process economy.
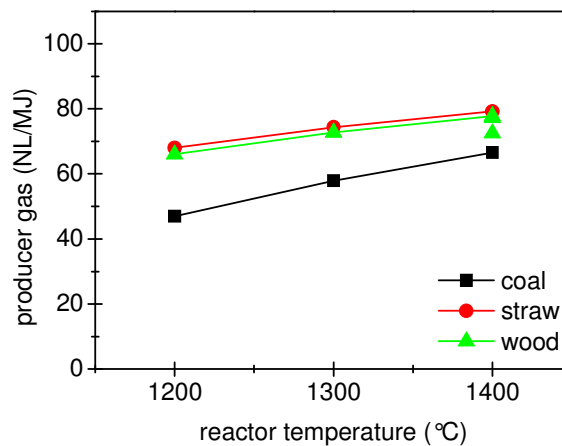

Figure 5.4 Producer gas yield during coal, straw, and wood gasification: $H_2O/C = 0.5$, $\lambda = 0.3$, and $O_2 = 21$ %
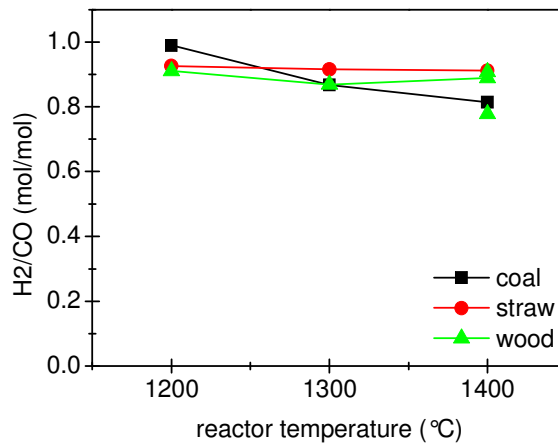

Figure 5.5 H_2/CO molar ratio during coal, straw, and wood gasification: $H_2O/C = 0.5$, $\lambda = 0.3$, and $O_2 = 21$ %

It is desirable to convert all fuel to gaseous products, particularly H_2 and CO. The producer gas yield (defined as the total amount of gas products including H_2, CO, CO_2, and C_xH_y) is another important indicator to evaluate the gasification process. The producer gas yield during coal, straw, and wood gasification is shown in Figure 5.4. It can be seen that it increased from about 67.0 to about 78.5 NL/MJ during both straw and wood gasification when the reactor

119

temperature was increased from 1200 to 1400 °C. At each temperature, compared with biomass gasification, the producer gas yield was lower during coal gasification because of the higher amount of unconverted solids, while its variation trend was the same. For different purposes of syngas utilization, different H_2/CO molar ratio is preferred, so this ratio is also an important indicator for a gasification process. Figure 5.5 shows the H_2/CO molar ratio during coal, straw, and wood gasification. When the temperature increased from 1200 to 1400 °C, the H_2/CO molar ratio decreased from 1.0 to 0.8 during coal gasification, while it kept nearly constant around 0.9 during both straw and wood gasification.

To compare the experimental condition with equilibrium condition, equilibrium calculations were conducted using the FactSage Program for experiments conducted at 1400 °C (NO. 3, 6, and 9, listed in Table 5.2). There was no carbon left in the equilibrium calculation, so the equilibrium syngas consisted of CO, CO_2, H_2, and H_2O. The product distributions of experiments and equilibrium calculations are compared in Figure 5.6. The majority of the undetermined product is water in these experiments (highest temperature with steam addition). Generally, the experimental results from straw and wood gasification were reasonably similar to the equilibrium calculation results, while the experimental results from coal gasification were different from the equilibrium calculation results to some degree mainly due to the low carbon conversion in the coal gasification experiment.
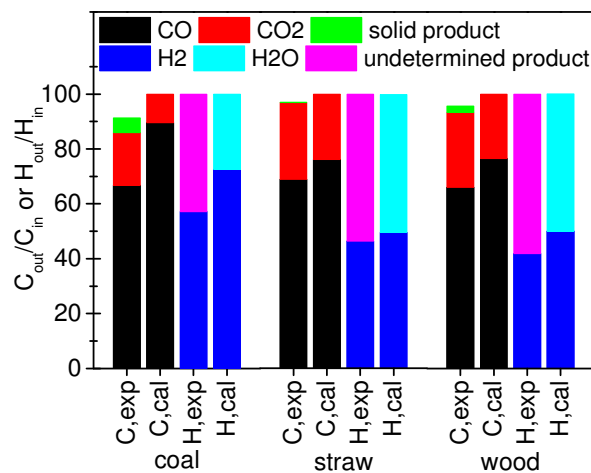

Figure 5.6 Comparison between the results of experiment and equilibrium calculation: the selected experiments are NO. 3, 6, and 9, listed in Table 5.2, with fixed operating parameters (T = 1400 °C, H_2O/C = 0.5, λ = 0.3, and O_2 = 21 %); C,exp and H,exp are the carbon and hydrogen balance in the experiment; C,cal and H,cal are the carbon and hydrogen balance in the equilibrium calculation

5.3.2 Co-gasification behaviors of fuel mixtures

The syngas composition during co-gasification of fuel mixtures is shown in Figure 5.7. The mixing ratio of any two fuels was increased from 0 to 100 th % with increments of 25 th % while the operating conditions in these experiments were fixed (reactor temperature = 1400 °C, steam/carbon ratio = 0.5, excess air ratio = 0.3, and oxygen concentration = 21 %). The calculated yield of each product (Y_{cal}) at any mixing ratio during co-gasification is

$$Y_{cal}\left(\frac{g, NL}{MJ}\right) = \sum_{i=1}^{2} r_{mix,fuel\,i}(th\,\%) \times Y_{exp,fuel\,i}\left(\frac{g, NL}{MJ}\right) \qquad (5.2)$$

where $r_{mix,\,fuel\,i}$ is the mixing ratio of the first fuel and second fuel respectively, and $Y_{exp,\,fuel\,i}$ is the product yield from gasification of the first fuel and the second fuel respectively. Figure 5.7 (a) – (c) depict the amounts of solid products (soot and char) in the co-gasification experiments. During co-gasification of straw/wood, no unreacted char was collected in the cyclone but soot was always collected by the metal filter. When the mixing ratio of straw increased, the soot yield decreased because straw gasification produced less soot than wood gasification. Furthermore, compared with the calculated values, the experimental yield of soot was lower, which indicates a synergistic effect on the soot yield in the co-gasification experiments of straw/wood. This is possibly owing to the high potassium content in straw that might have catalytic effect on soot formation and soot conversion [23]. During co-gasification of biomass/coal, char was collected in the cyclone only in the experiments with lower biomass mixing ratios (0 – 25 th %) and the amount of char decreased with an increase of biomass mixing ratio because biomass had a higher reactivity and a lower char yield. The difference in the char yield between calculation and experiment was not obvious because its yield was very low or zero during co-gasification of biomass/coal. However, solid particles were always observed on the metal filter and the organic matters in them might be mixtures of soot and fine char particles. When the biomass mixing ratio increased, the amount of soot and fine char mixtures decreased. Their amounts were lower than the calculated values, probably indicating that synergy might exist as well in this case. Some possible explanations of synergy are discussed below. Firstly, different local pyrolysis conditions caused by the different volatile contents of biomass and coal might affect soot formation. Secondly, the interaction of the potassium from straw with soot formation may take place through an ionic mechanism which could neutralize the charge on the soot particles and thereby inhibit their coagulation process [53]. Thirdly, the presence of potassium in the gas phase may act as sensitizers to

produce more OH radicals which react efficiently with soot and char [53]. Fourthly, the potassium and iron from straw and coal respectively, if initially released to the gas phase and then partly recondensed on the char and soot, may have a catalytic effect on soot and char gasification [54-64]. At present our experiments do not allow to firmly determine the relative importance of these possible explanations.
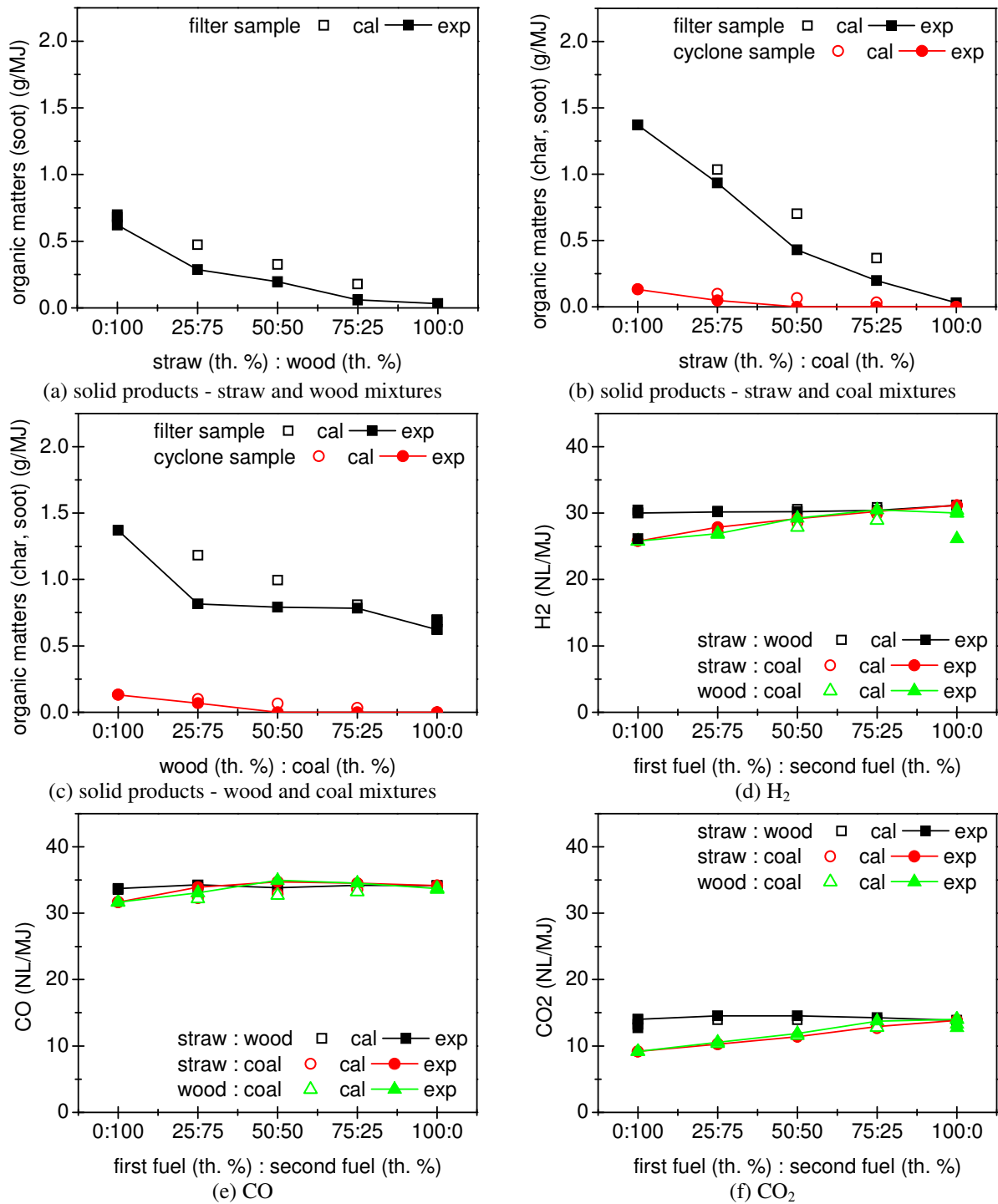

Figure 5.7 Product yields during co-gasification of fuel mixtures: cal and exp are calculated from the experiments with the pure fuels and experimental results respectively; T = 1400 °C, H_2O/C = 0.5, λ = 0.3, and O_2 = 21 %

Figure 5.7 (d) – (f) depict the yields of gas products during co-gasification. There were no hydrocarbons (C_xH_y) formed in the co-gasification experiments probably due to the applied high temperature of 1400 °C. During co-gasification of straw/wood, the yields of H_2, CO, and CO_2 stayed nearly constant at any mixing ratio because straw and wood gasification provided almost the same gas composition. During co-gasification of straw/coal, the yields of H_2, CO, and CO_2 increased from 25.8 to 31.2 NL/MJ, from 31.7 to 34.2 NL/MJ, and from 9.2 to 13.9 NL/MJ respectively when the straw mixing ratio increased from 0 to 100 th %. At each mixing ratio, the individual gas yields during co-gasification of wood/coal and straw/coal were almost the same. As we expected, biomass addition led to an increase of the gas products yields, because biomass char is more reactive than coal char and in the applied setup and under the applied conditions the formed coal char was not completely converted to gas. Besides, in Figure 5.7 (d) – (f), we observed that in all co-gasification experiments, the experimental yields of gas products were almost the same as the calculated values. This is because the improved conversion of solid particles (< 0.4 g/MJ), does not significantly change the amount of the gas products (< 1.5 NL/MJ) since the yield of gas is much higher than that of the solid products.
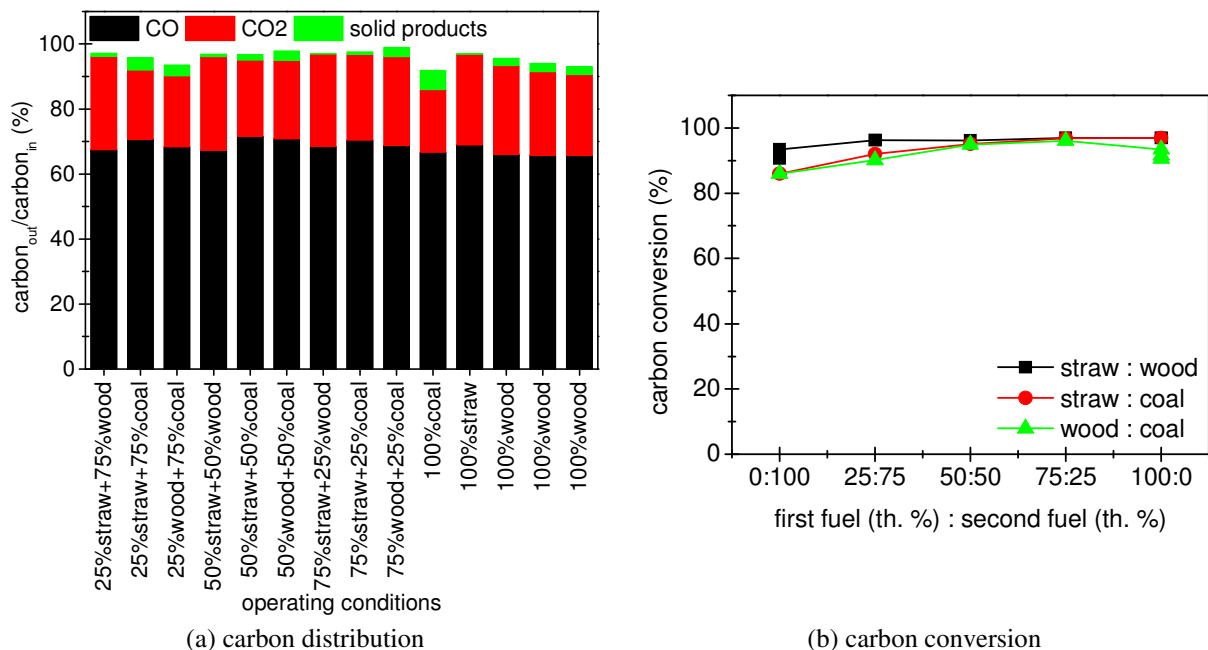

(a) carbon distribution

(b) carbon conversion

Figure 5.8 Carbon distribution and conversion during co-gasification of fuel mixtures: T = 1400 °C, $H_2O/C = 0.5$, $\lambda = 0.3$, and $O_2 = 21$ %

Figure 5.8 shows the carbon distribution and conversion during co-gasification. In Figure 5.8 (a), it can be seen that in all co-gasification experiments CO contributed the most (65 – 70 %) to the overall carbon balance, and CO_2 also gave an important contribution (20 – 30 %), while

the contribution from solid products (char and/or soot) was less than about 5 % and decreased with increasing biomass mixing ratio. The overall carbon balance in each experiment was better than 90 %. Figure 5.8 (b) shows that the carbon conversion during co-gasification of straw/wood was almost constant, about 95 %, which was nearly the same as the carbon conversion obtained during both straw and wood gasification. In the co-gasification experiments of biomass/coal, when the biomass mixing ratio was changed in the range of 0 – 100 th %, the carbon conversion increased from approximately 85 to 95 % mainly due to the higher yields of CO and CO_2. Therefore, biomass addition is helpful to improve carbon conversion during co-gasification of biomass and coal mixtures.
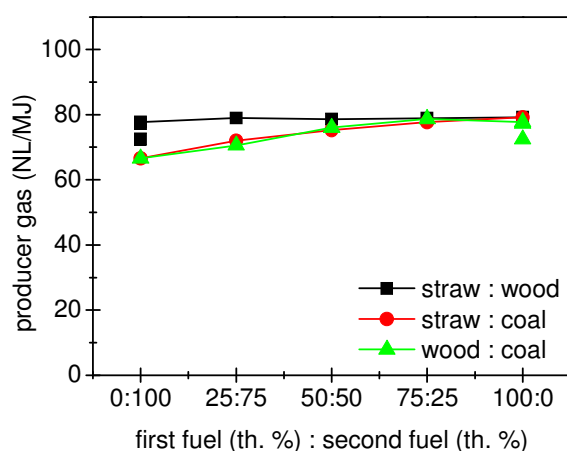
Figure 5.9 Producer gas yield during co-gasification of fuel mixtures: T = 1400 °C, H_2O/C = 0.5, λ = 0.3, and O_2 = 21 %

Figure 5.10 H_2/CO molar ratio during co-gasification of fuel mixtures: T = 1400 °C, H_2O/C = 0.5, λ = 0.3, and O_2 = 21 %

Figure 5.9 shows the producer gas yield during co-gasification. The producer gas yield kept constant around 78.7 NL/MJ for different mixing ratios during co-gasification of straw/wood, because straw and wood provided quite similar gas products. During co-gasification of

124

biomass/coal, an increase of the produced gas yield occurred from about 66.6 to about 78.5 NL/MJ when biomass was added from 0 to 100 th %, since biomass produced more gas products than coal. The H_2/CO molar ratio in the co-gasification experiments is shown in Figure 5.10. During co-gasification of straw/wood, the H_2/CO molar ratio was independent of their mixing ratio and stayed around 0.9. During co-gasification of biomass/coal, the H_2/CO molar ratio increased from 0.8 to 0.9 with biomass mixing ratio increasing from 0 to 100 th %, which indicates that adding biomass increased H_2 more than CO.

5.4 Conclusions

Three individual fuels, a bituminous coal, straw, and wood, were gasified at different temperatures with steam addition in a laboratory scale atmospheric pressure entrained flow reactor. Increasing reactor temperature from 1200 to 1400 °C reduced the amounts of char and soot from coal gasification and of soot from straw and wood gasification, which led to an improved carbon conversion. The yields of desired gas products, H_2 and CO, increased steadily, the yields of CO_2 decreased slightly, and thus the producer gas yield increased by elevating the reactor temperature. By increasing the reactor temperature from 1200 to 1400 °C, the H_2/CO molar ratio in the syngas decreased from 1.0 to 0.8 during coal gasification and kept constant around 0.9 during biomass gasification. C_xH_y was a minor gas product and CH_4 was the most abundant component of C_xH_y. The amount decreased from a very low yield at 1200 °C to disappear at 1400 °C. Compared with coal gasification, biomass gasification yielded more gas products because biomass had higher volatile content and a more complete fuel conversion.

Co-gasification experiments of straw/wood, straw/coal, and wood/coal were investigated at 1400 °C with steam addition in the same setup. The soot yield decreased with increasing straw mixing ratio during co-gasification of straw/wood, and the yields of char and soot decreased with increasing biomass mixing ratio during co-gasification of biomass/coal. The yield of soot in the co-gasification experiments of wood/straw was lower than the calculated value from their weighted yield in the individual fuel experiments, indicating a synergistic effect of co-gasification. This may be due to the high potassium content in straw which could have a catalytic effect on the gasification process. Similarly, the yield of char and/or soot during co-gasification of biomass/coal was also lower than the calculated value, indicating a synergistic effect here as well. The actual reason of the synergistic effect is still not clear, but some possible explanations have been discussed. There was no yield of C_xH_y during co-

gasification probably because of the applied high temperature of 1400 °C. During co-gasification of straw/wood, the amounts of H_2, CO, and CO_2 nearly remained unchanged with changed mixing ratio, because wood and straw gasification provided almost the same gas composition. During co-gasification of biomass/coal, the yields of H_2, CO, and CO_2 increased gradually when the biomass mixing ratio increased because of the improved char conversion resulting from the more reactive biomass char. Thereby the carbon conversion and producer gas yield also increased. The H_2/CO molar ratio increased from 0.8 to 0.9 with increasing biomass mixing ratio from 0 to 100 th %, showing that adding biomass increased H_2 more than CO.

5.5 References

[1] Basu P. Biomass gasification and pyrolysis: Practical design and theory. Oxford: Academic Press. 2010.

[2] Stevens DJ. Hot gas conditioning: recent progress with larger-scale biomass gasification systems. NREL Subcontractor Report: NREL/SR-510-29952. 2001.

[3] McLendon TR, Lui AP, Pineault RL, Beer SK, Richardson SW. High-pressure co-gasification of coal and biomass in a fluidized bed. Biomass Bioenergy 2004;26:377-88.

[4] Savolainen K. Co-firing of biomass in coal-fired utility boilers. Appl Energy 2003;74:369-81.

[5] Hamelinck CN, Faaij APC, den Uil H, Boerrigter H. Production of FT transportation fuels from biomass; technical options, process analysis and optimisation, and development potential. Energy 2004;29:1743-71.

[6] McKendry P. Energy production from biomass (part 3): gasification technologies. Bioresour Technol 2002;83:55-63.

[7] Higman C, Van Der Burgt M. Gasification. USA: Gulf Professional Publishing. 2003.

[8] Coetzer R, Keyser M. Experimental design and statistical evaluation of a full-scale gasification project. Fuel Process Technol 2003;80:263-78.

[9] Van Paasen S, Kiel J, Veringa H. Tar formation in a fluidised bed gasifier. ECN-report: ECN-C-04-013. 2004.

[10] Chaudhari S, Bej S, Bakhshi N, Dalai A. Steam gasification of biomass-derived char for the production of carbon monoxide-rich synthesis gas. Energy Fuels 2001;15:736-42.

[11] Kumabe K, Hanaoka T, Fujimoto S, Minowa T, Sakanishi K. Co-gasification of woody biomass and coal with air and steam. Fuel 2007;86:684-9.

[12] Fermoso J, Arias B, Plaza M, Pevida C, Rubiera F, Pis J, et al. High-pressure co-gasification of coal with biomass and petroleum coke. Fuel Process Technol 2009;90:926-32.

[13] Fermoso J, Arias B, Gil M, Plaza M, Pevida C, Pis J, et al. Co-gasification of different rank coals with biomass and petroleum coke in a high-pressure reactor for H_2-rich gas production. Bioresour Technol 2010;101:3230-5.

[14] Aigner I, Pfeifer C, Hofbauer H. Co-gasification of coal and wood in a dual fluidized bed gasifier. Fuel 2011;90:2404-12.

[15] de Jong W, Andries J, Hein KRG. Coal/biomass co-gasification in a pressurised fluidised bed reactor. Renewable Energy 1999;16:1110-3.

[16] Vélez JF, Chejne F, Valdés CF, Emery EJ, Londoño CA. Co-gasification of Colombian coal and biomass in fluidized bed: an experimental study. Fuel 2009;88:424-30.

[17] Alzate CA, Chejne F, Valdés CF, Berrio A, Cruz JDL, Londoño CA. Co-gasification of pelletized wood residues. Fuel 2009;88:437-45.

[18] Pinto F, Franco C, Andre RN, Tavares C, Dias M, Gulyurtlu I, et al. Effect of experimental conditions on co-gasification of coal, biomass and plastics wastes with air/steam mixtures in a fluidized bed system. Fuel 2003;82:1967-76.

[19] Pan Y, Velo E, Roca X, Manya J, Puigjaner L. Fluidized-bed co-gasification of residual biomass/poor coal blends for fuel gas production. Fuel 2000;79:1317-26.

[20] Li K, Zhang R, Bi J. Experimental study on syngas production by co-gasification of coal and biomass in a fluidized bed. Int J Hydrogen Energy 2010;35:2722-6.

[21] Hernández JJ, Aranda-Almansa G, Serrano C. Co-gasification of biomass wastes and coal– coke blends in an entrained flow gasifier: an experimental study. Energy Fuels 2010;24:2479-88.

[22] Lapuerta M, Hernández JJ, Pazo A, López J. Gasification and co-gasification of biomass wastes: effect of the biomass origin and the gasifier operating conditions. Fuel Process Technol 2008;89:828-37.

[23] Qin K, Jensen PA, Lin W, Jensen AD. Biomass gasification behavior in entrained flow reactor: gas product distribution and soot formation. Energy & Fuels 2012;26:5992-6002.

[24] Neves D, Thunman H, Matos A, Tarelho L, Gomez-Barea A. Characterization and prediction of biomass pyrolysis products. Progress in Energy and Combustion Science 2011;37:611-30.

[25] Chen JC, Niksa S. Coal devolatilization during rapid transient heating. 1. Primary devolatilization. Energy Fuels 1992;6:254-64.

[26] Chen JC, Castagnoli C, Niksa S. Coal devolatilization during rapid transient heating. 2. Secondary pyrolysis. Energy Fuels 1992;6:264-71.

[27] Fagbemi L, Khezami L, Capart R. Pyrolysis products from different biomasses: application to the thermal cracking of tar. Appl Energy 2001;69:293-306.

[28] Wei L, Xu S, Zhang L, Zhang H, Liu C, Zhu H, et al. Characteristics of fast pyrolysis of biomass in a free fall reactor. Fuel Process Technol 2006;87:863-71.

[29] Zhang H. Nitrogen evolution and soot formation during secondary coal pyrolysis. Ph.D Thesis, Department of Chemical Engineering, Brigham Young University. 2001.

[30] Xu WC, Tomita A. Effect of temperature on the flash pyrolysis of various coals. Fuel 1987;66:632-6.

[31] Sun S, Tian H, Zhao Y, Sun R, Zhou H. Experimental and numerical study of biomass flash pyrolysis in an entrained flow reactor. Bioresour Technol 2010;101:3678-84.

[32] Xu WC, Tomita A. Effect of coal type on the flash pyrolysis of various coals. Fuel 1987;66:627-31.

[33] Lopez B, Blanco C, Martinez-Alonso A, Tascon J. Composition of gases released during olive stones pyrolysis. J Anal Appl Pyrolysis 2002;65:313-22.

[34] Uzun BB, Putun AE, Putun E. Composition of products obtained via fast pyrolysis of olive-oil residue: Effect of pyrolysis temperature. J Anal Appl Pyrolysis 2007;79:147-53.

[35] Sharma R, Wooten J, Baliga V, Hajaligol M. Characterization of chars from biomass-derived materials: pectin chars. Fuel 2001;80:1825-36.

[36] Williams PT, Besler S. The pyrolysis of rice husks in a thermogravimetric analyser and static batch reactor. Fuel 1993;72:151-9.

[37] Van Heek K, Hodek W. Structure and pyrolysis behaviour of different coals and relevant model substances. Fuel 1994;73:886-96.

[38] Jakab E, Faix O, Till F. Thermal decomposition of milled wood lignins studied by thermogravimetry/mass spectrometry. J Anal Appl Pyrolysis 1997;40:171-86.

[39] Niksa S, Kerstein AR. FLASHCHAIN theory for rapid coal devolatilization kinetics. 1. Formulation. Energy Fuels 1991;5:647-65.

[40] Mill CJ. Pyrolysis of fine coal particles at high heating rate and pressure. Ph.D Thesis, School of Chemical Engineering and Industrial Chemistry, University of New South Wales Australia. 2000.

[41] Griffin TP, Howard JB, Peters WA. Pressure and temperature effects in bituminous coal pyrolysis: experimental observations and a transient lumped-parameter model. Fuel 1994;73:591-601.

[42] Scott DS, Majerski P, Piskorz J, Radlein D. A second look at fast pyrolysis of biomass--the RTI process. J Anal Appl Pyrolysis 1999;51:23-37.

[43] Zhang L, Xu S, Zhao W, Liu S. Co-pyrolysis of biomass and coal in a free fall reactor. Fuel 2007;86:353-9.

[44] Cho S, Marlow D, Niksa S. Burning velocities of multicomponent organic fuel mixtures derived from various coals. Combust Flame 1995;101:399-410.

[45] Xu WC, Tomita A. The effects of temperature and residence time on the secondary reactions of volatiles from coal pyrolysis. Fuel Process Technol 1989;21:25-37.

[46] Morf P, Hasler P, Nussbaumer T. Mechanisms and kinetics of homogeneous secondary reactions of tar from continuous pyrolysis of wood chips. Fuel 2002;81:843-53.

[47] Qin K, Lin W, Jensen PA, Jensen AD. High-temperature entrained flow gasification of biomass. Fuel 2012;93:589-600.

[48] Kriengsak SN, Buczynski R, Gmurczyk J, Gupta AK. Hydrogen production by high-temperature steam gasification of biomass and coal. Environ Eng Sci 2009;26:739-44.

[49] Xu B, Wu C, Luo Z, Zhou X. Kinetic study on biomass gasification. Solar Energy 1992;49:199-204.

[50] Fletcher TH, Ma J, Rigby JR, Brown AL, Webb BW. Soot in coal combustion systems. Progress in Energy and Combustion Science 1997;23:283-301.

[51] Koziski JA, Saade R. Effect of biomass burning on the formation of soot particles and heavy hydrocarbons: an experimental study. Fuel 1998;77:225-37.

[52] Kennedy IM. Models of soot formation and oxidation. Progress in Energy and Combustion Science 1997;23:95-132.

[53] Glarborg P. Hidden interactions - Trace species governing combustion and emissions. Proceedings of the combustion institute 2007;31:77-98.

[54] McKee DW. Mechanisms of the alkali metal catalysed gasification of carbon. Fuel 1983;62:170-5.

[55] McKee DW, Spiro CL, Kosky PG, Lamby EJ. Catalysis of coal char gasification by alkali metal salts. Fuel 1983;62:217-20.

[56] Lv D, Xu M, Liu X, Zhan Z, Li Z, Yao H. Effect of cellulose, lignin, alkali and alkaline earth metallic species on biomass pyrolysis and gasification. Fuel Process Technol 2009;91:903-9.

[57] Huang Y, Yin X, Wu C, Wang C, Xie J, Zhou Z, et al. Effects of metal catalysts on CO_2 gasification reactivity of biomass char. Biotechnol Adv 2009;27:568-72.

[58] Hüttinger KJ, Minges R. Catalytic water vapour gasification of carbon: Importance of melting and wetting behaviour of the 'catalyst'. Fuel 1985;64:491-4.

[59] El-Rub ZA, Bramer E, Brem G. Review of catalysts for tar elimination in biomass gasification processes. Ind Eng Chem Res 2004;43:6911-9.

[60] Sutton D, Kelleher B, Ross JRH. Review of literature on catalysts for biomass gasification. Fuel Process Technol 2001;73:155-73.

[61] Pande AR. Catalytic gasification of active charcoal by carbon dioxide: influence of type of catalyst and carbon particle size. Fuel 1992;71:1299-302.

[62] Nishiyama Y. Catalytic gasification of coals—Features and possibilities. Fuel Process Technol 1991;29:31-42.

[63] Song BH, Kim SD. Catalytic activity of alkali and iron salt mixtures for steam-char gasification. Fuel 1993;72:797-803.

[64] Lee WJ, Kim SD. Catalytic activity of alkali and transition metal salt mixtures for steam-char gasification. Fuel 1995;74:1387-93.

Chapter 6   A   model   for   high-temperature entrained flow gasification of biomass

Abstract

The objective of the present investigation is to simulate biomass entrained flow gasification. A mathematic model was developed, which included mixing, drying and pyrolysis, detailed gas phase chemistry, char and soot reactions, and mass and heat transfer. Experiments used for model validation were carried out in a laboratory-scale entrained flow reactor covering a wide range of operating conditions. The simulation results generally showed good agreement with the experimental results. They also coincided well with the equilibrium calculation results. The simulation result suggested that the soot can be completely converted and thereby the H_2 and CO yields can reach the maximum values with increasing the reactor length to 2.5 – 3 m under a reasonable condition (high temperature with steam addition).

6.1 Introduction

The transportation sector accounted for 27 % of the total world delivered energy consumption in 2008 and the share is expected to increase continuously [1]. Gasification is a thermochemical process currently available for syngas production, which can be subsequently used as raw material to synthesize liquid fuels in a catalytic process [2]. Thus, producing liquid fuels for transportation is an important utilization of gasification. One of the key problems to be solved in liquid fuels from syngas is to control the syngas quality, such as harmful impurities [3]. Entrained flow gasification operates at high temperature with small particles, which can achieve a high carbon conversion and produce a high-quality syngas without tar [4]. Among the renewable energy sources, biomass, as an important alternative fuel of coal, has a high potential due to the low net CO_2 emission. Thus using biomass as feedstock in entrained flow gasifiers attracts great interests.

In comparison to coal entrained flow gasification, the knowledge of biomass entrained flow gasification is limited and systematic investigations are still needed. Experimental work is a first and prerequisite step for attaining an insight into the effects of operating conditions on process performance. On the basis of the obtained knowledge and experimental results, a mathematic model can be developed and used to evaluate, predicted, and optimize the gasification process through a low-cost way.

The model of coal entrained flow gasification has already been studied and developed adequately. Some researchers [5-8] adopted a one-dimensional steady-state model to simulate coal entrained flow gasification, which was based on heterogeneous and homogeneous reactions and mass and energy balances in solid and gas phases. Govind et al.[9] developed the model by adding momentum balance. Besides, a numerical CFD model for coal entrained flow gasification was employed by many other researchers [10-15]. However, the reported model work on biomass entrained flow gasification is limited [16], since biomass is a new alternative fuel in recent years and rare experimental data can be found to support model validation.

The objective of the present work is to develop a mathematic model to describe biomass entrained flow gasification. Mixing, drying and pyrolysis, heterogeneous reactions, detailed homogeneous chemistry, and mass and heat transfer in solid and gas phases were included in the present model. The model was validated by our experimental results which involved biomass entrained flow gasification under a wide range of operating conditions.

6.2 Experimental

The setup used for gasification experiments was a laboratory-scale atmospheric pressure entrained flow reactor, shown in Chapter 3. The properties and particle size distribution of wood (beech saw dust) are given in Chapter 3.

Table 6.1 List of conducted experiments

NO.	primary flow		secondary flow			operating parameters				
	fuel feeding rate	feeder gas	main gas	steam	purge gas	t	O_2	λ	H_2O/C	T
	g/min	Nl/min	Nl/min	g/min	Nl/min	s	%	-	mol/mol	°C
1	12.8	10(N_2)	6.2(N_2)	0.0	0.3(air)+2.7(N_2)	2.6	0	0.00	0.0	1400
2	12.8	10(N_2)	6.2(N_2)	4.3	0.3(air)+2.7(N_2)	2.7	0	0.00	0.5	1400
3	12.8	10(N_2)	6.2(N_2)	8.6	0.3(air)+2.7(N_2)	2.8	0	0.00	1.0	1400
4	12.8	10(air)	6.2(air)	4.3	0.3(air)+2.7(N_2)	3.1	21	0.30	0.5	1400
5	15.9	10(air)	10.2(air)	5.4	0.3(air)+2.7(N_2)	2.5	21	0.30	0.5	1400
6	10.7	10(air)	3.5(air)	3.6	0.3(air)+2.7(N_2)	3.7	21	0.30	0.5	1400
7	12.8	6(air)	10.2(air)	4.3	0.3(air)+2.7(N_2)	3.1	21	0.30	0.5	1400
8	12.8	14(air)	2.2(air)	4.3	0.3(air)+2.7(N_2)	3.1	21	0.30	0.5	1400
9	9.7	10(air)	0.5(O_2)+5.7(N_2)	3.3	0.3(air)+2.7(N_2)	3.4	16	0.30	0.5	1400
10	15.8	10(air)	2.1(O_2)+4.1(N_2)	5.3	0.3(air)+2.7(N_2)	2.8	26	0.30	0.5	1400
11	15.3	10(air)	6.2(air)	5.2	0.3(air)+2.7(N_2)	2.8	21	0.25	0.5	1400
12	10.9	10(air)	6.2(air)	3.7	0.3(air)+2.7(N_2)	3.4	21	0.35	0.5	1400
13	12.8	10(air)	6.2(air)	0.0	0.3(air)+2.7(N_2)	3.2	21	0.30	0.0	1400
14	12.8	10(air)	6.2(air)	8.6	0.3(air)+2.7(N_2)	3.0	21	0.30	1.0	1400
15	12.8	10(air)	6.2(air)	4.3	0.3(air)+2.7(N_2)	3.8	21	0.30	0.5	1200
16	12.8	10(air)	6.2(air)	4.3	0.3(air)+2.7(N_2)	3.4	21	0.30	0.5	1300

The present model focused on high-temperature wood gasification. The conducted experiments are listed in Table 6.1. The studied operating parameters include residence time (2.4 – 3.6 s), feeder gas flow (6 – 14 NL/min), oxygen concentration (16 – 26 %), excess air ratio (0.25 - 0.35), steam/carbon ratio (0.0 – 1.0), and reactor temperature (1200 – 1400 °C).

6.3 Model description

Biomass gasification is a rather complicated process coupled with two-phase flow, mass and heat transfer, and heterogeneous and homogenous reactions. When biomass particles are injected into a high-temperature reactor, a series of physical and chemical process take place in the reactor. Biomass particles are quickly heated and the moistures are evaporated. Then, volatiles are escaped from the fuel particles and char particles are formed in the pyrolysis process. The pyrolysis products react with each other and other injected species depending on the surrounding environment and reaction mechanism. A completed description of the whole processes is not possible, due to the complexity and heterogeneity of biomass. Thus, some basic assumptions must be made to simplify the process. They include: both the gas and solid flows can be described by a plug flow model; there is no temperature gradient inside the solid particles; there is no slip velocity between solid particles and gas; there is a stagnant gas film layer surrounding the particles and the reactor wall, meaning that Nu ≈ 2 and Sh ≈ 2. Since the system is very dilute, interaction between particles is neglected. The biomass entrained flow gasification model has been implemented as a FORTRAN77 code that calls on the CHEMKIN III subroutine library [17] for calculations of gas phase reactions and some related parameters. The process of biomass entrained flow gasification is divided into the following sub-models.

6.3.1 Mixing

The mixing of the primary flow (including feeder gas entraining the biomass particles) and secondary flow (including steam, main gas, and purge gas) is considered as an important factor in a thermochemical process [18-22]. A satisfactory description of the mixing process becomes critical in the present model, because an assumption of instantaneous mixing may lead to considerable error in the prediction of reaction temperature and syngas products yields. In the present model, the mixing process was described by a modified Zwietering approach [23]. In this approach, the secondary flow gradually entered the primary flow. This was modeled by introducing some pseudo species (O_2^*, N_2^*, and H_2O^*) into the secondary flow.

These pseudo species became the actual species (O_2, N_2, and H_2O) through a set of reactions, shown in equation (6.1) - (6.3).

$$O_2^* \xrightarrow{k_{mixing}} O_2 \tag{6.1}$$

$$N_2^* \xrightarrow{k_{mixing}} N_2 \tag{6.2}$$

$$H_2O^* \xrightarrow{k_{mixing}} H_2O \tag{6.3}$$

Through these reactions the secondary flow entering the primary flow at a certain position (or time) can be calculated by equation (6.4) - (6.6).

$$\frac{dF_{O_2}}{dL} = \frac{1}{v}\frac{dF_{O_2}}{dt} = \frac{1}{v}k_{mixing}F_{O_2^*} \tag{6.4}$$

$$\frac{dF_{N_2}}{dL} = \frac{1}{v}\frac{dF_{N_2}}{dt} = \frac{1}{v}k_{mixing}F_{N_2^*} \tag{6.5}$$

$$\frac{dF_{H_2O}}{dL} = \frac{1}{v}\frac{dF_{H_2O}}{dt} = \frac{1}{v}k_{mixing}F_{H_2O^*} \tag{6.6}$$

The mixing rate constant, k_{mixing}, is determined by a measured or estimated mixing time, shown in equation (6.7). In the present model, the mixing time was taken as the time for which 95 % of the secondary flow was mixed with the primary flow ($k_{mixing} = \ln 20/t_{95\%}$).
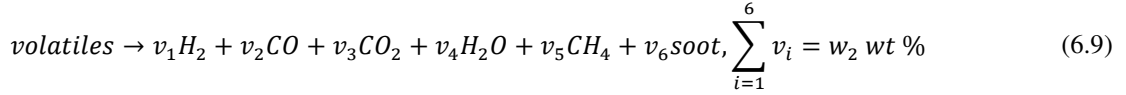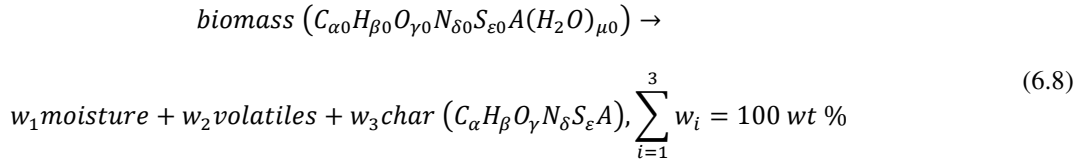
$$k_{mixing} = \frac{\ln(\frac{1}{F_{O_2^*,N_2^*,H_2O^*}|_{t=t}/F_{O_2^*,N_2^*,H_2O^*}|_{t=0}})}{t} \tag{6.7}$$

The cold primary flow and hot secondary flow were assumed to achieve a uniform mixing temperature instantaneously at the inlet of the reactor. The important advantage of this approach is that it is easily incorporated into CHEMKIN Software Package as additional first-order reactions for the reactants constituents in the secondary flow.

6.3.2 Drying and pyrolysis

When the biomass particles enter the reactor, drying and pyrolysis processes will follow. Due to the very high heating rate in the entrained flow reactor (high temperature employed and small particle size used), we assumed that drying and pyrolysis completed instantaneously. Consequently, the moisture released and pyrolysis products (volatiles and char) produced immediately at the inlet of the reactor. At high temperatures (> 1200 °C), the volatiles were considered to be composed by H_2, CO, CO_2, H_2O, lighter hydrocarbons, and soot. Thus, under
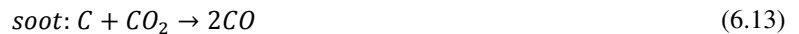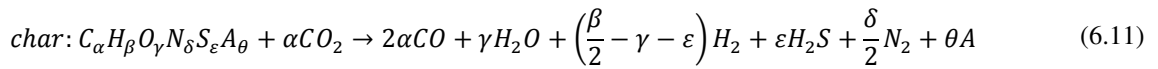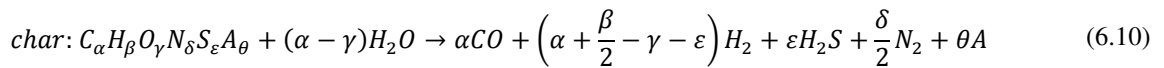
the applied operating conditions, the distribution of drying and pyrolysis products, which was prescribed on the basis of the biomass composition, is shown in equation (6.8) - (6.9).

$$biomass\left(C_{\alpha 0}H_{\beta 0}O_{\gamma 0}N_{\delta 0}S_{\varepsilon 0}A(H_2O)_{\mu 0}\right) \rightarrow$$

$$w_1 moisture + w_2 volatiles + w_3 char\left(C_\alpha H_\beta O_\gamma N_\delta S_\varepsilon A\right), \sum_{i=1}^{3} w_i = 100\ wt\ \% \tag{6.8}$$

$$volatiles \rightarrow v_1 H_2 + v_2 CO + v_3 CO_2 + v_4 H_2O + v_5 CH_4 + v_6 soot, \sum_{i=1}^{6} v_i = w_2\ wt\ \% \tag{6.9}$$

6.3.3 Homogeneous and heterogeneous reactions

The homogeneous reactions used in the present model were adopted directly from CHEMKIN III [17]. It was a detailed kinetic mechanism of gas phase chemistry, including 185 species in 1173 reactions [24]. Besides, the mixing was also incorporated into CHEMKIN III by adding 3 new species (O_2*, N_2*, and H_2O*) and 3 new reactions (equation (6.1) - (6.3)). Thus, the total network involved 188 species in 1176 reactions.

The heterogeneous reactions taking place in present work are shown in equation (6.10) - (6.12). The solid reactants involving these reactions are char and soot. In the present model, the char was composed by carbon, hydrogen, oxygen, nitrogen, sulfur, and ash (specified as silicon dioxide), and the soot was considered as pure carbon. As soon as the pyrolysis gases released, they consumed the insufficient oxygen very quickly. Therefore only char and soot gasification reactions with H_2O and CO_2 were considered in the present model.

$$char: C_\alpha H_\beta O_\gamma N_\delta S_\varepsilon A_\theta + (\alpha - \gamma)H_2O \rightarrow \alpha CO + \left(\alpha + \frac{\beta}{2} - \gamma - \varepsilon\right)H_2 + \varepsilon H_2S + \frac{\delta}{2}N_2 + \theta A \tag{6.10}$$

$$char: C_\alpha H_\beta O_\gamma N_\delta S_\varepsilon A_\theta + \alpha CO_2 \rightarrow 2\alpha CO + \gamma H_2O + \left(\frac{\beta}{2} - \gamma - \varepsilon\right)H_2 + \varepsilon H_2S + \frac{\delta}{2}N_2 + \theta A \tag{6.11}$$

$$soot: C + H_2O \rightarrow CO + H_2 \tag{6.12}$$

$$soot: C + CO_2 \rightarrow 2CO \tag{6.13}$$

6.3.4 Mass and heat transfer

The char-gas reactions and soot-gas reactions were described by the progressive conversion model with particle shrinkage [25], because in the previous STA experiments shown in Chapter 3, we found that the conversion of wood char and soot obtained from entrained flow

gasification were adequately described by this model. The shrinking particles were assumed to have a constant density and not to form an ash layer. In the high-temperature entrained flow reactor, the conversion rate of porose solid particles is usually affected by pore diffusion limitation, thus the effectiveness factor (η) [26] is included in the particle conversion model. The mole balance for char and soot particles is described by equation (6.14) and (6.15) respectively. The gas phase mole balance is described by equation (6.16), which includes the contributions from both gas phase reactions (the first term) and solid-gas reactions (the second and third terms). In the present model, isothermal conditions were applied since all the experiments were conducted in an electrical heated entrained flow reactor and the employed fuel feeding rates were low. The energy balance for char and soot particles and gas species is described by equation (6.17).

$$\frac{dF_c}{dL} = \sum_i \frac{1}{v} \eta_{c,i} A_{c0,i} \exp\left(-\frac{E_{c,i}}{RT_c}\right) P_{c,i}^{m_{c,i}} \left(\frac{F_c}{F_{c0}}\right)^{n_{c,i}} F_{c0}$$

$$\Rightarrow \frac{dR_c}{dL} = \sum_i \frac{1}{v} \eta_{c,i} A_{c0,i} \exp\left(-\frac{E_{c,i}}{RT_c}\right) P_{c,i}^{m_{c,i}} \left(\frac{R_c}{R_{c0}}\right)^{3n_{c,i}} \frac{R_{c0}^3}{3R_c^2}$$

(6.14)

$$\frac{dF_s}{dL} = \sum_i \frac{1}{v} \eta_{s,i} A_{s0,i} \exp\left(-\frac{E_{s,i}}{RT_s}\right) P_{s,i}^{m_{s,i}} \left(\frac{F_s}{F_{s0}}\right)^{n_{s,i}} F_{s0}$$

$$\Rightarrow \frac{dR_s}{dL} = \sum_i \frac{1}{v} \eta_{s,i} A_{s0,i} \exp\left(-\frac{E_{s,i}}{RT_s}\right) P_{s,i}^{m_{s,i}} \left(\frac{R_s}{R_{s0}}\right)^{3n_{s,i}} \frac{R_{s0}^3}{3R_s^2}$$

(6.15)

$$\frac{dF_{g,j}}{dL} = \sum_i A r_{g,j} + \sum_i \theta_{ij} \frac{1}{v} \eta_{c,i} A_{c0,i} \exp\left(-\frac{E_{c,i}}{RT_c}\right) P_{c,i}^{m_{c,i}} \left(\frac{R_c}{R_{c0}}\right)^{3n_{c,i}} F_{c0}$$

$$+ \sum_i \theta_{ij} \frac{1}{v} \eta_{s,i} A_{s0,i} \exp\left(-\frac{E_{s,i}}{RT_s}\right) P_{s,i}^{m_{s,i}} \left(\frac{R_s}{R_{s0}}\right)^{3n_{s,i}} F_{s0}$$

(6.16)

$$\frac{dT_c}{dL} = \frac{dT_s}{dL} = \frac{dT_g}{dL} = 0$$

(6.17)

6.3.5 Input parameter estimation

In the previous work, shown in Chapter 3, we observed that increasing feeder gas flow can improve the mixing condition, thus in the model different mixing rate constants were employed when different feeder gas flows were used, which are listed in Table 6.2. At different reactor temperature (1200 – 1400 °C), the different drying and pyrolysis products during wood gasification are listed in Table 6.3. The char composition was calculated by the

present model on the basis of fuel composition and moisture and volatiles distribution. The properties of char and soot particles are given in Table 6.4.

Table 6.2 Mixing rate constant for using different feeder gas flow [22]

feeder gas flow	6 NL/min	10 NL/min	14 NL/min
k_{mixing}	2	5	8

Table 6.3 Composition of wood drying and pyrolysis products at different temperatures [27-29]

(a) The drying and pyrolysis products

wood		T_w=1200 °C	T_w=1300 °C	T_w=1400 °C
mositure	w_1, %	9.04	9.04	9.04
voilatiles	w_2, %	81.86	83.96	85.96
char	w_3, %	9.00	7.00	5.00

(b) The volatiles composition

volatiles		T_w=1200 °C	T_w=1300 °C	T_w=1400 °C
H_2	v_1, %	0.40	0.70	1.00
CO	v_2, %	18.00	21.00	24.00
CO_2	v_3, %	28.50	24.50	20.50
H_2O	v_5, %	7.96	9.96	11.96
CH_4	v_4, %	16.10	14.80	13.50
soot	v_6, %	7.00	11.00	15.00

(c) The char composition

char	T_w=1200 °C	T_w=1300 °C	T_w=1400 °C
$C_\alpha H_\beta O_\gamma N_\delta S_\varepsilon A$	$C_{0.8504}H_{0.0723}O_{0.0275}N_{0.0234}S_{0.0008}A$	$C_{0.6753}H_{0.2500}O_{0.0527}N_{0.0103}S_{0.0003}A$	$C_{0.6256}H_{0.3005}O_{0.0598}N_{0.0066}S_{0.0002}A$

Table 6.4 Properties of wood char and soot [24,30-34]

char			soot		
d_{c0}	µm	200	d_{s0}	nm	100
ρ_c	kg/m³	500	ρ_s	kg/m³	2000
d_{cpore}	µm	2	d_{spore}	nm	1
ε_c	-	0.8	ε_s	-	0.1
τ_c	-	2	τ_s	-	9
e_c	-	0.9	e_s	-	0.9

Table 6.5 Measured kinetic parameters of wood char and soot gasification reactions in STA

in STA	char-CO_2	char-H_2O	soot-CO_2	soot-H_2O
	measured	estimated	measured	estimated
temperature interval	610 – 820 °C	-	670 – 910 °C	-
gas environment	10, 15, and 20 vol % O_2 in N_2	-	10, 50, and 90 vol % CO_2 in N_2	-
E (kJ/mol)	213	194	247	228
A_0 (s^{-1}MPa^{-m})	1.25×10^8	1.04×10^8	3.61×10^9	3.01×10^9
m	0.12	0.22	0.54	0.64
n	0.5	0.5	0.5	0.5

In the previous work, shown in Chapter 4, the kinetic parameters for char-CO_2 and soot-CO_2 reactions were obtained by non-isothermal measurement from about 600 to about 900 °C in STA, given in Table 6.5. The estimated kinetic parameters for solid-H_2O reaction were based on the reaction rate of solid-CO_2 reaction [13,35]. In the present model, at 1200 – 1400 °C,

the calculated reaction rate of solid-H_2O was approximately $2 - 3$ times faster than that of solid-CO_2 when the partial pressure of H_2O and CO_2 was in the range of $0.01 - 0.09$ MPa.

The reaction kinetics was obtained in a low-temperature range in the STA, thus the kinetics might be unauthentic and could cause unaccepted error when they were applied in a high-temperature range. In the present work the changes of the char reaction kinetics were not performed, because char was completely converted at the outlet of the reactor in the applied experiments listed in Table 6.1 and its conversion profile along with the reactor length was unknown. When the soot reaction kinetics obtained in the STA was used in the model, we found the soot was completely consumed just at the top of the reactor, which cannot fit the experimental results at all. Therefore, the soot reaction kinetics in the applied entrained flow gasification condition ($1200 - 1400$ °C) must be different from that in STA. We assumed that the reaction order for solid phase and gas phase, n and m, were unchanged, the activation energy, E, was decreased in the high-temperature range. And the changes of kinetics took place at 910 °C (soot reaction kinetics obtained at $670 - 910$ °C in STA), thereby the changed pre-exponential factor, A_0, was obtained at this temperature. Five sets of different kinetics were investigated in the present model. They are listed in Table 6.6 and the different soot-CO_2 reaction rates are compared in Figure 6.1.

Table 6.6 Applied kinetic parameters of the wood soot gasification at 910-1400 °C

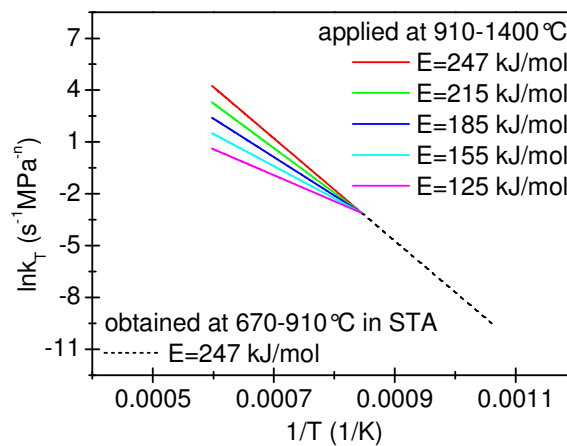| NO. | soot-CO_2 | | | | soot-H_2O | | | | remark |
---	E	A_0	m	n	E	A_0	m	n	
	kJ/mol	$s^{-1}MPa^{-m}$	-	-	kJ/mol	$s^{-1}MPa^{-m}$	-	-	
A	247	3.61×10^9	0.54	0.5	228	3.01×10^9	0.64	0.5	obtained in the STA
B	215	1.39×10^8	0.54	0.5	196	1.16×10^8	0.64	0.5	-
C	185	6.60×10^6	0.54	0.5	166	5.50×10^6	0.64	0.5	-
D	155	3.13×10^5	0.54	0.5	136	2.61×10^5	0.64	0.5	-
E	125	1.48×10^4	0.54	0.5	106	1.23×10^4	0.64	0.5	used in the model in section 6.4.2

Figure 6.1 Arrhenius plots of different soot-CO_2 reaction rates: $k_T = A_0\exp(-\frac{E}{RT})$

138

6.4 Results and discussion

6.4.1 Input parameter sensitivity study

The experiment, NO.4 listed in the Table 6.1, was selected as the standard experiment, because each operating parameter in this experiment was set as a reasonable value in the entrained flow gasification process. The standard experiment was used to investigate the sensitivity of simulation results to some selected input parameters, such as soot reaction kinetics, soot property, and mixing rate.

6.4.1.1 Effect of soot reaction kinetics

Figure 6.2 shows the sensitivity of predicted product yield and temperature to soot reaction kinetics. In Figure 6.2 (a), with gradually changing the soot reaction kinetics from A to E (listed in Table 6.6), the simulation result of soot yield was close to the experimental result step by step. When the reaction kinetics E was employed in the model, the predicted soot yield fitted the experimental result well. In Figure 6.2 (b), it can be observed that the varied soot reaction kinetics had a little influence on the char conversion along with the reactor length. However, when any soot kinetics was employed in the model, the char was completely converted at approximate 0.6 m. In Figure 6.2 (c) – (f), we found that the varied soot reaction kinetics had an obvious influence on the profiles of gas products yields along with the reactor length, while it had negligible influence on the final gas products yields. In compassion to the profile of the CO_2 and CH_4 yields along with the reactor length, the profile of the H_2, CO, and H_2O yields changed a lot with using different kinetics. This probably reveals that the soot-H_2O reaction is more important than the soot-CO_2 reaction in the gasification process. When the reaction kinetics A, B, and C were used in the model, the soot was gasified very fast and completely consumed at the top of the reactor. When the reaction kinetics D was used in the model, the soot was completely converted in the middle of the reactor (approximate 1.1 m). In Figure 6.2 (g), the initial available O_2 from primary gas flow was very quickly consumed by gas-phase reactions. The rest O_2 from the secondary gas flow gradually mixed with the primary gas flow. In Figure 6.2 (f), the added steam from the secondary gas flow also gradually mixed with the primary gas flow. The mixing process was accomplished at approximate 0.6 m. On the whole, soot reaction kinetics E was reasonable, which made the predicted soot yield fit the experimental result and hardly affected the final yields of other product. Thus, soot reaction kinetics E was used for parameter validation in section 6.4.1.4.
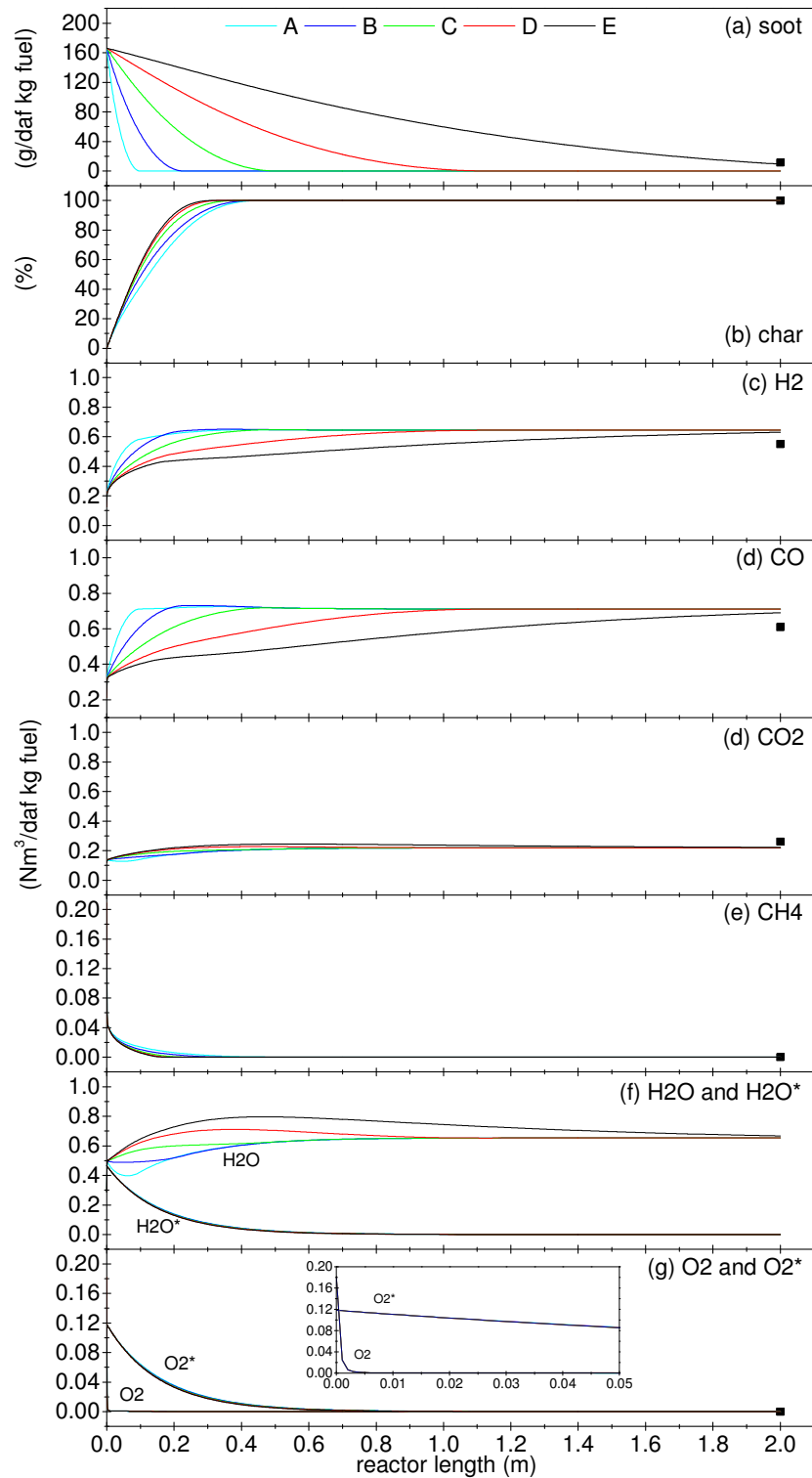
Figure 6.2 Sensitivity of predicted product yield and temperature to soot reaction kinetics: kinetics A-E listed in Table 6.6; symbols – experimental results (experiment NO.4 listed in Table 6.1); lines – simulation results

6.4.1.2 Effect of soot property

Table 6.7 presents the sensitivity of predicted product yield to soot property including pore size, porosity, tortuosity, particle density, and particle initial size. The soot pore property

(pore size, porosity, and tortuosity) hardly affected the product yield. This is probably because in the present model the calculated effectiveness factor (η) was always close to one due to the very small size of soot particle, indicating the effect of pore diffusion limitation could be ignored. The changed soot particle density only affected the effectiveness factor (pore diffusion) rather than intrinsic reaction kinetics in the present model. However, the effectiveness factor almost stayed at one, thus the soot particle density had negligible influence on the product yield in the model. The varied initial size of soot particle, from 50 nm to 200 nm, changed the soot yield a little, resulting from the changed intrinsic reaction kinetics. As shown in equation (6.15), decreasing the initial particle size tended to increase the reaction rate and vice versa. According to the above discussion, the soot property did not have significant influence on the product yields, thus the standard values of soot property (listed in Table 6.7) were used for parameter validation in section 6.4.1.4.

Table 6.7 Sensitivity of predicted product yield to soot property

	ρ_s kg/m^3	d_{s0} nm	d_{spore} nm	ε_s -	τ_s -	soot g/daf kg fuel	H_2	CO Nm^3/daf kg fuel	CO_2
standard values	2000	100	1.0	0.1	9	9.170	0.630	0.691	0.221
change d_{spore}	2000	100	0.5	0.1	9	9.204	0.630	0.691	0.221
	2000	100	2.0	0.1	9	9.153	0.630	0.691	0.221
change ε_s	2000	100	1.0	0.4	9	9.145	0.630	0.691	0.221
	2000	100	1.0	0.7	9	9.141	0.630	0.691	0.221
change τ_s	2000	100	1.0	0.1	6	9.159	0.630	0.691	0.221
	2000	100	1.0	0.1	3	9.148	0.630	0.691	0.221
change ρ_s	1500	100	1.0	0.1	9	9.162	0.630	0.691	0.221
	1000	100	1.0	0.1	9	9.153	0.630	0.691	0.221
change d_{s0}	2000	50	1.0	0.1	9	9.145	0.630	0.691	0.221
	2000	200	1.0	0.1	9	9.273	0.630	0.691	0.221

6.4.1.3 Effect of mixing rate

Figure 6.3 and Table 6.8 show the sensitivity of predicted product yield and temperature profile to mixing rate. In the standard experiment (NO.4 listed in Table 6.1), 10 NL/min feeder air was employed to entrain the fuel particles to the reactor in the primary flow. The rest air and added steam were supplied by the secondary flow. Three different mixing rates were studied under the standard condition. When k_{mixing} increased from 2 to 8, the location for complete mixing moved up from the middle to top of the reactor. In Figure 6.3 (a) and Table 6.8, we observed that the mixing rate affected the soot yield to some degree. The mixing was slower, the produced soot was more. This is probably because of the decreased soot gasification rate owing to the slower release of H_2O^* and O_2^* and thereby slower formation of H_2O and CO_2 at lower mixing rate. In Figure 6.3 (b), char was always completely converted at any used mixing rate, but the decreased mixing rate delayed the char conversion. In Figure

6.3 (c) – (g) and Table 6.8, we found that the decreased mixing rate had certain influence on the profiles of gas products yields due to the slower released and formed reactants, while it hardly affected the final gas product yield. For parameter validation in section 6.4.1.4, a moderate value of mixing rate ($k_{mixing} = 5$) was used.
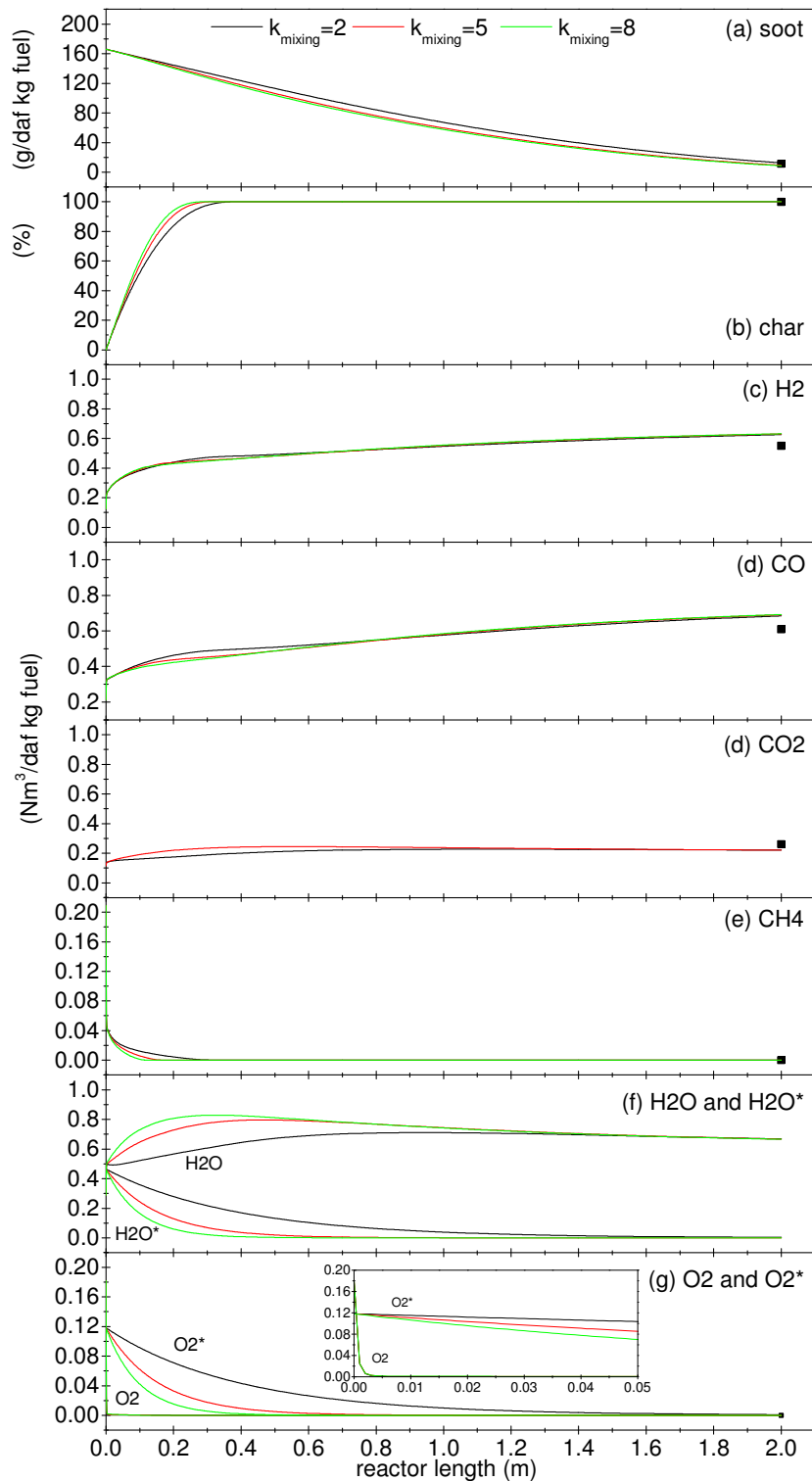

Figure 6.3 Sensitivity of predicted product yield and temperature to mixing rate: symbols – experimental results (experiment NO.4 listed in Table 6.1); lines – simulation results

Table 6.8 Sensitivity of predicted product yield to mixing rate

k_{mixing} s^{-1}	complete mixing location m	soot g/daf kg fuel	H_2	CO Nm^3/daf kg fuel	CO_2
2	1.214	12.456	0.626	0.685	0.221
5	0.474	9.170	0.630	0.691	0.221
8	0.293	8.478	0.631	0.693	0.221

6.4.1.4 Parameter validation

In order to further investigate the validity of the input parameters, soot reaction kinetics E and other input parameters shown in Table 6.2 – Table 6.4 were employed in the present model under the pyrolysis conditions with different steam/carbon ratios (same as the conditions of experiments NO.1, 2, and 3 listed in Table 6.1). The comparison between the simulation and experimental results are shown in Figure 6.4 and Figure 6.5. It can be observed that for both the soot and gas product yields, the simulation results were globally in good agreement with the experimental results. Thus, the used input parameters were reasonable and reliable at the applied reaction temperature, and these parameters were used in the following simulations.
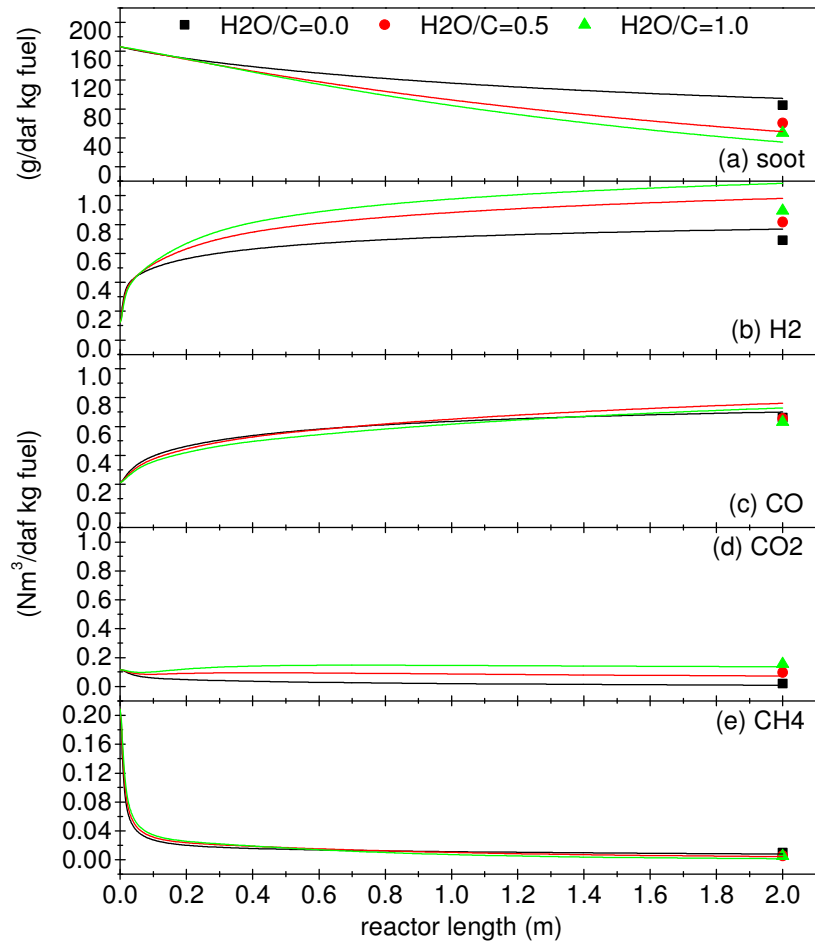
Figure 6.4 Pyrolysis products distribution along with the reactor length at different steam/carbon ratio: symbols – experimental results (experiments NO.1, 2, and 3 listed in Table 6.1); lines – simulation results
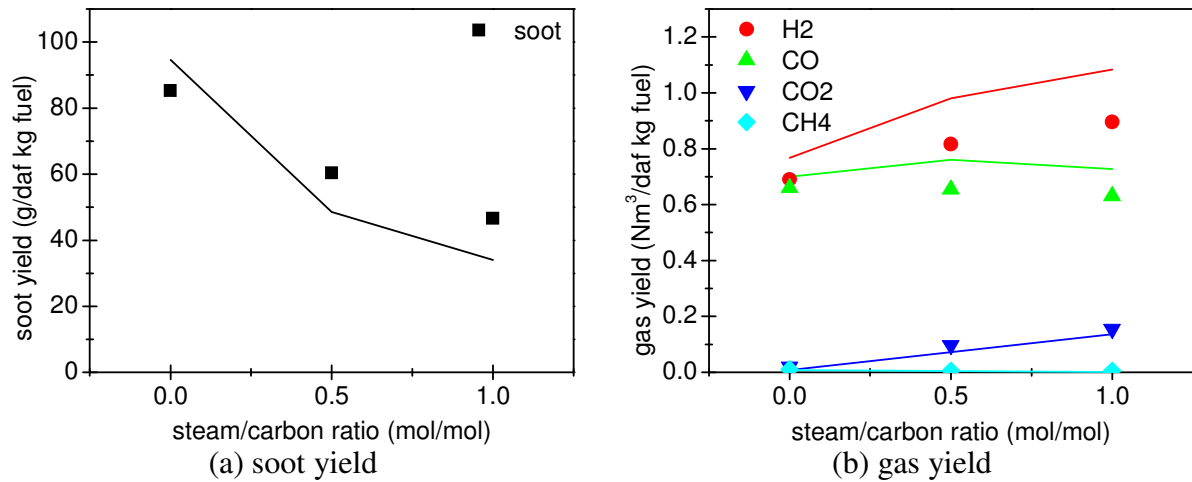
Figure 6.5 Pyrolysis product yields at different steam/carbon ratio: symbols – experimental results (experiments NO.1, 2, and 3 listed in Table 6.1); lines – simulation results

6.4.2 Comparison between experiment and simulation
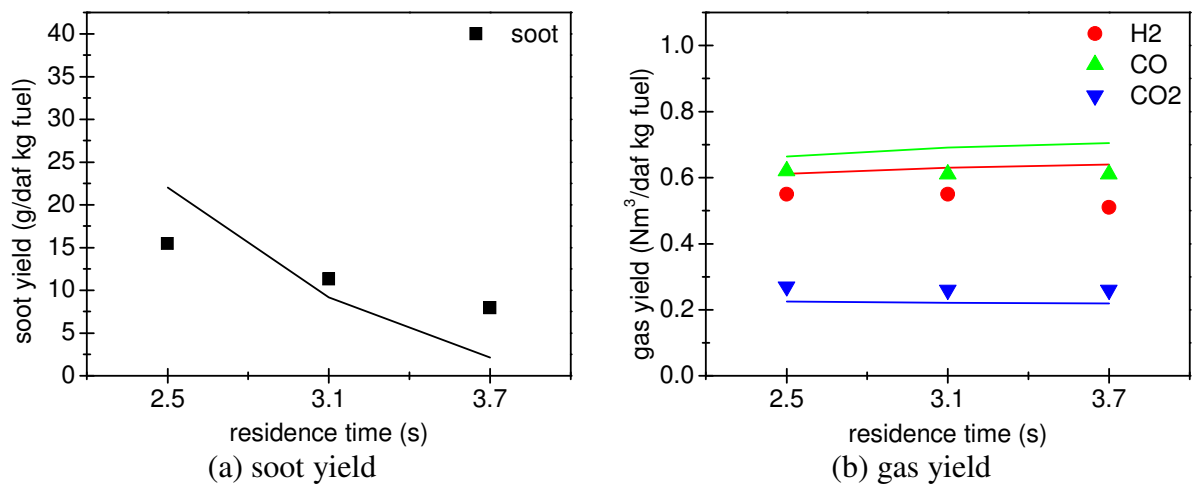
6.4.2.1 Effect of residence time

Figure 6.6 Effect of residence time on product yield: symbols – experimental results (experiments NO.4, 5, and 6 listed in Table 6.1); lines – simulation results

Figure 6.6 shows the comparison between experimental and simulation results of product yield as a function of residence time. The simulations were conducted for experiments NO. 4, 5, and 6 listed in Table 6.1. It can be observed that in both experiments and simulations, the soot yield decreased and the yield of the individual gas species almost kept constant with increasing residence time from 2.5 to 3.7 s. The simulation results captured the trend of product yield in the experiments well. At shorter (2.5 s) and longer (3.7 s) residence time, the simulation result obviously overestimated and underestimated the soot yield respectively. This is might be related to the errors in the employed reaction rate of soot and assumed initial produced amounts of soot. For the gas products, their yields were not so sensitive to the initial

144

pyrolysis products distribution, probably because operating conditions were close to the equilibrium conditions [27].

6.4.2.2 Effect of feeder air flow

Figure 6.7 shows the comparison between experimental and simulation results of product yield as a function of feeder air flow. The simulations were conducted for experiments NO. 4, 7, and 8 listed in Table 6.1. In the present model, we assumed that different feeder air flows only affected the mixing, thus the employed k_{mixing} was varied from 2 to 8 with increasing feeder air flow from 6 to 14 NL/min. It can be observed that in both experiments and simulations, the soot yield decreased and the yield of the individual gas species increased a little with increasing feeder air flow. On the whole, the simulation results were in good agreement with the experimental results, which confirmed the expectations that mixing was very important for the formation of soot. When feeder air flow of 6 NL/min was employed, the simulation result clearly underestimated the soot yield and overestimated the H_2 yield. It is probably because in the experiment employed lower feeder air flow, the mixing at the top of the reactor was poor, which led to more soot formation because of tar being converted to soot instead of cracking to light gases, mostly H_2. However, in the present model, the initial produced amounts of soot at different feeder air flows were assumed the same.
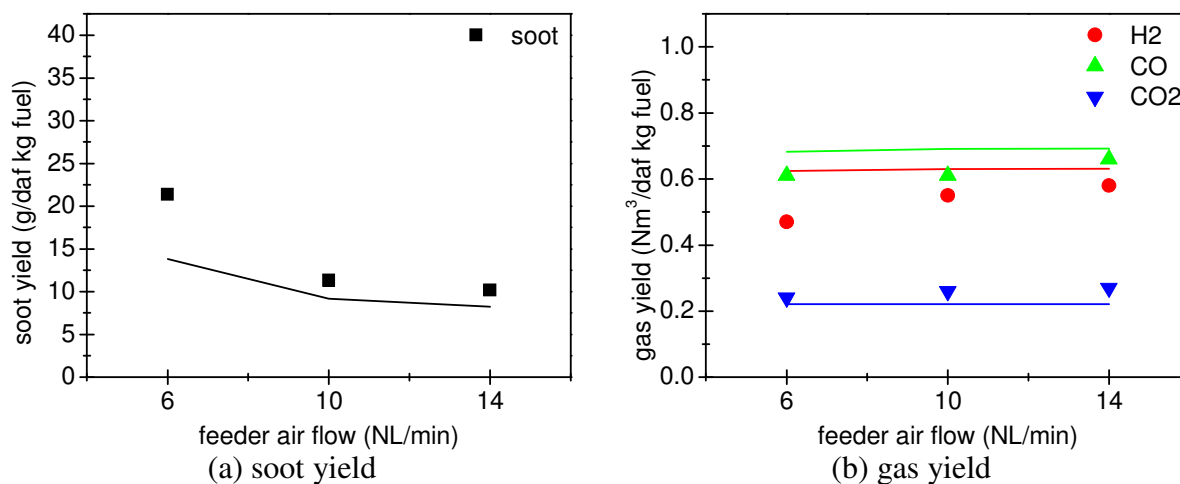

(a) soot yield (b) gas yield

Figure 6.7 Effect of feeder air flow on product yield: symbols – experimental results (experiments NO.4, 7, and 8 listed in Table 6.1); lines – simulation results

6.4.2.3 Effect of oxygen concentration

Figure 6.8 shows the comparison between experimental and simulation results of product yield as a function of oxygen concentration. The simulations were conducted for experiments NO. 4, 9, and 10 listed in Table 6.1. It can be observed that in both experiments and

simulations, the soot yield increased a little and the yield of the individual gas species almost kept constant with increasing oxygen concentration from 16 to 26 %. The simulation results were globally in good agreement with the experimental results. In the experiments, we thought that the increasing oxygen concentration could raise the flame temperature, which may cause more soot formation [36]. In the present model, we assumed that the initial produced amounts of soot at different oxygen concentrations were the same. However, in the simulation the soot yield still increased with increasing oxygen concentration. This probably reveals that the increased initial produced amounts of soot are not the main reason to increasing the soot yield in the experiments. In the experiments and simulations, the increased oxygen concentration was obtained by increasing fuel feeding rate and changing gas composition but fixing the flows of feeder gas, main gas, and purge gas. At oxygen concentration of 16 %, a smaller amount of fuel was carried by the fixed amount of feeder gas, which may lead to a higher local excess air ratio at the top of the reactor owing to the premixed feeder air and fuel. Thus, much more H_2O and CO_2 produced locally, resulting in more soot was gasified and finally lower soot left at the outlet of the reactor. The gas products were nearly independent of the oxygen concentration, because they were close to equilibrium at the nominal reactor temperature.

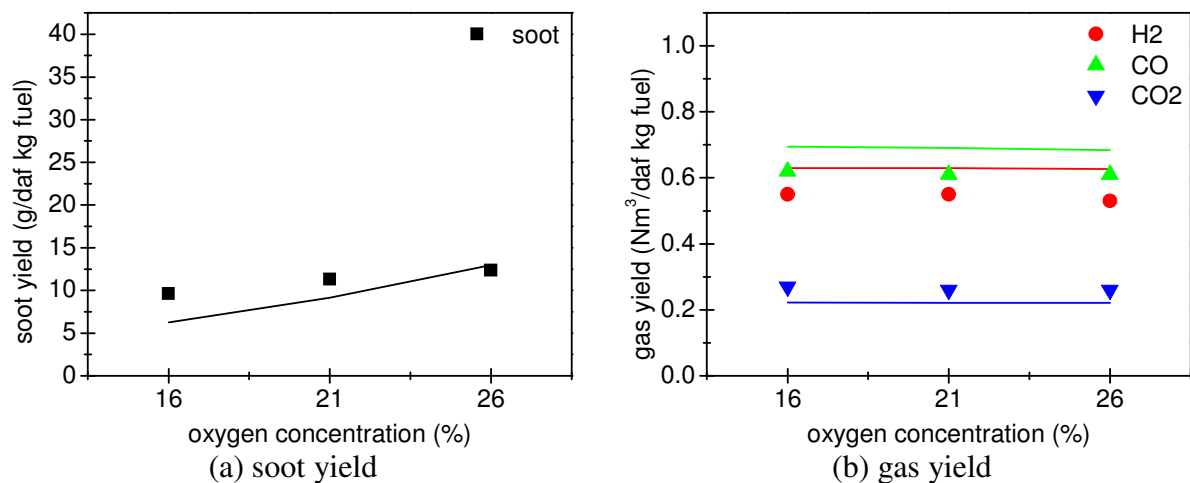

(a) soot yield   (b) gas yield

Figure 6.8 Effect of oxygen concentration on product yield: symbols – experimental results (experiments NO.4, 9, and 10 listed in Table 6.1); lines – simulation results

6.4.2.4 Effect of excess air ratio

Figure 6.9 shows the comparison between experimental and simulation results of product yield as a function of excess air ratio. The simulations were conducted for experiments NO. 4, 11, and 12 listed in Table 6.1. In the experiments and simulations, the increased excess air ratio was achieved by decreased the fuel feeding rate but fixing the flows of feeder gas, main

gas, and purge gas. It can be observed that in both experiments and simulations, the yields of soot, H_2, and CO decreased while the CO_2 yield increased with increasing excess air ratio from 0.25 to 0.35. The simulation results were globally in good agreement with the experimental results. At excess air ratio of 0.25, the simulation result clearly underestimated the soot yield. This is probably because in the present model, we assumed that the initial produced amounts of soot at different excess air ratios were the same. However, in the experiments, the initially generated soot might be higher at the lower excess air ratio due to the higher fuel feeding rate and lower oxygen content resulting in more soot formation at the top of the reactor [27]. The errors in the yields of gas products between the simulations and experiments might be related to the gas phase reaction kinetics.
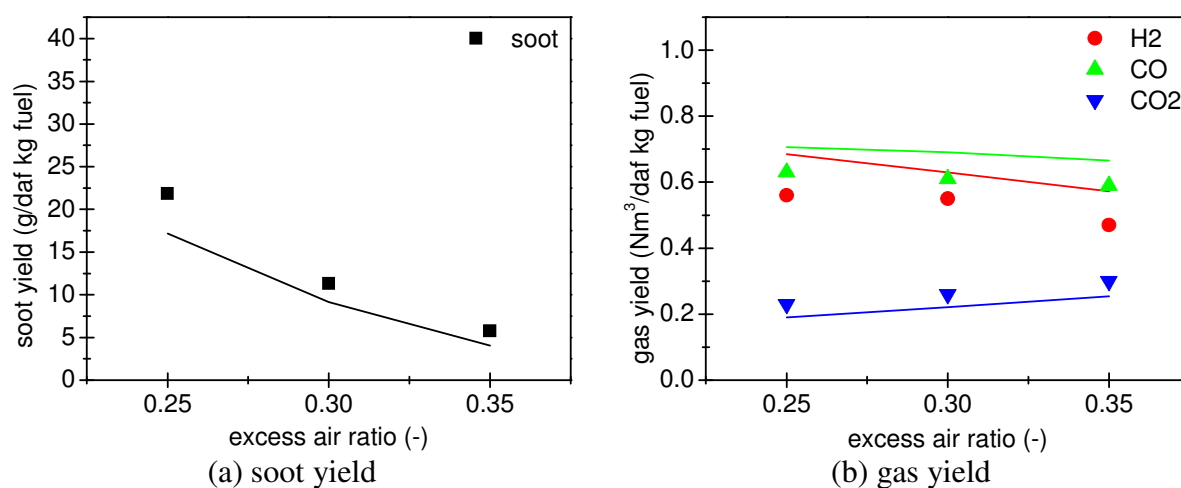

(a) soot yield
(b) gas yield

Figure 6.9 Effect of excess air ratio on product yield: symbols – experimental results (experiments NO.4, 11, and 12 listed in Table 6.1); lines – simulation results

6.4.2.5 Effect of steam/carbon ratio

Figure 6.10 shows the comparison between experimental and simulation results of product yield as a function of steam/carbon ratio. The simulations were conducted for experiments NO. 4, 13, and 14 listed in Table 6.1. It can be observed that in both experiments and simulations, the yields of soot and CO decreased while the yields of H_2 and CO_2 increased with increasing steam/carbon ratio from 0.0 to 1.0, because steam addition promoted the soot-steam gasification reaction and the water gas shift reaction. On the whole, the simulation results were in good agreement with the experimental results. The differences in the yields of soot, H_2, and CO between the simulations and experiments are probably due to the errors in the estimation of soot- H_2O reaction kinetics.
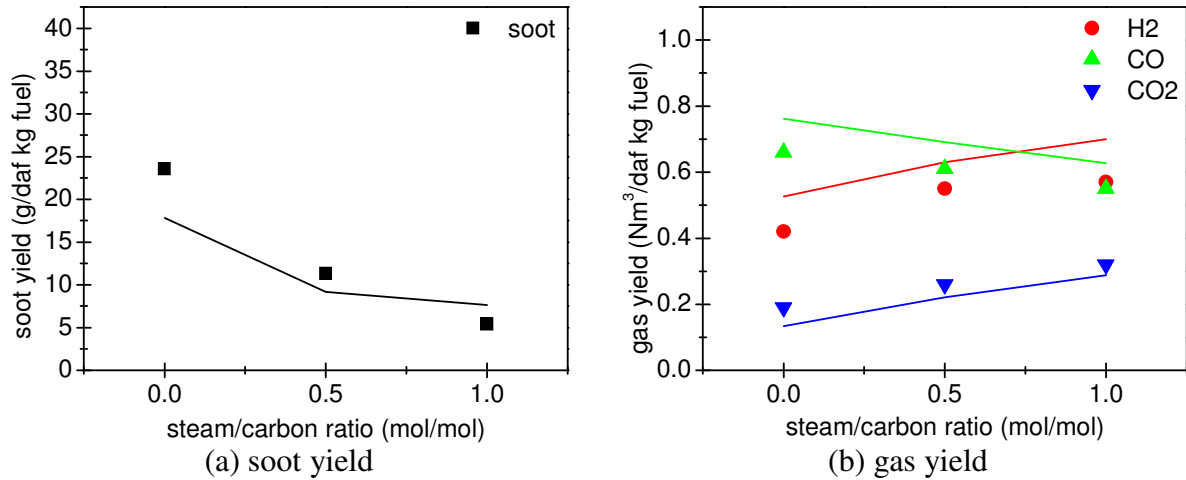
(a) soot yield

(b) gas yield

Figure 6.10 Effect of steam/carbon ratio on product yield: symbols – experimental results (experiments NO.4, 13, and 14 listed in Table 6.1); lines – simulation results

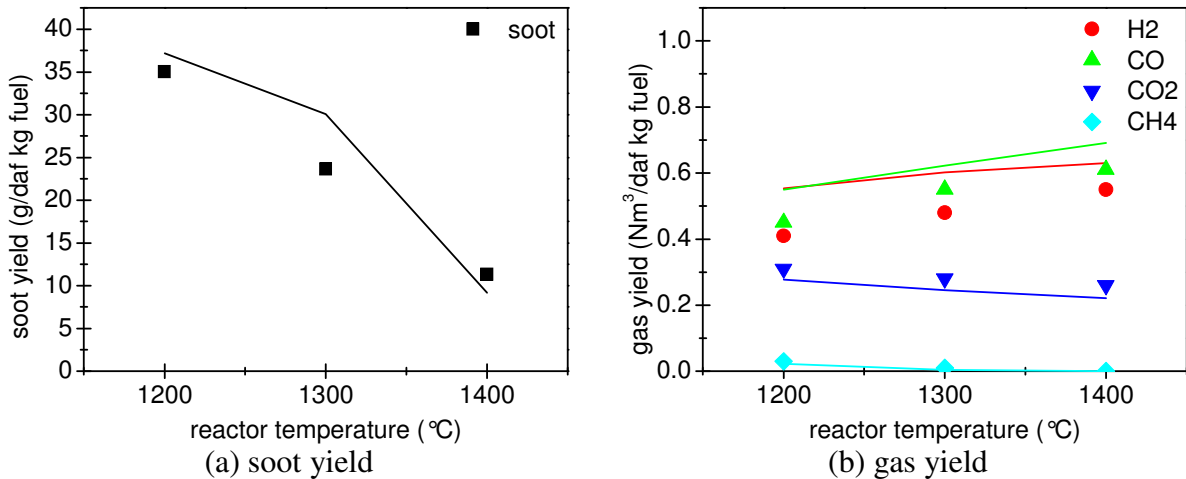### 6.4.2.6 Effect of reactor temperature

(a) soot yield

(b) gas yield

Figure 6.11 Effect of reactor temperature on product yield: symbols – experimental results (experiments NO.4, 15, and 16 listed in Table 6.1); lines – simulation results

Figure 6.11 shows the comparison between experimental and simulation results of product yield as a function of reactor temperature. The simulations were conducted for experiments NO. 4, 15, and 16 listed in Table 6.1. In the present model, the distributions of pyrolysis products at different reactor temperatures were assumed different. Higher pyrolysis temperature tended to generate more soot while less char in the initial pyrolysis products [37]. Besides, in the present model, we assumed that the soot particles as well as the char particles produced at different temperatures had the same reaction kinetics. It can be observed that in both experiments and simulations, the yields of soot, CO_2, and CH_4 decreased while the yields of H_2 and CO increased with increasing reactor temperature from 1200 to 1400 °C. The simulation results were globally in good agreement with the experimental results. The errors

in the yields of gas products between the simulations and experiments might be related to the employed pyrolysis products distributions and gas phase reaction kinetics.

6.4.3 Comparison among experiment, simulation and equilibrium calculation

In comparison to the experimental results of wood gasification, simulation and equilibrium calculations were performed for the standard experiment, No .4 listed in Table 6.1. There was no carbon left in the equilibrium calculation, therefore the equilibrium syngas consisted of CO, CO_2, H_2, and H_2O. The comparison among experimental, simulation, and equilibrium calculation results are shown in Figure 6.12. In the experiment, H_2O cannot be measured and thus its yield is estimated on the basis of the hydrogen mass balance. Generally, the results obtained from the experiment, simulation, and equilibrium calculation were reasonably similar. Comparison between simulation and equilibrium calculation results, it can be found that their gas product yields were quite similar. This probably indicates that the gas phase reaction kinetics used by the CHEMKIN III subroutine library in the simulation and by the FactSage Program in the equilibrium calculation must be very similar in the current operating condition (high temperature with steam addition).
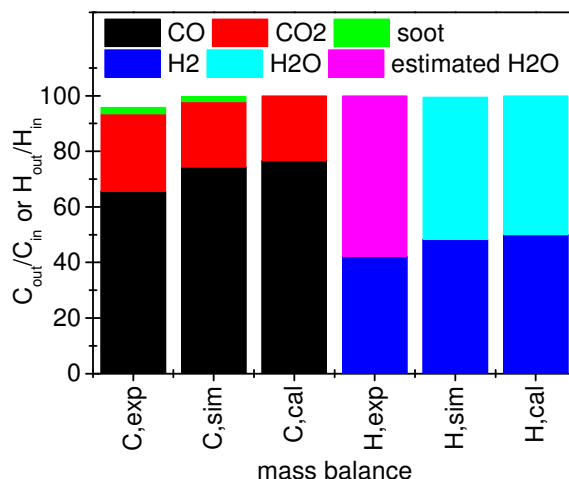

Figure 6.12 Comparison among experimental (experiment NO.4 listed in Table 6.1), simulation, and equilibrium calculation results

6.4.4 Model evaluation

Figure 6.13 compares the simulation results with the experimental results shown in Figure 6.6 – Figure 6.11, in total 16 experimental data for each product. The data shown in Figure 6.13 included a wide range of operating parameters discussed in the previous sections. In Figure

6.13, it can be seen that the largest deviation between simulation and experimental results was about 15 % absolute errors. Therefore, it can be conclude that the model generally provided a satisfactory description of biomass entrained flow gasification under the applied operating conditions.
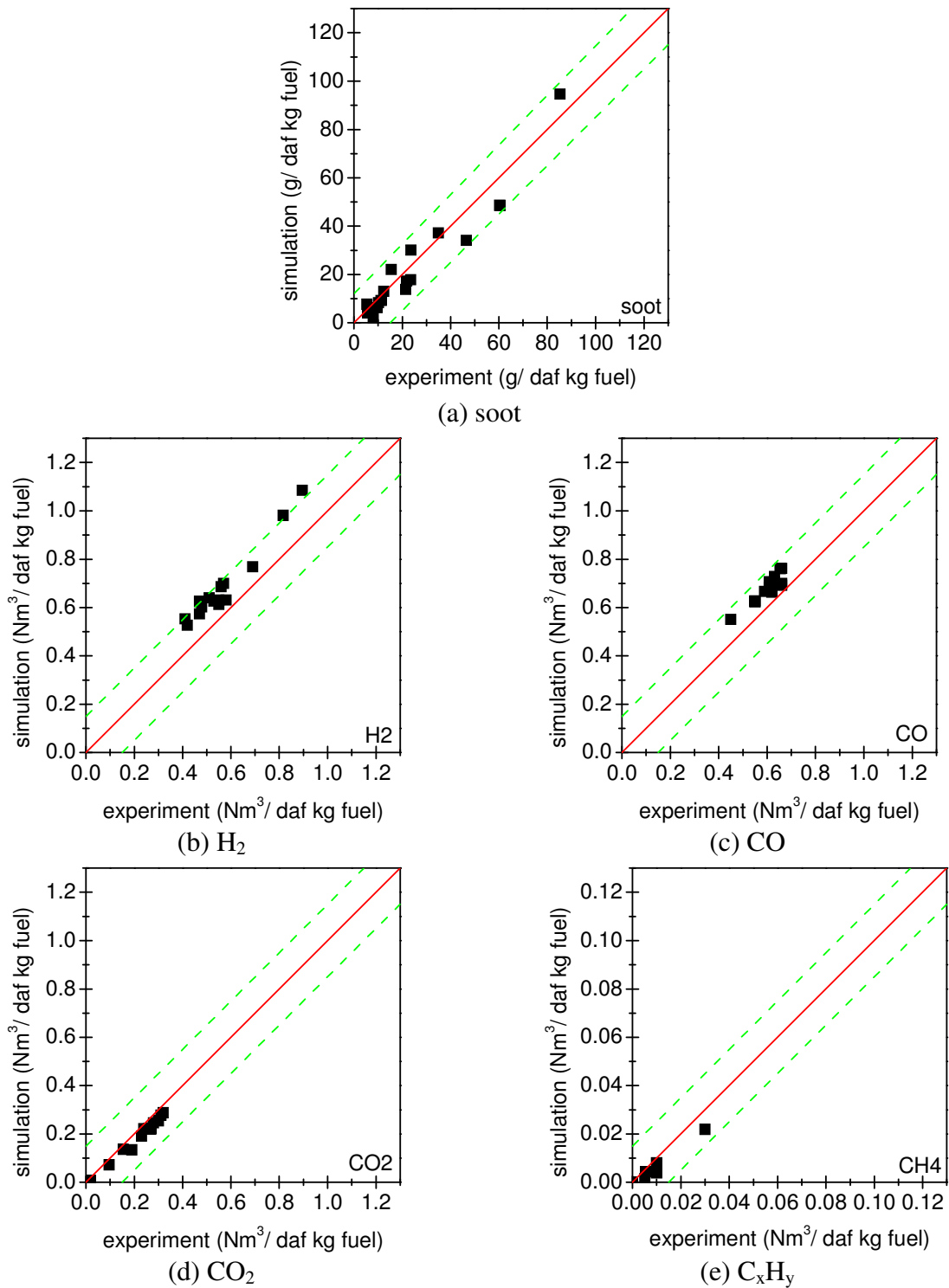

(a) soot

(b) H_2

(c) CO

(d) CO_2

(e) C_xH_y

Figure 6.13 Comparison between experimental and simulation results in ± 15 % absolute errors

6.4.5 Model prediction on complete soot conversion

Soot, produced at high-temperature entrained flow gasification, is an undesired byproduct, which could generate fouling problem in gasification devices [33,38]. Besides, unconverted soot in the syngas reduces the efficiency of the gasification process and makes further syngas cleaning more comprehensive. In the applied experiments, listed in Table 6.1, char was completely converted but soot was always left. Thus, in the present model, the reactor length was prolonged to 3 m to improve soot conversion. The standard experiment, No.4 listed in Table 6.1, was employed to investigate the effect of reactor length on the soot yield and gas product yield. The simulation results are shown in Figure 6.14. It can be observed that with increasing the reactor length, the soot was completely converted after 2.5 m. When the reactor length was between 2 and 2.5 m, the yields of H_2 and CO increased while the CO_2 yield almost kept constant. When the reactor length was longer than 2.5 m, these gas products yields nearly remained unchanged. Therefore, it is suggested that the reactor length of 2.5 – 3 m is suitable for soot removal in the present work.
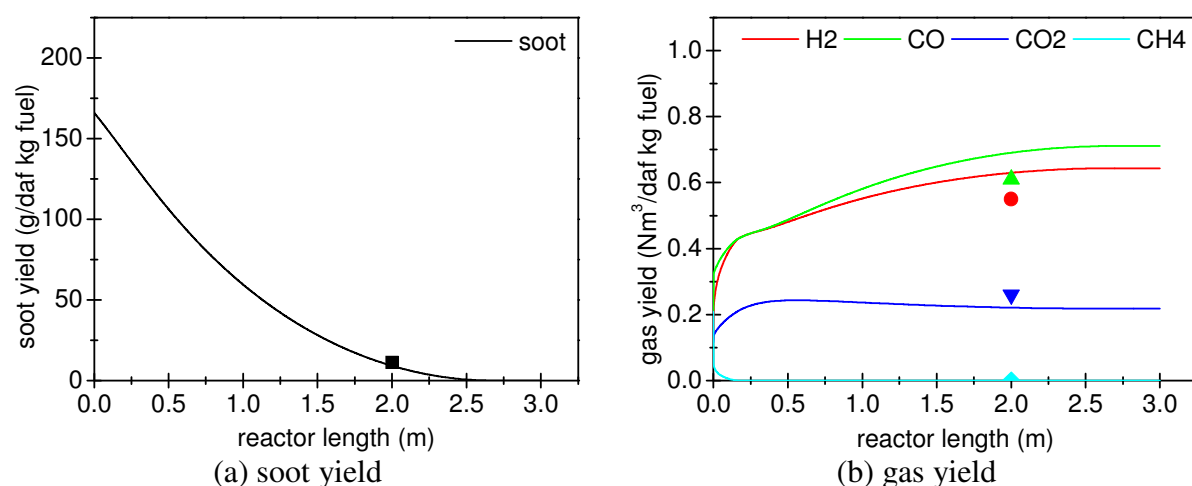

(a) soot yield   (b) gas yield

Figure 6.14 Effect of reactor length on product yield: symbols – experimental results (experiment NO.4 in Table 6.1); lines – simulation results

6.5 Conclusions

A mathematic model with detailed gas phase chemistry was developed to describe entrained flow gasification of biomass. The present model included mixing, drying and pyrolysis, homogeneous and heterogeneous reactions, and mass and heat transfer in solid and gas phase. It is able to predict syngas composition, particularly soot, under different operating conditions.

The simulations were performed under different operating conditions by changing residence time, feeder air flow, oxygen concentration, excess air ratio, steam/carbon ratio, and reactor

temperature. All the simulation results of the soot and gas product yields generally coincided with the experimental results well. The differences between simulation and experimental results for each product might be mainly caused by the errors in the estimation of the pyrolysis product distribution, solid-gas reaction kinetics, and simple assumption of mixing, which were below approximate 15 % absolute error. The experimental, simulation, and equilibrium calculation results under the standard condition were compared. Generally, they were reasonably similar, especially the simulation and equilibrium calculation results, probably related to the similar gas phase chemistry used in them. Under a reasonable gasification condition (t = 3.1 s, feeder air flow = 10 NL/min, oxygen concentration = 21 %, excess air ratio = 0.3, steam/carbon ratio = 0.5, and reactor temperature = 1400 °C), 2.5 – 3 m reactor is suitable for completely soot conversion and optimizing the gas composition (maximum yields of H_2 and CO). On the whole, it can be confirmed that most features of biomass entrained flow gasification under a wide range of operating conditions can be identified and predicted reliably by the present model.

6.6 Notation

A	=	cross section area of entrained flow reactor	(m^2)
A_{c0}	=	pre-exponential factor in char gasification reaction	$(s^{-1}MPa^{-m})$
A_{s0}	=	pre-exponential factor in soot gasification reaction	$(s^{-1}MPa^{-m})$
a_{sc}	=	total external surface area of char particles	(m^2s^{-1})
a_{ss}	=	total external surface area of soot particles	(m^2s^{-1})
a_w	=	external surface area of entrained flow reactor per length	(m)
C_{pc}	=	molar heat capacity of char	$(Jmol^{-1}K^{-1})$
C_{pg}	=	molar heat capacity of gas	$(Jmol^{-1}K^{-1})$
C_{ps}	=	molar heat capacity of soot	$(Jmol^{-1}K^{-1})$
E_c	=	activation energy in char gasification reaction	$(Jmol^{-1})$
E_s	=	activation energy in soot gasification reaction	$(Jmol^{-1})$
e_c	=	char emissivity	$(-)$
e_s	=	soot emissivity	$(-)$
d_{c0}	=	initial diameter of char	(m)
d_{s0}	=	initial diameter of soot	(m)
d_{cpore}	=	diameter of pore in char	(m)
d_{spore}	=	diameter of pore in soot	(m)
F_c	=	molar flow rate of char	(mol/s)
F_g	=	molar flow rate of gas	(mol/s)
F_s	=	molar flow rate of soot	(mol/s)
F_{c0}	=	initial molar flow rate of char	(mol/s)
F_{s0}	=	initial molar flow rate of soot	(mol/s)
F_{wc}	=	view factor between reactor wall and char particles	$(-)$
F_{ws}	=	view factor between reactor wall and soot particles	$(-)$
F_{O2}	=	molar flow rate of oxygen	(mol/s)
F_{N2}	=	molar flow rate of nitrogen	(mol/s)

F_{H2O}	=	molar flow rate of steam	(mol/s)
h_{sc}	=	convection heat transfer coefficient between char and gas	$(Wm^{-2}K^{-1})$
h_{ss}	=	convection heat transfer coefficient between soot and gas	$(Wm^{-2}K^{-1})$
h_w	=	convection heat transfer coefficient between wall and gas	$(Wm^{-2}K^{-1})$
ΔH_c	=	heat of char gasification reaction	$(Jmol^{-1})$
ΔH_g	=	heat of gas phase reaction	$(Jmol^{-1})$
ΔH_s	=	heat of soot gasification reaction	$(Jmol^{-1})$
L	=	reactor length	(m)
m_c	=	reaction order for gas phase in char gasification reaction	(-)
m_s	=	reaction order for gas phase in soot gasification reaction	(-)
n_c	=	reaction order for solid phase in char gasification reaction	(-)
n_s	=	reaction order for solid phase in soot gasification reaction	(-)
P_c	=	gas partial pressure at the char surface	(MPa)
P_s	=	gas partial pressure at the soot surface	(MPa)
R	=	ideal gas constant	$(Jmol^{-1}K^{-1})$
R_c	=	radius of char	(m)
R_s	=	radius of soot	(m)
R_{c0}	=	initial radius of char	(m)
R_{s0}	=	initial radius of soot	(m)
r_c	=	char gasification reaction rate	$(mols^{-1}m^{-1})$
r_g	=	gas phase reaction rate	$(mols^{-1}m^{-3})$
r_s	=	soot gasification reaction rate	$(mols^{-1}m^{-1})$
T_c	=	char temperature	(K)
T_g	=	gas temperature	(K)
T_s	=	soot temperature	(K)
T_w	=	reactor wall temperature	(K)
t	=	residence time	(s)
v	=	gas and solid velocity	(m/s)
ε_c	=	porosity of char	(-)
ε_s	=	porosity of soot	(-)
η_c	=	effectiveness factor in char gasification reaction	(-)
η_s	=	effectiveness factor in soot gasification reaction	(-)
θ	=	stoichiometric ratio in solid-gas reaction	(-)
ρ_c	=	density of char	(Kgm^{-3})
ρ_s	=	density of soot	(Kgm^{-3})
σ	=	Stefan-Boltzmann constant	$(Wm^{-2}K^{-4})$
τ_c	=	tortuosity of char	(-)
τ_s	=	tortuosity of soot	(-)
subscript			
i	=	reaction number	(-)
j	=	gas species	(-)

6.7 References

[1] International energy outlook 2011. Available from: http://www.eia.gov/forecasts/ieo/pdf/0484(2011).pdf.

[2] Stiegel GJ, Maxwell RC. Gasification technologies: the path to clean, affordable energy in the 21st century. Fuel Process Technol 2001;71:79-97.

[3] Christensen JM, Jensen PA, Jensen A. Effects of feed composition and feed impurities in the catalytic conversion of syngas to higher alcohols over alkali-promoted cobalt-molybdenum sulfide. Ind Eng Chem Res 2011;50:7949-63.

[4] Higman C, Van der Burgt M. Gasification. Burlington: Gulf Professional Publishing. 2008.

[5] Wen C, Chaung T. Entrainment coal gasification modeling. Industrial & Engineering Chemistry Process Design and Development 1979;18:684-95.

[6] Kalinenko R, Levitskii A, Mirokhin YA, Polak L. Mathematical model of the pyrolysis and gasification of coal. Kinet.Catal.(Engl.Transl.);(United States) 1987;28.

[7] Vamvuka D, Woodburn ET, Senior PR. Modelling of an entrained flow coal gasifier. 1. Development of the model and general predictions. Fuel 1995;74:1452-60.

[8] Beath AC. Mathematical modelling of entrained flow coal gasification. Ph.D thesis, Department of Chemical Engineering, University of Newcastle, Australia. 1996.

[9] Govind R, Shah J. Modeling and simulation of an entrained flow coal gasifier. AIChE J 1984;30:79-92.

[10] Soelberg NR, Smoot LD, Hedman PO. Entrained flow gasification of coal: 1. Evaluation of mixing and reaction processes from local measurements. Fuel 1985;64:776-81.

[11] Chen C, Horio M, Kojima T. Numerical simulation of entrained flow coal gasifiers. Part I: modeling of coal gasification in an entrained flow gasifier. Chemical Engineering Science 2000;55:3861-74.

[12] Watanabe H, Otaka M. Numerical simulation of coal gasification in entrained flow coal gasifier. Fuel 2006;85:1935-43.

[13] Choi Y, Li X, Park T, Kim J, Lee J. Numerical study on the coal gasification characteristics in an entrained flow coal gasifier. Fuel 2001;80:2193-201.

[14] Vicente W, Ochoa S, Aguillon J, Barrios E. An Eulerian model for the simulation of an entrained flow coal gasifier. Appl Therm Eng 2003;23:1993-2008.

[15] Liu XJ, Zhang WR, Park TJ. Modelling coal gasification in an entrained flow gasifier. Combustion Theory and Modelling 2001;5:595-608.

[16] Fletcher D, Haynes B, Christo F, Joseph S. A CFD based combustion model of an entrained flow biomass gasifier. Appl Math Model 2000;24:165-82.

[17] Kee RJ, Rupley FM, Meeks E, Miller JA. CHEMKIN-III: A FORTRAN chemical kinetics package for the analysis of gas-phase chemical and plasma kinetics. Report No. SAND96-8216. 1996.

[18] Østberg M, Glarborg P, Jensen A, Johnsson JE, Pedersen LS, Dam-Johansen K. A model of the coal reburning process. Symposium (International) on Combustion 1998;27:3027-3035.

[19] Vilas E, Skifter U, Jensen AD, López C, Maier J, Glarborg P. Experimental and modeling study of biomass reburning. Energy Fuels 2004;18:1442-50.

[20] Glarborg P, Kristensen PG, Dam-Johansen K, Alzueta M, Millera A, Bilbao R. Nitric oxide reduction by non-hydrocarbon fuels. Implications for reburning with gasification gases. Energy Fuels 2000;14:828-38.

[21] Alzueta MU, Bilbao R, Millera A, Glarborg P, Østberg M, Dam-Johansen K. Modeling low-temperature gas reburning. NO x reduction potential and effects of mixing. Energy Fuels 1998;12:329-38.

[22] Hashemi H, Hansen S, Toftegaard MB, Pedersen KH, Jensen AD, Dam-Johansen K, et al. A model for nitrogen chemistry in oxy-fuel combustion of pulverized coal. Energy Fuels 2011.

[23] Zwietering TN. The degree of mixing in continuous flow systems. Chemical Engineering Science 1959;11:1-15.

[24] Brix J. A model for entrained flow gasification of solid fuels for syngas production. Master Thesis, Technical University of Denmark. 2007.

[25] Gavhane KA. Chemical reaction engineering II. Maharashtra: Nirali Prakashan. 2009.

[26] Fogler HS. Elements of chemical reaction engineering. New Jersey: Prentice-Hall International. 1999.

[27] Qin K, Jensen PA, Lin W, Jensen AD. Biomass gasification behavior in entrained flow reactor: gas product distribution and soot formation. Energy & Fuels 2012;26:5992-6002.

[28] Septien Stringel S. High temperature gasification of millimetric wood particles between 800° C and 1400° C. Ph.D Thesis, National Polytechnic Institute of Toulouse. 2011.

[29] Zhang Y, Kajitani S, Ashizawa M, Miura K. Peculiarities of rapid pyrolysis of biomass covering medium-and high-temperature ranges. Energy Fuels 2006;20:2705-12.

[30] Neoh K, Howard J, Sarofim A. Effect of oxidation on the physical structure of soot. Symposium (International) on Combustion 1985;20:951-957.

[31] Marcuccilli F, Gilot P, Stanmore B, Prado G. Experimental and theoretical study of diesel soot reactivity. Symposium (International) on Combustion 1994;25:619-626.

[32] Sivathanu Y, Gore J. Coupled radiation and soot kinetics calculations in laminar acetylene/air diffusion flames. Combust Flame 1994;97:161-72.

[33] Stanmore BR, Brilhac JF, Gilot P. The oxidation of soot: a review of experiments, mechanisms and models. Carbon 2001;39:2247-68.

[34] Qin K, Lin W, Fæster S, Jensen PA, Wu H, Jensen AD. Characterization of residual particulates from biomass entrained flow gasification. Energy & Fuels 2013;27:262-70.

[35] Di Blasi C. Combustion and gasification rates of lignocellulosic chars. Progress in energy and combustion science 2009;35:121-40.

[36] Glassman I, Yaccarino P. The effect of oxygen concentration on sooting diffusion flames. Combustion Sci Technol 1980;24:107-14.

[37] Septien S, Valin S, Dupont C, Peyrot M, Salvador S. Effect of particle size and temperature on woody biomass fast pyrolysis at high temperature (1000–1400° C). Fuel 2012;97:202-10.

[38] Chen G, Zhang Y, Zhu J, Cao Y, Pan W. Coal and biomass partial gasification and soot properties in an atmospheric fluidized bed. Energy Fuels 2011;25:1964-9.

Chapter 7   Conclusions and suggestions for future work

The objective of the present work is to contribute to an increased knowledge on biomass entrained flow gasification. This information should be helpful to support the development of commercial entrained flow biomass gasifiers. A comprehensive literature study of biomass entrained flow gasification was presented. An experimental study on biomass entrained flow gasification was conducted, and a mathematic model of biomass entrained flow gasification was developed on the basis of the obtained experimental results. An experimental study on entrained flow co-gasification of biomass and coal was also conducted, because the first step to use biomass is to apply it together with coal in the plants originally designed only for coal. The conclusions are summarized and suggestions for further work are given.

7.1 Conclusions

Biomass gasification was investigated in a laboratory-scale atmospheric pressure entrained flow reactor. The experimental study focused on the effects of operating parameters and biomass types on the yields of gas (H_2, CO, CO_2, and light hydrocarbons) and residual particulates (char and soot). Six operating parameters, reactor temperature (1000 – 1400 °C), steam/carbon ratio (0.0 – 1.0), excess air ratio (0.25 – 0.50), oxygen concentration (5 – 26 %), feeder gas flow (6 – 14 NL/min), and residence time (2.4 – 6.0 s) were selected due to their intimate association with practical application. Wood (beech sawdust), straw (pulverized wheat straw pellets), and lignin (byproduct from a straw ethanol plant), which are typical forestry, agricultural, and industrial wastes respectively, were used as biomass fuels. In all gasification experiments, most biomass carbon was partitioned to CO and CO_2. The part of biomass carbon to light hydrocarbons decreased gradually with increasing the reactor temperature. Moreover, the biomass carbon that was not completely converted to gas only appeared as soot particles except for two experiments performed at 1000 °C without steam addition where a very small amount unconverted of char was also left. In the high-temperature gasification experiments (> 1200 °C), the carbon mass balance closures were reasonable, typically higher than 90 %, except for a few experiments conducted at 1000 and 1100 °C (approximate 10 – 20 % gap) probably due to the deposited carbonaceous products on the reactor wall. H_2 and CO are the desired products during entrained flow gasification, while soot is the main byproduct and is required to be removed or minimized. Increasing the

157

reactor temperature, increasing the steam/carbon ratio, and decreasing the excess air ratio were beneficial to increasing the H_2 yield. Increasing the reactor temperature, decreasing the steam/carbon ratio, and decreasing the excess air ratio were helpful to increasing the CO yield. Changing oxygen concentration, feeder air flow, and residence time did not affect the H_2 and CO yield noticeably. The soot yield was reduced by employing a higher reactor temperature, higher steam/carbon ratio, higher excess air ratio, lower oxygen concentration, larger feeder air flow, and longer residence time. Wood, straw, and lignin gasification exhibited similar gas compositions. However, the soot yield was much lower during straw gasification than that during both wood and lignin gasification, probably related to the high potassium content in straw. Besides a comprehensive experimental study on biomass gasification, a few biomass pyrolysis experiments were also conducted to obtain a better understanding of the whole gasification process. In the pyrolysis experiments, besides the contribution of CO and CO_2, soot also contributed obviously to the closure of carbon mass balance. In comparison to gasification, higher yields of H_2, CO, and soot were produced during pyrolysis. On the basis of our present work, it can be concluded that high-temperature (> 1200 °C) entrained flow air/steam gasification of biomass can achieve a high carbon conversion within a few seconds of residence time and a high-quality syngas without tar while with a low but not negligible amount of soot. Increasing the excess air ratio, feeder air flow, and residence time can further reduce the amount of soot in syngas. In addition, FactSage Program was employed to calculate the equilibrium product composition under the applied operating conditions in the gasification experiments. At high temperature with steam addition, the experimental results were close to the gas composition obtained by equilibrium calculation. Therefore, high temperature and steam addition can help the experimental results approaching to the equilibrium product composition.

In all biomass gasification experiments, residual particulates were always left in the metal filter, while residual particulates were observed in the cyclone only in two experiments conducted at 1000 °C without steam addition. STA was employed to analyze the composition (moisture, organic matters, volatilizable inorganic compound, and residual ash), reactivity and kinetics of the obtained solid samples. SEM with EDS was employed to analyze their morphology and elemental distribution. During wood gasification, soot was the major part of the filter sample, which appeared as agglomerated nano-size spheres (< 100 nm) being rich in carbon. In comparison to wood gasification, the filter sample obtained from straw gasification had quite low content of soot while high contents of volatilizable KCl and K_2SO_4 and

appeared as irregular crystals (> 100 nm) due to the deposited KCl and K_2SO_4 on the soot surface. The filter sample obtained from the lignin gasification experiment mainly consisted of soot and non-volatilizable inorganic matter due to the high silica and calcium contents in lignin. The obtained cyclone sample was char. The parent wood particles and the derived wood char particles had a layered structure with a loose and porous texture and appeared as similar size and shape. However, the derived wood char particle surface looked smoother. These observations indicated that only some degree of melting rather than complete melting took place on the wood char particles which were obtained from the gasification experiment conducted at 1000 °C without steam addition. In the study on the reactivity and kinetics of the wood soot and wood char, it can be found that the wood char was more reactive than the wood soot with respect to both oxidation and CO_2 gasification probably due to a less ordered structure of carbon in the char compared to the soot. For both the wood soot and char, the reaction order with respect to the solid phase was found to be 1.0 during oxidation and to be 0.5 during gasification. In the wood soot and char oxidation, the reaction order with respect to the gas phase was 0.99 and 0.71 respectively. In the wood soot and char CO_2 gasification, the reaction order with respect to the gas phase was 0.54 and 0.12 respectively. The activation energy of the wood soot conversion is higher than that of the wood char conversion. This difference in reactivity was a possible evidence to explain why char was generally fully converted in the conducted biomass gasification experiments while soot was not. Moreover, we also found that the wood soot produced at a higher temperature was more reactive than the soot produced at a lower temperature.

Coal gasification and biomass and coal co-gasification experiments were performed in the same entrained flow reactor. Compared with biomass gasification, coal gasification yielded less gas products because coal had lower volatile content and a relatively worse fuel conversion. This indicates that lower oxygen to fuel ratio is needed to accomplish biomass gasification, which is beneficial to the process economy. The effect of mixing ratio on co-gasification of straw/wood, straw/coal, and wood/coal were investigated at 1400 °C with steam addition. The yields of residual particulates decreased with increasing straw fraction during straw/wood co-gasification and with increasing biomass fraction (straw or wood) during biomass/coal co-gasification. Moreover, the measured yields of residual particulates in the co-gasification experiments were lower than the calculated values from their weighted yields in the individual biomass gasification experiments, indicating a synergistic effect of co-gasification. The yields of H_2, CO, and CO_2 nearly kept constant with changing mixing ratio

during straw/wood co-gasification due to the similar gas composition in straw and wood gasification, while increased with increasing biomass mixing ratio during biomass/coal co-gasification because of the more reactive biomass char leading to an improved char conversion. The H_2/CO molar ratio increased with increasing biomass mixing ratio, indicating that adding biomass increased H_2 more than CO.

A mathematic model was developed to describe biomass entrained flow gasification. The model included mixing, drying and pyrolysis, char-gas and soot-gas reactions, detailed gas-phase reactions, and mass and heat transfer. The simulations were performed under different operating conditions applied in the wood gasification experiments. The simulation results usually compared well with the experimental data. However, there were still certain difference between the simulation and experimental results, which might be mainly caused by the errors in the estimation of the pyrolysis product distribution, solid-gas reaction kinetics, and simple assumption of mixing. Besides, the simulation and equilibrium calculation results were also similar. On the whole, the model has a reasonable ability to predict syngas composition, particularly the amount of soot, under different gasification conditions. Moreover, the simulation result suggested that 2.5 – 3 m reactor was suitable for complete soot conversion and optimizing the gas composition (maximum yields of H_2 and CO) under a reasonable gasification condition (reactor temperature = 1400 °C, steam/carbon ratio = 0.5, excess air ratio = 0.3, oxygen concentration = 21 %, feeder air flow = 10 NL/min, and residence time = 3.1 s).

7.2 Suggestions for future works

In all experiments conducted in the entrained flow reactor, the syngas products were obtained at the outlet of the reactor, so the intermediate process and product along with the reactor length is unknown. If the syngas products can be sampled at different location along with the reactor length in the future work, a more comprehensive understanding of the whole gasification process and deeper information of reaction mechanism can be obtained.

The carbon mass balance closure was reasonable in all experiments, typically > 90 %, except for biomass gasification experiments conducted at 1000 – 1100 °C and coal gasification experiments conducted at 1200 °C (the lowest temperature used in coal gasification experiments). The gap (approximate 10 – 20 %) was probably caused by the deposited carbonaceous products (e.g. unreacted char, soot, and tar) on the reactor wall, uncollected tar compounds by Petersen column, and unmeasured tar by the employed method. A standard

method of tar sampling and analysis should be used during relatively low-temperature gasification in the future work, which can determine the relative importance of these possible reasons.

In the biomass gasification experiments, we found that straw gasification yielded much less soot than both wood and lignin gasification. This is probably related to the high potassium content in straw but is still unclear. In the biomass and coal co-gasification experiments, a synergistic effect on the yield of residual particulates (char and soot) was observed. The possible reasons were discussed in the present work but the main reason is still undetermined. Thus, pretreated materials, such as wood with additives, leached straw, and leached coal, are expected to be used during individual fuel gasification and mixtures of these pretreated materials are also expected to be used during co-gasification experiments. These new increased results can be used to verify the discussed explanations.

In the biomass gasification experiments conducted at high temperatures, char was completely converted but soot was always left. The unconverted soot particles reduce the fuel conversion and gasification efficiency and are required to be removed or minimized. Thus, the knowledge on characterization of soot is needed. The composition, morphology, and kinetics (oxidation and CO_2 gasification) of soot were investigated by STA and SEM with EDS analysis in the present work. However, some additional information of soot is still required: elemental composition, particle size distribution, intrinsic structure, and soot-H_2O reaction kinetics.

In the model work on biomass entrained flow gasification, the initial pyrolysis products distribution was estimated on the basis of the final products distribution obtained at the outlet of the reactor in the pyrolysis experiments. During high-temperature pyrolysis, the considerable difference between the initial pyrolysis products distribution at the top of the reactor and final pyrolysis products distribution at the bottom of reactor might exist, especially for solid particles due to their rapid consuming rate. If the pyrolysis products can be sampled at the top of the reactor in the future experimental investigation, then the measured initial pyrolysis products distribution can be applied to the model and thereby improve the prediction accuracy. Besides, if the pyrolysis products can be sampled at different location along with the reactor length, the obtained experimental data should be helpful to further model validation. With respect to tar destruction and soot formation in the model, we assumed that tar was completely converted to soot immediately in the high-temperature pyrolysis process (> 1200 °C). If the composition of tar and soot and the reaction mechanism of tar destruction and soot formation can be included, then the model can predict

the soot yield with greater accuracy during high-temperature gasification and also can predict the tar and soot yields during relatively low-temperature gasification. Moreover, the soot reaction kinetics was measured at low temperatures (< 1000 °C) in STA. Soot reaction kinetics at high temperatures used in the model was estimated by the measured kinetics at low temperatures, which may lead to certain errors in the prediction. If the kinetics of soot reaction can be measured at high temperatures, the uncertainty of soot reaction rate in the model can be reduced.

Appendix

A.1 Temperature profile in the entrained flow reactor

The axial temperature profile in the entrained flow reactor at setting temperature of 1000 °C without fuel feeding was roughly monitored by using a thermocouple of S type (the positive wire: 90 % platinum and 10 % rhodium; the negative wire: 100 % platinum). The measured axial temperature profile is shown in Figure A.1. It can be observed that a reasonably uniform temperature, which was close to the setting temperature, was achieved in the reaction tube except its top and end. A lower temperature at the top of the reactor was caused by the injection of cold feeder gas (10 NL/min). The temperature at the end of the reactor dropped sharply due to the applied water-cooled bottom. Therefore, in an experiment, as the fuel and gas are injected into the reactor, they and/or the products undergo a sequence of three thermal processes: heating, isothermal, and cooling.
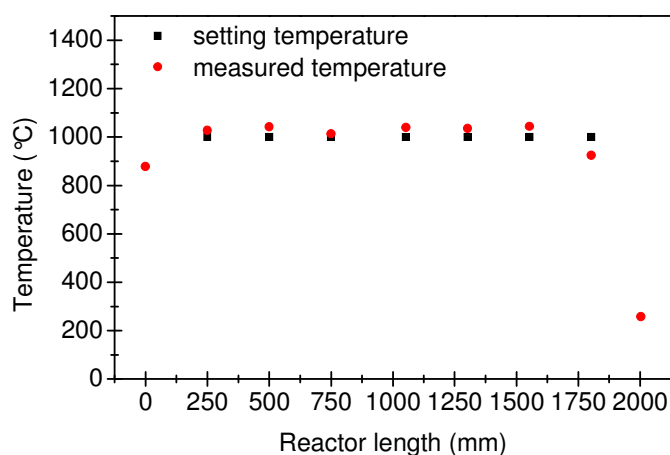
Figure A.1 Temperature profile in the entrained flow reactor at setting temperature of 1000°C without fuel feeding

A.2 Fuel feeding rate and syngas composition

During an experiment, numerous data were logged. Most data were sampled automatically by Labview, such as reactor pressure, fuel feeding rate, and gas concentration (measured by the NDIR gas analyzer). The data were typically logged with an interval of one second. Other data were logged manually or semi-automatically, such as reactor temperature, gas flow, and gas concentration (measured by the Micro GC). Figure A.2 and Figure A.3 show the most important online data (the fuel feeding rate and the gas concentration measured by the NDIR gas analyzer) automatically logged during some typical gasification and co-gasification

163

experiments. These typical experiments were conducted under the same operating condition: feeder air flow = 10 NL/min, oxygen concentration = 21 %, excess air flow = 0.3,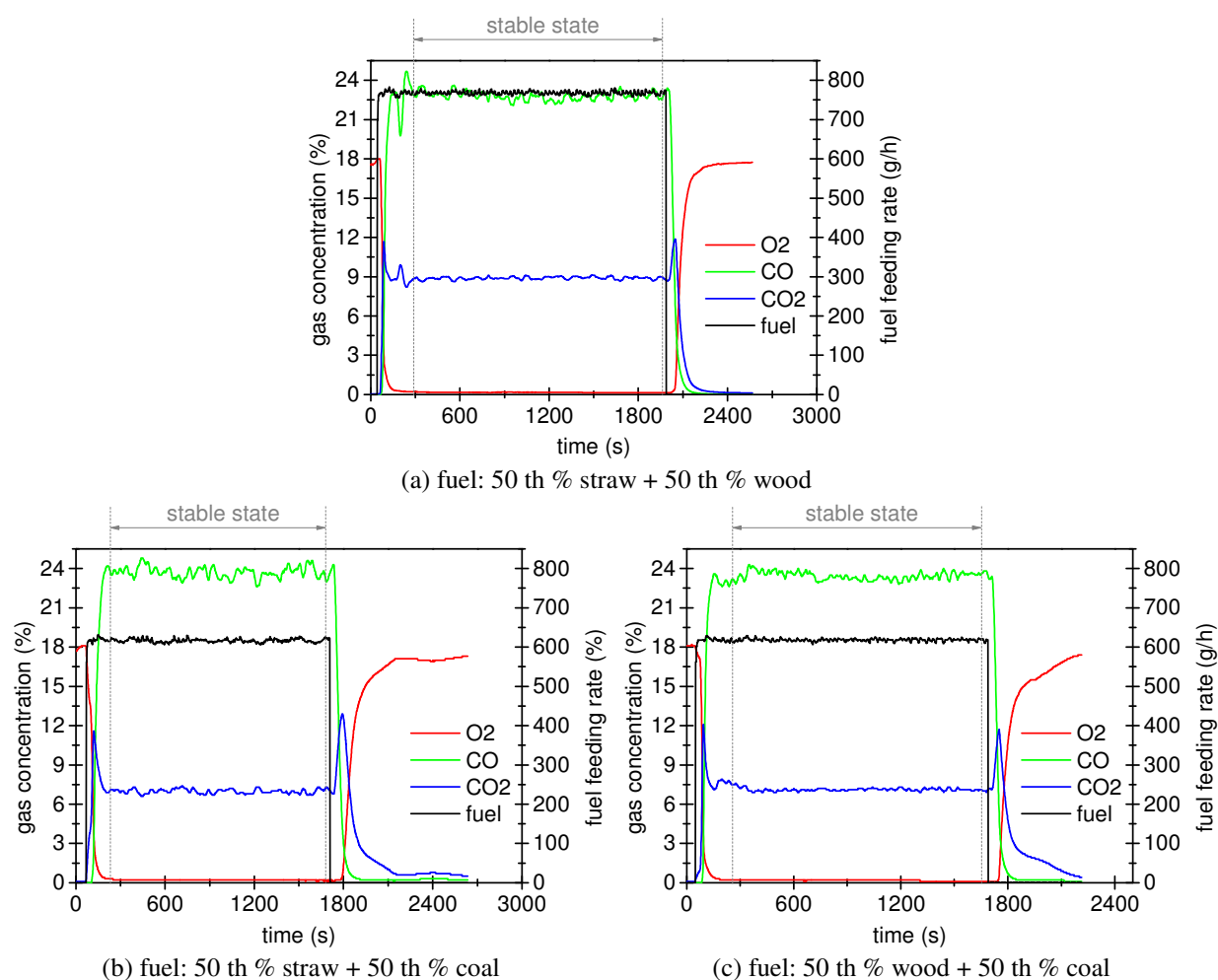 steam/carbon ratio = 0.5, and reactor temperature = 1400 °C. The setting point of fuel feeding rate during these experiments is listed in Table A.1. A small deviation (< 2 %) between the attained fuel feeding rate and the setting point was observed when the experimental condition reached a stable state. The NDIR gas analyzer was calibrated every day prior to the experiment. The general information about measurement and calibration of the NDIR gas analyzer is listed in Table A.2. In Figure A.2 and Figure A.3, it can be observed that the produced CO concentration was out of the calibrated measurement range that was restricted by the range of upper limit and calibrating gas composition, thus the accuracy of CO measurement was uncertain. The data collected by the NDIR gas analyzer were used as reference values to compare with the collected data by the Micro GC. Besides, these data were also used to determine if the experimental condition reached a stable state.

(a) fuel: wood

(b) fuel: straw

(c) fuel: dried lignin

(d) fuel: coal
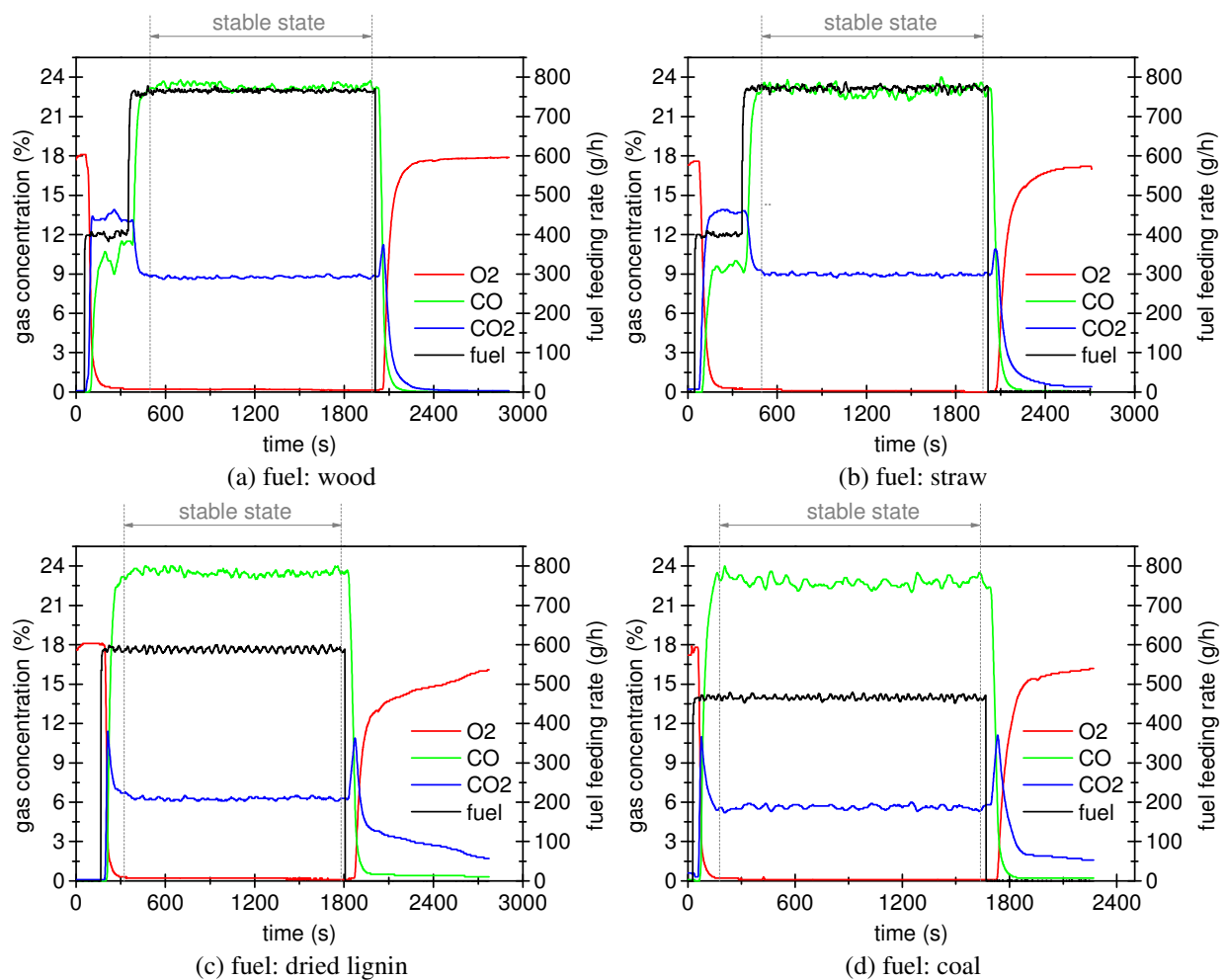
Figure A.2 The fuel feeding rate and the syngas composition measured by the NDIR gas analyzer during some typical gasification experiments (operating condition: feeder air flow = 10 NL/min, oxygen concentration = 21 %, excess air flow = 0.3, steam/carbon ratio = 0.5, and reactor temperature = 1400 °C)

(a) fuel: 50 th % straw + 50 th % wood

(b) fuel: 50 th % straw + 50 th % coal

(c) fuel: 50 th % wood + 50 th % coal

Figure A.3 The fuel feeding rate and the syngas composition measured by the NDIR gas analyzer during some typical co-gasification experiments (operating condition: feeder air flow = 10 NL/min, oxygen concentration = 21 %, excess air flow = 0.3, steam/carbon ratio = 0.5, and reactor temperature = 1400 °C)

Table A.1 The setting point of fuel feeding rate during some typical gasification and co-gasification experiments (operating condition: feeder air flow = 10 NL/min, oxygen concentration = 21 %, excess air flow = 0.3, steam/carbon ratio = 0.5, and reactor temperature = 1400 °C)

fuel	fuel feeding rate
-	g/h
wood	766.4
straw	770.6
dried lignin	588.3
coal	465.1
50 th % straw + 50 th % wood	768.5
50 th % straw + 50 th % coal	617.9
50 th % wood + 50 th % coal	615.8

Table A.2 The general information about measurement and calibration of the NDIR gas analyzer

gas species	range of upper limit	calibrating gas
-	%	%
O_2	10	9.52
CO	5	4.51
CO_2	25	18.8

The Micro GC was started to measure the gas concentration when the fuel feeding rate and the gas concentration measured by the NDIR gas analyzer reached a stable state. The general information about the Micro GC is listed in Table A.3. The sampling interval for the Micro GC measurement is significantly longer than one second obtainable for the NDIR gas analyzer. Typically, the Micro GC provides data with a six-minute interval. The employed calibrating gas for the Micro GC calibration is listed in Table A.4. The measured syngas composition during some typical gasification and co-gasification experiments is listed in Table A.5. The operating conditions of these typical gasification and co-gasification experiments were mentioned above. The corresponding measured chromatograph data during these typical gasification and co-gasification experiments are shown in Figure A.4 - Figure A.10. Compared Table A.5 with Figure A.2 and Figure A.3, good correlation between the NDIR gas analyzer and the Micro GC measurement was observed.

Table A.3 The general information about the Micro GC

channel	column	carrier gas
A	molsieve, 30m×320μm×12μm	He
B	plotU, 8m×320μm×30μm	He
C	molsieve, 10m×320μm×12μm	N_2

Table A.4 The employed calibrating gas for the Micro GC calibration

calibrating gas	gas species in N_2									
NO.	O_2	CO	CO_2	CH_4	C_2H_6	C_2H_4	C_2H_2	C_3H_8	C_3H_6	H_2
1	1%	-	-	-	-	-	-	-	-	-
2	9.52%	4.51%	18.8%	-	-	-	-	-	-	-
3	-	-	1.9%	-	-	-	-	-	-	-
4	-	50%	-	-	-	-	-	1000ppm	-	-
5	-	-	-	1%	-	-	-	-	-	-
6	-	-	-	5%	-	-	-	-	-	-
7	-	-	-	-	1.01%	1.02%	0.996%	-	5%	-
8	-	-	-	-	-	-	-	-	-	10%
9	-	-	-	-	-	-	-	-	-	50%

Table A.5 The syngas composition measured by the Micro GC during some typical gasification and co-gasification experiments (operating condition: feeder air flow = 10 NL/min, oxygen concentration = 21 %, excess air flow = 0.3, steam/carbon ratio = 0.5, and reactor temperature = 1400 °C)
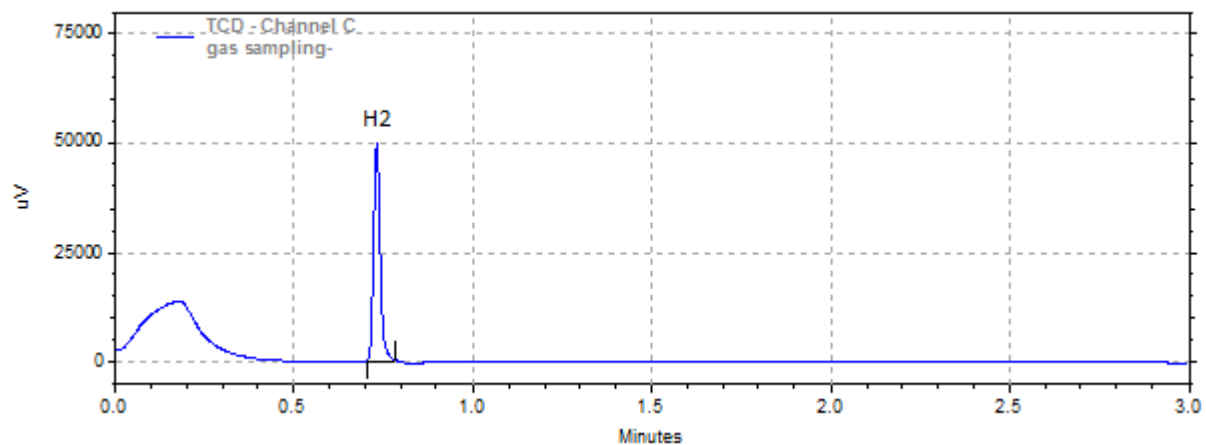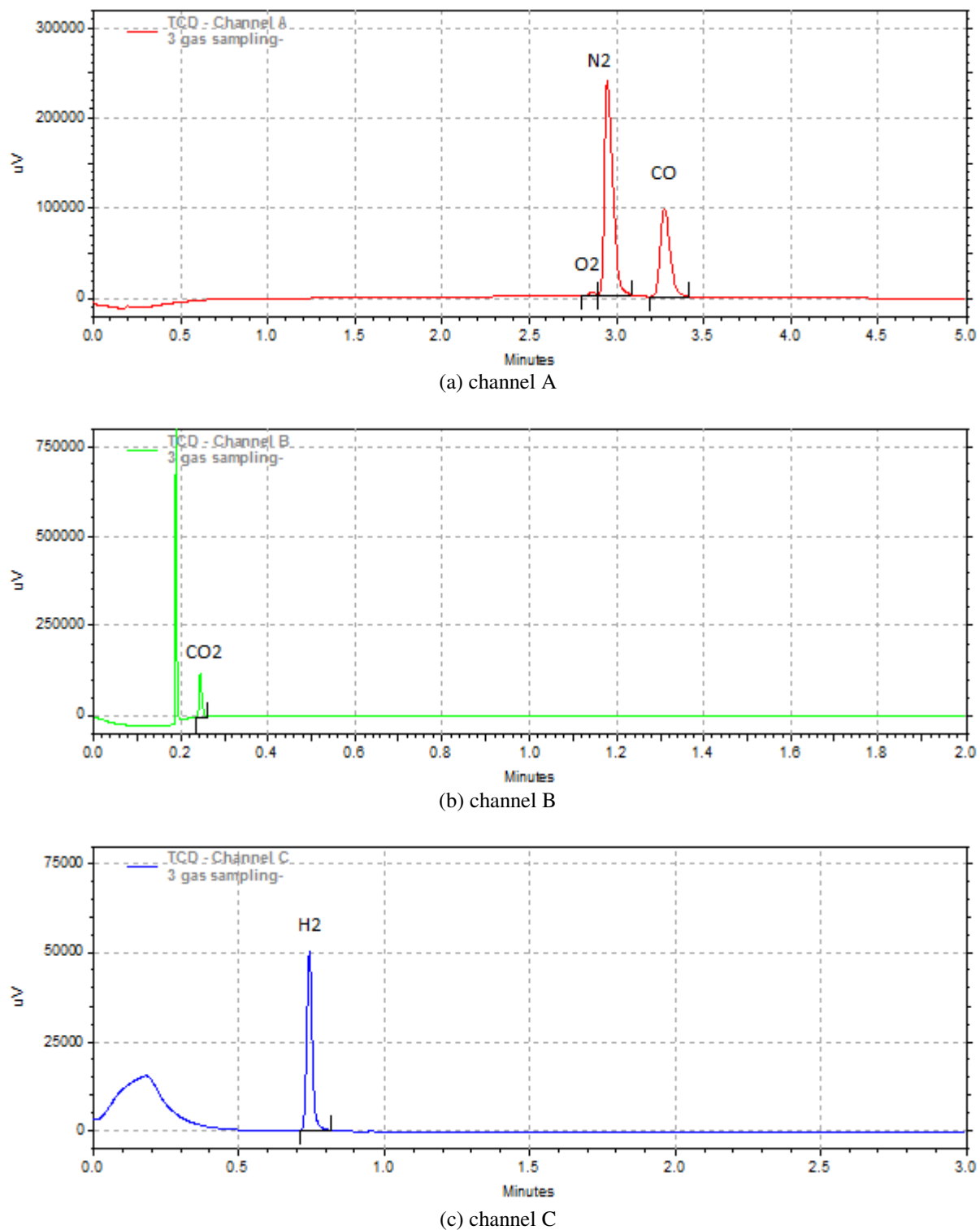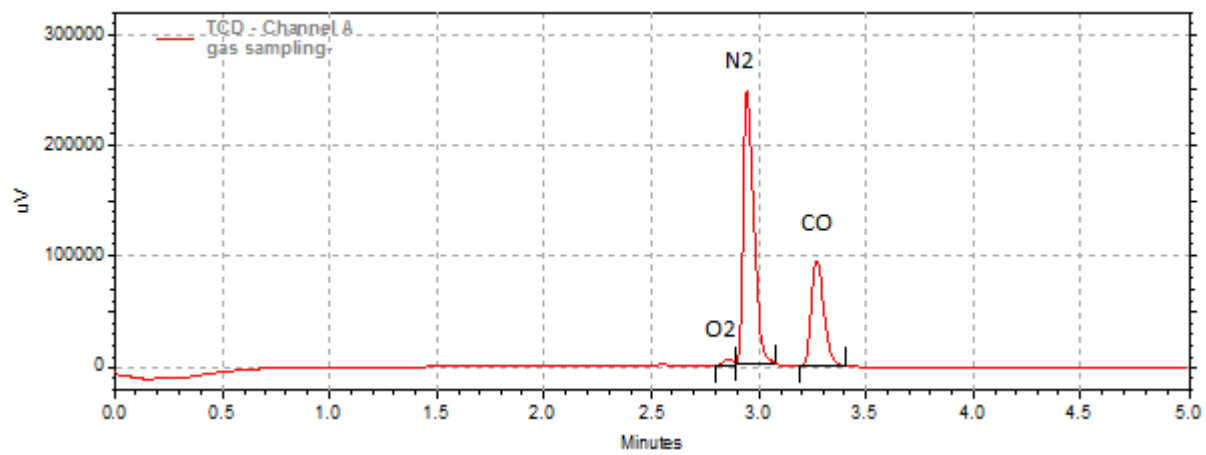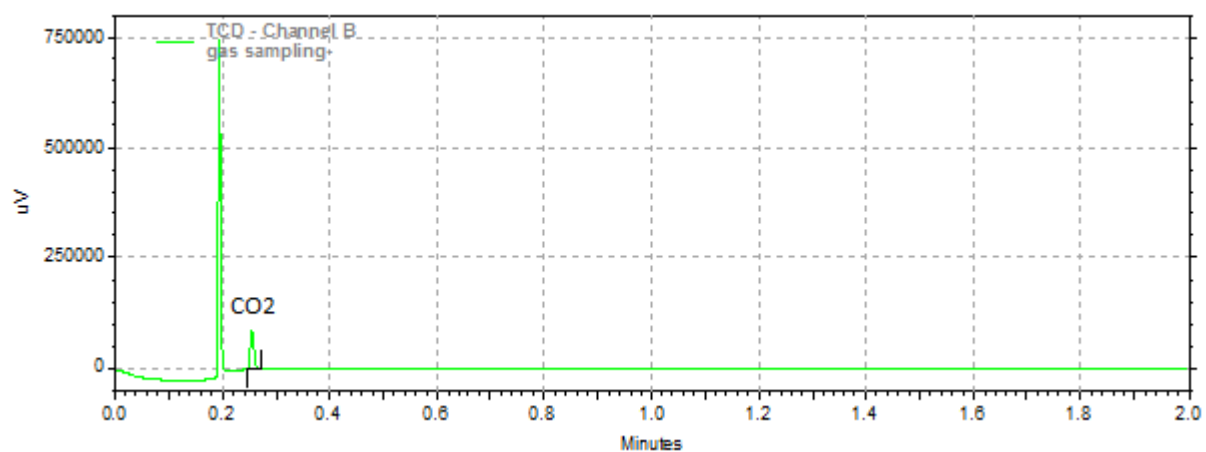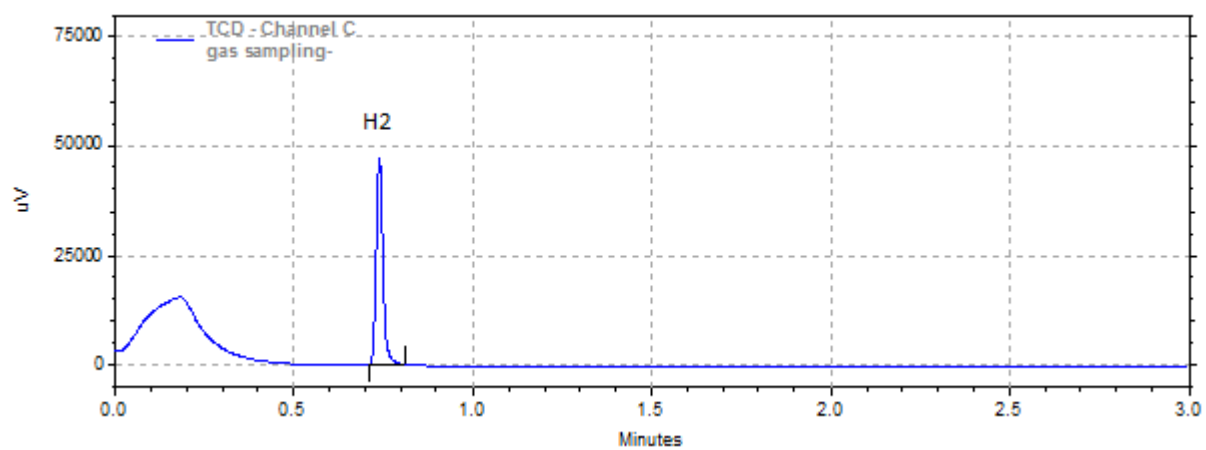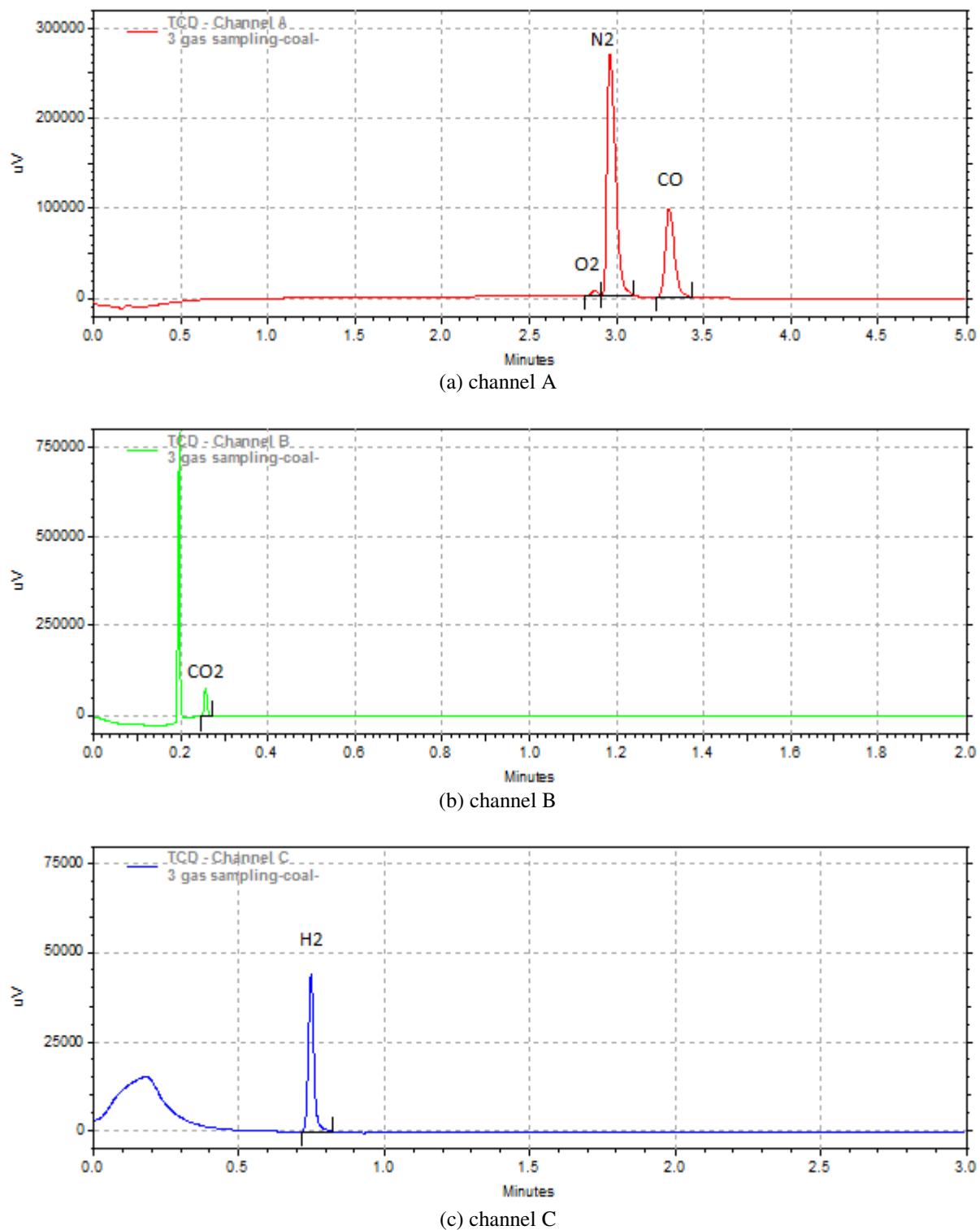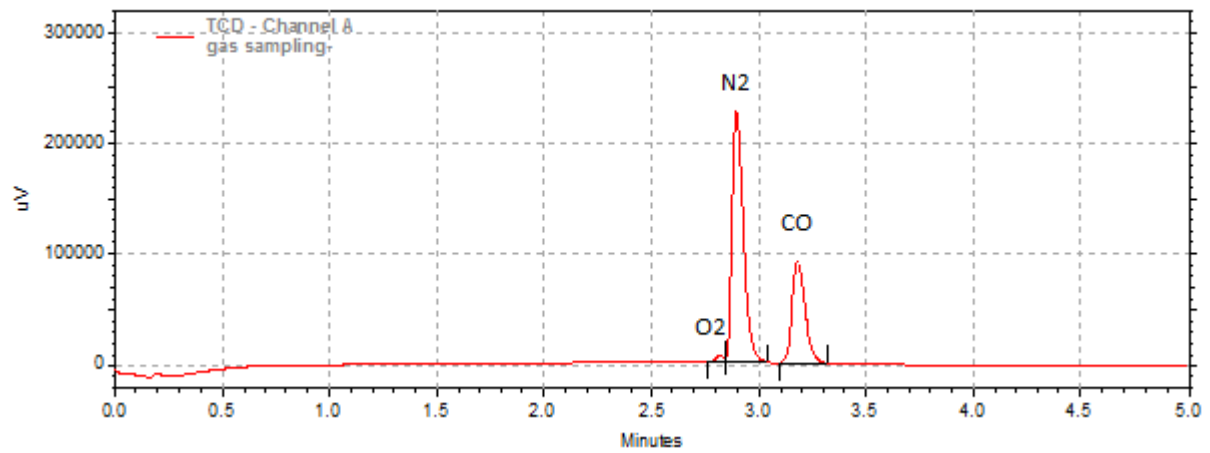
fuel	gas concentration (%)				
-	O_2	N_2	CO	CO_2	H_2
wood	0.92	48.93	22.05	9.17	19.60
straw	0.68	46.98	22.34	9.06	20.37
dried lignin	0.92	50.18	22.72	6.95	19.00
coal	0.92	52.16	21.89	6.34	17.82
50 th % straw + 50 th % wood	0.81	48.34	22.30	9.69	19.99
50 th % straw + 50 th % coal	0.89	49.82	23.44	7.71	19.69
50 th % wood + 50 th % coal	0.93	48.97	22.71	7.72	19.00
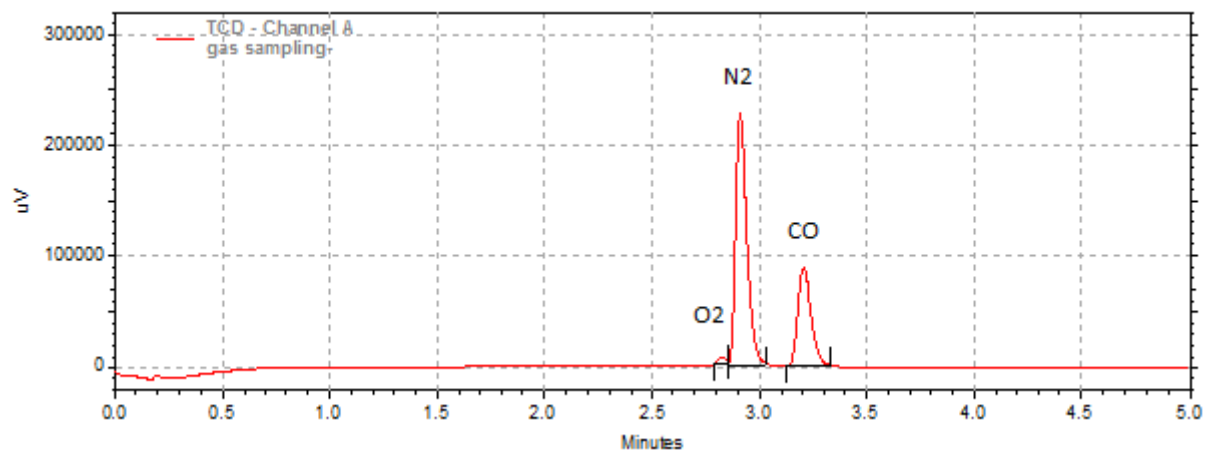
(a) channel A
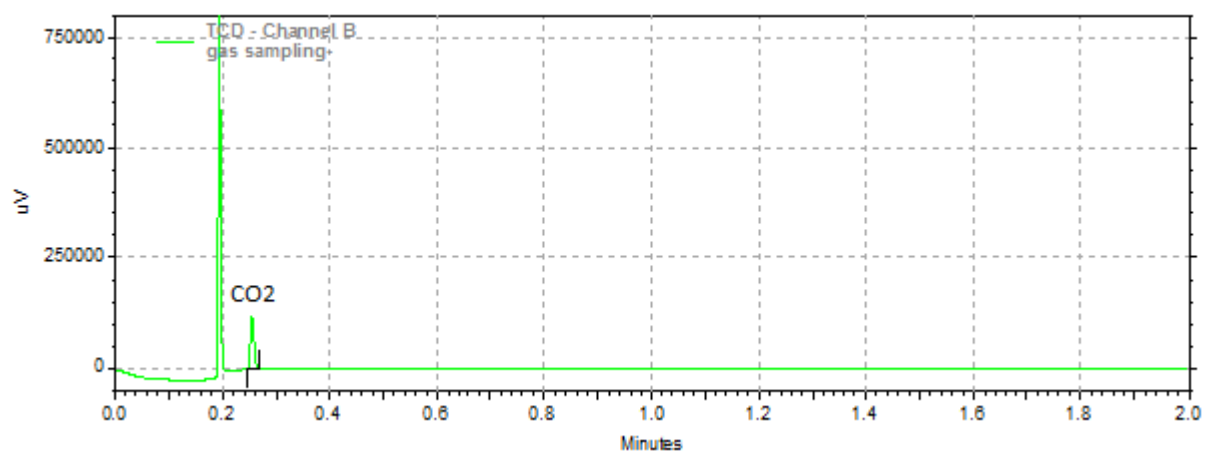
(b) channel B

(c) channel C

Figure A.4 The chromatograph data of syngas composition measured by the micro GC during wood gasification experiment (operating condition: feeder air flow = 10 NL/min, oxygen concentration = 21 %, excess air flow = 0.3, steam/carbon ratio = 0.5, and reactor temperature = 1400 °C)
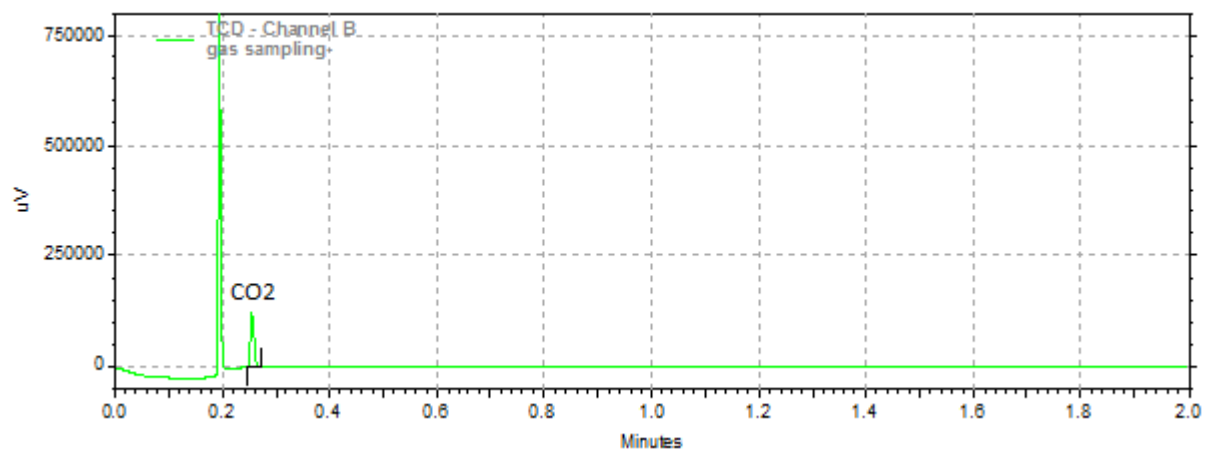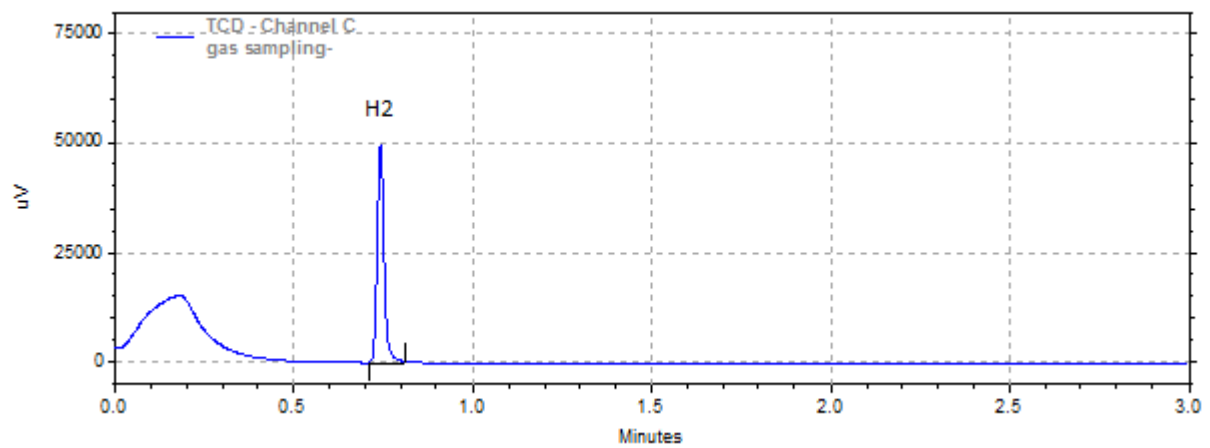
(a) channel A

(b) channel B

(c) channel C

Figure A.5 The chromatograph data of syngas composition measured by the micro GC during straw gasification experiment (operating condition: feeder air flow = 10 NL/min, oxygen concentration = 21 %, excess air flow = 0.3, steam/carbon ratio = 0.5, and reactor temperature = 1400 °C)
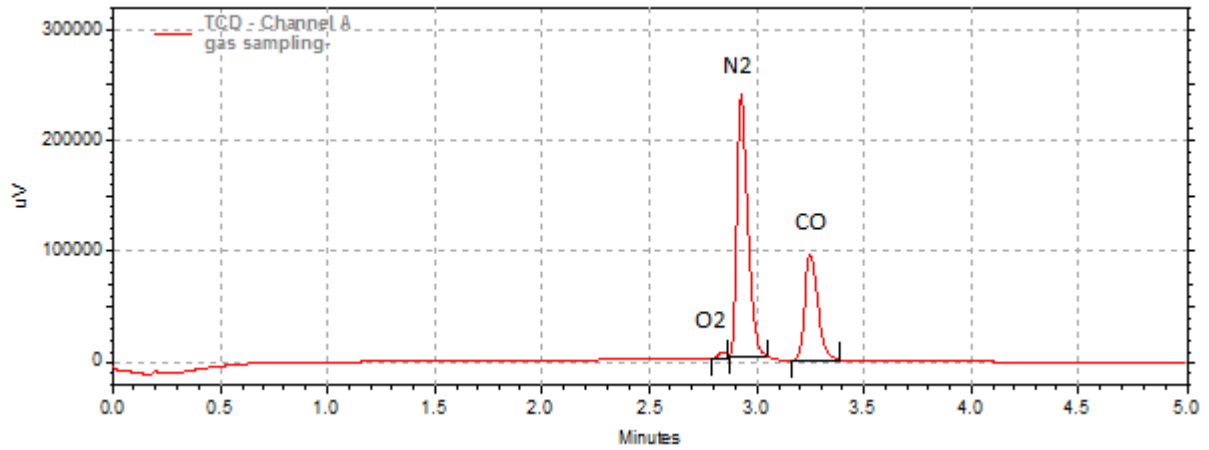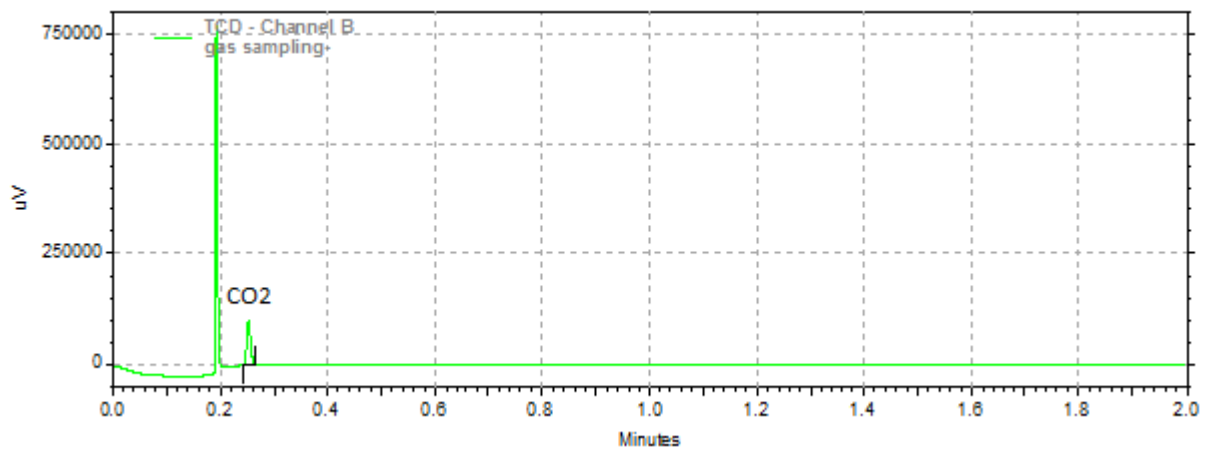
(a) channel A

(b) channel B

(c) channel C

Figure A.6 The chromatograph data of syngas composition measured by the micro GC during dried lignin gasification experiment (operating condition: feeder air flow = 10 NL/min, oxygen concentration = 21 %, excess air flow = 0.3, steam/carbon ratio = 0.5, and reactor temperature = 1400 °C)

(a) channel A
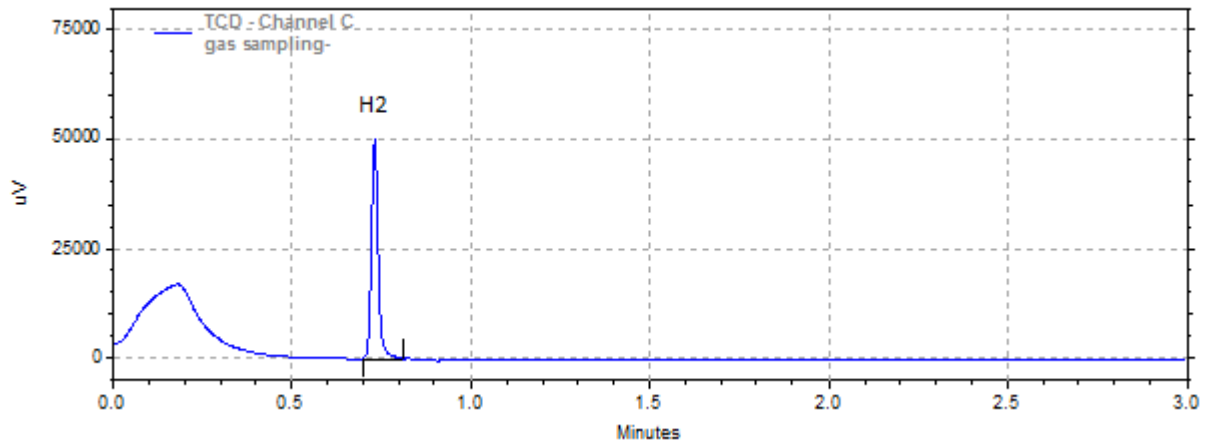

(b) channel B

(c) channel C

Figure A.7 The chromatograph data of syngas composition measured by the micro GC during coal gasification experiment (operating condition: feeder air flow = 10 NL/min, oxygen concentration = 21 %, excess air flow = 0.3, steam/carbon ratio = 0.5, and reactor temperature = 1400 °C)
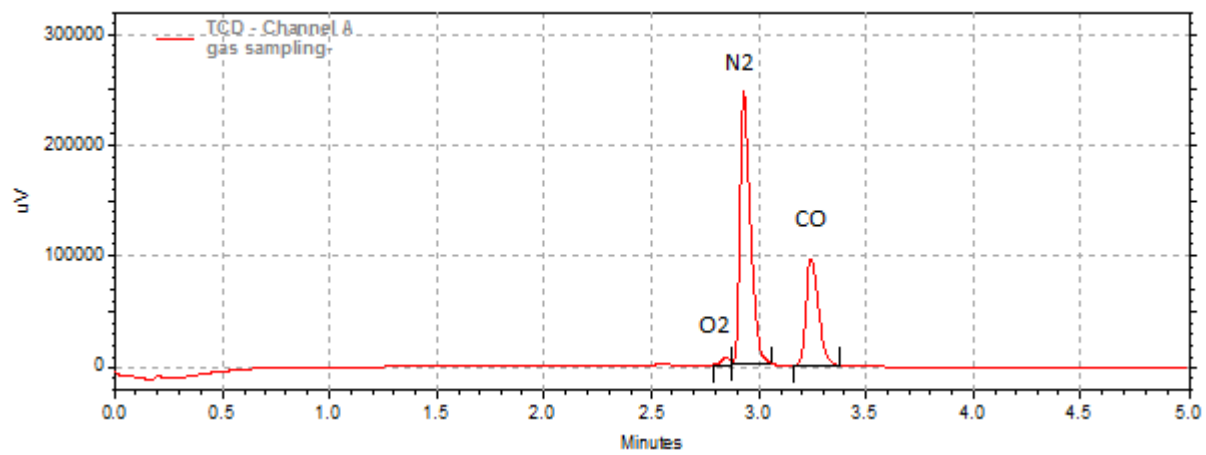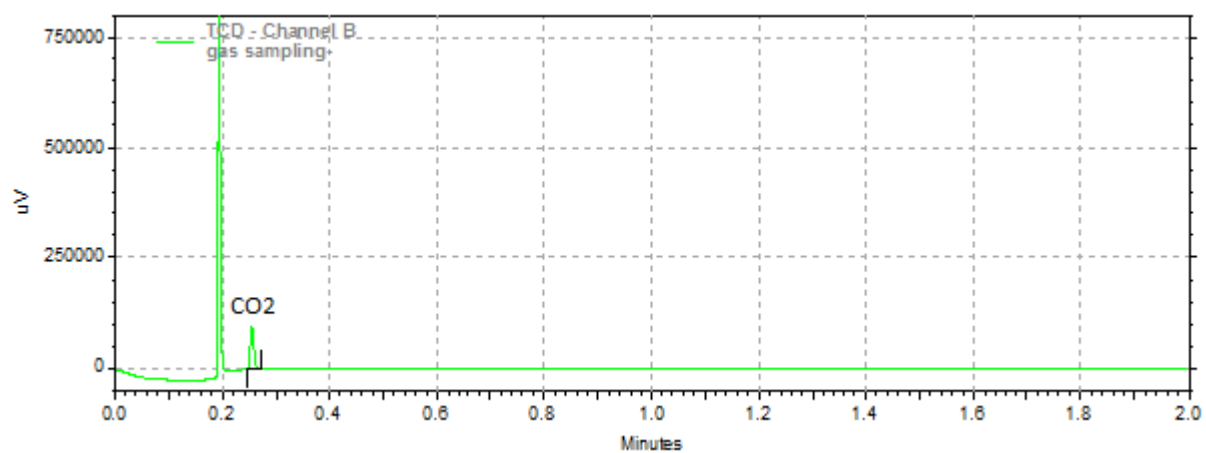
(a) channel A

(b) channel B

(c) channel C

Figure A.8 The chromatograph data of syngas composition measured by the micro GC during 50 th % straw and 50 th % wood co-gasification experiment (operating condition: feeder air flow = 10 NL/min, oxygen concentration = 21 %, excess air flow = 0.3, steam/carbon ratio = 0.5, and reactor temperature = 1400 °C)

171

(a) channel A
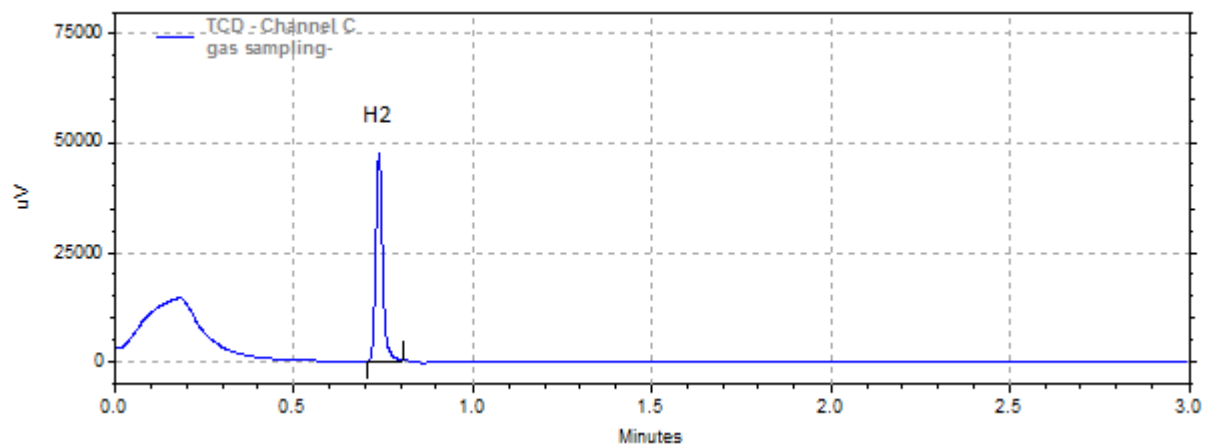

(b) channel B

(c) channel C

Figure A.9 The chromatograph data of syngas composition measured by the micro GC during 50 th % straw and 50 th % coal co-gasification experiment (operating condition: feeder air flow = 10 NL/min, oxygen concentration = 21 %, excess air flow = 0.3, steam/carbon ratio = 0.5, and reactor temperature = 1400 °C)

(a) channel A

(b) channel B

(c) channel C

Figure A.10 The chromatograph data of syngas composition measured by the micro GC during 50 th % wood and 50 th % coal co-gasification experiment (operating condition: feeder air flow = 10 NL/min, oxygen concentration = 21 %, excess air flow = 0.3, steam/carbon ratio = 0.5, and reactor temperature = 1400 °C)